Advances in rapid compression machine studies of low- and intermediate-temperature autoignition phenomena

S.S. Goldsborough [1]*
S. Hochgreb [2]
G. Vanhove [3]
M.S. Wooldridge [4]
H.J. Curran [5]
C.-J. Sung [6]

[1] Center for Transportation Research
Argonne National Laboratory
Argonne, IL 60439, USA

[2] Department of Engineering
University of Cambridge
Cambridge, CB2 1PZ, United Kingdom

[3] Université Lille, CNRS, UMR 8522
PC2A - Physicochimie des Processus de Combustion et de l'Atmosphère
F-59000 Lille, France

[4] Department of Mechanical Engineering
University of Michigan
Ann Arbor, MI 48109, USA

[5] Combustion Chemistry Centre
National University of Ireland Galway
Galway, Ireland

[6] Department of Mechanical Engineering
University of Connecticut
Storrs, CT 06269, USA

* Corresponding author
scott.goldsborough@anl.gov
+1-630-252-9375

Abstract

Rapid compression machines (RCMs) are widely-used to acquire experimental insights into fuel autoignition and pollutant formation chemistry, especially at conditions relevant to current and future combustion technologies. RCM studies emphasize important experimental regimes, characterized by low- to intermediate-temperatures (600–1200 K) and moderate to high pressures (5–80 bar). At these conditions, which are directly relevant to modern combustion schemes including low temperature combustion (LTC) for internal combustion engines and dry low emissions (DLE) for gas turbine engines, combustion chemistry exhibits complex and experimentally challenging behaviors such as the chemistry attributed to cool flame behavior and the negative temperature coefficient regime. Challenges for studying this regime include that experimental observations can be more sensitive to coupled physical-chemical processes leading to phenomena such as mixed deflagrative/autoignitive combustion. Experimental strategies which leverage the strengths of RCMs have been developed in recent years to make RCMs particularly well suited for elucidating LTC and DLE chemistry, as well as convolved physical-chemical processes.

Specifically, this work presents a review of experimental and computational efforts applying RCMs to study autoignition phenomena, and the insights gained through these efforts. A brief history of RCM development is presented towards the steady improvement in design, characterization, instrumentation and data analysis. Novel experimental approaches and measurement techniques, coordinated with computational methods are described which have expanded the utility of RCMs beyond empirical studies of explosion limits to increasingly detailed understanding of autoignition chemistry and the role of physical-chemical interactions. Fundamental insight into the autoignition chemistry of specific fuels is described, demonstrating the extent of knowledge of low-temperature chemistry derived from RCM studies, from simple hydrocarbons to multi-component blends and full-boiling range fuels. Emerging needs and further opportunities are suggested, including investigations of under-explored fuels and the implementation of increasingly higher fidelity diagnostics.

Key Words

Rapid Compression Machine

Low Temperature Combustion

Chemical Kinetics

Physical-Chemical Interactions

Table of Contents

0. Nomenclature

Acronyms	
CC	Crevice Containment
CFD	Computational Fluid Dynamics
CHRJ	Camelina Hydro-processed Renewable Jet fuel
CI	Compression Ignition
CMOS	Complementary Metal Oxide Semiconductor
CR	Compression Ratio
DCN	Derived Cetane Number
DDT	Deflagration to Detonation Transition
DLE	Dry Low Emissions
DNS	Direct Numerical Simulation
EGR	Exhaust Gas Recirculation
FACE	Fuels for Advanced Combustion Engines
FFT	Fast Fourier Transform
GC	Gas Chromatography
GT	Gas Turbine
HACA	H-abstraction/acetylene-addition
HCCI	Homogeneous Charge Compression Ignition
HRM	Homogeneous reactor model
HRR	Heat Release Rate
IC	Internal Combustion
ICCD	Intensified Charge Coupled Device
ITHR	Intermediate Temperature Heat Release
JSR	Jet Stirred Reactor
LES	Large Eddy Simulation
LIF	Laser Induced Fluorescence
LPG	Liquefied Petroleum Gas
LTC	Low Temperature Combustion
LTHR	Low Temperature Heat Release
nCC	No Crevice Containment
NG	Natural Gas
NTC	Negative Temperature Coefficient
PDF	Probability Distribution Function
PIHR	Pre-Ignition Heat Release
PIV	Particle Image Velocimetry
PLIF	Planar Laser Induced Fluorescence
PM	Particulate Matter
PRF	Primary Reference Fuel
RAMEC	Ram Accelerator Mechanism
RCEM	Rapid Compression Expansion Machine
RCM	Rapid Compression Machine
RDT	Rapid Distortion Theory

RMS	Root Mean Squared
RON	Research Octane Number
SI	Spark Ignition
SRM	Stochastic reactor Model
SWACER	Shock Wave Amplification by Coherent Energy Release
TCI	Turbulence-Chemistry Interactions
TDC	Top Dead Center
THRJ	Tallow Hydro-treated Renewable Jet fuel
UHC	Unburned Hydrocarbons
Variables	
ϕ	Equivalence Ratio
A	Surface Area
c_v	Specific Heat at Constant Volume
d	diameter
Da	Damköhler Number
E	Activation Energy
h	Convection Coefficient
K	Sensitivity Parameter
m	Mass
P	Pressure
q	Chemical Energy Released
Q	Heat Release, Heat Transfer
R	Gas Constant
Re	Reynolds Number
T	Temperature
t_{50}	Time for the last 50% of Pressure Rise
t_{50T}	Time for the last 50% of Temperature Rise
τ_C	Compression Time
τ_D	Molecular Diffusion Time,
τ_R	Reaction/Induction Time
τ_T	Turbulent Diffusion Time
τ_θ	Characteristic Time of Heat Release
V	Volume
W	Work transfer
Ze	Zeldovich Number
Subscripts	
γ	Ratio of Specific Heats
λ	Mixing Scale
c	Compressed
eff	Effective
i	Initial
k	Reaction

ℓ	Integra Scale
w	Wall
Research Organizations	
ANL	Argonne National Laboratory
GRI	Gas Research Institute
LLNL	Lawrence Livermore National Laboratory
MIT	Massachusetts Institute of Technology
NUIG	National University of Ireland Galway
UAkron	University of Akron
UConn	University of Connecticut
ULST	Université de Lille 1 Sciences et Technologies
UPMC	Université Pierre et Marie Curie
Chemical species	
2-EHN	2-Ethyl Hexyl Nitrate
DIB	Diisobutylene
DEA	Diethylamine
DEC	Diethyl Carbonate
DME	Dimethyl Ether
DTBP	Ditertbutyl Peroxide
MCH	Methylcyclohexane
MTBE	Methyl Tert Butyl Ether
TEL	Tetra Ethyl Lead
THF	Tetrahydrofuran
TMS	Trimethyl Silanol
TRF	Toluene Reference Fuel

1. Introduction

1.1. Background

Over the past few decades, research into the operation and performance of internal combustion (IC), as well as gas turbine (GT) engines has been undergoing a quiet revolution. These advances address the need for both maintaining or increasing engine efficiency, currently at a peak of 45–50% for compression ignition engines and 60% for combined cycle GT engines, whilst decreasing emissions beyond what is currently achievable with costly aftertreatment, to values lower than 80 mg/km for nitric oxides (NO_x) and below 5 mg/km for particulate matter (PM) (Euro 6) (19 mg/km NO_x and 1.9 g/km PM (U.S. Tier 3)), and below 0.67 and 0.03 mg/kWh for NO_x and PM, respectively, for stationary applications [1,2].

Historically, reciprocating IC engines have been divided into premixed, spark-ignited (SI) gasoline engines and diffusion-controlled, compression-ignition (CI) diesel engines. However, the demand for high efficiency, combined with ever lower emissions regulations has led to a wide range of experimentation into autoignition-driven combustion regimes using a variety of fuels and operating conditions. The range of new operating modes aims to reach an optimum balance between creating premixed operation, which both reduces peak combustion temperatures, thus NO_x and soot formation, while maintaining ignitability for combustion phasing just after top dead center (TDC), which increases thermal efficiency. The fine balance must also maintain high enough exhaust temperatures to allow sufficient oxidation of remaining unburned hydrocarbons (UHCs), carbon monoxide (CO) and PM or soot. The CI operating strategies based on these concepts rely on modifying the injection, mixing and exhaust gas concentration to modulate the autoignition and heat release rate of the resulting globally fuel lean, fully- or partially-mixed reactants.

The variations on a particular strategy of autoignition-driven combustion are designated by the extent of premixing and mode of exhaust gas recycling such as homogeneous charge compression ignition (HCCI). A popular nomenclature from diesel studies has been the idea of low temperature combustion (LTC) to differentiate from flame-driven combustion. In this paper, we use the term LTC to denote the class of autoignition-controlled, or chemical kinetically modulated processes, where both volumetric autoignition and local deflagrative fronts can be present. Recent review papers have discussed potential opportunities and challenges to the application of these techniques in engine operation [3–5]. The opportunities arise from the ability to increase compression ratios and burn very lean or dilute mixtures, leading to high efficiencies and low emissions. A simple energy analysis for an engine cycle with combustion at TDC, i.e., the Otto cycle, shows that increasing compression ratios increases the thermal efficiency of engines in proportion to $(1 - CR^{1-\gamma})$, where CR is the compression ratio and γ is the ratio of specific heats of the

working fluid. Higher compression ratios and higher specific heat ratios, which are obtained for more overall fuel lean and/or more dilute mixtures, increase engine efficiency. Trends are similar for gas turbine engines where pressure ratios and γ dictate efficiencies. Limitations come from two related processes. First, since autoignition of the mixed reactants is inherently controlled by chemical kinetics, some LTC operating strategies are challenged by the inability to precisely control combustion timing via spark and/or fuel injection events, particularly over a broad range of state and mixture conditions. Instead, the combination of reaction and mixing after a given fuel injection time modulates the start of combustion. Second, the rate of heat release in kinetically-modulated schemes is no longer completely controlled by flame propagation or fuel injection rates, but by the often rapid reaction rates of chemical processes distributed throughout the combustion chamber. Finally, pollutant emissions depend greatly on the local equivalence ratio and temperature-time history of the mixture. This complex situation creates opportunities for low temperature, low emission combustion, but in a scenario where many external and internal parameters determine the local temperature and state of mixedness, and ultimately reaction rates.

Original work by Onishi *et al.* [6] highlighted the possibilities of premixed autoignition using internal exhaust gas recirculation (EGR) in two-stroke engines. Najt and Foster [7] extended the work to four-stroke engines, and highlighted limitations regarding control. The topic was reawakened by a series of papers by Johansson and coworkers [8–10], who demonstrated the ability to control the process using a combination of injection control, variable supercharging and EGR. Work in the U.S. and Japan demonstrated the use of diesel fuel in HCCI mode [11–15]. The latter work spawned a number of studies on variations of HCCI, as discussed below. Although there have been numerous contributions to the literature on the subject since then, difficulties in controlling ignition of premixed charges remain. However, the original ideas have found fertile ground in existing diesel engines in the form of LTC by leveraging the recent advances in the ability to deliver multiple injections in CI systems.

The concept of LTC was highlighted by Akihama *et al.* [16], who neatly described the tradeoffs between soot and NO_x formation in a regime diagram (which has been highly cited since) showing calculated soot and NO_x contours as a function of temperature, T, and equivalence ratio, ϕ, for a given residence time. The diagram allowed examination of desirable ϕ-T pathways that have the potential to avoid the formation of either NO_x or soot towards the low temperature regions, using either fuel rich or fuel lean strategies. The diagram shows a narrow valley at combustion temperatures which can attain low NO_x and low PM. Following this idea, the concept has been exploited in practice, and indeed adopted into

practical engines via multiple injections, high EGR, and high boost concepts, to name a few, such as the Toyota UNIBUS [17], or the Nissan MK [18] systems and extensively discussed in other review articles [4]. In particular, very high efficiencies, low emissions have been demonstrated by the use of low cetane fuels at intermediate compression ratios between those typical of CI and SI engines [19,20]. Further, dual fuel concepts such as reactivity controlled compression ignition employ a combination of low and high cetane fuels, delivered through separately timed injection events, to achieve similar fuel economy and emissions performance. Numerous studies have recently explored the very wide operating space including fuel, engine parameters and operating conditions [21,22].

The need to understand and control autoignition has been strongly motivated by a growing interest in HCCI and LTC concepts in recent years. Additionally, parallel development in highly boosted, downsized direct injected, spark-ignited gasoline engines has highlighted some limitations of the current autoignition database. Downsized, boosted SI engines offer advantages in overall engine size, weight, and fuel consumption, yet a byproduct of boosting has been the onset of knock and especially random episodes of violent autoignition [23,24], sometimes referred to as superknock. The origins of superknock are still under debate, but it appears to be associated with a mixed mode of combustion, in which an early local deflagration or autoignition event (produced for example, by non-uniformities in fuel-air ratio or the presence of easily ignitable lubricants) leads to a sudden pressure wave across the chamber, which, depending on the state of the gas and the turbulent dissipation of the localized reaction, can trigger subsequent reactions throughout the system, in a state approaching a developing detonation [25–27].

High pressures lead to high efficiencies in continuous thermal cycles, so gas turbines have also offered targets for understanding autoignition. Current gas turbines for power production typically operate at pressure ratios between 15–30, and aeroengine turbines operate at pressure ratios around 40–45 [28]. An overall higher pressure ratio offers the highest efficiencies for a single stage, though most stationary gas turbines optimize the efficiency of the overall combined cycle, including multiple staged heat additions with a range of mixing scenarios. Aeroengine turbines are designed based on fuel properties of conventional kerosene and jet fuels, and are typically not premixed, but rather fuel-lean, direct injection, where the fuel and air are introduced shortly before the combustor to avoid autoignition and instabilities. Aeroengines operate over a wide range of pressures, temperatures and flow rates, and must guarantee operability over the entire operating map for safety reasons – premixing is thus limited, and uncontrolled autoignition must be avoided. Gas turbines for power generation make extensive use of fuel-air premixing with a variety of strategies, called dry - low emissions (DLE), to differentiate from other methods for

lowering NO_x such as steam-injection or humid cycles. Gas turbines for engine cycles can also use autoignition to stabilize the second heat addition in combined cycle combustors, such as the sequential combustor of Alstom [29][30], allowing for heat release rates under dilute conditions, thus minimizing NO production. Gas turbines must balance the propensity for autoignition, flashback and instabilities, whilst still being operable for a variety of fuels, typically natural gas, with a wide range of minor gas compositions (mainly H_2 and higher hydrocarbons in methane, as highlighted in Section 6), but also synthesis gases, biogases, and new synthetic and modified liquid fuels and biofuels. Synthetic fuels vary widely in composition and corresponding propensities for autoignition [31], so it is challenging to design premixed or direct injection systems that work well with a wide variety of fuels using a fixed geometry. Fuel chemistry and interactions with the turbulent flows can influence burning rates and important combustor parameters, such as the lean blowout limit [32,33]. Furthermore, low- and intermediate-temperature chemistry, and associated heat release can perturb the flame structure, especially under complex mixing scenarios used in modern gas turbine engines [34,35]. As such, the availability of reliable, verified chemical kinetic mechanisms for the pressures and temperatures prevalent in the premixing (autoignition) zone of gas turbines (initial pressures up to 50 bar, temperatures up to 1200 K) is essential to aid future turbine design.

The development of engines and fuels has followed largely separate paths. Gasoline became available to replace coal gas in steam engines, and diesel and kerosene were originally available as safe alternatives to coal gas for street lamps at the time when Otto and Diesel were testing their inventions [36]. Once the infrastructure for fuel distribution was established engines adapted to the available fuels rather than optimizing the fuels for the engines. In recent years, there have been relatively large scale efforts to introduce infrastructure for alternative fuels, particularly oxygenated fuels such as ethanol (in Brazil and the U.S.), methanol (in Sweden), along with liquefied petroleum and natural gas conversions in various parts of the world. The requirement for the success of new cycles or fuels however, has often been that the fuels must use the existing infrastructure. Furthermore, whereas some fuels such as ethanol may allow higher efficiencies owing to higher octane ratings, these benefits are often not realized, as in many markets the need to operate on a range of fuels restricts the ability of engines to dynamically adapt to fuels. In Brazil for example, most light duty vehicles are adapted by automakers to operate using either 100% ethanol or a blend of ethanol and gasoline. In these systems, the oxygen sensor varies the engine calibration according to the fuel in use, but the overall vehicle fleet achieves largely sub-optimal efficiencies using either fuel. If maximum fuel efficiency gains are to be realized, along with associated reductions in greenhouse gas emissions, a much more detailed understanding of autoignition associated

with LTC processes of a wide range of fuels is needed to design novel and robust engine hardware and operating strategies.

1.2. Measurements of autoignition phenomena

The ability to design and control reciprocating engines and gas turbine engines that utilize highly promising LTC and DLE approaches, along with new varieties of fuels, depends on the availability of well validated models for: (i) the chemical kinetics of the autoigniting mixture, (ii) the rate of turbulent dissipation of species and heat through the reaction process, and (iii) the interaction between turbulence, thermal/compositional gradients, and chemistry. As mentioned, these needs are also relevant to modern SI and CI engines that employ techniques such as downsizing and charge boosting, since LTC phenomena including low- and intermediate-temperature heat release (LTHR and ITHR, respectively) can become evident as boost pressure becomes significant [37,38]. These issues represent substantial challenges to the combustion community. While models exist based on theory and interpretation of engine data, experimental validation of proposed fundamental chemical and physical mechanisms is still needed to cover the range of operating conditions found in engines, since unacceptable discrepancies and uncertainties still persist in existing models.

1.2.1 Autoignition chemistry

A significant database for autoignition chemistry of various fuels at engine-relevant conditions has been compiled ever since IC engines have existed, where early interest targeted gasoline engine knock, and to some extent diesel fuel autoignition. Recent efforts have also targeted jet fuels. Chemical kinetic models are typically formulated based on data from a variety of sources, including rapid compression machines (RCMs) [39], motored or skip-fired engines [40], flow/jet reactors [41,42], and shock tubes [43]. Typical ranges of operation for these apparatuses are summarized in Fig. 1 and Table 1; though some facilities operate outside of these ranges. Figure 1 is presented to highlight the thermodynamic conditions of these devices, but the reactor, as well as chemical time scale of the mixture, which is discussed in Section 1.4, are also important.

All devices have intrinsic optimal ranges of temperatures and pressures, limited either by physical material constraints or the achievable reaction times of interest. Starting with reciprocating engines, these were the original devices where autoignition was detected and from which many historical studies originated. A motored engine is typically a continuously reciprocating device, without direct fuel injection or spark, which can produce repeated compression events for the resident mixture inside the engine. The bulk composition inside the chamber can potentially be controlled by purging post-reaction gases over

many cycles, *i.e.*, skip-firing, so as to produce well-controlled initial, bottom dead center conditions on average. Given the character of the compression process, however, the mixture experiences the many processes typical of engine flow, including heat transfer to the walls, and characteristic turbulent disturbances produced by the inlet and outlet conditions with moving valves. This means that whereas the bulk conditions in the engine are statistically stationary, each single stroke experiences a different detailed distribution of temperature and velocity, which affects the chemical reaction rates. Thus, the statistical distribution of autoignition times or critical compression ratios ascertained from motored engines typically reflects the distribution of operating conditions. One advantage of motored engines is that species evolution can typically be obtained by timed sampling events relative to the crankangle position, or by extraction from the exhaust gas flow.

Flow and jet reactors attempt to separate the confluence of mixing and reaction by providing very fast mixing conditions throughout the system, so fluctuations of temperature or species concentration across the volume of the reactor (in the case of a jet-stirred reactor) or across the radial dimension (for plug flow reactors) can be considered negligible. The challenge in this case is to maintain the reactor at high and uniform temperature, as well as high pressure. This is typically accomplished through external heating of the diluent gas and walls. An advantage of these reactors is the ability to vary composition, pressure and temperature independently, and the straightforward extraction of samples for chemical analysis. Flow reactors can measure a limited range of ignition times, based on location downstream of the inlet. Jet reactors must be operated using very dilute conditions, e.g., < 1% O_2, to ensure temperature homogeneity across a section.

Shock tubes offer the ability to reach the highest temperatures of the techniques considered, e.g., 2500 K, by a combination of incident and reflected shocks. Shock tubes are single shot devices that create transient test conditions, so probing reactions is most amenable to fast response optical and laser-based diagnostics, as physical sampling can be challenging for the shorter test times available (typically <5 ms), though a few techniques have been developed, especially for very dilute mixtures [44,45]. Shock tubes are typically designed with consideration for minimizing boundary layer influences on the gas dynamics, while some have been extended to lower temperature operation and longer reaction times, e.g., 10–50 ms [43,46], by careful tailoring of the mixture used in the driver section, and extension of the length of the driver section to minimize expansion wave and contact surface interactions with the test gas mixture (see [47] and references therein). A particular strength of shock tube studies remains higher temperature

dilute mixture conditions, which are particularly well suited to studies of elementary chemical reactions and can be more straightforward to model without considering complex boundary conditions [48].

RCMs also offer well-controlled state conditions for studying the ignition properties of fuels while using realistic (*e.g.*, dilute to undiluted) mixtures. Like shock tubes, the single-shot character of RCMs affects the nature of diagnostics used to access the state of reaction; and, long test times of RCMs enable physical sampling and other experimental techniques. Much historical and recent effort has been undertaken to address challenges associated with RCMs, including heat transfer induced boundary layer growth, as well as others. The current work reviews many contributions of RCM studies to the understanding LTC and DLE relevant autoignition chemistry.

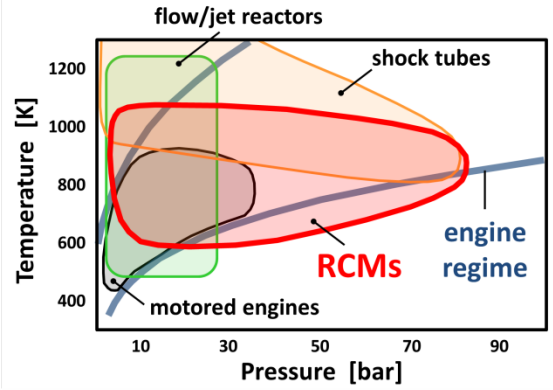

Figure 1. Temperature–pressure diagram of typical operating conditions for experimental devices and combustion engines.

Table 1. Typical features and operating conditions of devices used to acquire data for autoignition / LTC phenomena

Method	Motored engine	Flow / jet reactor	Shock tube	RCM
Temperature (K)	400–900	<1500	800–2500	400–1200
Pressure (bar)	5–40	<30	2–80	5–80
Reaction times (ms)	1–10	10–10000	0.01–2	2–150
Operation	Multi-shot, unsteady	Continuous	Single-shot, unsteady	Single-shot, unsteady
Flow conditions	Turbulent	Turbulent	Laminar (transition to turbulent)	Laminar, Turbulent
Advantages	Inexpensive, moderate pressures / temperatures	Continuous (sampling straightforward)	High pressures / temperatures, instantaneous compression	Inexpensive, high pressures / temperatures, pressure history similar to engines
Disadvantages	Limited range, turbulent, high residual concentrations	Limited range of ignition times / significant dilution required	Single shot, boundary layers, test times	Single shot, heat transfer

1.2.2 Physical-chemical interactions

A significant database for physical-chemical interactions covering a range of engine-relevant conditions has been developed through the use of steady flow / constant pressure devices like burners and [49,50]. These configurations have the ability to generate statistically stationary conditions (more so than motored engines) and are able to provide wide diagnostic access for the implementation of optically-based configurations, as well as physical sampling based ones. These steady flow devices are able to cover a wide range of flow rates and power levels, but can be limited in, for instance pressure ratings. Achieving energy densities that replicate reciprocating and gas turbine engines is also challenging. Single-shot devices like combustion bombs [51,52] and spray chambers [53] have also been used to achieve IC engine-relevant conditions, but the diagnostic access is reduced, while shot-to-shot variability complicates analysis of the data, and comparison with models. Some datasets relevant to physical-chemical interactions have also been acquired via controlled-turbulence RCMs, and these unique contributions are discussed here, with suggestions for possible future work in this area.

Computational databases for physical-chemical interaction studies are also growing covering the finest scales through direct numerical simulation [54–58], as well as larger scales via large eddy simulation [59,60]. Extremeley beneficial insight has been drawn, but the applicable Reynolds and Mach numbers, and other regimes, e.g., Damköhler, can be limited.

1.3. Rapid compression machines

RCMs have been used since the earliest days of engine research to study autoignition phenomena, and a description of the evolution of the hardware is presented in Section 2. These single-shot, piston-based machines produce relatively fast compression of the gases in a chamber, creating high pressure and temperature and nearly adiabatic conditions. Modern RCMs are often designed so the test mixtures and conditions are decoupled from the fluid mechanics and mixing that result from the gas exchange process in production reciprocating engines, thereby allowing the study of autoignition at conditions controlled by the design of the device. Importantly, the boundary and initial conditions can be well specified. Moreover, autoignition processes in RCMs are representative of those that occur within combustion engines, where these evolve through many thermo-chemical regimes, and this complicated evolution can be different than that experienced in temperature/pressure controlled devices, as discussed, for example, in [61].

RCMs have progressed significantly in design so that modern configurations are able to create well-specified, thermo-chemical state conditions within the reaction chamber which are well controlled for

long periods of time (2–150 ms), and thus enable the study of autoignition chemistry. Additionally, some arrangements are also able to generate controlled non-uniformities for investigation of physical-chemical interactions, as highlighted in the previous section. A variety of temporally- and spatially-resolved diagnostics can be implemented to acquire a wide range of measurements towards the development and validation of autoignition chemistry and turbulence-chemistry interactions (TCI) models, as well as understanding how full-boiling range fuels behave at engine relevant conditions. Various diagnostic techniques are discussed in detail in Section 3. There are currently nearly thirty laboratories worldwide that utilize RCMs for investigations of gas-phase autoignition processes. An overview of the physical characteristics and capabilities of these facilities is provided in the Supplementary Material. In addition, another fifteen laboratories employ RCMs to investigate spray combustion phenomena [62]. The relative simplicity, range of accessible pressure and temperature conditions and the ability to tailor and control the reactant composition have allowed data acquired from RCMs to reliably quantify the reactivity and reaction pathways of a large range of fuels, as well as provide valuable data for the development and validation of chemical kinetic mechanisms. Recent reviews by Kéromnès [63] and Sung and Curran [39] describe state-of-the-art techniques for applying RCMs in this manner. The current manuscript extends these works to additionally cover utilization for studying physical-chemical interactions, as well as detailed design considerations, diagnostic implementation and insight, and alternative approaches to modeling RCM processes.

Early RCM studies primarily addressed high load (*i.e.* high energy density), near stoichiometric conditions relevant to SI engine knock, where trends in fuel reactivity at some select conditions were an initial focus. Substantial insights were contributed by a number of groups, including Jost *et al.* at Philipps-Universität Marburg [64–67], Leary *et al.* at the Massachusetts Institute of Technology (MIT) [68,69], and Fish *et al.* at Shell Thornton [70–73]. Griffiths *et al.* at the University of Leeds [74–78] and Minetti *et al.* at Université Lille Sciences et Technologies (ULST) [79–84] expanded upon these and acquired more quantitative datasets utilizing sophisticated diagnostics over a wider range of conditions. Recent developments in LTC and DLE engines require extension of experimental databases covering an expansive range of pressures (p = 5–100+ bar), temperatures (T = 600–1100 K), and dilution levels (O_2 = 5–30 %), from very lean to rich fuel loadings (ϕ = 0.25–4.0), and a range of residual gas concentrations (EGR = 0–60 %), specifically to understand the role of CO_2, H_2O, NO_x and UHC present in dilution strategies. Hydrocarbon fuels were the initial focus for RCM studies, while recent developments in the fuel industry have prompted expansion beyond conventional fuels, and into alternatives such as oxygenated structures.

A summary of the results of RCM studies of natural gas, gasoline surrogates, full-boiling range fuels and fuel additives is provided in Section 6.

The evolution of certain reaction systems is highly dependent on the molecular structure of the fuel as well as the temperature- and pressure-time histories. A well-studied example is the delayed autoignition phase in long-chain hydrocarbons, whereby an increase in temperature can lead to longer ignition times, and thus an apparent "negative temperature coefficient" (NTC) region when ignition delay time data are plotted using Arrhenius or inverse temperature coordinates. This region, which appears around 700–850 K for *iso*-octane at a pressure of 20 bar in air levels of dilution (*i.e.* 21% O_2, mole basis), is identified in Fig. 2 [62]. Under these conditions there is a shift in the main reaction routes from the formation of hydroperoxides that result from interactions between the fuel radicals and molecular oxygen, and its associated LTHR which dominate at lower temperatures, to the non-branching formation of stable olefins/ethers/carbonyls, accompanied by ITHR. The chemical kinetic processes, and observed behavior depend on the temporal evolution of temperature and pressure throughout the experimental tests, and thus can complicate interpretations of the measurements, as well as comparisons between different RCM, shock tube, and reciprocating engine datasets where different operating characteristics affect the state preparation and induction period. For example, ignition delay time measurements in the NTC region can vary by $\pm$25 % or more for hydrocarbons displaying this behavior, and this can be seen in Fig. 2 [62]. The data presented here include results from several RCM facilities in the 2nd International RCM Workshop, and highlight the need for rigorous specification of the initial and boundary conditions for each test, e.g., heat loss characteristics. Furthermore, this illustrates challenges associated with comparing experimental results when only on a single characteristic parameter, such as compressed temperature is used as the basis.

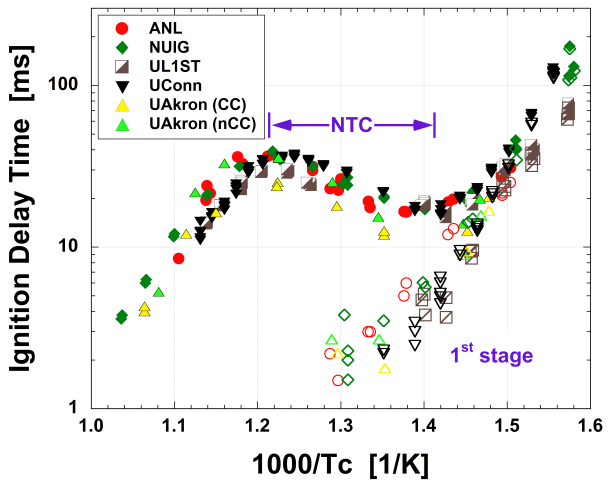

Figure 2. Arrhenius plot of selected *iso*-octane ignition delay time data at a pressure of 20 (±0.65) bar from the 2nd International RCM Workshop [62]. Open symbols indicate first-stage ignition (where the first-stage reaction chemistry is often attributed to cool flame processes), closed symbols are total ignition times. (ANL – Argonne National Laboratory, NUIG – National University of Ireland Galway, UL1ST – Université de Lille 1 Sciences et Technologies, UConn – University of Connecticut, UAkron – University of Akron (CC – crevice containment, nCC – no crevice containment) [85]).

All experimental devices are subject to operating constraints which may limit the range of conditions available. For RCMs which acquire data to quantify fuel reactivity, understand autoignition chemistry, and investigate interactions between chemistry and the scalar/velocity fields, particular attention needs to be given to the measurement of local thermal conditions. As in all physical devices, the state conditions can be affected by boundary layer growth and gas motion, since different temperatures prevail near the walls relative to the center, or core of the test sections. As discussed earlier, the onset of autoignition and rate of heat release can be altered, intentionally (as in reciprocating engines) or unintentionally, by the presence of inhomogeneities, mixing, and turbulence in the combustion chamber. In many current RCMs, significant effort has been directed towards suppressing undesirable non-uniformities; some historical data indicate that when these non-uniformities are present substantial scatter can result [69]. Strategies to address these are covered in Section 2. In order to achieve low uncertainties towards the development of reliable chemical kinetic information and models, and the formulation of more accurate phenomenological insight coupled with quantitatively accurate simulations, comparisons of experimental RCM data need to go beyond evaluation of ignition delay times. Indeed, detailed evaluations require sound understanding of the physical and chemical phenomena taking place within the system and the influence of these on commonly measured, pressure-time histories. These issues are clearly not unique to RCMs – boundary layer and turbulence-chemistry interactions appear in other devices such as shock

tubes and flow/jet reactors [86,87]. The present review surveys different approaches to resolve these issues, and identifies 'best practices' and opportunities.

1.4. Characteristic time scales

Autoignition phenomena that occur within piston engines and gas turbines can be substantially affected by states of mixing and turbulence, and the developing chemical kinetics represents one component of knowledge necessary to accurately predict ignition and heat release in practical devices and thus facilitate engine design. How to identify and model the onset of autoignition has been explored using direct numerical simulations (DNS) [88,89], where the propagation of autoignition events can be distinguished from deflagrative processes. Experimental approaches for investigating coupled autoignition and deflagration phenomena, as well as developing detonation phenomena using RCMs are discussed in this review.

Characteristic time scales associated with LTC phenomena in engines and RCMs, include: compression time, τ_C, reaction, or induction time, τ_R, molecular diffusion time, τ_D, and turbulent diffusion time, τ_T. The compression time is determined by the driving force on the piston and the stroke of the machine. For typical RCM studies of autoignition chemistry the compression time is often designed to be as low as possible to minimize overall heat transfer and extent of reaction before the test conditions are reached, yet the velocity is limited to the low Mach number limit, to keep acoustic disturbances to a minimum. Furthermore, turbulence should be inhibited by avoiding high strain rate conditions. The reaction time is a function of the composition of the mixture and the local temperature and pressure. A related quantity is associated with the rate at which the local temperature (and pressure) rises due to chemical heat release, relative to the reaction, or ignition delay time. The normalized sensitivity of the rate of temperature rise is given by a modified Zeldovich number $Ze = \tau_R/\tau_\theta = (q/c_v T)(E/RT)$ where τ_θ is the characteristic time of chemical heat release (sometimes referred to as an excitation time [90]), q is the chemical energy released, c_v the specific heat at constant volume, while E and R are the activation energy and the gas constant, respectively. When Ze is large, the local heat release can lead to large thermal gradients followed by, for instance, gas dynamic or other phenomena, *e.g.,* knock [91]. The molecular diffusion time is a function of the diffusion of heat and species across the mixture, which also depends on the pressure, temperature and mixing conditions in the chamber. The turbulent diffusion time depends on the turbulence characteristics in the system.

The ratios of the time scales, or Damköhler number, for uniform composition systems indicate a wide range of possible behaviors as proposed in Fig. 3, from fully uniform autoignition to ignition in stratified

layers. The behaviors change dynamically depending on the initial condition or operation point. For typical RCM studies of autoignition chemistry, the objective is to achieve laminar autoignition in the adiabatic region, called the core, which ideally does not mix with the cooler regions near walls. At the other extreme, machines can be configured to achieve a well-mixed, non-adiabatic reactor regime, for instance, to investigate turbulence-chemistry interactions.

The panel on the right in Fig. 3 compares time scales for laminar and turbulent diffusion and reaction. At laminar conditions with high rates of molecular diffusion, reaction can be quenched by heat transfer. Low rates of turbulence and diffusion are ideal conditions for laminar rapid compression machines with adiabatic conditions in the core region. High rates of turbulence relative to reaction and laminar diffusion lead to uniform stirred conditions, such as in a turbulent engine at high speeds. For intermediate regimes, even if the system starts at a uniform temperature, regions of cold gas can be intermixed with higher temperature, autoigniting regions. The panel on the left in Fig. 3 compares the rates of diffusion, temperature rise and reaction. Cases where the rate of temperature rise is small or gradual and the rate of diffusion is low, lead to adiabatic and steady conditions. When diffusion rates are low and reaction rates are high, rapid heat release can lead to detonation and knock (depending on the rate of heat release and heat loss relative to the local speed of sound, which is not considered in the present diagram). The NTC region significantly complicates the characterization of the state of the system, as the relative rate of heat transfer and heat release can cause the temperature to transition into or out of the NTC region. This can become a source of scatter in autoignition measurements in the NTC region, as shown by the data from different facilities in Fig. 2.

For the present discussion on the contributions of RCM studies to understanding low and intermediate temperature chemistry, insight into diffusion and heat transfer effects on reaction as well as heat release rate at different experimental conditions is critical to determining the uncertainty and accuracy of RCM measurements. The relative importance of these physical and chemical mechanisms must also guide experimental design and the appropriate modeling approaches, as discussed in Sections 2 and 4.

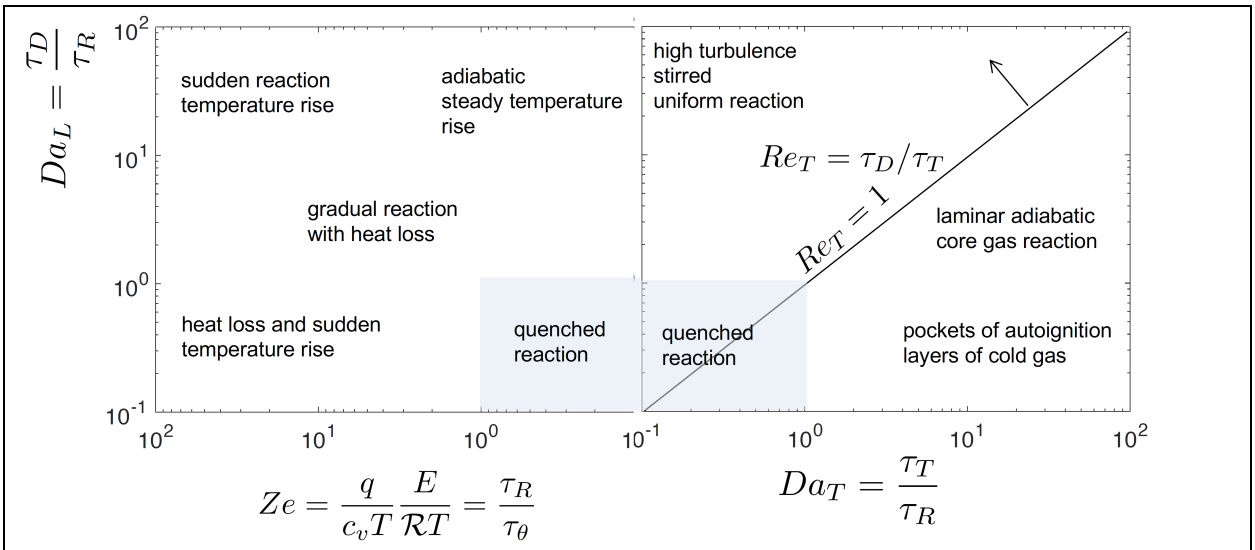

Figure 3. Autoignition regimes in engines and RCMs categorized based on relative characteristic times.

1.5. Overview

The objective of this paper is to extend the recent reviews by Kéromnès [63], and Sung and Curran [39], and present a summary of important advances that have been achieved via rapid compression machines as experimental platforms towards improving the understanding, development and validation of models for low temperature combustion. Thanks to both historical and recent innovations, uncertainties associated with the reaction chemistry of the LTC regime have been substantially reduced. Further improvements are still necessary so that predictive capabilities can be achieved toward the design of advanced combustion engines. The focus within this review is primarily on gas phase phenomena covering autoignition chemistry and associated physical–chemical interactions. While spray combustion has been investigated in RCMs, these studies are not reviewed here. The organization of this paper is as follows. Section 2 describes the evolution of machine configurations from simple, uncontrolled falling weight devices to sophisticated apparatuses where the thermo-chemical/fluid dynamic fields can be precisely controlled during the test period for studies focused on either autoignition chemistry or physical-chemical interactions. Section 3 covers the implementation of various diagnostic techniques, both intrusive and non-intrusive, in order to probe the evolution of the reactive system within the test chamber. Section 4 further discusses autoignition regimes and associated modeling approaches where facility-specific effects can be taken into account. Section 5 presents results of RCM investigations of physical-chemical interactions, including effects of large- and small-scale phenomena. Section 6 reviews advances made towards the understanding and modeling of autoignition chemistry for a wide range of fuels, from hydrogen to gasoline and jet fuel. Finally, current needs and opportunities for combustion

research using RCMs, in terms of novel topics and the implementation of emerging diagnostics, are highlighted in Section 7.

2. RCM designs and configurations

RCMs have been employed since the beginning of the 20th century to access thermo-physical conditions relevant to conventional and advanced combustion schemes. These regimes cover the transition from low to intermediate-temperature autoignition phenomena, including tight coupling between the scalar and velocity fields so that mixed deflagrative-autoignitive processes can take place. Continual progress has been achieved towards accurately specifying the state of the mixture during and post compression, enabling detailed investigations of the chemical transformations that occur throughout the ignition delay period prior to the main explosion or heat release, as well as interactions between the evolving scalar and velocity distributions. These studies have provided unique insights into LTC phenomena, while advancements in RCM design have enabled the thermo-physical conditions of the reacting mixtures to be more precisely controlled, and facilitated the implementation of advanced diagnostics.

The intent of this section is to review the progress and increasing sophistication of RCM designs in order to highlight experimental techniques which have provided access to important combustion regimes. Challenges with the experiment and ways to address these are also discussed. There are currently nearly thirty machines in use worldwide to study LTC phenomena, generally emphasizing either homogeneous autoignition chemistry or physical-chemical interactions. This section segregates these two topics, and discusses geometrical and operational needs of each, as well as means to address these accordingly. The first part details progress in RCM design towards achieving well-behaved conditions during and post-compression for autoignition studies, as well as some characterization results that have motivated the need for new technological concepts, including manipulation of the piston trajectory, temperature and mixture homogeneity. The second part of the chapter focuses on recent RCM developments which, for example, seek to create non-homogeneous conditions necessary to study turbulence-chemistry interactions, and other phenomena. Improvements in RCM configurations have been critical in reducing uncertainties associated with the measurements as well as interpretations of acquired data, while historical advances have provided guidance and insight into the design and operation of modern and future machines. Important findings are summarized at the end of the section.

2.1. RCMs for autoignition chemistry / fuel reactivity studies

In order to understand the autoignition behavior and reactivity characteristics of fuel components, blends and full-boiling range fuels, the capability to generate a wide range of temperatures and pressures is required. RCMs have been developed to access relevant combustion conditions without complications

of flow and gas exchange. However, the long experience with these devices has shown that RCM design and operation must be undertaken with care, as with all experimental facilities, to avoid adverse influence on the measurements. Here we specifically discuss challenges associated with, and strategies to control: (i) the gas compression process, (ii) piston creep and rebound, (iii) the state and uniformity of the reacting gas, and (iv) piston crevice containment. Approaches to interpret the data are covered in Section 4.

For studies of autoignition chemistry, ideally the volumetric compression process would be instantaneous to eliminate pre-test fuel reactivity and provide well-defined initial conditions, while the chemical reactions during the constant volume process would occur at conditions that are spatially uniform and without heat loss. These characteristics are impossible to achieve in practice: as an example, instantaneous piston acceleration/deceleration necessitates unwieldy mechanical forces, and generates compressibility effects leading to complex gas dynamics, as well as the development of turbulent, inhomogeneous conditions. Heat transfer must inevitably take place, since the walls of the reaction chamber are in general much cooler than the reacting gas, and heat loss therefore occurs during the test period, decreasing the temperature and pressure in the test chamber and stratifying the mixture.

Since ideal operation cannot be achieved, all designs represent some compromise. An optimal, but realistic configuration is one that can compress the gas in a time short enough to decouple the chemical time scales from the piston motion, while simultaneously ensuring that the arresting of the piston occurs smoothly and without rebound, minimizing the generation of gas dynamics and turbulence within the reaction chamber. Additionally, the configuration should achieve a good degree of thermal and compositional uniformity throughout the test gas by suppressing fluid motion within the reaction chamber. The hot core gases in the center of the reaction chamber should be segregated from the cold walls by minimizing the thickness and volume of the boundary layer relative to the reacting gas. Dead volumes associated with ports and diagnostics should be as small as possible, while chemical contamination due to lubricants or seal materials, or catalytic effects at the walls should be eliminated. Furthermore, the reaction chamber should incorporate fast sensors for measurement and control, and optical access or sampling capabilities to enable implementation of advanced diagnostics. As with all ignition studies the experimental results should be consistent and repeatable. Finally, flexible configurations, e.g., clearance height control, can facilitate convenient modification of the thermodynamic state of the reacting mixture for each test. The following sub-section describes some historical efforts undertaken towards developing machines to achieve these goals, as well as modern techniques. For the interested reader, comprehensive reviews of early RCMs can be found in refs. [68,92].

2.1.1. Early designs

The first RCMs were created in response to industrial safety concerns. These were designed with the goal to measure 'minimum ignition temperatures,' where it was expected that the autoignition process would be instantaneous when these temperatures were reached. The first known efforts in this direction were initiated by Nernst and realized by Falk [93,94]. One of the RCMs used in their work is pictured in Fig. 4a).

Falk's RCMs were actuated by a falling weight that drove the compressing piston within the cylinder until autoignition occurred. The pressure increase then drove the unconstrained piston backwards. The lowest position of the piston inside the cylinder was recorded by a moving ring, allowing a calculation of the maximum adiabatic compressed temperature. Seals made from hemp cord were used and lanoline was employed as a lubricant to seal the combustion chamber. In their studies using hydrogen, gas mixtures were synthesized by electrolysis and introduced in the chamber through a tube. The chamber was then sealed by moving the piston past the injection port. Dixon and Crofts [95] used an improved version of the Falk design that recorded the piston position history via a revolving drum, and used a tuning fork as a time reference. They identified an influence of lanoline on the measured ignition temperatures and raised concerns regarding the effects of particles on the experiments. Visualization techniques were employed in order to provide insight into these interactions with the autoignition process. Related issues have been noted by subsequent researchers [96]. To enable photographic techniques, a pendulum RCM, equipped with a glass reaction chamber, was used by Dixon *et al*. [97], as pictured in Fig. 4b).

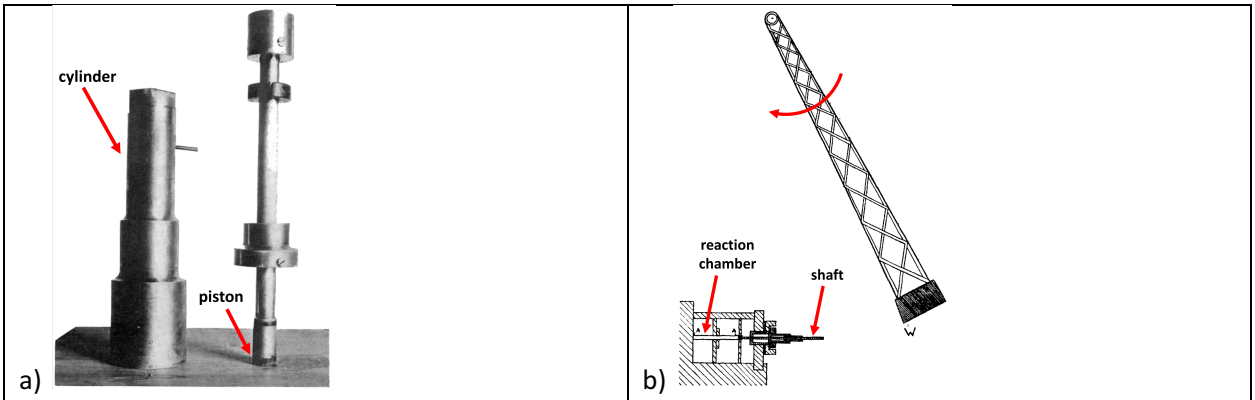

Figure 4. a) Falk's RCM [93,94]: the cylinder is the component on the left, the compression piston is on the right (adapted from [93,94], J Am Chem Soc.) b) Dixon *et al*.'s pendulum RCM (adapted from [97] , J Chem Soc Trans.) The reaction chamber was made of glass to allow for photographic observation of the combustion process.

Cassel *et al*. also used a falling weight apparatus [98], which was equipped with lead washers and a brake in order to minimize rebound issues at the end of the compression. The compression time was reduced to around 40 ms, and the measured volume histories were used to deduce experimental pressure profiles by supposing adiabatic compression, as shown in Fig. 5. Both of these developments uncovered evidence of a time delay before autoignition was observed. This first evidence of an ignition delay time agreed with the contemporary visualization work of Dixon *et al*. [97]. These studies initiated interest in reducing the duration of the compression phase duration in order to better decipher this period. This finding opened new avenues for evaluating and characterizing fuels based on induction time covering a range of conditions, and has resulted in unique insights into fuel decomposition and oxidation chemistry, such as the discovery of NTC behavior. This early RCM work also led to the eventual use of shock tubes to explore reaction times at conditions not achievable in RCMs, e.g., τ_R less than about 1 ms, and temperatures greater than 1200 K [99–101].

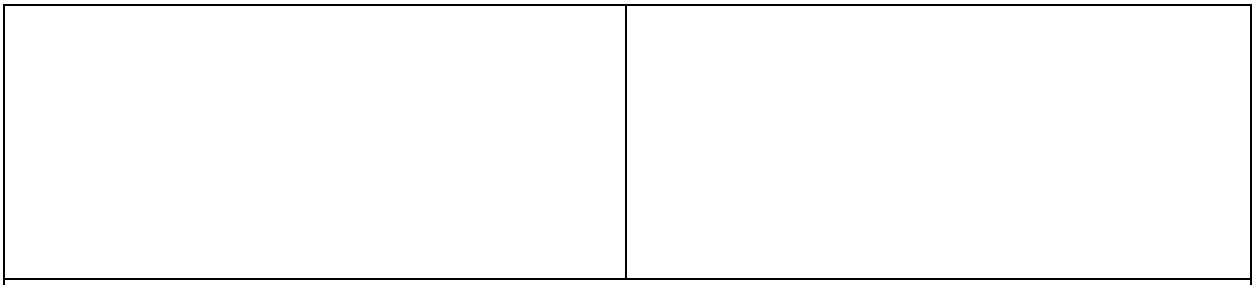

Figure 5. Experimental results from Cassel *et al*. [98] for an H_2/O_2 mixture (reprinted from [98] Ann Phys.) a) Raw experimental data, showing the measured volume history and time reference. b) Deduced pressure profile showing the existence of an ignition delay after the end of compression.

2.1.2. Control of the compression phase

The volumetric compression phase, or state preparation period of the experiment is critically important towards achieving a well-defined test and ensuring minimal reactivity before the test conditions are reached. In terms of evaluating the compression phase duration, a typical parameter, $t_{50,}$ can be used and defined as the time for the last 50% of the pressure rise to occur. This parameter is slightly shorter than the time required for the last 50% of the temperature rise, t_{50T}, due to the different non-linear behaviors of pressure and temperature during isentropic compression. The t_{50} and t_{50T} times are useful since they provide an indication of the duration that the mixture spends at elevated state conditions before the constant-volume test conditions are reached. This can be particularly important when very reactive mixtures are used and measured ignition delays are short, e.g., < 3 ms.

Figure 6 illustrates three simulated piston trajectories and the associated pressure and temperature histories for the reacting gas. The piston travel is normalized based on the stroke of the machine and an assumed compression time, while the gas pressures and temperatures are calculated based on an assumption of isentropic compression of air with a fixed heat capacity where the initial temperature and pressure are T_i = 300 K and p_i = 1 bar, respectively. The stroke and clearance height are kept constant between these cases with a compression ratio CR = 12, while the velocity profiles are modified.

Case 1 generates a fairly constant velocity profile during compression where the acceleration and deceleration periods are confined to the beginning and end of the piston stroke, respectively. In Case 2, the piston is accelerated through most of its displacement such that the velocity peaks after the piston has traveled 80% of the stroke, near an instantaneous compression ratio of 4. The trajectory used for Case 2 has been adjusted so that the stroke, compression time and t_{50} are identical to Case 1; although these constraints are not realistic for an actual configuration, they are used here for illustrative purposes. The resulting t_{50T} for this configuration is about twenty percent shorter than for Case 1, while the temperature-time history indicates that the mixture is much cooler through most of the piston travel. This characteristic could be beneficial for minimizing pre-reaction chemistry when investigating very reactive mixtures. On the other hand, the peak piston velocity is more than twice that of Case 1, while the deceleration rate is 50% larger. These features have implications with regards to the mechanical intricacies and structural requirements needed to ensure safe and consistent operation, as well as minimizing the generation of aerodynamic heating and turbulence within the reaction chamber as discussed in [102]. Furthermore, boundary layer growth, bulk fluid motion, turbulence, and heat loss can also be affected by the piston trajectory in complicated ways, but this is not discussed here.

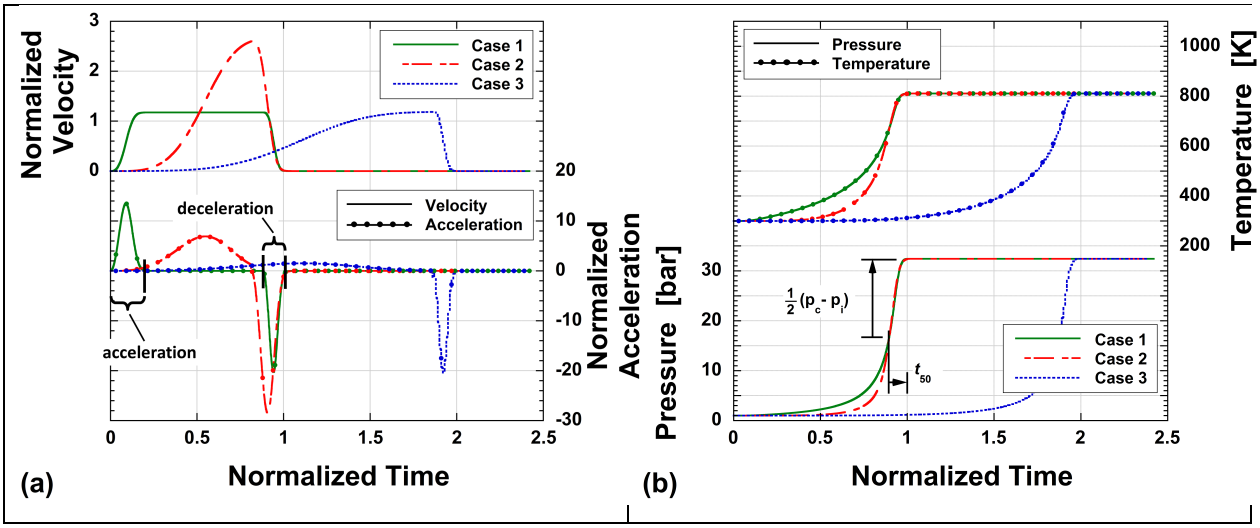

Figure 6. Comparison of various 0-dimensional simulated piston trajectories and associated isentropic pressure and temperature histories. Time is normalized based on the compression time of Case 1, and position by the stroke of the machine. The normalized velocity and acceleration are the first and second derivatives, respectively of the normalized position with respect to normalized time.

Case 3 uses a profile similar to Case 2, but the peak piston velocity and deceleration rates are limited to the maximum values used in Case 1. For the same stroke, this requires an extension of the overall compression time to nearly twice that used with Case 2. This modification, while addressing the concerns just mentioned, could have undesirable influences on heat loss and the boundary layer growth that occurs during compression, as discussed later in this section. The resulting t_{50} and t_{50T} times are nearly identical to those realized by Case 1. In Cases 1 and 2, the final 50% of the temperature and pressure rise are entirely contained within the deceleration period. This highlights the fact that it is the deceleration and piston seating processes that are the primary influences on these parameters, and thus the state preparation period, and the mechanical design of the arresting mechanism must be undertaken with care.

There are a number of methods that can be used to facilitate fast piston acceleration and deceleration, as well as control the velocity profile through the stroke. Pneumatics, hydraulics or explosive charges can be used to drive the piston, while pneumatics, hydraulics or impact mechanics can be used to arrest the piston motion. Hydraulic shear and mechanical cams can be employed to modulate the velocity of the piston through its displacement. Each approach has challenges and limitations. The development and resulting characteristics of some of the methods are discussed next in the context of historical machine development, with an outlook to future capabilities.

Pneumatic driving systems, which typically use compressed air as the gas, provide a fast way to accelerate the piston, whereby a separate driving piston can be employed on a shaft using an area ratio force multiplier that allows lower gas pressures in the pneumatic driving chamber. The ratio of the piston areas dictates the allowed ratio of pressures between the driving chamber and the combustion chamber, where the maximum pressure in the combustion chamber is typically the maximum compressed pressure or the pressure at ignition. While these limits are usually determined based on static analyses of the design configuration, the dynamics of the piston deceleration can be affected as the pressure limits are approached, leading to extended t_{50} times. A separate, large air reservoir can be used to maintain consistent pressure in the pneumatic chamber as the piston is displaced. This principle was first put into practice for the construction of several RCMs developed at MIT [103], but also served in the development of the RCM later used by Jost *et al.* [66,104,105], and is employed in many contemporary machines.

To achieve rapid pressurization of the driving chamber, Leary *et al.* [68] employed a poppet valve that separated a high pressure section from a lower pressure section in the driving chamber, as shown in Fig. 7. The poppet valve was raised with a screw jack, and held in place by shear pins. A falling weight would break the pins and allow compressed air to enter the lower section of the chamber. The lowest section of this chamber, at first filled by a lower pressure of air, was compressed by the piston and served as an air cushion with the purpose to slow the compression piston and avoid mechanical shock. Meticulous adjustment of the air pressures was needed. This RCM was able to reach compression times as fast as τ_C = 6 ms, with t_{50} around 1 ms, owing to its very short stroke (~9 cm). These times are still fast by today's standards. The peak piston velocity was near 20 m/s. A strain gage was used as a pressure sensor and the piston position was evaluated from high speed photographs of the piston relative to position references of equally spaced black and white lines. The data from this machine, however, suffered from reproducibility issues, and under certain conditions, pressure ringing at ignition. The inconsistencies would be attributed in later work to temperature inhomogeneities within the reaction chamber, as observed in direct photographs and schlieren images [69,106]. Inhomogeneities most likely originated from the vigorous compression process and the concave geometries of the piston and cylinder head, which led to undesirable fluid motion and turbulence within the reaction chamber. Nevertheless, data from this device enabled early insight into the chemical kinetic effects of knock inhibitors such as tetraethyl lead as well as features of mild ignition, which is associated with convolved deflagrative/autoignitive processes, for a variety of fuels, and these are discussed in more detail in Sections 5 and 6.

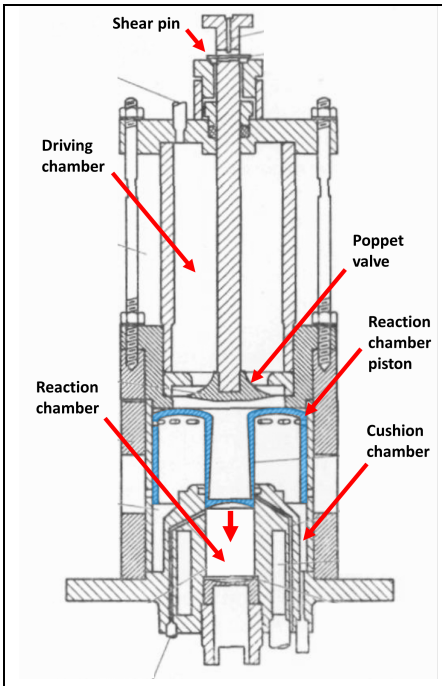

Figure 7. Schematic of the RCM developed at MIT by Leary *et al.* (adapted from [68]).

Other approaches to control the start of the experiment in pneumatically-driven systems include the use a diaphragm such as employed in shock tubes [107], a globe valve [108] or a converging nozzle geometry [109]. The rupturing of the diaphragm, opening of the valve or unseating of the nozzle induces rapid pressurization of the driving piston and therefore starts the compression process in a controlled and rapid manner [107]. However, the compression phase duration, and to a lesser extent the pressure at TDC, can be subject to variability in these designs, as reported in Shiga *et al.* [110].

The use of a hydraulic driving system is one way to reduce the required piston area ratio for a device, since much higher hydraulic pressures can be safely employed (e.g., ~40 MPa compared to 2–4 MPa for pneumatic systems) [111]. In addition, the initial and final piston positions and the piston trajectory can be controlled with fairly good precision. However, significant amounts of hydraulic fluid must be transported into the driving chamber as the piston is displaced in order to maintain the driving pressure. The timing and capacity of the servo valves and hydraulic accumulators used to actuate and control this can therefore influence performance. As a result, slower compression times have generally been reported for hydraulically-driven machines, e.g., 40–60 ms [112,113].

In an effort to reduce the mechanical complexity and time required to replace pins or diaphragms on pneumatic driving systems, other configurations have been devised. The RCM designed at Shell Thornton

by Affleck *et al.* [114], and now in use at the National University of Ireland Galway [115] was configured with a hydraulic section between the pneumatic and reaction chambers where this can be used to lock the piston in place before compression and achieve controlled, consistent actuation. Hydraulic fluid in front of an integrated hydraulic piston, shown in Fig. 8, is pressurized to a level that prevents the piston from moving at the retracted position, even after the high pneumatic pressure is applied to the driving piston. The retracted location is indicated by the dashed line in Fig. 8, while the pressure on the opposite side of the hydraulic piston is kept near atmospheric levels. The discharge of a small volume of the fluid from the main chamber (i.e., in front of the piston) provides proper actuation of the experiment as this causes the hydraulic pressure differential to disappear, and the piston subsequently moves. The timing of depressurization of the main chamber can be used to synchronize the motion of the two pistons for this opposed-piston geometry.

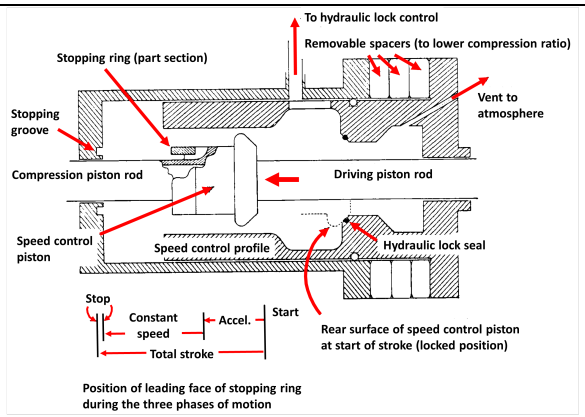

Figure 8. Schematic of the hydraulic system of the Shell Thornton RCM (adapted from [114] with permission of Proc Inst Mech Eng).

The hydraulic section in the Shell Thornton machine was carefully designed to modulate the piston velocity through the stroke. This was inspired by novel braking configurations developed by Rogowski at MIT [116], and Voinov *et al*. at the Institute of Chemical Physics, USSR [117]. The large inner bore of the chamber at the retracted location allows the piston to accelerate freely at the start of the test with little hydraulic resistance. Partway through the stroke, the bore of the chamber narrows so that when the piston enters this section there is substantial hydraulic shear on the circumference of the piston, as well as pressurization of the fluid in front of the piston. The gap between the piston circumference and the inner bore was sized so the resulting hydraulic forces balance the pneumatic driving force and this causes the velocity of the piston to become nearly constant through the main portion of the stroke, similar to the profile seen for Case 1 in Fig. 6a. Fast compression times were also achieved with this machine due to its

opposed-piston configuration and short stroke for each piston, with $\tau_C \approx 13$ ms, and $t_{50} \approx 1.5$ ms. The robust design enabled the Shell group to acquire a range of ignition and speciation data covering cool flame and two-stage ignition chemistry [70–73]. The machine at the University of Leeds [118] is of nearly identical design and utilizes this hydraulic chamber arrangement, though only one piston is employed in order to facilitate a range of optical diagnostics in the end wall of the reaction chamber, as discussed further in the next section of this review.

Following this idea, the machine at the Université Pierre et Marie Curie (UPMC) was designed to utilize dynamic control of various hydraulic servo valves to regulate the hydraulic pressure in front of the piston during the stroke and thus achieve similar constant-velocity piston trajectories [113]. This was only possible however at longer compression times, $\tau_C > 40$ ms, with maximum velocities around 5 m/s, due to servo valve limitations.

Another means to control the piston trajectory is the use of coupled mechanical parts, as first demonstrated in Tizard and Pye's RCM, developed by Ricardo [119]. This machine employed a flywheel-driven crank that brought the piston to TDC in approximately 120 ms before disconnecting, leaving it locked in that position. More recent developments have yielded the construction of a number of right-angled RCMs [120–124], such as the one presented in Fig. 9. These devices employ a moving cam to couple the motion of the driving piston with the motion of the compressing piston, where the advantage is precise control over the piston velocity and compression ratio, although relatively longer compression times typically result ($\tau_C > 30$ ms). With an arrangement of this type, a range of piston trajectories can be easily prescribed by utilizing different cam profiles [125,126]. Before compression, the driving piston is usually kept in place by a hydraulic jack while the driving chamber is pressurized.

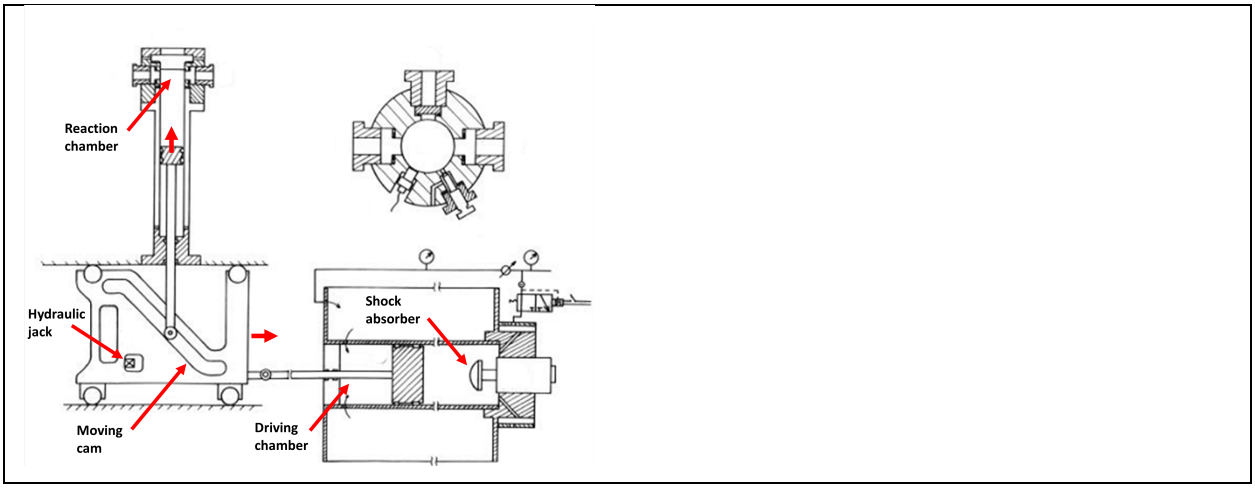

Figure 9. Schematic of the right-angle, cam-equipped RCM from the Université de Lille 1 Sciences et Technologies (adapted from [120] with permission of J Chim Phys).

As discussed earlier, the deceleration phase of the piston is critical towards ensuring short t_{50} and t_{50T} times. One successful method to achieve rapid stoppage of the piston without significant gas oscillations is to use impact mechanics, where the momentum of the piston is transferred to another component of the machine upon impact, as was originally done by Jost *et al.* [66,105] at Philipps-Universität Marburg, and as currently employed at the University of Michigan [108], Nihon University [127] and the University of Cape Town [128]. Final t_{50} times on the order of 0.5–1.5 ms are possible with this approach. Jost's RCM used an elastic shock between the vertical, pneumatically driven piston and a floating buffer mass on springs, as shown in Fig. 10a, to achieve high deceleration rates. The masses of the shock damping system and of the piston were similar, so the piston would come to rest nearly instantaneously, while the floating mass was displaced further. This RCM was most likely the first to be equipped with a piezoelectric pressure sensor since the issue of mechanical vibration at piston arrest was successfully resolved, and test times of several tens of milliseconds allowed Jost's group to build a wide and comprehensive understanding of the ignition of C_4–C_8 alkanes. They reported data on two-stage ignition, effects of temperature, pressure, ϕ and of alkyl chain length on the ignition delays, as well as evidence of NTC behavior for some fuels. The effects of tetraethyl lead as an octane booster for gasoline surrogates were also investigated, as highlighted in Fig. 10b-d. Their interpretation of the data suggested that while the first stage of ignition was due to chemical branching, the second stage was made possible because of thermal runaway. These findings provided early foundational support towards the current understanding of causes for two-stage ignition: indirect chemical branching through the formation of unstable peroxides leading to LTHR, and thermal decomposition of H_2O_2 accumulated from H-atom abstraction reactions involving HO_2 for the second stage, as discussed more thoroughly in Section 6. Furthermore, by studying the LTHR during autognition of *n*-heptane/air mixtures with tetraethyl lead addition, the additive was found to be effective only when the reaction temperature was high enough to facilitate its decomposition and subsequent radical scavenging, so that the second-stage ignition times were extended, while the first-stage ones were typically unaffected.

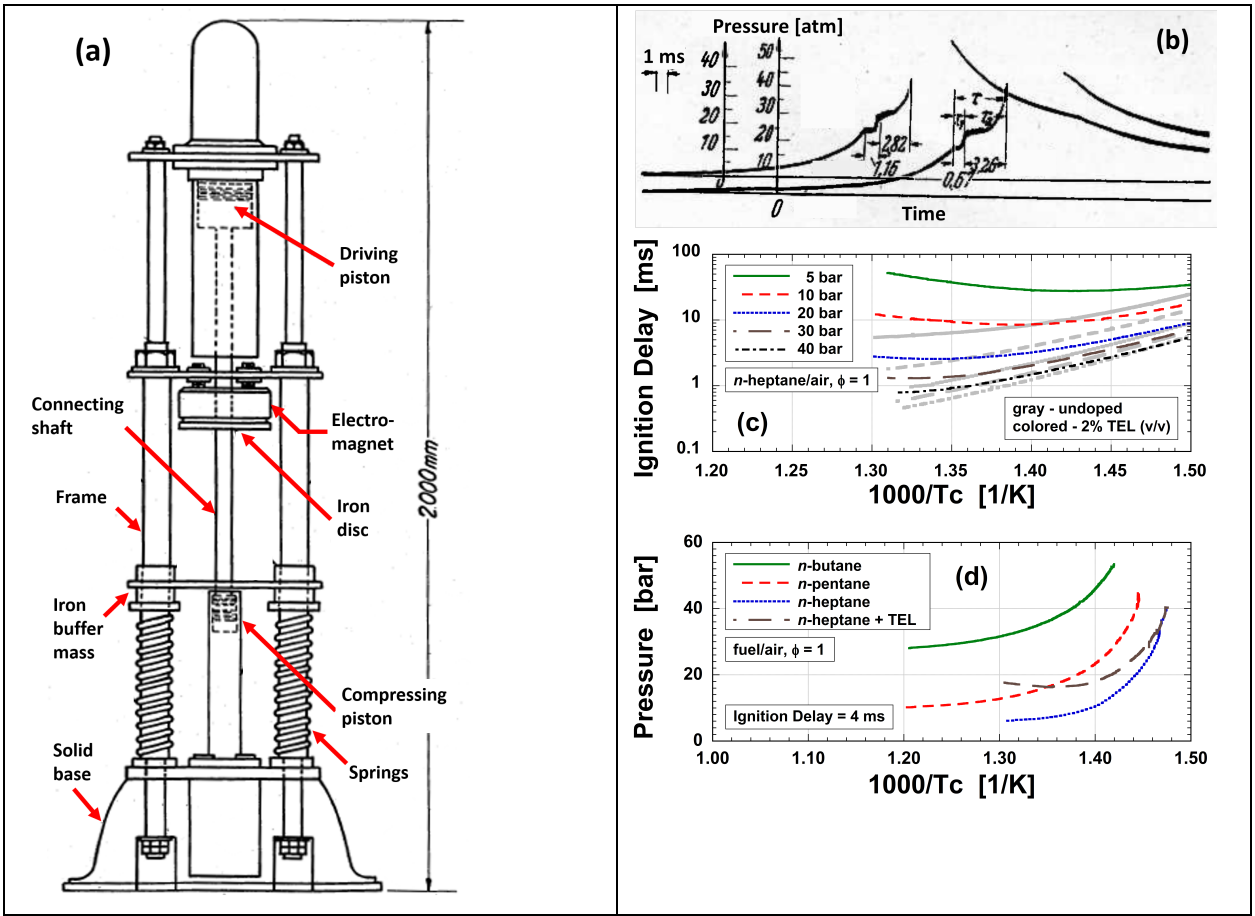

Figure 10. The redesigned RCM used by Jost and Rögener *et al*. and some representative results, redrawn here for clarity (adapted from [64–66] with permission of Symp. Combust. Flame, Explos. Phen.) (a) Schematic of the RCM. (b) Pressure-time histories for two experiments exhibiting two-stage ignition of an *n*-heptane/tetraethyl-lead/air mixture. (c) Effect of temperature and pressure on the ignition delay of *n*-heptane/air, showing evidence of NTC behavior and the influence of tetraethyl lead (TEL) addition. (d) Measured isopleths of ignition delay time, or isolags, for various alkanes presented as a function of temperature and pressure, where Rögener [104], following the work of Maccormac and Townend [129], suggested that such curves could be used to indicate a fuel's knocking propensity, with higher temperature-pressure conditions yielding higher octane ratings.

Ikegami *et al.* [130] and later Donovan *et al.* [108] developed configurations that used tapered pistons made of deformable material, e.g., ultra-high-molecular-weight polyethylene, to absorb the kinetic energy of the piston. These arrangements also seal the reaction chamber during the test period. Schmidt *et al*. [131] and Watanabe *et al.* [127] employed buckling of calibrated aluminum tubes to decelerate the piston. In principle, it was possible to vary the stroke by adjusting the thickness of the tubes. Both of these concepts required disassembly of the machine between tests in order to unseat the piston or replace the shock absorbing tubes. To minimize the interval between tests, Evezard [128] developed a hydraulically-coupled momentum trap to decelerate the piston. Careful adjustment of the distance

between the momentum trap position before the impact and the final resting place of the impacting end was needed, but this design, along with its two-stage pneumatic driving system, yields piston velocities as high as 8 m/s just before the end of compression. Because of the unique configuration of the coupled momentum trap, the combustion chamber in this RCM has a toroidal geometry.

An alternative method to achieve fairly rapid, though somewhat slower piston deceleration is based on hydraulic oil displacement. In this concept a ring-groove [114], or similar geometry [102,116], is used within the hydraulic chamber wherein oil must be displaced as the ring, located on the fore side of the hydraulic piston, enters a stopping groove near the end of the piston stroke, as depicted in Fig. 8. Compression of oil within the groove increases the pressure quickly and this resistive force slows the piston's motion, while the oil seeps from the groove back into the main hydraulic chamber. Careful adjustment of the ring-groove clearances, and any additional transfer ports, e.g., radially through the ring, is needed to achieve precise control of the deceleration profile [132]. Numerous machines currently in use employ this technique.

Finally, controlled piston deceleration can also be achieved via a prescribed cam profile or modulation of servo valves within hydraulically driven configurations, as highlighted previously. Deceleration rates can be limited due to the allowable stresses on the roller bearings used in the cam design, and the piston motion is often damped using a shock absorber or a hydraulic brake. Servo valve limitations can lead to fairly long deceleration rates, e.g., $t_{50} \approx 6.5$ ms.

2.1.3. Control of piston creep and rebound

It is possible for piston creep and/or rebound can occur during the piston seating process, with rebound also possible during chemical heat release. Creep is defined as slow movement of the piston in the compressive direction, while rebound is defined as movement in the expansive direction. Following the work of Cassel *et al.* [98], it was identified that slight changes in the volume of the reaction chamber at TDC can significantly alter the gas temperature, and therefore lead to tremendous changes in the global reaction rate of the mixture. It is thus crucial to ensure the volume of the chamber is well controlled, at least for the duration of the ignition delay, or longer if analyses are conducted through the main ignition process, e.g., rate of heat release measurements. Hydraulically damped systems are more prone to creep and rebound during piston seating due to the dynamics of the oil displacement process and this needs to be considered in the design. Creep has however been proposed as a way to counteract the influence of heat loss however, with the intent to reduce the rate of pressure fall-off that can occur in the early portion of the ignition delay period [133]. This does not prevent the growth of the thermal boundary layer in the

reaction chamber, but simply maintains the elevated pressure and temperature of the core gases for a slightly longer period of time, e.g., 10–15 ms.

At the end of compression, the piston can be locked in its TDC position by a combination of mechanical elements or driving pressure, in such a manner that eventual heat release does not push the piston back. The most frequently used solution in linear RCMs is to impose a higher pneumatic force on the driving piston than the force resulting on the combustion chamber piston, so the compression piston is not displaced by the heat release. A very large bore driving piston, or large driving pressure can be required in order to ensure the absence of piston rebound. This can be challenging when high compressed pressures are used, *e.g.*, $p_c > 30$ bar, since the reaction chamber pressure can alter the piston dynamics during the deceleration process, as well as at the point of heat release.

Hydraulically-assisted schemes have been used in hydraulically decelerated machines wherein the main hydraulic chamber is maintained in a pressurized state during the actuation process while the pressure in the groove at the endwall is reduced after piston seating, e.g., via connection to a low pressure reservoir, [134]. Additionally, a variety of mechanical solutions have been used, starting with the clamping mechanism first demonstrated in Aubert and Pignot's RCM [135]. Two pins mounted on springs were engaged in corresponding holes on the compression piston axis and held in place at TDC. The disadvantage of this system is of course its relative fragility and ensuing limitation in terms of maximum pressure obtained while the ignition takes place, as well as the possibility to induce piston creep at the final stages of compression.

Tizard and Pye's RCM [119] and its flywheel-controlled compression phase also offered an early solution to this problem, with the compromise of a longer compression phase. In a similar fashion, some in-line RCMs are currently equipped with hinged arms, i.e., two-bar linkages, that keep the piston in place at TDC [136][137]. Kim *et al.* [138] used a system of gears to connect the movement of the driving piston and of the compression piston, which allows easy variation of the compression ratio. Right-angled RCMs also keep the combustion chamber volume rigorously constant after compression, as a result of the mechanical linkage between the driving piston and the compression piston.

2.1.4. Control of the reacting gas

The autoignition behavior of the reacting mixture is critically dependent on the gas temperature. To minimize uncertainties associated with the experiment and understanding derived from the measurements, the thermodynamic state of the gas must be accurately determined, including any non-

uniformities in the reaction chamber. Temperature can be measured directly in RCM studies, as discussed in Section 3, but this is difficult and under some conditions the uncertainties are high, and thus most often temperature is inferred from other direct measurements like pressure. The first RCM studies considered the compression process to be fully adiabatic with homogeneous conditions in the reaction chamber, i.e., isentropic; it was assumed compression was sufficiently rapid that heat losses and non-uniformities were negligible. The temperature obtained after compression was calculated based on the geometric compression ratio with this hypothesis in mind. Nevertheless, measurements by Tizard and Pye [139] proved this assumption to be wrong. In their tests, the compression time was varied between τ_C = 50 and 200 ms, and the measured pressure at TDC was compared with the calculated adiabatic pressure. These data are shown in Fig. 11. Here the pressure at maximum compression, p_c, is plotted as a function of overall compression time, with the instantaneous, adiabatic values marked by extrapolation to zero compression time, determined using a fixed specific heat ratio, γ, for the mixture. The results show how increasing compression times leads to pressures lower than adiabatic, which is attributed to heat transfer during compression.

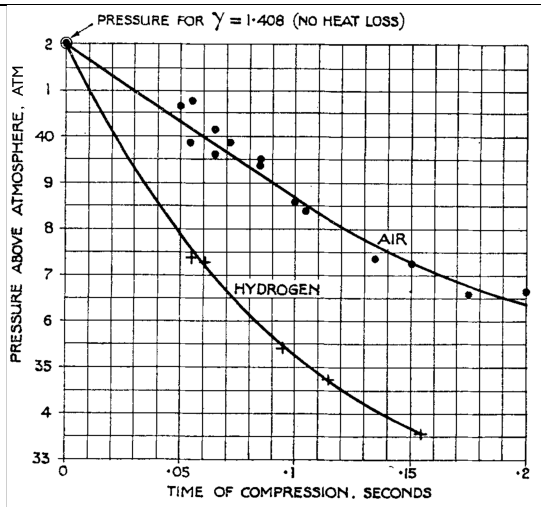

Figure 11. Comparison of measured compressed pressure (symbols) with the predicted adiabatic pressure (labeled as t = 0, no heat loss) as a function of the compression time (reprinted from [139] Philos Mag Ser.)

Tizard and Pye [139] further highlighted the competition between reaction rates and rates of gas cooling during the ignition delay period covering a number of different fuels, including *n*-heptane, diethyl ether and carbon disulphide. They explored differences between 'quiescent' conditions and cases where an internal fan was used to stir the gases in the reaction chamber, and they noted shifts in measured ignition times as well as quenching limits for the tests. Leary and co-workers [69,106] were one of the

first groups to identify, based on schlieren and direct imaging, the possibility of generating non-uniformities within the reaction chamber during compression due to piston-wall interactions, as the boundary layer can be scraped from the wall to produce turbulent gas motion. Park and Keck [102], using insight derived from IC engines studies, further described the development of flows at the piston-wall interface, where it is possible to generate a toroidal structure during compression. Griffiths *et al.* [140] were then one of the first groups to employ computational fluid dynamics (CFD) to better understand interactions between large-scale thermal non-uniformities and the progress of autoignition. Their calculations, while coarse in terms of spatial resolution and chemistry (*e.g.,* 14 x 50 cells with 30 species participating in 70 reactions representing ditertbutyl peroxide (DTBP) mixtures), highlighted boundary layer effects and the evolution of the corner vortex. The work by Griffiths *et al.* [140] showed that reactivity can develop faster in cooler rather than hotter regions of the reaction chamber for fuels with NTC behavior, though this is dependent on the compressed conditions, as well as fuel loading. Similar observations of induced non-uniformities and their influence on the autoignition chemistry were subsequently described in further multi-dimensional simulation studies conducted by Lee and Hochgreb [141], Guézet and Kageyama [121], Chen and Karim [142], and Frolov *et al.* [143]. Experimental measurements, based on Rayleigh scattering [144] and microthermocouples [145], confirmed the development of toroidal structures, which were observed to persist well into the ignition delay period under some conditions, e.g., for longer than 50 milliseconds. The results from studies such as these motivated research towards improving the homogeneity of the test gases for experiments focused on autoignition chemistry.

When designing their RCM, Park and Keck [102] made several recommendations to mitigate the detrimental behavior of gas motion in the reaction chamber and the ensuing development of temperature non-uniformities. Their scaling analyses indicated that the Reynolds number, *Re*, based on stroke and mean piston speed, should be less than about 10^5 in order to keep the boundary layer laminar, while the Mach number of the piston should be less than 0.08 to avoid significant heating of the gases by sound waves generated by the piston. For their configuration, these constraints resulted in piston velocity limits of 10 and 20 m/s, respectively. Their remaining recommendations aimed to reduce the mixing of the boundary layer with the central core gases. Firstly, they proposed a criterion for the minimum ratio of the bore to height of the chamber, which should be greater than 5. Consequently, the bore would exceed the vortex diameter by at least tenfold, so as to minimize the extent of vortex influence on the temperature field. Secondly, they proposed implementing a crevice volume machined around the circumference of the piston that could capture the thermal boundary layer which develops along the cylinder walls during the

compression phase, and thereby prevent the vortex formation and subsequent mixing with the core gases. This concept can be seen in Fig. 12, where the core and boundary layer gases are shown schematically for a creviced and an uncreviced, or flat piston.

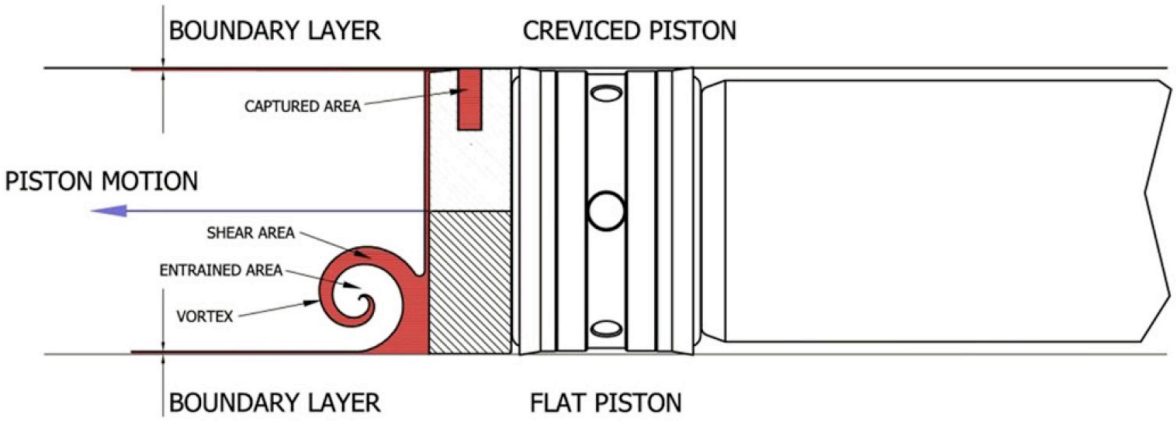

Figure 12. Capture of the wall vortex during compression in a piston cylinder geometry. The top panel illustrates a creviced piston configuration while the bottom panel shows the behavior of a flat piston geometry (reprinted from [39] with permission of Elsevier).

Park and Keck's piston crevice design (highlighted in Fig. 13, column (a)) was improved further by Lee and Hochgreb on the same RCM [141], where a different geometry was suggested, with the following points in mind: (i) the clearance between the piston crown and the wall should be larger than the boundary layer but small enough to limit reemergence of the crevice contents back into the reaction chamber during the delay period, (ii) the crevice should have a shape able to quickly cool the captured boundary layer gases to a temperature where reactivity can be considered negligible, and (iii) the crevice volume should be large enough to contain the corresponding volume of boundary layer gases. The improved configuration is identified in column (b) of Fig. 13.

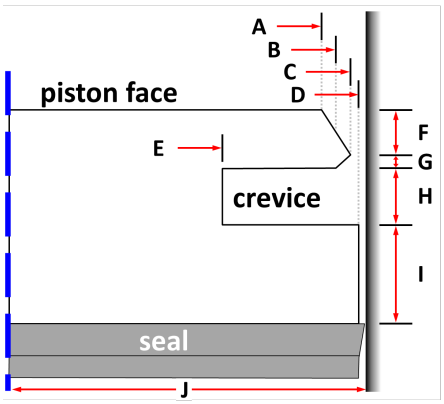

	(a)	(b)	(c)	(d)
A	0.52	0.48	0.46	0.50
B	2.72	0.72	na	0.15
C	0.52	0.12	na	0.15
D	0.23	0.23	na	na
E	2.72	4.75	9.00	1.50
F	0.00	4.00	2.20	4.00
G	2.20	0.60	0.60	0.00
H	0.00	1.40	2.20	20.00
I	4.90	1.10	4.00	na
J	25.40	25.40	19.07	25.40

Figure 13. Configuration of different piston crevice designs reported in RCM studies (dimensions in mm): (a) Park and Keck [102], (b) Lee and Hochgreb [141], (c) Würmel and Simmie [146], and (d) Mittal and Sung [147],

The effectiveness of this strategy was demonstrated by follow-on detailed CFD studies [146,148], using higher spatial resolution and improved physical sub-models resolving down to a 0.1 mm cell thickness in the boundary layer, corresponding to 9000 cells at TDC. The associated crevice geometries are presented in columns (c) and (d) of Fig. 13, respectively. Würmel and Simmie [146] suggested that the dimension of the entrance of the crevice may not play a significant role, once it is larger than a value sufficient to capture the thickness of the boundary layer. They found that diluent gasses with different heat transfer properties could significantly alter the boundary layer growth during piston compression, and thus the effectiveness of the crevice. The size of successful crevice volumes were around 12–14 % for the RCM system used by Würmel and Simmie [146], and 9–13% for the RCM system used by Mittal and Sung [147], relative to the compressed reaction chamber volume. The capability of these crevices to reduce the vortex formation was observed in the computational results, and confirmed experimentally using acetone planar laser induced fluorescence (PLIF) thermometry [148]. More recommendations on the crevice design and limitations for vortex formation were provided based on additional CFD calculations in Mittal *et al.* [149], who noted that a longer stroke can result in a larger vortex, while a wider clearance at TDC could mitigate the influence of the vortex. This last finding is contradictory with the recommendations of Park and Keck [102], though the investigated geometries were slightly different. Large bore-to-height ratios proposed in [102] generally lead to higher surface area to volume ratios, and therefore greater heat loss and thermal stratification under long test time conditions. In any event, producing crevices large enough to trap the entire thermal boundary layer during compression can be challenging for experiments that utilize mixtures with high thermal diffusivities, such as under low pressure conditions ($p_c \approx 5–8$ bar), as the thermal diffusivity is inversely proportional to pressure. Mittal *et al.* [149], summarized the influence of the corner vortex for a range of pressures and strokes, and this is depicted in Fig. 14.

From these studies, it is clear that properly configuring the piston crevice for particular machine geometry and operating conditions is key to adequately suppressing the corner vortex formation, and that a single configuration may not be appropriate across a wide range of facilities, or a range of experimental conditions explored during an experimental campaign. Yousefian *et al*. [150] used non-dimensional scaling to highlight that Peclet number, bore:stroke aspect ratio, and crevice volume : swept volume ratio

are key overall parameters towards suppressing fluid motion and minimizing thermal non-uniformities. Care must be taken in the crevice design and implementation to ensure that flow stratification, heat transfer and boundary layer effects are minimized for a particular test series.

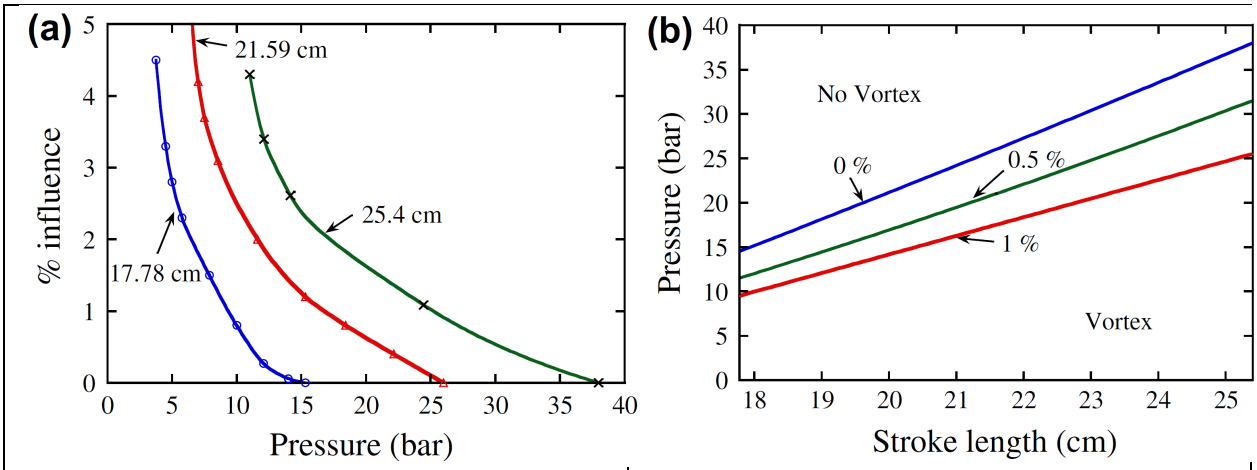

Figure 14. Calculated extent of corner vortex influence as a function of the compressed pressure and stroke length within the University of Connecticut RCM. The % influence is defined as the normalized difference between the adiabatic core temperature and the mass average temperature of the gas in the reaction chamber. In the left panel the stroke lengths are indicated for each of the three curves; in the right panel the % influence is indicated for each of the three curves. (reprinted from [149] with permission from Elsevier).

2.1.5. Piston crevice containment

The development of creviced piston configurations has been a significant advancement in the design of RCMs towards studying autoignition chemistry and fuel reactivity, and has substantially improved the quality of data recorded and reduced uncertainties in datasets from these machines. Improved piston designs have enabled better descriptions of the gas mixture during and post compression via the adiabatic core model which is presented and discussed in Section 4. For many reactive systems this approximation is sufficiently accurate, as long as the thermal boundary layer represents only a small portion of the reaction chamber volume, isolated at the walls of the chamber. There are many ways to conduct chemical kinetic simulations using this hypothesis which are reviewed in Section 4. A particularly popular method employs a zero-dimensional framework with a time-varying volume derived from pressure records using non-reactive experiments. It has been demonstrated that during multi-stage ignition however, and even under slightly exothermic conditions, e.g., ITHR, mass flow from the main reaction chamber volume to the crevice can be significant, and can affect observed ignition delay times [85,151]. These processes are not taken into account in most adiabatic core simulation frameworks [152]. In addition, creviced geometries

can lead to uncertainties associated with the gas composition when samples of the gas are physically extracted from the reaction chamber for chemical analysis and if unreacted/quenched components from the crevice are extracted along with reacted gases from the core [153].

These issues have been targeted through the development of crevice containment configurations, whereby the crevice volume is isolated from the main reaction chamber once the compression phase is completed. This has been implemented at the University of Akron [154] by an O-ring seal around the circumference of the piston that engages at piston seating, while the reaction chamber design employed at the University of Michigan [108] naturally seals the convergent section of the chamber from the crevice volume with the nose-cosed sabot that seats using an interference fit. These geometries are illustrated in Fig. 15. Challenges exist when utilizing this technique however. For instance, CFD calculations of the temperature fields performed in Mittal and Bhari [154] suggested that under some conditions high velocity flow can be forced into the reaction chamber from the crevice volume as the seal engages, so that a small vortex can be generated and evolve during the delay period. Furthermore, the O-ring seal used to isolate the crevice from the main reaction chamber can be subjected to severe mechanical deformation during piston sealing, so that care must be exercised to avoid particle generation and transport into the reaction chamber due to seal degradation, as described in [154].

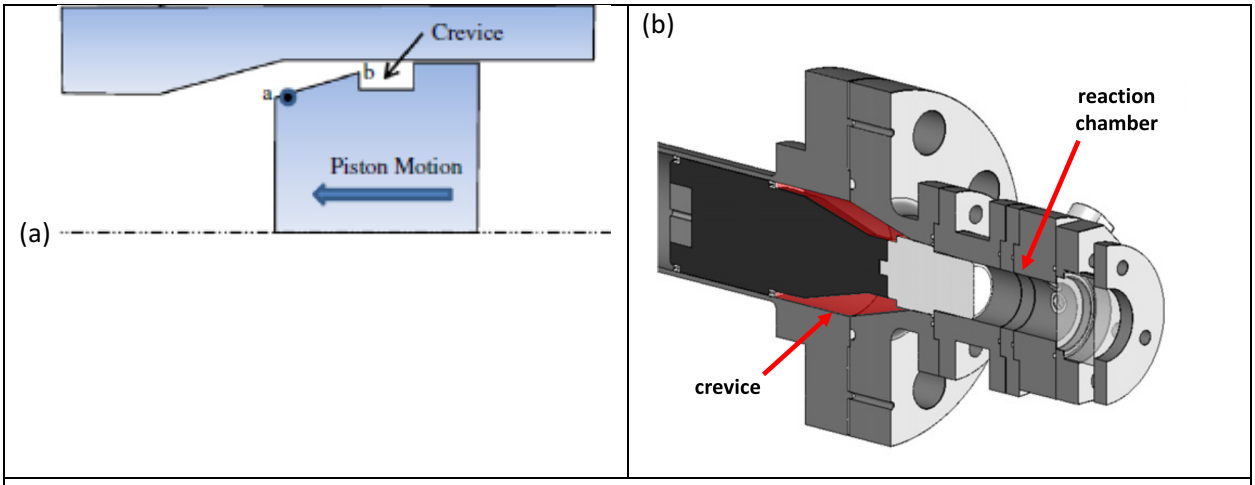

Figure 15. Two strategies for crevice containment. (a) O-ring seal equipped piston at the University of Akron (reprinted from [154] with permission of Elsevier). (b) Interference fit using deformable material at the University of Michigan (adapted from [108] with permission of Elsevier).

2.1.6. Aerosol fueling and direct test chamber methods

RCMs, like shock tubes, are typically limited to high volatility fuels. This is especially pertinent when targeting undiluted conditions where high concentrations of vaporized fuel are needed, e.g., 1–3% mole

fraction. Conventionally, tests utilize pre-vaporized mixtures of fuel, oxygen and diluent, often mixed externally, though sometimes within the reaction chamber, so the capability to supply the gas-phase fuel is restricted by the vapor pressure of the fuel. Large molecular weight components of jet and diesel fuel have very low vapor pressures, e.g., 10 mbar and 0.5 mbar, respectively, at temperatures typical of the initial test conditions, e.g., T_i = 25–120 ^{o}C. Oxygen containing molecules can also have very low vapor pressures. As the need grows for understanding the autoignition chemistry of large fuel molecules and oxygenates, new techniques are needed to facilitate tests with RCMs. Aerosol fuel loading and direct test chamber methods have been suggested to address this issue without having to resort to extremely high premixing tank and reaction chamber temperatures.

In the aerosol fueling method [155], which was initially developed for shock tubes [156,157], a mixture of suspended fuel droplets is created external to the reaction chamber, with the carrier, or bath gas consisting of the oxidizer and diluent components. The multi-phase mixture is delivered to the RCM in a continuous flow manner. Just before the start of the test, the flow is interrupted and the reaction chamber is sealed. As volumetric compression proceeds, the increase in bath gas temperature leads to vaporization of the fuel droplets, so by the end of compression the fuel is completely vaporized and mixed with the oxidizer/diluent gas. In designing such an experiment, the fuel droplets need to be uniformly distributed within the flow, and must be small enough to ensure complete vaporization and diffusive mixing by the end of the compression stroke. This type of experiment is more complicated than typical tests of gas-phase reactants and higher experimental uncertainties can therefore result. Challenges are associated with the effects of droplet impingement during aerosol delivery to the reaction chamber, residual fluid motion during the piston compression process, as well as accurate determinations of the gas phase fuel concentration at the end of compression.

Allen *et al.* [155] investigated the aerosol delivery process and mixing in the reaction chamber with help from CFD simulations and Mie scattering imaging. They also noted that the evaluation of the compressed gas temperature can be complicated because of the cooling effects associated with evaporation of the droplets. The concept of aerosol RCMs and the near-droplet phenomena, including evaporation and fuel vapor transport into the surrounding gas were later studied through a droplet vaporization model developed by Goldsborough *et al.* [158,159]. These studies provided guidelines on experimental configurations and the interpretation of data. In order to avoid thermal and compositional stratification, the droplet diameters need to be on the order of just a few micrometers, with the maximum useable droplet diameters dependent on the fuel volatility. The use of neon as a diluent over argon and

nitrogen was recommended, because of its higher thermal diffusivity, which can aid evaporation and thus help reduce local compositional stratification.

In the direct test chamber method [160,161], small quantities of low volatility fuel are directly injected into the reaction chamber using a multi-pulse injection strategy with a gasoline-style injector. The multi-pulse approach is intended to achieve precise control over the total quantity of injected fuel while facilitating the generation of small droplets within the reaction chamber which aids the evaporation rates. This approach was motivated by the fact that since the partial pressure requirements of the fuel are lower in the reaction chamber, as compared to a large external mixing vessel, it may be possible to achieve better fuel vaporization. In Allen *et al*. [160] the fuel vapor was allowed to diffusively mix in the reaction chamber for a short period of time, generally 2 minutes, before the compression process was initiated. As with the aerosol loading technique, issues regarding direct confirmation of the gas phase fuel concentration for each test, as well as the uniformity of the mixture at the end of compression are challenging. While the potential of these two novel techniques has been experimentally demonstrated, additional work is needed to further develop these concepts and demonstrate uncertainties low enough to be equivalent with modern pre-vaporized/premixed test practices.

2.2. RCMs to study physical-chemical interactions

Physical-chemical interactions play an important role in combustion engines where, for example the timing of ignition or location of flame stabilization, and rates of heat release are affected by both physical and chemical mechanisms. Interactions can facilitate stable combustion, or lead to unstable conditions which can result in excessive pollutant formation, poor efficiencies and other detrimental behavior. In extreme cases, the combustion chamber or engine can be destroyed. Interactions evolve due to temperature and/or compositional gradients/fluctuations, as well as fluid dynamic processes.

While the study of autoignition chemistry is a primary focus of modern RCM experiments and has motivated the design of most machines, RCMs can also be used to investigate coupled physical-chemical phenomena, including those associated with large-scale gradients, turbulence, plasmas and localized gradients created by phase change. The following briefly discusses these topics and some design requirements, and directs the interested reader toward relevant work. Configurations used for these studies pose different challenges than those used to investigate autoignition chemistry, including the creation of appropriate test conditions, e.g., generation of desired plasma, as well as integration of requisite diagnostics. Particularly critical is the requirement for spatially and temporally resolved data that can complement conventional, volumetrically-averaged measurements, like pressure, and provide

insight into the physical-chemical interactions. Advanced diagnostics for such studies are highlighted in Section 3 of this review, while investigations exploring these interactions are discussed in Section 5.

2.2.1. Stratified autoignition

Stratified autoignition describes conditions where large-scale gradients lead to a cascade of ignition events within the reaction chamber, generally via a propagating wave, as opposed to a deflagrating front. Stratified autoignition can be used in engine applications to mitigate pressure rise rates in a range of LTC modes, *e.g.,* HCCI [162]. RCMs designed to investigate these processes must generate controlled, large-scale thermal and/or compositional stratification prior to the chemical induction period.

Iida and co-workers [163–167] at Keio University configured an RCM with a non-uniform heating system to thermally stratify the mixture prior to initiation of compression. The reaction chamber was mounted horizontally with hotter temperatures located on the upper side of the cylinder, enhancing buoyancy effects. Pöschl and Sattelmayer [168] at Technische Universität München implemented a similar configuration in their machine. A continuous flow system was used at Keio University to deliver the mixture through three intake valves located at the base of the cylinder, i.e., bottom-dead-center, and out two exhaust valves located in the head. The temperatures of the three gas manifolds were individually controlled. Under steady flow operation, where the gas had an axial velocity of 1.5 cm/s ($Re \approx 100$), the mixture had a relatively small radial thermal gradient ($\Delta T \approx 10$ K), with similar differences in the axial direction. The overall distribution for an early system design had large bimodal peaks located near the entrance and the exit of the cylinder; later tests reported better thermal control, with root mean squared (RMS) values near $\pm$1.5%. After closing the valves and a short residence time (~2 min) to allow the fluid motion to decay, piston compression was used to increase the stratification to $\Delta T \approx$ 25–52 K, with RMS values near $\pm$2.0–2.5%. The design features of this RCM led to bulk gradients near 1 K/mm at the initiation of compression, which increased to span $\Delta T \approx$ 50–200 K across the bore. Compositional stratification was also possible in this device by varying the seeding rate of fuel and/or simulated exhaust gas residuals (CO_2 and N_2) through each intake port. For instance, under some scenarios, fuel was excluded from two of the ports (so only O_2 and diluent flowed), with the fuel was directed through the remaining port. The fuel gradient could be positively or negatively correlated to the lateral thermal gradient. Creviced pistons were not included in this design, and the compression process was relatively slow, with a maximum piston velocity of 6 m/s, τ_C = 185 ms, and t_{50} = 25 ms. Since a flat piston was used in this machine, in-cylinder fluid motion and its influences may have been present during the tests, but these were not documented.

2.2.2. Turbulence–chemistry interactions

Turbulence–chemistry interactions (TCI) occur when small-scale gradients and fluctuations are present within the reacting mixture and the turbulent time scale is on the same order as the characteristic times for chemical reaction. These important phenomena have been identified in many flame-driven combustion schemes, but can also be relevant to autoignition-driven, LTC modes [169]. In early TCI work using RCMs, the turbulence fields were typically not well-controlled. Modern studies have focused on accurately characterizing these conditions within RCM reaction chambers. Large-scale motion, such as corner vortices, can influence the measurements and must be considered when designing RCMs for studies of small-scale turbulence effects, while diagnostic implementation, including location, timing and correlation of events, represent challenges in machine configuration and operation.

Griffiths and Franck, and Nimmo and co-workers [75,78] employed two methods to generate turbulence in their RCM test chamber. Their first approach, like Tizard and Pye [139], used an internal fan to stir the gases in the reaction chamber. They also designed a configuration where perforated mesh plates were placed at the entrance to the reaction chamber in order to generate turbulent flows during piston compression. As gas is forced through the holes in the plate, high velocity flows are created in the reaction chamber. A range of hole sizes and blockages ratios were employed to achieve different turbulent conditions. Franck *et al*. [78] demonstrated the influence of turbulence intensities on the measured ignition delay times, as well as the minimum compressed temperatures required for autoignition. Guibert *et al.* [113] at UPMC employed a similar approach with mesh plates. Because their geometry used a nose cone where the crevice volume was compressed, or squished, during the piston seating process such that the crevice gas was forced into the reaction chamber, high velocity fields were generated in the reaction chamber at TDC. The reaction chamber was made from transparent sapphire which provided excellent optical access, and utilized an octagonally shaped external surface to ease visual bias correction. The optical arrangement enabled measurements of the rates of turbulent kinetic energy decay during the delay period.

Park and Keck [102] highlighted through scaling analyses that turbulence can also be generated in the reaction chamber when the piston velocity based *Re* exceeds 10^5, or the boundary layer is not captured by a creviced piston. Ihme [170] used stochastic, reduced-order modeling to demonstrate the turbulence field can be significantly enhanced via high strain rate operation, i.e., high piston speeds, and through the use of high compression ratios, e.g., $CR > 30$. Strozzi *et al*. [126] configured a square cross-section, flat (uncreviced) piston geometry to generate turbulent flows during piston compression, while the flat walls

of the reaction chamber facilitated complete optical access without the need to correct for distortions due to curvature. Another approach to generate turbulence is to create large scale motion in the reaction chamber before piston compression, as applied in Kojima and Suzuoki [171], where an initial swirling flow was obtained using gas injectors placed on the periphery of the reaction chamber. A particular challenge for designing RCM hardware for TCI studies is the transient nature of RCM operation, and the time decaying statistics of the flow field. Consequently, it is difficult to achieve reliable, 'high turbulence, well-stirred uniform reaction' conditions, as identified in Fig. 3, within RCM configurations constructed to date.

2.2.3. Knock

Knock is associated with the evolution of gas dynamics within the combustion chamber, initiated by localized pressure spikes that result from non-uniform, uncontrolled chemical heat release. The propagation of pressure waves can remain sonic, or they can transition to supersonic detonation waves. Analogous processes occur within RCMs and shock tubes, but the confined dimensions of RCMs and associated wave – wall interactions are more representative of IC engines. There is a long history of knock investigation within IC engine platforms, and many theories have been proposed to describe its causes and development [172]. Recent work has also focused on processes leading to superknock [27], as discussed in Section 1. Some fuels are more prone to knock [173], while the combustion chamber geometry [174], including the location of any spark plugs, as well as the operating conditions [175] are influential. Conventional knock measurements conducted using variable compression ratio engines [176,177] can be influenced by many factors including evaporative cooling of the fuel, complex temperature and composition fields due to filling processes, and turbulent flame propagation rates.

Taylor *et al*. [178], designed one of the first configurations capable of simultaneous end wall visualization, and measurements of the reaction chamber pressure and piston position during knocking events. A strain guage was integrated into the crown of the piston, while a high speed camera recorded markings on the piston shaft as it traversed its stroke. Optically accessible cylinder heads were also used by Griffiths *et al*. [74,179–181], Hayashi *et al*. [182], Katsumata *et al*. [183], Wang *et al*. [184–187] and Tanoue *et al*. [188], while Tanaka *et al*. [189] and Pöschl and Sattelmayer [168] employed Bowditch-style pistons. Pöschl and Sattelmayer [168] also integrated fiber optic access into their cylinder head, while Affleck and Fish [71] located an optical port into the side-wall of their opposed-piston configuration. These transmissive heads, pistons and ports enable recording of spatially-resolved emissions, including direct and spectrally-filtered, as well as density gradients through the autoignition and wave generation

process. Affleck and Fish [71] implemented a rapid sampling valve and expansion chamber to extract product gases for quantification of individual species generated during the knocking process.

Spark probes have been utilized to investigate forced-ignition conditions where the probes have been centrally located [71], or situated in the side-wall of the reaction chamber [168]. Side-wall configurations allow non-symmetric conditions to be studied, for instance flame propagation across a positive, or negative temperature gradient. The use of multiple pressure transducers located across the reaction chamber can allow a deconvolution of the gas dynamic processess [168]. Finally, very high speed diagnostics, including kilohertz imaging (250–300 kfps) and pressure measurements (200 kHz), as discussed in Section 2, are necessary in order properly capture the very high speed phenomena that occur during knock.

2.2.4. Plasma-enhanced autoignition

Plasma-enhanced autoignition is an emerging field with potential application to reciprocating engines and gas turbines. Numerous techniques have been developed to generate non-equilibrium plasmas, e.g., nano-second pulsed discharge, where these plasmas differ significantly from conventional, equilibrium-type plasmas, e.g., spark discharge [190]. For non-equilibrium plasmas, much higher electron temperatures can be achieved along with lower electron number densities. Furthermore, non-equilibrium plasmas are more kinetically active due to the rapid production of active radicals and excited species via electron impact dissociation, excitation and subsequent energy relaxation. Little is understood about plasma-enhanced ignition at engine-relevant conditions, and much of the work to date has been conducted at low pressure and for simple fuels such as methane. Open questions include how the kinetic pathways of plasma-enhanced ignition are dependent on the plasma properties, gas temperature and fuels, and particularly what interactions occur between the plasma chemistry and low temperature chemistry of the fuel.

Few RCM studies have explored plasma-enhanced autoignition phenomena and opportunities exist for new methods. RCMs must be integrated thoughtfully with a method to generate the plasma, either inside the reaction chamber or externally. Boumehdi and co-workers [191,192] used a high-voltage electrode (d = 20 mm) located directly on the head of the reaction chamber (bore = 50 mm) to create a nanosecond pulsed, surface dielectric barrier discharge plasma. Takahashi *et al.* [193] used a reactor tube located in the inlet manifold of the RCM to generate a pulsed, dielectric barrier discharge plasma.

Specialized plasma diagnostics are required in addition to conventional RCM diagnostics where important measurements include number densities of key radicals, e.g., ȮH, Ö, and Ḣ, ions and electron densities and local temperature. Plasma generation is not a volumetric process but occurs near the surfaces of the electrodes, so the capability for spatial resolution in the measurements is important. Techniques for controlling fluid and aerodynamics, along with prescribing non-stimulated autoignition chemistry are also relevant for studies of plasma-enhanced autoignition in an analogous way, as for autoignition chemistry experiments.

2.2.5. Phase-change induced gradients

Phase-change induced gradients are particularly relevant to engine operation where fuel stratification due to spray events can be used to facilitate an array of LTC schemes. At the smallest scales, gradients in temperature and composition induced by evaporation from fuel droplets can alter the chemical kinetic processes leading to autoignition. The gradients and induced transport can be much larger than those generated by wall effects. Single droplets are one way to experimentally investigate the effects of small-scale gradients in a well-controlled manner, and have been utilized previously in studies in constant volume vessels. There are only few data at pressure and temperature conditions representative of LTC however. In such tests, a single droplet is suspended in the reaction chamber using a wire, and the surrounding gas subsequently compressed volumetrically by the piston(s). The rising gas temperature induces evaporation (similar to aerosol fuel loading techniques), and in oxidizing environments this can lead to autoignition. Open questions include how thermal/compositional gradients and transport influence the evolution of autoignition chemistry, including the dynamics of cool flame development and propagation [194].

Design and operational considerations for these tests include piston trajectory control to minimize the convolution of the gas compression with fuel volatility, minimization of gas motion near the droplet surface during and post compression, and ensuring the wire and wall effects are minimal during the test period. The wire must be sufficiently strong to withstand the compression heating and thermal expansion/contraction, yet also sufficiently low mass to reduce impacting the local state conditions. Fuel evaporation and autoignition must occur on scales relevant to the gas compression and heat loss. Necessary diagnostics include optical access and capability to monitor the two- or three-dimensional coupled physical-chemical phenomena; especially the means to locate spatially and temporally the phase interface, gas phase transport of the fuel and resulting compositional / thermal gradients, and initiation/evolution of the reaction front.

Kim *et al.* [195–198] used a single-piston RCM geometry with the droplet (400–600 μm) suspended in the center of the final compressed volume using a K-type, fine wire thermocouple (50 μm wires, 100 μm bead diameter) to study single and bi-component droplet ignition where effects of fuel volatility and reactivity were investigated. Compression ratios could be varied from *CR* = 13 to 18 but with relatively long compression times of τ_C = 170–210 ms (v_{max} < 1 m/s). Optical access through the end wall provided a means to record the droplet size throughout the compression, evaporation and ignition processes. In some of the tests, advection due to buoyancy and flow past the droplet during piston compression was evident near the droplet surface, highlighting challenges towards mitigating this phenomenon and ensure diffusive-controlled transport. Better resolution and measurement of the fuel concentration and temperature fields could lead to improved fundamental understanding that can be derived from the tests.

2.3. Summary

RCM design and configuration have developed significantly over the past century, and especially during the past two decades, with increasing control and manipulation of the reacting gas for both autoigntion chemistry studies, and those of coupled physical-chemical processes. A number of 'best practices' have emerged where these indicate that:

- Lubricants, oils and tiny particles can significantly foul the measurements and should thus be avoided.
- The gas compression process can affect the fuel/oxidizer chemistry, turbulence evolution and intensity, as well as heat loss, and care should therefore be taken.
- Compressed air provides the fastest rates of compression, while the use of hydraulics requires sophisticated control mechanisms, and hydraulic systems can be more prone to creep and rebound.
- Though an important contribution has been the development of creviced pistons, it is clear that properly configuring the piston crevice for particular machine geometry and operating conditions is key to adequately suppressing the corner vortex formation, and that a single configuration may not be appropriate across a wide range of facilities, or a range of experimental conditions explored during an experimental campaign.
- Since most facilities are one-of-a-kind fabrications, designers of new components and devices are encouraged to leverage past advances, and to publish detailed descriptions and characterization work that demonstrate new capabilities, or limitations of concepts. It is good practice to apply high-fidelity and/or reduced-order models before prototyping new concepts.

There are many opportunities to develop new configurations, especially for continued investigation of physical-chemical interactions, the implementation of increasingly higher fidelity diagnostics, some of which are discussed in the next Section, and the utilization of challenging fuels and extreme combustion regimes.

3. Development and application of standard and advanced RCM diagnostics

In this section, methods for and results from the application of standard and advanced diagnostics are described. These diagnostics are necessary to achieve accurate observation of autoignition chemistry and physical-chemical interactions using RCMs. Some advanced experimental methods target high fidelity measurements which can supplement information provided by standard diagnostics, such as pressure histories, and highlight opportunities for RCM research and discoveries. Temporal, spatial, and other limiting resolutions for typical conditions are provided (when available), as well as methods to overcome experimental challenges.

Accurate measurements of pressure and estimates of the corresponding temperature are minimum requirements for extracting the necessary chemical reactivity characteristics for RCM experiments. Measurements of pressure-time histories have been used since the 1930s to deduce ignition delay times for reacting mixtures. The pressure data have been particularly useful in developing an understanding of reactivity trends covering a range of temperatures, as well as providing insight into heat loss and preliminary heat release prior to the main ignition event. It should be noted that ignition time measurements inferred from pressure traces are a result of the convolved pressure-temperature history experienced during the induction period, and thus the pressure and temperature information cannot be easily deconvolved without additional information, as described in Section 1. Additional details including temperature or species concentration measurements can be acquired via supplementary diagnostics to provide more complete information on the reactive system. Details on the thermometry diagnostics are provided in the references cited in this section and in comprehensive textbooks on combustion diagnostics (see [199,200] for example).

A wide range of diagnostics has been applied to RCM studies to enhance the understanding of the chemistry and flow physics important for LTC processes. Much has been learned about key reaction pathways during ignition, as well as the effects of temperature, pressure, heat loss, and fluid motion. The diagnostics can be categorized as intrusive, where the application directly affects the sample region, as in the case of thermocouples and gas sampling; or non-intrusive, which generally leverage optical strategies like laser absorption and laser induced fluorescence (LIF). All modern RCMs are equipped with pressure transducers to acquire pressure histories, and many use passive imaging in the form of high speed cameras or photodiodes. A more complete picture of LTC phenomena could be assembled via detailed descriptions of the spatial distribution and time history of pressure, temperature, intermediate species and velocity

fields. However, the experimental complexity involved in spatially resolved fast diagnostics is prohibitive, and often not necessary, to acquire sufficient understanding for developing and adequately validating predictive combustion models.

In the following sub-sections, we briefly introduce dynamic pressure measurements and describe the implementation and some of the major results obtained in RCM studies using many advanced diagnostics. Measurements of temperature within the reaction chamber are discussed, including examples of intrusive (e.g. thermocouple) and non-intrusive techniques (e.g. fluorescence). This is followed by a description of measurements to identify and quantify stable and radical species, again including intrusive (e.g. physical sampling) and non-intrusive (e.g. chemiluminescence, laser absorption and extinction, etc.) methods. The section ends with some examples of flow field measurements (e.g. particle image velocimetry (PIV)), which are vital in studies of physical-chemical interactions. The material in this section is meant to introduce the topics of diagnostic measurements in RCMs, but the review is not intended to be exhaustive. The reader is encouraged to consult original references for details on the experimental hardware, analysis, and subtleties associated with advanced diagnostic methods. Opportunities to implement novel and emerging diagnostics are discussed in Section 7.

3.1. Pressure measurements

There are numerous documents in the scientific, engineering and commercial literature concerning how to make accurate measurements using pressure sensors (typically based on piezoelectric crystals) including topics of thermal shock, chemical compatibility, durability and other important concerns [201–203]. The IC engine community has extensively documented methods that thoughtfully consider these issues and others, such as the appropriate placement of pressure transducers, analog-to-digital converter resolution, charge amplifier matching, and triggering. Pressure history data are routinely conditioned using filtering and averaging methods. Because pressure measurements are the cornerstone of most RCM studies, researchers should provide explicit documentation of the data acquisition and conditioning applied in each study, as well as examples of typical pressure data for a range of experiments. Researchers new to RCM investigations are encouraged to explore texts like the work by Rogers [201] and other important references on 'best practices' for pressure sensor measurements. Data conditioning affects the end-of-compression pressure and therefore end-of-compression temperatures as well, if they are derived from the pressure data. The uncertainty analyses should include the effects of different methods of conditioning pressure data as well as different means of defining end-of-compression (e.g. based on local pressure maxima, pressure derivatives, pre- or post-data conditioning, etc.). Even though the effects

of pressure data conditioning on state conditions are critical, reporting such analysis is not standard among RCM studies, although it should be. Some examples of 'best practices' for considering pressure data analysis can be found in Mansfield *et al.* [204].

3.2. Temperature measurements

Autoignition is significantly influenced by the local temperature, often in an exponential manner. Therefore, even small temporal and spatial variations in temperature can significantly affect the evolution of reactions. Thermal gradients and localized hot spots are particularly associated with the development of non-uniform ignition phenomena in RCMs. Most RCM studies do not directly measure temperature, but rather infer temperature from pressure measurements, e.g., via the adiabatic core hypothesis, as discussed in Section 4. However, many efforts have pursued measurements of temperature in RCMs with varying levels of spatial and temporal fidelity. These endeavors have been critically important towards reducing the uncertainty associated with investigations of LTC processes within RCMs, and are discussed in detail here.

3.2.1. Schlieren techniques

Some of the earliest RCM studies took advantage of large areas of optical access provided by transparent end-wall and side-wall windows to apply schlieren imaging to study flow physics during autoignition experiments [69,106]. Later studies applied schlieren imaging to consider flame progress in RCMs equipped with spark plugs, e.g. [205,206], and others have applied schlieren and shadowgraph methods to image fuel spray development in RCMs e.g. [112,206–208] and engine knock phenomena e.g. [182,209–211]. Often, these studies include photographic records of combustion and ignition chemiluminescence, which offer further information on the levels of homogeneity within the test chamber of the RCM experiments.

Schlieren imaging provides a measure of the density gradient, which is a direct, qualitative indication of the thermal gradient, when there are no pressure oscillations in the test chamber and the mixture is homogeneous and non-reacting. With careful calibration, schlieren imaging can be used for quantitative line-of-sight averaged temperature measurement; however, schlieren methods have been predominantly applied for qualitative studies in autoignition experiments.

In the seminal work by Livengood and Leary [106], the authors present schlieren images of *iso*-octane and benzene autoignition with comparison to non-reacting schlieren images of compressed air. Significant non-uniformities were observed during the ignition process of the different fuels. The authors

proposed that the observed temperature inhomogeneities could be attributed (in part) to the piston travel during the compression phase where this "scrapes off the boundary layer of air from the cylinder walls, producing a turbulent region at the periphery of the chamber…" The work by Livengood and Leary [106] was the first to suggest caution in the exclusive use of pressure measurements to characterize autoignition, both with regards to ignition time measurements, as well as determination of the characteristic state conditions for the test. The schlieren imaging data of Griffiths *et al.* [212], similar to earlier results [69,106], showed spatial aspects to ignition of *n*-pentane and the formation of ignition kernels. Later work by Strozzi *et al.* [126] used qualitative schlieren imaging to show the formation of roll-up vortices at the corners of the piston and test chamber for their square cross-sectioned, flat piston RCM. The same data describe the extent of thermal homogeneity within the test section and the time scales of fluid-motion enhanced transport. These studies provided the foundation for further work on the flow physics of RCMs, how these influence the ignition measurements and how they can be mitigated, and motivated the quantitative measurements of temperature fields that develop in RCM studies.

3.2.2. Thermocouple measurements

Thermocouples provide well established methods to quantify the temperature field in combustion systems, while recognizing such measurements require corrections for radiation, conduction and convection heat transfer, and researchers must be aware of potential catalytic interactions. Additionally, fine wires and small junctions are required for adequate time response and good spatial resolution, which necessitates the use of fragile experimental equipment. However, there are several RCM studies that have successfully applied thermocouples for accurate temperature measurements with good spatial and temporal fidelity.

The pioneering work of Desgroux *et al.* [144] demonstrated Rayleigh scattering to measure core gas temperatures in an RCM. The optical measurements were complemented with fine wire thermocouple measurements [145]. The thermocouple measurements were placed across the radius of the RCM at 5 mm intervals in the central region of the test section, with higher resolution (1 mm) in the thermal boundary layer near the wall. The single thermocouple, inserted through a 1.2 mm double-bore ceramic rod was relocated after each test to build a composite image of the temperature profile within the reaction chamber. The time response of a thermocouple is a function of both the size of the thermocouple bead and the local gas dynamic conditions. For reference, Desgroux *et al.* [145] used 12 μm chromel-alumel wire with an estimated time response of less than 3 ms, and a data sampling rate of 25 kHz. Compression times were adjusted to a duration of τ_C = 100 ms in order to minimize the effects of the

reaction chamber wall thermal dynamics. The results were the first to provide spatially and temporally resolved data on the thermal fields as they evolve during a typical RCM test. The studies of non-reacting and reacting experiments conducted with a non-creviced piston showed regions of fairly good thermal uniformity, where bulk gradients on the order of 5 K/mm [145,213] were observed in the time immediately after the end of compression, as seen in Fig 16. The data presented in Fig. 16 are for mixtures with 1.65% *iso*-octane, where the 20.65% oxygen is replaced with N_2 in the non-reacting mixture. The non-reacting data, as mentioned in Section 2, indicated the formation of a cooler toroidal region surrounding the central portion of the RCM test section. Comparison of the non-reacting and reacting data showed that heat release during the preliminary stages of ignition, i.e., LTHR, attenuated this stratification and led to a more thermally though not compositionally homogeneous mixture. The thermocouple measurements by Desgroux *et al.* [145] and later work by Donovan *et al.* [108] indicated that the thermal boundary layers that formed near the walls of the respective RCMs could be on the order of 3–5 mm after 50 ms post-compression, where bore-to-height ratios were 2.3 and 0.5–1.0, respectively. While the fine wire thermocouples used in these studies (12 μm wire in [145] and 25 μm wire in [108]) provided good spatial and temporal resolution (around ~1–10 ms for ignition experiments; where the time response varies as a function of the bead size, material and the Nusselt number of the RCM test conditions, as discussed in [108]), the thermocouples are often not sufficiently robust to withstand the conditions of autoignition, especially with undiluted mixtures.

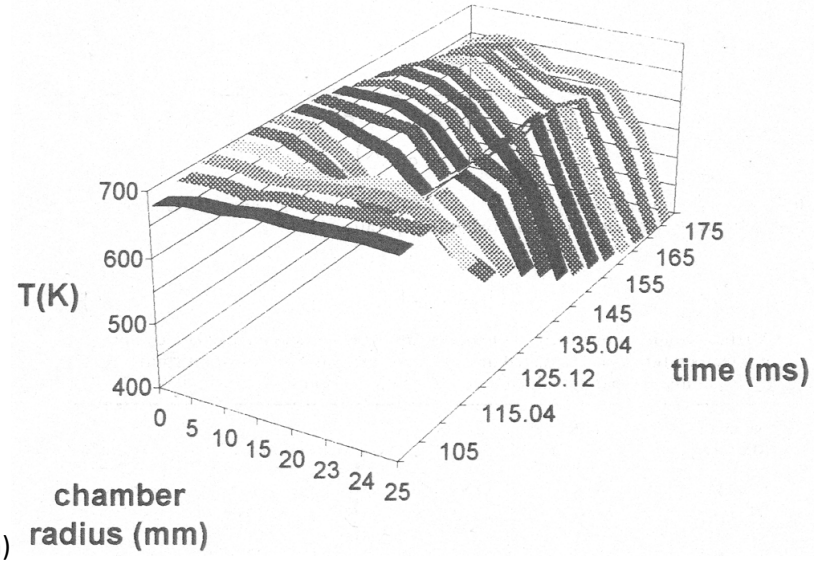

a)

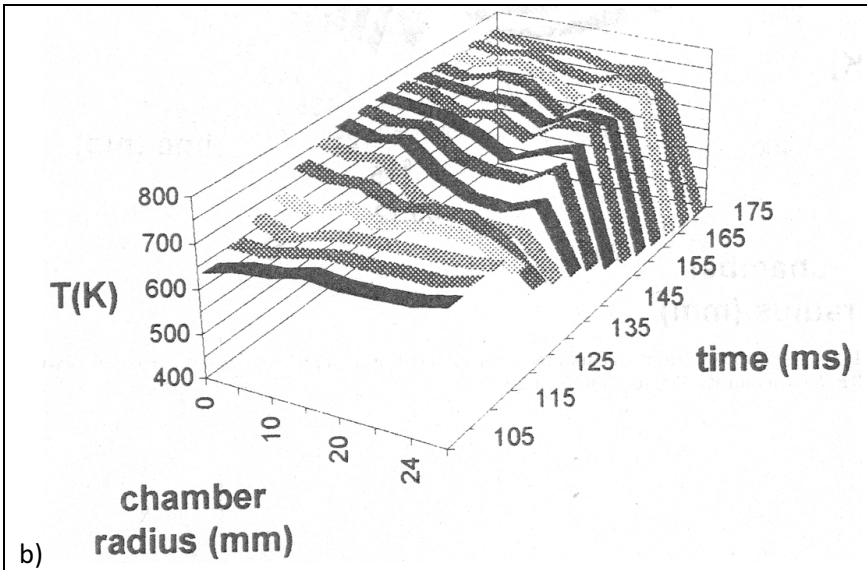

b)

Figure 16. Uncorrected thermocouple measurements of temperature in a) a non-reacting RCM experiment and b) a reacting RCM experiment. End of compression is 100 ms in both panels where $T_c \approx 700$ K and $p_c \approx 8$ bar. The data show the good thermal uniformity that can be achieved in the core, or central region of the RCM immediately after the end of compression, and how a toroidal thermal structure evolves near 125 ms, 25 ms after the end of compression. LTHR within the reacting mixture attenuates the magnitude of the temperature gradient as a function of time. (reprinted from [145] with permission of Taylor & Francis)

3.2.3. Rayleigh Scattering, Fluorescence and Absorption Techniques

Optical diagnostics are more complex to deploy, but more robust than thermocouples while providing adequate spatial and temporal resolution. The spatial fidelity is generally better and the response time faster, but data acquisition rates, which are a function of laser pulse repetition, may be slower. Signal to noise issues can also result in larger uncertainty bands for the measurements, and the data cannot be easily averaged, as is often done in reciprocating engine studies where the cycle repetition rates are much higher than for most RCMs. Optical access in RCMs can vary from the large windows used in schlieren and chemiluminescence studies, to small ports with windows around 1 cm in diameter. Line of sight diagnostics such as laser absorption, typically use opposed ports, whereas Rayleigh scattering and fluorescence require orthogonal optical access.

Desgroux *et al.* [144,145] were the first to use Rayleigh scattering measurements for temperature measurements. The repetition rate of their laser (10 Hz, a pulsed frequency doubled Nd:YAG laser providing emission at 532 nm) limited the measurements to discrete intervals after the end of compression in their RCM (nominally one data point each, taken 100 ms after the end of compression),

and high interference from reflections limited measurements near the wall [144,145]. The authors quoted a temperature accuracy of 3–4%, or ±30 K, at the experimental conditions studied. The path-averaged measurements provided some corroboration with the thermocouple data, though questions arose regarding discrepancies between the datasets, including differences in fidelity and tradeoffs between the techniques.

Clarkson *et al.* [214] extensively characterized the temperature field in their RCM using acetone LIF and Rayleigh scattering of non-reacting and reacting test gas mixtures. LIF and Rayleigh scattering signals, like many optical diagnostics, are sensitive to the density of the test gas mixture as well as the composition. Thus, quantifying the measurements from these diagnostics requires an understanding of the evolution of the state conditions and extent of chemical reaction during autoignition. Clarkson *et al.* [214] made recommendations on how to successfully apply LIF and Rayleigh methods to identify spatial structures in RCM flow fields. Similarly to Desgroux *et al.* [144,145], the authors conjectured that a toroidal structure existed for their RCM hardware at the conditions studied, consisting of a vortex formed at the end of compression where the center or core region of the test gases could experience temperatures colder than the surrounding fluid. The evidence for the fluid motion included higher LIF signals in the center of test chamber than the surroundings, as shown in Fig. 17(a). The LIF data also showed that the thermal stratification was attenuated to a more uniform profile by 30 ms after the end compression, as seen in Fig. 17(b). To further study thermal stratification in the RCM, Clarkson *et al.* [214] also used ditertbutyl peroxide (DTBP) as a thermo-chemical marker, where exothermicity from the decomposition of the DTBP amplified the pre-existing temperature field. Calibration of these optical methods for quantitative data is challenging. However, as noted in [214], qualitative data can yield significant insight into the flow physics in RCMs, just as in other reactors. Particularly, as identified in Section 2, these measurements have been crucial towards the development of RCM configurations that can achieve more uniform conditions in the reaction chamber for autoignition chemistry studies.

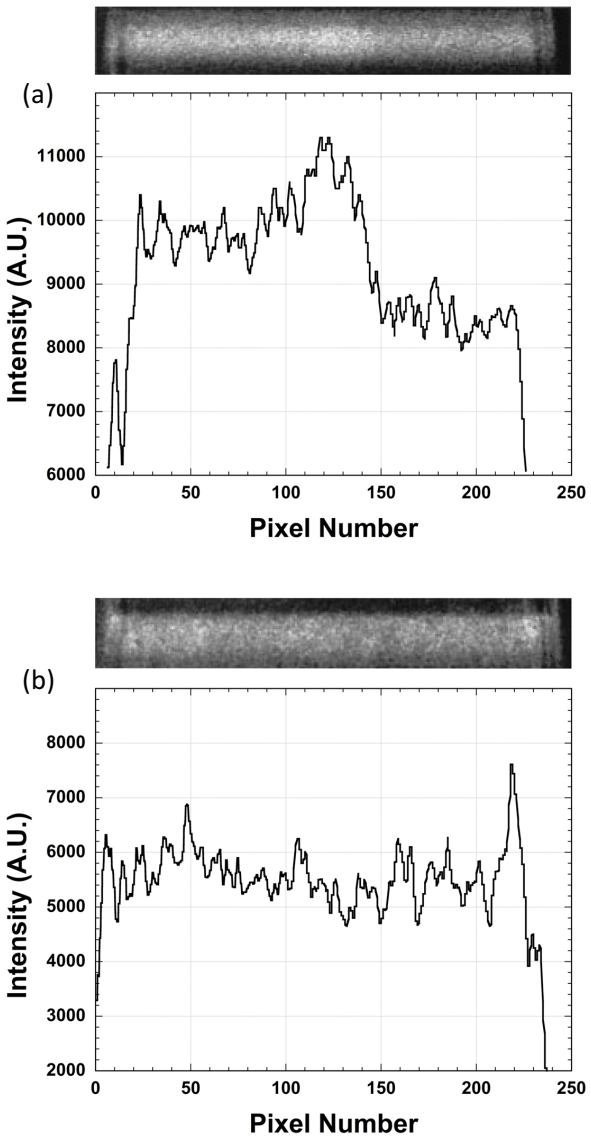

Figure 17. LIF signals for acetone/N_2 mixtures in RCM experiments imaged in a sheet across the central plane of the reaction chamber, indicating the temperature field at (a) 1.1 ms and (b) 30 ms after the end of compression, where $T_c \approx 700$ K and $p_c \approx 8$ bar. The upper panels present the recorded planar LIF signals and the lower panels present the LIF intensity (arbitrary units, since the signal was not calibrated) integrated over the width of the laser beam. The pixel number represents the distance across the width of the end-view imaging of the RCM (~0.2 mm/pixel). (reprinted from [214] with permission of Elsevier)

Optical diagnostics can also provide insight via semi-quantitative measurements, where the measurements can be normalized, or compared relative to a reference condition. For example, Griffiths and co-workers used planar Rayleigh scattering to provide quantitative measurements of the relative temperature field in their RCM [74]. Representative scattering intensity data from [74] are presented in Fig. 18. When composition and pressure are constant within the test volume, the scattering data can

show the variation and evolution in the temperature field at each discrete measurement time. It should be highlighted that due to the 10 Hz laser repetition rate, the images for each of these panels represent data averaged from four different tests. The authors claimed excellent repeatability of the tests, however. The two columns in the figure show data for *n*-pentane/air ignition studies at two end of compression temperatures, T_c = 690 K and 770 K. Because the state and composition change as a function of time during the autoignition experiments, the primary goal of the measurements was to understand the evolution of the temperature field at each point of the reaction progress. As seen in Fig. 18, the temperature fields appear to be quite uniform in the core of the chamber shortly before ignition (*t* = -2.8 ms) where random, localized fluctuations were on the order of ±4–9 K, with gradients near 10–30 K/mm. For the T_c = 690 K condition (Fig. 18a), the higher signals at the center of the test section that develop at later times indicate cooler gases in the center relative to the surrounding gases. The thermal stratification is attributed to a roll-up vortex as the piston did not incorporate a crevice. The higher signals at the edges of the images are attributed to interference from reflection off the windows. The lower gradients in the signals outside of the region of interference were attributed to the development of the thermal boundary layer, where this was interpreted as approximately 5 mm thick. Assuming a uniform thickness of the boundary layer around the core of the reactive gas, this suggests that the boundary layer region occupied about 70% of the volume at these conditions. Given the large bore to height ratio geometry, most of the boundary layer penetration is in the axial direction. For T_c = 770 K (Fig. 18b), the temperature profile appears to evolve in a skewed fashion, which the authors attributed to the formation and propagation of a flame across the reaction chamber, where this led to knock at these conditions [74]. Though the measurements of the temperature field are made at discrete time intervals during the delay period and only relative temperature can be deduced from the data, the temporal and spatial resolution of this application of Rayleigh scattering is very good.

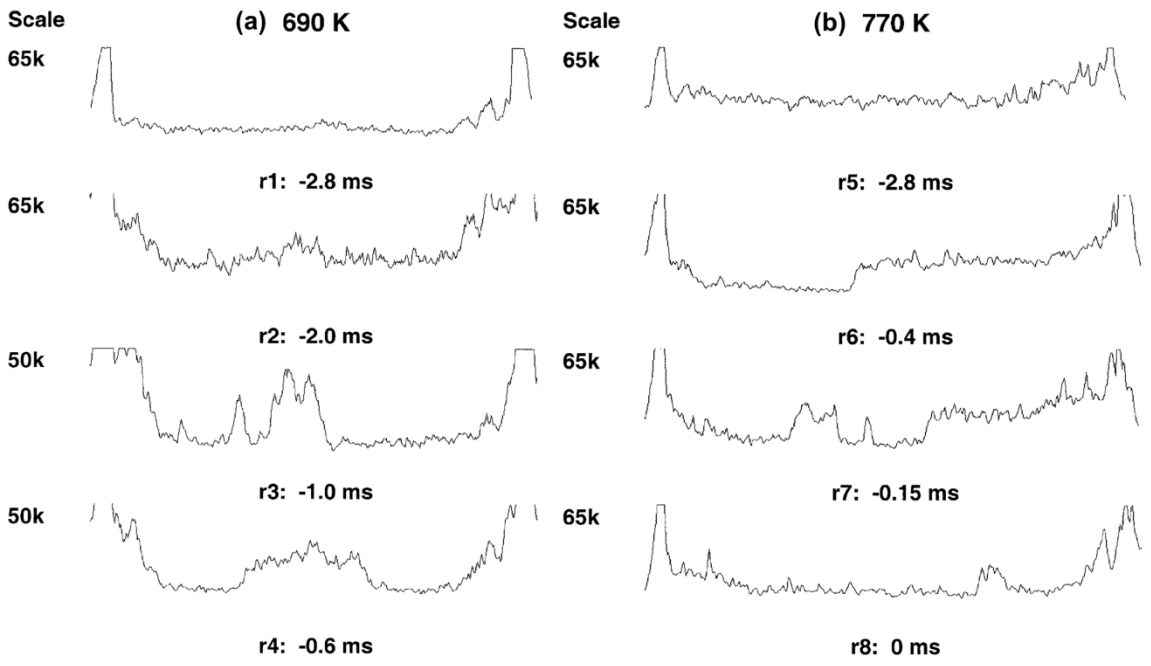

Figure 18. Statistically averaged Rayleigh scattering intensities obtained during stoichiometric *n*-pentane/air RCM autoignition experiments where the intensities correspond to relative temperatures across the diameter of the RCM, noted to the left of each profile. The time before the maximum pressure due to ignition is provided below each temperature profile. Data in the left (non-knocking) and right (knocking) columns correspond to end of compression temperatures of (a) T_c = 690 K and (b) T_c = 770 K, respectively, with $p_c \approx 8$ bar. Depth of field resolution, 2 mm, resolution 0.2 mm/pixel, 10 Hz laser pulse frequency, temperature difference detectivity limit 60 K, temperatures averaged over a 1 cm wide laser sheet. (reprinted from [74] with permission of Elsevier).

Mittal and Sung [148] employed one-dimensional acetone LIF using non-reacting mixtures to compare the temperature gradients formed in an RCM equipped with a creviced piston to results using a non-creviced piston. The authors applied a correction for absorption that improves the sensitivity of this LIF method, and with some assumptions and the use of a simplified one-dimensional gas model, absolute temperatures were obtained from the data. Uncertainties in temperature were estimated to be around ±1.5% (±11 K), while the scatter in the measurements was close to ±0.5%. The spatial resolution was twice that obtained by Griffiths *et al*. [74], around 0.1 mm/pixel, while the experiments were similarly conducted using a 10 Hz pulsed laser with data acquired at one discrete time during each test. The LIF results showed that gradients due to uncontrolled bulk fluid motion from the corner vortex could be on the order of 50–100 K/mm. When the authors utilized a creviced piston, the corner vortex could be suppressed and the temperature of the gas in the reaction chamber was more uniform, with bulk gradients measured to be on the order of 1–5 K/mm, while peak local gradients were near 5–10 K/mm.

Random temperature fluctuations were observed to be less than 1% in the core gas for the creviced piston, but larger (1.5–3.0%) for the flat piston.

More recently, Strozzi *et al.* [122,215] applied planar laser induced fluorescence (PLIF) to oxygen-free toluene mixtures to measure the instantaneous two-dimensional temperature field formed in their RCM, which was designed with a square cross-section to facilitate (in part) planar imaging, and utilized a non-creviced piston. Their configuration was not designed to suppress fluid dynamic motion, but to achieve turbulent conditions that are similar to operating IC engines. In the absence of oxygen, toluene provides higher fluorescence signals compared to acetone, and toluene fluorescence has high sensitivity to temperature for the conditions studied. The authors used a frequency quadrupled Nd:YAG laser with 10 Hz repetition rate and the fluorescence data were recorded with a 10 Hz sampling rate using an intensified charge coupled device (ICCD) camera. As with earlier investigations, multiple tests were required in order to build a composite dataset of the evolution of the temperature field. Their optical arrangement yielded similar spatial resolution as Mittal and Sung [148] of about 0.1 mm/pixel. Careful calibration methods were used to create accurate, absolute, quantitative temperature measurements. The spectroscopic theory and data analytics applied are well described in Strozzi *et al.* [122]. Some results of their study are shown in Fig. 19, where the data indicate both the large- and small-scale features of the temperature field resolved in these PLIF studies. The uncertainty in temperature was estimated to be ±5% (±45 K) at the highest temperatures, which were found in the core region, and ±1% (±10 K) at colder temperatures, e.g., in the vortex or boundary layer. RMS temperatures across the core of the reaction chamber were near ±30–60 K, where local fluctuations were close to ±14 K. Representative gradients are indicated in the Fig. 19.

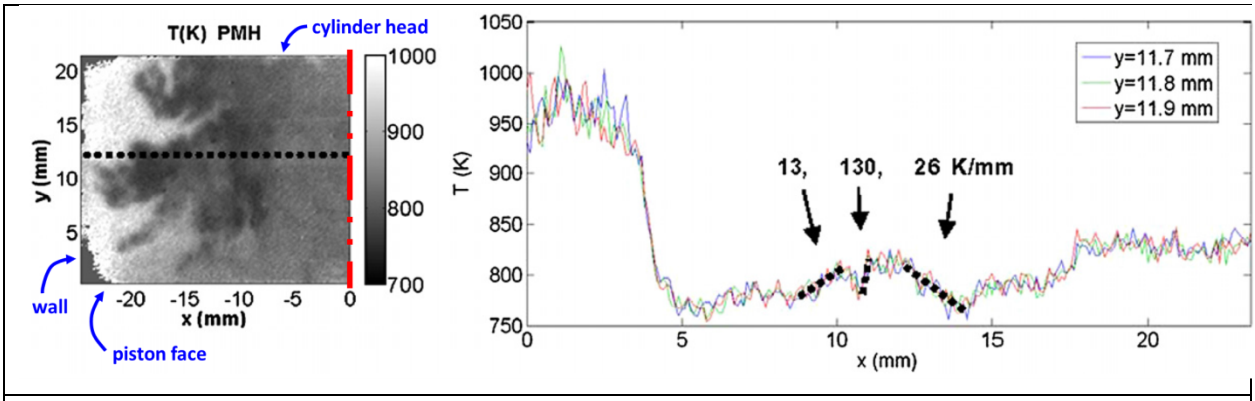

Figure 19. Results of PLIF thermometry to characterize the two-dimensional temperature fields created at the end of compression in a high compression ratio (*CR* = 18) RCM with a square cross-section and flat piston, where at this point in time the roll-up vortex has penetrated into the bulk of the reaction

chamber and the remaining core gas is located near the wall of the cylinder. For this test T_c = 950 K, and p_c = 40 bar. (reprinted from [122] with permission of IOP Publishing Ltd.)

Due to the high quenching rate of toluene by oxygen, toluene-based PLIF cannot be applied to igniting mixtures; however, Griffiths *et al.* [212] applied PLIF of acetone for thermometry and PLIF of formaldehyde to reacting mixtures to study the complex effects of thermal feedback, comparing an NTC (*n*-pentane) with a non-NTC (DTBP) fuel. The PLIF data of the formaldehyde formed during ignition were not converted to temperatures, but rather used as markers of the intermediates formed during ignition of the two parent fuels. The interactions between the reaction kinetics and the intrinsic temperature fields created in their RCM led to interesting observations regarding the relative reactivity of the fuel mixtures in cooler and hotter zones. The authors concluded that a zero-dimensional approximation of the test may be valid for RCM ignition studies using fuels with positive temperature dependent reaction, even when spatial inhomogenieties are present. However, the same could not be said for NTC fuels exhibiting two-stage ignition behavior; in this case the validity of a zero-dimensional approach and the interpretation of appropriate state conditions for the experiments were described as questionable.

Nasir and Farooq [216] recently applied quantum cascade laser absorption to make time-resolved temperature measurements (with time resolution <10 μs) in both non-reacting (CO/N_2) and reacting (*n*-pentane/air doped with CO) mixtures. The temperature measurements were line-of-sight averaged and based on two-line resonance absorption spectroscopy of CO. As with many of the studies previously discussed, the results confirmed the RCM compression was well-represented as an adiabatic core process. They estimated the measurement uncertainty at ±6.3% or approximately ±50 K, and with this diagnostic showed discrepancies in both the time of first-stage ignition, and extent of low temperature heat release compared to a detailed chemical kinetic model. The time resolution of the quantum cascade laser diagnostic enables further studies to potentially apply inversion methods to multiple probe beams to evaluate spatial effects in RCMs.

3.3. Species measurements: radicals, stable intermediates and products

Similar to temperature measurements in RCMs, species measurements can be categorized as intrusive (e.g. physical sampling) or non-intrusive (e.g. laser absorption). Sampling measurements tend to allow a large range of species to be identified and quantified simultaneously, whereas optically based methods can provide measurements of short-lived radicals, as well as provide additional temporal and spatial fidelity in comparison to gas sampling. However, the range of species measurements demonstrated with

optical techniques is more limited. Highlights and examples of both approaches are provided in the following subsections.

3.3.1. Gas sampling methods

Physical sampling of the test gases in RCM experiments has yielded powerful insights into important reaction pathways during autoignition. Physical sampling combined with analytical methods like gas chromatography (GC) can be used to measure a broad range of species including the stable reactants, intermediates, and products of combustion. There are two general strategies employed for gas sampling: quench all the gases in the test chamber to increase the volume of gas available for analysis, or extract a small sample that minimizes the impact on the rest of the test gases in the RCM. Figure 20 shows schematics of the typical hardware used for the two approaches. Both methods have merits and challenges, and sampling durations for both methods are typically on the order of 1–2 ms. The physical sampling times limit these methods to autoignition regimes where the chemical time scales are longer than the sampling duration, to allow adequate time resolution. The use of a punctured diaphragm, as indicated in Fig. 20a, minimizes the sampling time for the former approach. In all cases an evacuated chamber is connected to the test section of the RCM, and the the gas sample is extracted by expansion. The pressure differential between the test section and the sample chamber ensures that the reaction progress of the test gas mixture is quenched by rapidly decreasing the temperature. When sampling valves are used, the studies are usually limited to compressed pressures of $p_c < 30$ bar due to difficulties of rapidly actuating and sealing the sampling valves. All methods require an understanding of the quenching process and quantification of any “dead” or unreacted volume of the test section, e.g., piston crevice, and sampling system. The unreacted volume of gases dilutes the sample and is a factor in the uncertainty of the gas sampling measurements.

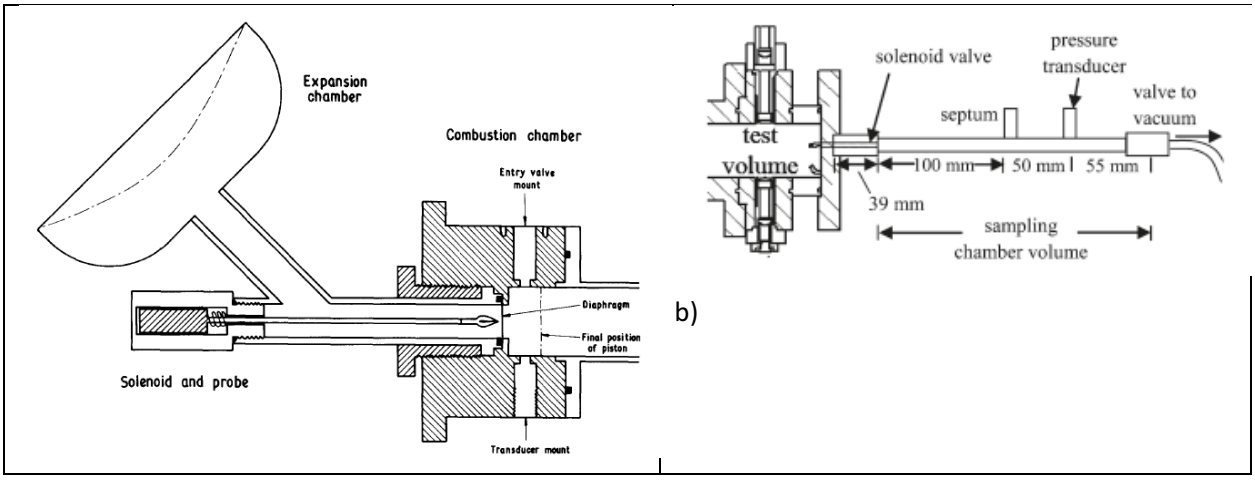

a)	
Figure 20. Schematics of the typical equipment used in gas sampling systems that a) quench the entire test section gases (reprinted from [118] with permission of Elsevier), and b) quench a small sample of the test section gases (reprinted from [217] with permission of American Chemical Society).	

Gas-sampling has been applied to RCM experiments for decades led by the pioneering work of Martinengo *et al.* [218], Roblee [219] and Fish *et al.* [73]. Roblee [219] sampled intermediates by rupturing a diaphragm and rapidly expanding and quenching the entire test gas mixture into an expansion chamber. The geometry and size of the expansion chamber is critical to quenching the reactivity of the test gas mixtures as described in Roblee [219]. The sampling system used by Fish *et al*. [73] expanded the test chamber gases into nitrogen, using expansion cooling and dilution to prevent further reaction.

The ignition study by Fish *et al.* [73] demonstrated how insightful gas sampling can be in terms of elucidating reaction chemistry. Using sampling and gas chromatography, the authors quantified over 40 intermediate species formed during 2-methylpentane/air ignition studies, as well as upper limits on 7 additional species. By referencing the species measured to the initial fuel concentration, the authors identified the yields in the major classes of intermediate species (alkenes, aldehydes, ketones, alcohols, etc.) and used the data to describe the reaction pathways of cool flame and two-stage ignition chemistry.

The study by Fish *et al*. [73] is an example of how the mass balance of the parent fuel can be closed by taking into account all of the important reaction pathways. Such studies provide further information on branching fractions of overall reaction pathways, as well as absolute reaction rates. Often however, not all peaks in the gas chromatograms can be identified or quantified. Calibration standards are required for each species, and this is an expensive and time consuming process. Additionally, standards are often not available or are highly toxic. Fortunately, flame ionization detectors often allow calibration factors to be extrapolated from similar species (same number of carbon atoms, same functional groups), at the expense of increased uncertainty relative to calibration factors based on absolute standards. Detection limits for species with absolute standards vary, but can readily be sub-part per million. Multiple gas chromatography ovens, columns and temperature programs are required to accurately separate a broad range of species. Carbon recovery can be challenging for intermediates from some constituents such as heavier hydrocarbons or very polar species, which can adsorb or absorb to the walls of the sampling vessel or condense in the manifold that connects the reaction chamber to the analytical unit. However, quantitative and accurate measurements can be readily made for many species, and recent improvements

in analytical techniques, such as multidimensional GC [220], hold promise for providing isomeric distinction between many intermediate species.

Following these early works, gas sampling has become a useful diagnostic for RCMs. Speciation studies conducted at the University of Leeds have applied gas sampling to RCM autoignition studies of isopropyl nitrate [118] and normal/branched paraffins [77]. Speciation studies at ULST have applied gas sampling to RCM ignition studies covering a wide range of fuel structures including: normal alkanes and alkenes [80,81,84,221–223], saturated and unsaturated cyclic alkanes [83], alkyl cycloparaffins [224], alkyl-substituted aromatics [225] and methyl esters [226]. At the University of Michigan, the approach of using small gas samples has been developed and applied to a range of fuels including alkanes [227–229], alcohols [217,228], and esters [230–232]. The results of these studies have provided new insights into autoignition chemistry. For example, recent work by Wagnon *et al.* [232] identified high uncertainties in the reaction chemistry of unsaturated esters and the reaction pathways involving smaller unsaturated and poly-unsaturated stable and radical species. Representative results from this work are illustrated in Fig. 21 where noticeable achievements were made in model predictions. Similarly, recent gas sampling measurements from RCM studies at Tsinghua University have highlighted discrepancies in model predictions of intermediate species during *iso*-butanol ignition [233].

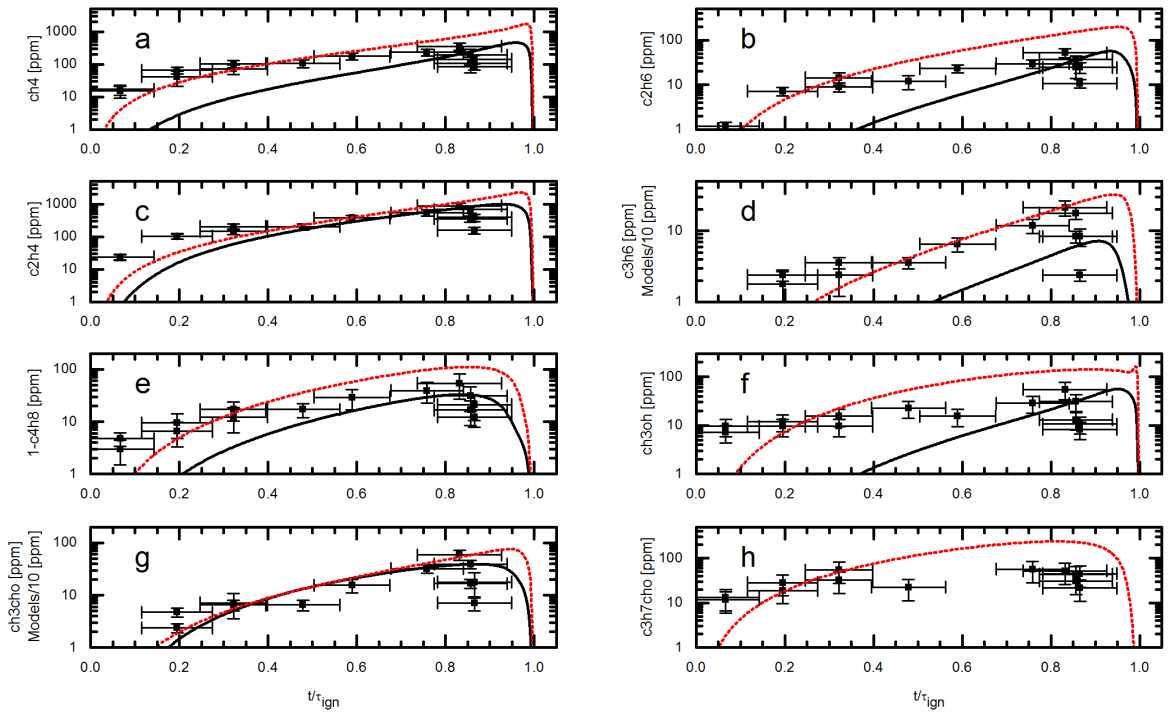

Figure 21. Stable intermediate time histories (mole fraction) during methyl trans-3-hexenoate autoignition: a) CH_4, b) C_2H_6, c) C_2H_4, d) C_3H_6, e) 1-C_4H_8, f) CH_3OH, g) CH_3CHO, h) C_3H_7CHO. The

experimental data are represented as symbols and the lines are model predictions. The black solid, and red dotted lines indicate the original and updated model results, respectively. Average conditions for the experiments were T_c = 934 K, p_c = 10.4 bar, ϕ = 0.30, diluent:O_2 = 3.76. (reprinted from [232] with permission of American Chemical Society).

Exhaust gas analyzers provide another means to measure the products of combustion (CO, CO_2, NO_x, UHCs, etc.) and have been used to quantify combustion efficiency in RCM fuel studies [234] and to measure NO_x production [189,234,235]. The primary products of combustion are typically measured post-ignition. By physically sampling at different times after the end of compression, physical sampling and exhaust gas analyzers, like GCs, can be used to create quantitative time histories of these key species during and after the ignition delay period. A challenge to measurements using exhaust gas analyzers is the relatively high minimum detectable limit and the relatively large sample volumes required for some devices. However, Van Blarigan *et al.* [234] described procedures to address these issues.

3.3.2. Absorption, emission, and fluorescence spectroscopy

Short-lived radicals provide excellent targets for validating and developing reaction mechanisms for autoignition processes relevant to LTC. Because radicals recombine during most physical sampling methods, attractive *in situ* diagnostics to measure radicals are absorption, emission and fluorescence spectroscopy. Of course, stable species can be measured using absorption and emission diagnostics, and such measurements also provide insight into fuel consumption and major product reaction pathways. However, absorption, emission and fluorescence diagnostics require accurate understanding of the bulk and local temperature, pressure and composition in order to extract quantitative data on the radical or stable species. Conversely, accurate understanding of the composition is required to extract quantitative measurements of temperature. Thus, there are many challenges as the reaction chemistry evolves and with it ensuing endo- or exothermicity. Some methods combine spectral features and methods to measure species concentrations and temperature at the same time [236][237]. Line-of-sight methods are further enabled by good spatial homogeneity of the conditions probed by the laser or other light source, and thus the development of strategies such as optimized creviced pistons has significantly improved the capability to confidently implement these techniques.

Some of the earliest combustion chemistry studies using RCMs like the work by Fish *et al*. [73] and Beeley *et al*. [118] applied absorption spectroscopy using broad band light sources (such as deuterium or tungsten-iodine lamps) which were spectrally filtered (e.g., using monochromators) to target measurements of the species of interest like NO_2 and HNO [118]. As noted in [73], care must be taken to

correct for interfering species, background emission and other optical phenomena. Generally, these studies also include careful execution of calibration experiments or validation of important spectroscopic constants, like absorption cross sections and broadening coefficients. In some measurements and studies, absorption and emission features can be used to identify unknown intermediate species: in [73] ultraviolet absorption was identified as due to the formation of unsaturated carbonyl and β-dicarbonyl intermediates during 2-methylpentane combustion with oxygen. The same absorption measurements were combined with gas chromatography measurements, and allowed the authors to propose a detailed oxidation pathway for 2-methylpentane at intermediate temperatures and high pressures (T_c = 713–933 K, p_c = 10–40 bar).

Emission from chemiluminescence has been extensively applied to RCM studies to document the spatial and temporal characteristics of autoignition. These measurements have been enabled by dramatic improvements in the past decade in the time response and sensitivity of high-speed complementary metal oxide semiconductor (CMOS) cameras. The high intensities of chemiluminescence that occurs during ignition are well captured using modern CMOS cameras which can provide temporal resolution of over 250,000 frames per second. Results of high speed imaging studies include identifying conditions associated with homogeneous and inhomogeneous ignition behavior [204,238,239], characterizing the effects of charge stratification and induced turbulence [113,240,241], identifying spatial features associated with knocking conditions [74,183,242] such as the formation of shock waves during knocking [127,241], and the effects of thermal stratification on ignition [164,167,215]. Figure 22 presents chemiluminescence imaging data acquired by Griffiths *et al.* [74] during studies of knocking and non-knocking ignition of *n*-pentane at two thermodynamic state conditions. The images demonstrate the physical changes in the ignition characteristics associated with knocking conditions [212].

(ICCD cameras have also been applied to chemiluminescence studies in RCM facilities. In addition to good sensitivity in the visible wavelength region, ICCD cameras are particularly sensitive in the ultraviolet, where key species like ȮH and NO have resonant features and are often used as the sensor array in fluorescence studies which are discussed below. In the work by Lim *et al*. [163], the authors used ICCD imaging to characterize the effects of buoyant thermal stratification on autoignition, with spatial resolution of 0.67 mm/pixel and 8 images per cycle, using exposure times of 0.44 ms.

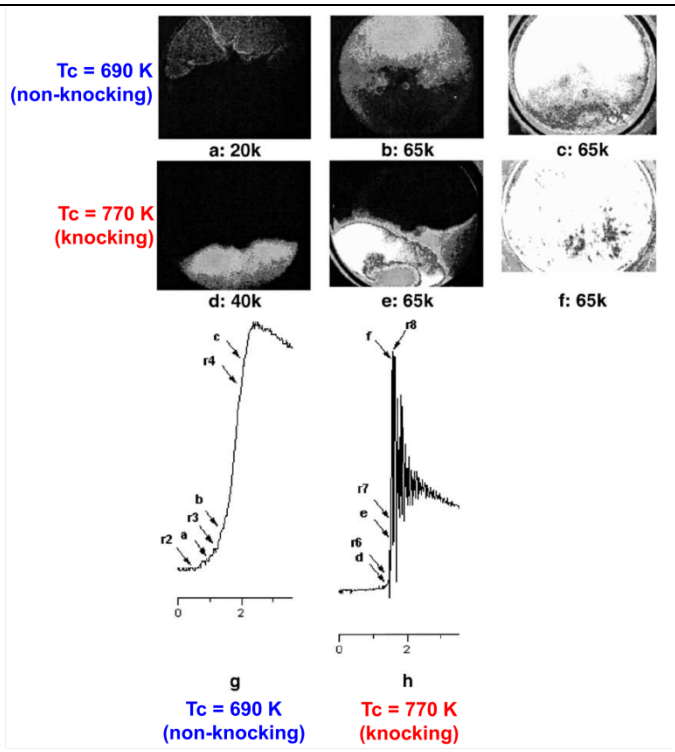

Figure 22. Chemiluminescence images during RCM studies of *n*-pentane at non-knocking (panels a, b, c, and g) and knocking (panel d, e, f, and h) conditions where T_c = 690 K and 770 K, respectively, with p_c = 8 bar. (reprinted from [74] with permission of Elsevier).

Absorption, emission and fluorescence methods can be applied using naturally occurring species as in chemiluminescence investigations, or by doping the reactant mixtures with additives. Recently, laser absorption methods have been applied to RCM studies to measure targeted species, where this is different from early absorption or emission studies which used recorded spectral characteristics to identify various species. When additives such as acetone, toluene or water are used, experimental validation must typically be undertaken in order to demonstrate that the autoignition processes are not significantly perturbed (chemically, thermally or otherwise) by the additives.

He *et al.* [243] were the first to apply narrow-line absorption of ultraviolet emission to ȮH measurements during ignition studies of *iso*-octane. Following this, Sung and co-workers [236,244] applied quantum cascade lasers to use near infrared laser scanning (200 Hz) to obtain line-of-sight averaged temperature measurements based on H_2O spectra with both non-reacting and reacting gases in a creviced-piston RCM. The studies demonstrated the application of high-fidelity laser absorption methods in RCMs to investigate reaction chemistry with part-per-million detectivity limits as seen in Fig. 23 [243], and thermometry with experimental and simulated temperature-time histories as seen in Fig.

24 [236]. Uncertainties in temperature and H_2O concentration were reported to be ±11% and ±16%, respectively, for undoped conditions, which were reduced to nearly ±1% and ±5%, respectively, for tests where 0.6% H_2O was seeded into the test mixture, and these were within ±5 K of adiabatic core calculations. Multiple passes of the laser beam (e.g., 6) was found to also reduce the measurement uncertainties. Care was taken in these tests to ensure that the thermal boundary layer occupied, at most, 5% of the laser path for each reported measurement.

Line-of-sight, broadband attenuation of He-Ne emission at 632.8 nm was used by Tanaka *et al*. [189] to quantify particulate formation during ignition of *n*-heptane. By combining the laser attenuation diagnostic with exhaust gas analysis, the authors were able to identify mixture compositions and state conditions where NO_x and particulate emissions were simultaneously lowered. Kitsopanidis and Cheng [245] followed this laser extinction study with measurements of soot formation under rich *n*-butane/O_2/Ar conditions, while Di Sante [246] used similar techniques to measure soot yields for blends of *n*-heptane/toluene under rich conditions (ϕ = 3), covering a range of temperatures from T_c = 675 to 800 K at p_c = 11 bar.

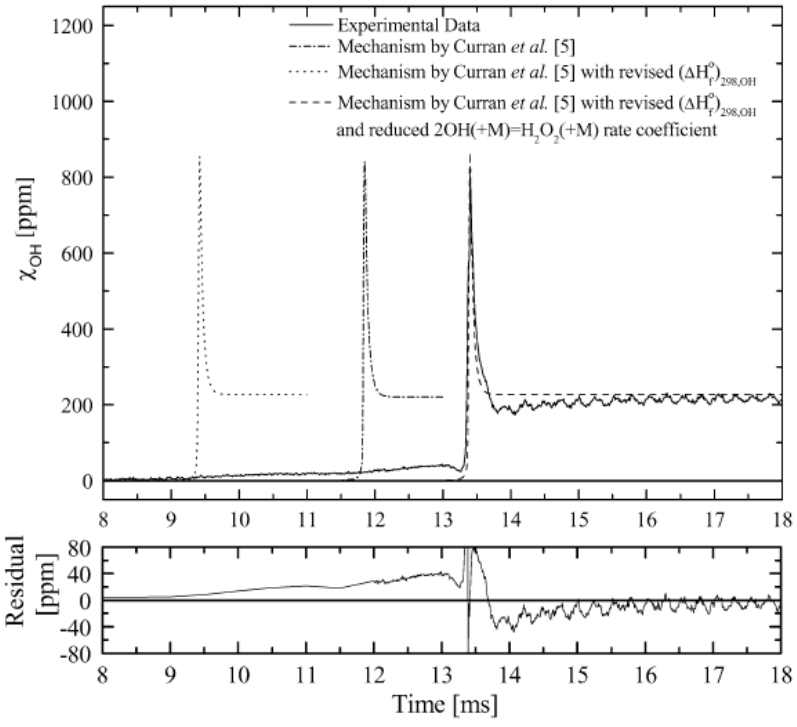

Figure 23. Time histories of ȮH obtained using near ultraviolet laser absorption spectroscopy during RCM autoignition studies of *iso*-octane and air. The experimental data (solid line) are compared with

simulation results using different reaction mechanisms and thermodynamic data. The residual presented in the lower panel is the difference between the experimental data and the simulation results for the updated mechanism. T_c = 971 K and p_c = 14.5 bar for this test. (reprinted from [243] with permission of Elsevier).

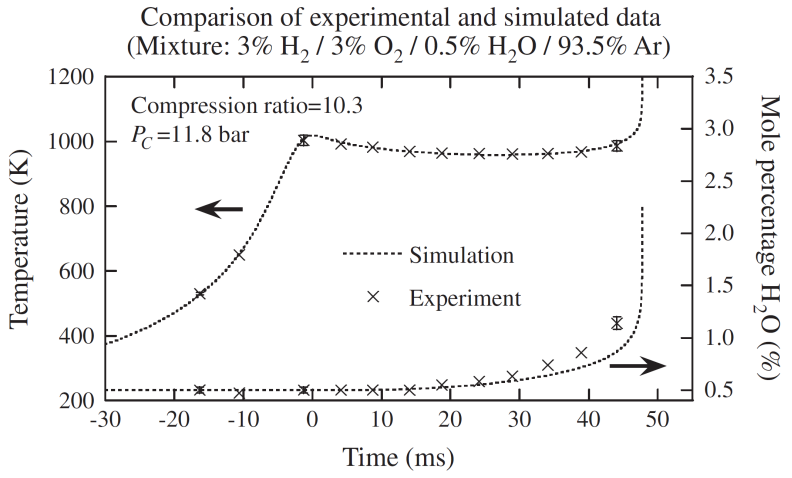

Figure 24. Temperature and H_2O measurements obtained using near infrared laser absorption spectroscopy during H_2/O_2 RCM autoignition studies where the test mixture was seeded with 0.5% H_2O. Simulation results using the adiabatic core hypothesis are presented as the dashed lines and the experimental data are represented by the symbols where representative error bars are shown. (reprinted from [236] with permission of Elsevier).

3.4. Velocity field characterization

Few RCM studies have focused on quantifying flow field velocities, even though such data can be important towards understanding a number of physical-chemical interaction phenomena. The lack of data may be attributed to challenges associated with making these measurements. In particular, intrusive methods such as hot wire anemometry [205,247] can distort the flow field, and are generally limited to point measurements, while optically based methods require good optical access, significant signal calibration, and typically need some means to seed the flow [113,215,240]. Due to the non-continuous nature of RCM operation, it is difficult to seed the gas with particles and prevent them from settling prior to initiation of the test. However, these challenges are offset by the significant understanding provided by quantitative knowledge of the flow field. One important area of current research is improving the quantitative understanding of the effects of turbulence on chemical reactivity. RCM studies provide an excellent opportunity to address these fundamental issues, as demonstrated in [113,215,240]. It should be noted that studies to date have been conducted in machines designed to encourage turbulent flow

fields, as opposed to geometries configured to suppress fluid dynamic processes, as described in Section 2. There are no experimental velocimetry studies to date which have used creviced piston configurations.

As an example, Strozzi *et al*. [215] used PIV, seeded with zirconium oxide particles (d_{mean} = 5 μm, d_{max} = 14 μm) deposited directly into the evacuated reaction chamber and subsequently mixed with the test gases *in situ*, using a pre-test residence time of 2 min to minimize residual flows. They conducted measurements of the flow fields created in their square cross-section RCM where autoignition of lean methane/air mixtures was studied. They combined the PIV data (acquired using a laser pulse interval of 40 μs) with chemiluminescence (acquired at 5–9 kHz, 0.13–0.26 mm/pixel), and PLIF thermometry (described earlier) to provide a comprehensive understanding of the ignition characteristics in terms of the ignition criterion first proposed by Zeldovich [248] and Gu *et al*. [249], and extended by Sankaran *et al*. [250]. In particular, the data presented in Fig. 25 show that the initial location of the ignition kernel is consistent with the hottest region identified in the temperature field and this region is where the local ignition delay time is the shortest. Heat is released by a combination of deflagrative and autoignitive processes, depending on the local conditions. The authors conducted extensive analysis of the two-dimensional experimental data and used fundamental theory to quantify the thermal stratification and the effects on the local ignition environment.

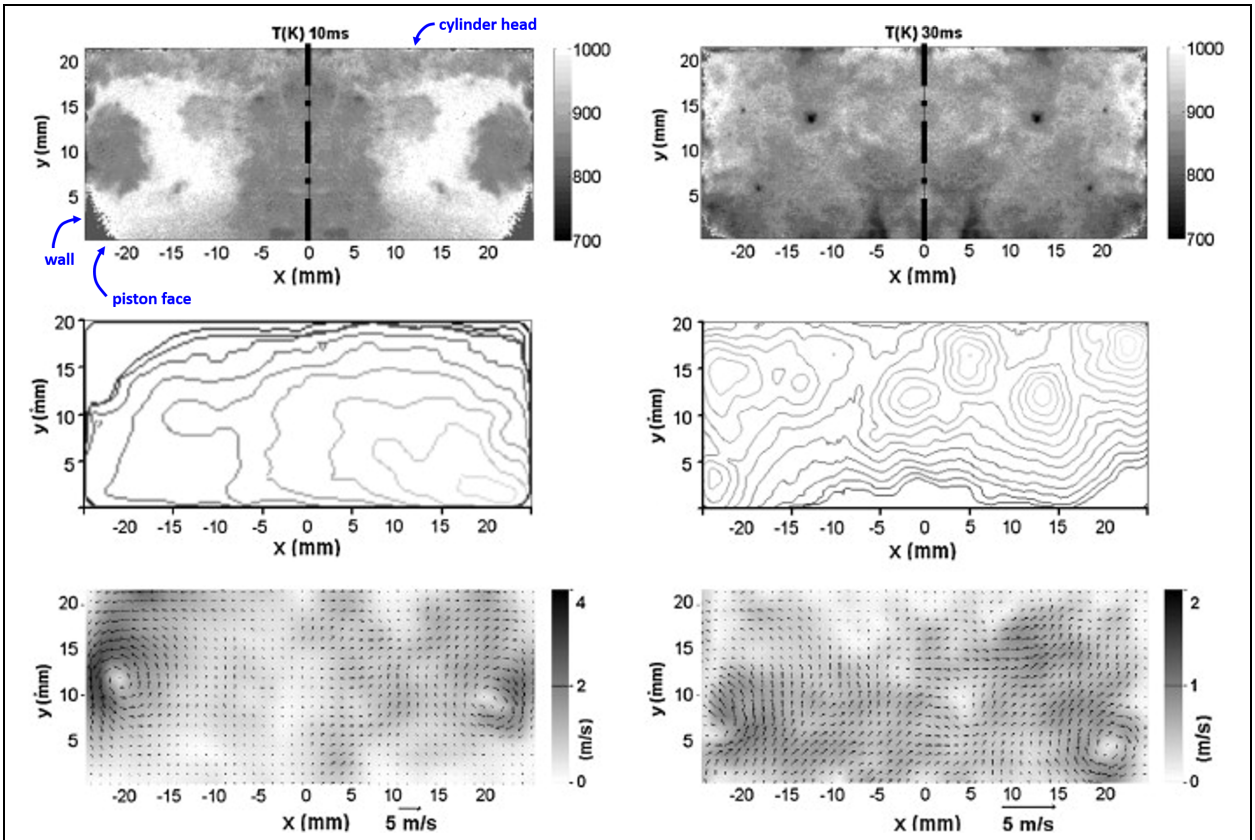

Figure 25. Temperature (top panel), contours of spontaneous emission intensity (middle panels) and velocity fields (bottom panels) from methane-air autoignition study. 'x' is the distance from the center of the reaction chamber, and 'y' is the distance from the piston face. The temperature and velocity field data were acquired from non-reacting experiments at 10 ms (left panels) and 30 ms (right panels) after the end of compression, where the reacting mixtures ignited at 10 and 30 ms, respectively. The temperatures were determined using toluene PLIF and the velocities were determined using PIV during separate tests. Note that the PLIF measurements, due to signal to noise ratio limitations, were conducted for only one half of the reaction chamber bore and the uniformly symmetric temperature field is assumed and imposed in the top panels. The emission intensity contours were acquired from high speed imaging using a CMOS camera where T_c = 945 and 928 K and p_c = 38.4 and 40.7 bar, respectively. (adapted from [215] with permission of Elsevier)

The study by Guibert *et al.* [240] similarly leveraged multiple advanced diagnostics and further considered the effects of turbulence intensity on autoignition behavior in the test section of their RCM. Fig. 26 presents instantaneous results from the PIV measurements where starch particles with d_{mean} = 20 μm were used and delivered via entrainment in the intake manifold of the machine. The PIV data, acquired using a laser pulse interval of 1.4 ms, were used to determine mean kinetic energy data, where some results as a function of the time after the end of compression are presented in Fig. 27. The RCM in the study employed a nose-cone geometry and a small crevice volume at the exterior of the larger, main bore of the machine to control the vortex rollup and capture some of the boundary layer gases. However,

most of the rollup gases are forced into the smaller bore reaction chamber near the time of piston seating. Because of this arrangement, the flow fields in the reaction chamber exhibit high velocities; much higher than with the geometry used in [122]. The data for the tests showed the characteristic time for the rate of turbulence dissipation can be of the same order as the characteristic times for autoignition for the fuel-air mixtures studied. The data indicated that the residual turbulence levels in the reaction chamber can affect the progress of autoignition, and thus measured ignition delay times and pressure rise rates. This is of course dependent on the particular mixtures used, operating conditions explored and RCM hardware utilized, though it is clear that for shorter ignition times there will be a greater competition between the kinetics and turbulence.

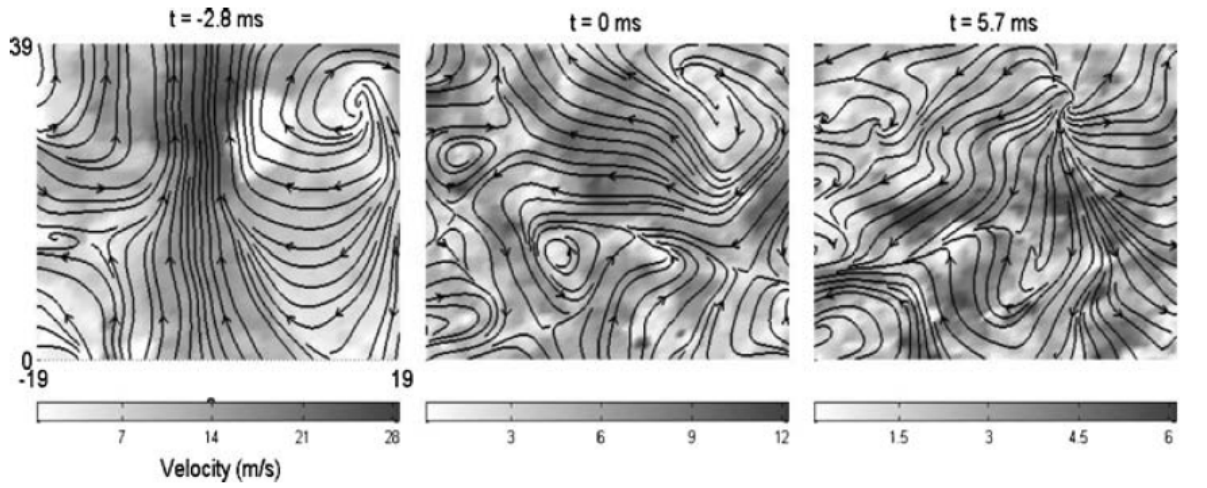

Figure 26. Instantaneous velocity fields and streamlines measured for non-reacting test gas mixtures at times before and after the end of compression (t = 0 ms) using PIV where T_c = 840 K and p_c = 37 bar (reprinted from [240] with permission of Springer Science).

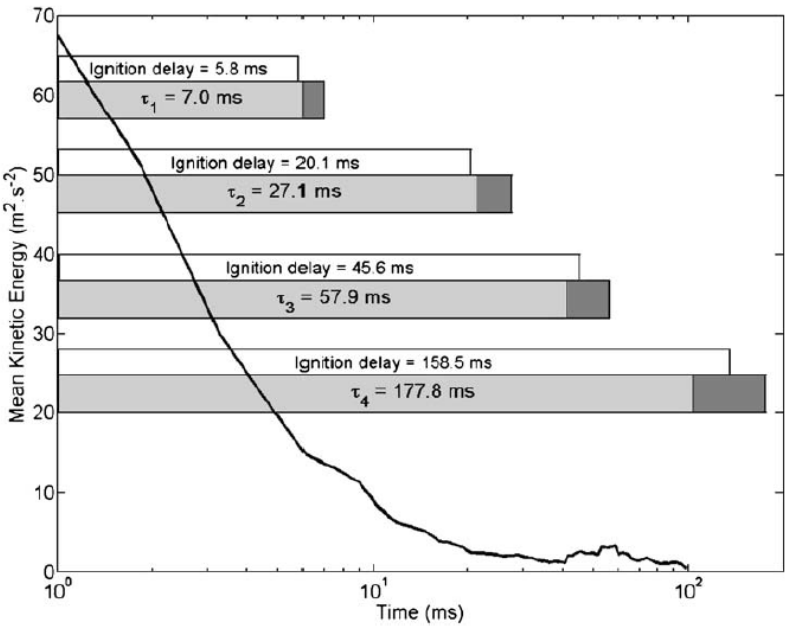

Figure 27. Mean total kinetic energy derived from PIV data as a function of time after the end of compression. The unshaded bars show the average measured autoignition delay time at $T_c \approx 840$ K and $p_c \approx 37$ bar. The shaded bars represent the time from the end of compression to the maximum pressure, where the darker portions indicate the time when visible emissions were recorded using the CMOS camera. The ignition data correspond to four fuels: 1-hexene, primary reference fuel blend of 90% iso-octane and 10% n-heptane (PRF90), methylcyclopentane and *iso*-octane, in order of increasing ignition delay time. (reprinted from [240] with permission of Springer Science).

3.5. Summary

The development and application of standard and advanced RCM diagnostics have followed an exciting evolution. Whereas the studies discussed here indicate a general pattern for temperature field measurements, one should be cautious with generalizations. Mixture composition and operating pressure can affect the heat transfer properties of the experiments, via the thermal diffusivity, while RCMs use different strategies to create the experimental conditions of interest, for example square versus circular cross-sections, with and without piston crevice volumes, wall heating versus ambient surroundings, compression ratio versus diluent composition change, reacting versus non-reacting mixtures, and so on. Therefore, the reaction chamber conditions, for example the presence and strength of thermal gradients, are not identical from one study to the next. Furthermore, variability in each experiment can also affect interpretation of the results for techniques that utilize line-of-sight averaging, ensemble, or other composite methods. Absolute, quantitative temperature measurements are challenging and the data currently available, albeit for limited conditions and facility configurations, are invaluable for the design of experiments and interpretation of the resulting data, but uncertainties must

be considered. Additionally, all results to date have been one- or two-dimensional measurements, although the data indicate three-dimensional flow fields can be formed during RCM experiments. Within these caveats, the results of the studies presented here suggest that for RCMs configured to study autoignition chemistry by suppressing large scale fluid motion, thermal boundary layers can grow to 5 mm thick during the test period, and random fluctuations in temperature can be lowered to less than 1%, with bulk and local gradients near 1 to 10 K/mm. Larger scale features associated with uncontrolled fluid motion, like the vortex roll-up in non-creviced piston geometries, have been identified with associated thermal gradients from 50 to 100 K/mm and temperature fluctuations of $\pm$2–3%.

Species measurements coupled with ignition delay time measurements provide higher fidelity data for developing reaction theory and for validation combustion kinetics. For example, excellent agreement between experimental and model predictions for ignition delay time have been demonstrated for a broad range of fuels and conditions, as presented and discussed in Section 6. However, time-resolved species measurements sometimes show significant discrepancies between the model predictions and the experimental data, even though the ignition delay times are in good agreement. Such discrepancies indicate potential problems with the predictive certainty of the models for important intermediates like small alkenes, as well as trace species such as pollutants. Gas-smpling techniques have matured in the past decade both with respect to the temporal fidelity of the physical sampling hardware and with respect to advances in the gas analysis. Multi-dimensional gas chromatography and mass spectroscopy provide more information with higher accuracy than previous achieveable.

Laser diagnostics have also advanced providing higher temporal and spatial resolution than physical sampling methods, albeit for fewer species. Readers are directed to the numerous excellent reviews of these spectroscopic methods for more information on the implementation details of laser diagnostics, e.g. [251–255]. Simultaneous application of independent measurements (gas sampling or optically based) will provide further opportunities to refine reaction rate theory and improve the predictive capabilities of modeling combustion chemistry.

The work in [215] and [113] were the first of their kind to apply such in-depth and complementary measurements and analysis for low and high turbulence conditions, respectively. The studies highlight opportunities for future explorations of turbulence and chemistry interactions, while also indicating the care that must be used in understanding the complex fluid motion and chemistry interactions within RCMs. The results also highlight the high quality experimental evidence that can be acquired using RCMs to understand turbulence - combustion chemistry interactions at conditions that are highly relevant to

current and next generation combustion systems. In particular, RCMs provide powerful experimental platforms to develop and validate combustion theory that is described in Section 4. Few experimental platforms provide the time scales necessary for such studies.

4. Autoignition regimes and modeling

Autoignition regimes are distinguishable based on characteristic time scales including compression, reaction, heat release and diffusion (molecular and turbulent), as discussed in Section 1. Fundamentally, these are associated with competing and/or coupled physical-chemical processes. Various regimes are targeted during an RCM experimental campaign via specialized machine configuration and/or operating conditions. Modeling is often undertaken to complement RCM experiments, for instance towards the development and validation of chemical kinetic and other models, to facilitate analysis of the experimental data, or assist in the creation of more robust or diverse experimental configurations. To some degree, it is necessary to account for facility influences and/or physical interactions during any RCM test, as it is for most experimental measurements [256].

This section provides additional detail on autoignition regimes, specifically as they relate to RCM tests, and definitions of parameters used later in this text. Furthermore, various modeling frameworks are described, where these are able to provide, with increasing fidelity, representations of facility effects and coupled physical-chemical interactions that can occur within a reaction chamber during a test. There are still many open questions concerning modeling approaches for RCM experiments so that rigorous recommendations of 'best practices' cannot be made at this time, however the state-of-the-art is summarized at the end of the section.

4.1. Definitions

Factors which influence the development of autoignition behaviors include thermal and/or compositional stratification, chemical kinetic sensitivity, endo-/exothermicity and the transport characteristics of the reacting medium. Stratification and/or fluctuations in temperature or composition within the reacting gas can favor different chemical pathways, while kinetic sensitivity can cause the mixture to react on significantly different time scales depending on the local conditions. Endo- and exothermicity provides thermal and/or pressure feedback to some processes. Finally, the properties of the mixture, such as the acoustic velocity and thermal diffusivity, can affect the response of the system to localized heat release.

Various aspects of these features as they relate to RCM experiments have recently been discussed by Grogan *et al.* [257] and references therein, where a regime diagram was constructed to parameterize the gas behavior during a test. This operating map, which is depicted in Fig. 28, was formulated in terms of Damköhler and Reynolds numbers (*Da* and *Re*, respectively), with demarcations estimated to indicate transitions between various phenomena. The Damköhler number used ignition delay time as the chemical

time scale (i.e., τ_T/τ_{ign}), while the Reynolds number was parameterized by the mean piston velocity and the bore of the reaction chamber. It was assumed that laminar conditions in the test chamber are only possible at very low *Re* based on diameter (of order or below unity), although it should be realized that the transition is expected to occur at higher *Re* [102], while creviced piston configurations can extend this even further. The parameterization used for Fig. 28 requires some adjustment for the wide range of machine configurations in use today, covering those designed to investigate autoignition chemistry, as well as those used for turbulence-chemistry interaction (TCI) studies, and this is an area of active investigation. The evolution of various phenomena and their demarcation boundaries will shift accordingly. Nevertheless, analogous diagrams have been created for other experimental devices, e.g., [258,259], and are useful since they can aid experimental design, for both machine arrangement as well as selecting operating conditions.

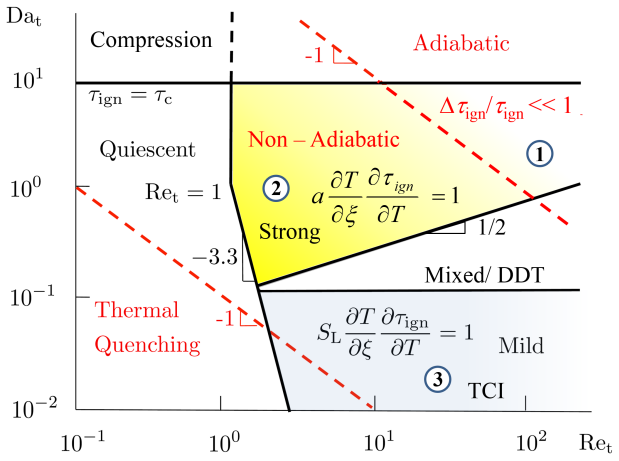

Figure 28. Operating map illustrating various autoignition regimes that can be encountered during RCM experiments. Tests focused on autoignition chemistry are typically conducted in the region labeled ①. (adapted from [257] with permission of Elsevier).

Modern RCMs used to study autoignition chemistry are configured to minimize non-uniformities and other physical effects such as boundary layer growth, and thus tend to operate within the region labeled ① in Fig. 28. This region is bounded by the 'compression' limit ($\tau_{ign} = \tau_C$), the 'loss of adiabaticity' limit ($\Delta\tau_{ign}/\tau_{ign}<<1$), and the 'mixed/detonation to deflagration, or DDT' limit ($f(Re^{1/2})$). RCMs designed to probe physical-chemical interactions operate intentionally outside of these boundaries. For instance, stratified autoignition studies typically access the mixed ignition regime or region ②, and TCI investigations operate in region ③.

When expressed on an Arrhenius diagram, the limits for region ① can be manifested roughly as shown in Figure 29. Here, the boundaries indicate conditions where reliable autoignition chemistry data can be acquired with relatively low uncertainties. Experiments are typically conducted within this window via adjustments to p_c, ϕ, and diluent:O_2 ratio, in a manner similar to shock tubes. The locations of these boundaries are somewhat facility dependent, being functions of t_{50}, surface area to volume ratio, etc., but normally ignition times greater than 2 ms and less than 150 ms are within these limits. The kinetic sensitivity of the reactive mixture can also shift the 'mixed/DDT' limit to shorter or longer times, and this generally will not coincide with other limits. Additional work to rigorously evaluate these boundaries could benefit our understanding of autoignition regimes.

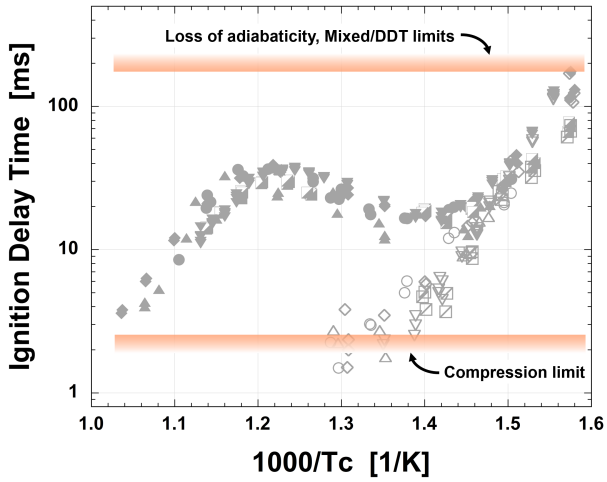

Figure 29. Representative Arrhenius plot for RCM ignition delay data of stoichiometric *iso*-octane/air mixtures at 20 (±0.65) bar [62].

Autoignition experiments typically use pressure-time measurements as the primary diagnostic. Representative experimental traces are presented in Fig. 30 for reacting and non-reacting tests using *iso*-octane/air mixtures [62]. The air in RCM experiments is typically a synthetic blend of O_2 and N_2/Ar and non-reacting tests are performed by replacing the O_2 with N_2, since these gases have similar thermo-physical properties. The non-reacting tests provide an indication of the heat loss or heat gain experienced during a particular test, and can also be used to evaluate processes such as the evolution and extent of preliminary exothermicity, e.g., LTHR or ITHR [260].

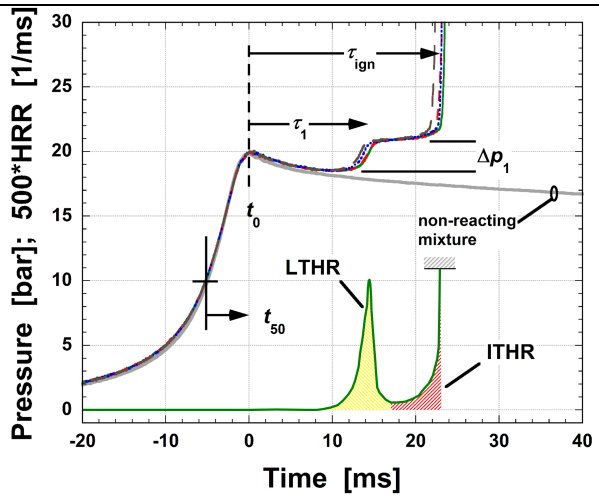

Figure 30. Representative experimental pressure-time histories, and associated derived heat release rates (HRR) for a stoichiometric *iso*-octane/air mixture [62]. The reactive tests include five individual experiments, with the derived HRR of just one shown.

In Fig. 30 the parameters t_0, t_{50}, τ_1, τ_{ign}, and Δp_1 are identified. The reference time, t_0, is often specified as the location where the pressure-time curve peaks during compression of a non-reacting mixture, though some other definitions have also been used [102,133]. The thermodynamic state conditions are typically evaluated at this point. The time shown here does not necessarily correspond to the end of piston travel, since at the elevated temperature conditions there is significant competition between heat loss and compression heating, so the pressure can begin to decrease before the piston motion is completely arrested. The piston typically stops moving 0.25–3.0 ms after *dp/dt* becomes negative, but this can be as long as 40 ms in some configurations. The parameter t_{50} is the time required for the last 50% of the pressure and associated temperature rise. This parameter is especially important for studies where highly reactive fuels are investigated in order to avoid the 'compression' limit, since the pressure and temperature of the reacting gas are significantly elevated near the end of piston compression. Low values of t_{50} are thus essential for preventing fuel reactivity during the compression process, and also reducing uncertainties associated with the evaluated thermodynamic state for a particular test condition. The time τ_{ign} from the reference time is the induction period, or ignition delay time, defined here where *dp/dt* is greatest. Studies have also used a pressure-rise threshold or ȮH emissions to mark the main ignition point. The intermediate time interval, τ_1, is defined based on the location of the inflection in the pressure trace, or the peak of the derived heat release rate (HRR), shown in Fig. 30 normalized by the lower heating value of the mixture, and may be observed for mixtures where there is substantial LTHR. As seen in Fig. 30, LTHR, which is quantified as the integral of the HRR curve during the first-stage peak,

and whose source is discussed further in Section 6, generally involves a sharp rise in pressure, Δp_1, , while ITHR, which can occur subsequent to, or without LTHR, involves a more gradual rise in pressure that results from coupled self-heating processes, but without a sharp inflection point preceding the main ignition.

4.2. Modeling

A number of options exist for modeling RCM experiments, where various levels of fidelity are used to account for facility influences and/or physical interactions that occur during a test. As discussed earlier, these interactions and influences can be moderate, like the piston trajectory used within a device and the diffusive growth of a laminar boundary layer, or they can be complex, with mixing and transport processes spanning a range of length and time scales, as with TCI studies. Realistic modeling of these along with detailed chemical kinetic representations can be straightforward, or it can be computationally intensive [261]. Detailed CFD studies conducted to date have highlighted challenges associated with accurately describing the laminar-turbulent transitional flows that exist within RCMs, and have indicated that low-fidelity turbulence models, e.g., Reynolds Averaged Navier Stokes *k-ε*, may be inadequate towards properly simulating this regime [148]. Few high-fidelity simulations have been reported which can replicate the physical characteristics, i.e., fluctuations, experimentally measured in some RCMs, such as the LIF measurements of [148], and further work using high-fidelity multi-dimensional simulations such as DNS [261] would help bracket physical phenomena. In many cases though, it is possible to describe the systems in terms of a limited set of thermodynamic parameters. These reduced-order models are generally classified as either homogeneous or non-uniform, and are discussed in detail next. The end of this section summarizes the state-of-the-art for modeling RCM experiments.

4.2.1. Homogeneous reactor models

Homogeneous reactor models (HRMs) utilize the simplest computational paradigm wherein the chemical reactions are assumed to proceed in a spatially uniform manner within the reaction chamber where the temperature and chemical composition are uniform, or at least that reactions are limited to a specified range of locations such as the core gas outside the boundary layer. In this case, only one state is needed to describe the reaction progress. Very limited physical interactions can be implemented with this approach, and generally only specific facility effects of piston compression and heat losses are taken into account.

Tizard and Pye [119,139] constructed the first HRM for an RCM. They utilized an energy balance or conservation formulation and incorporated heat loss using a linear expression for the heat loss.

$$\frac{d(Nc_vT)}{dt} = Q_K - hA(T - T_w) - p\left.\frac{dV}{dt}\right|_{\exp} \quad (1)$$

where N is the number of moles of gas, c_v the mixture specific heat at constant volume, T the temperature, Q_K the heat release rate due to reaction, $hA(T\text{-}T_w)$ the rate of heat loss from the gas with h representing the convection coefficient, A the surface area of the reaction chamber, T_w the wall temperature, p the pressure and $dV/dt|_{\exp}$ the experimentally measured rate of change of the reaction chamber volume. Linear, or Newtonian representations for cooling often assume spatial averaging across the thermal gradient that exists between the walls of the reactor and the hot gases so that the time-integrated thermodynamic state of the mixture corresponds to a volume-averaging of the gas within the reaction chamber. This is similar to a mixture-average temperature that results from application of the ideal gas law based on the measured pressure and volume of the chamber. The heat loss coefficient in [119,139] was determined based on non-reacting tests using inerts including air, and was adjusted for different operating conditions, as well as times past the end of compression. They did not consider the compression process within their simulations, and utilized single-step kinetics for the autoignition chemistry. Halstead and co-workers [262,263] followed a similar approach for their HRM where heat loss was also included as a linear term. The coefficients were determined empirically covering a wide range of conditions via non-reacting experiments, and expressed in terms of Reynolds and Grashof numbers. The piston compression process was incorporated within their analysis using simplified expressions for the measured piston trajectory. The compression process was segregated into three constant velocity intervals, where different values were used to approximate the acceleration, coasting and deceleration periods. Halstead *et al*. implemented a more complicated kinetic scheme using 11 reactions and 12 species, commonly referred to as the Shell model, which was able to replicate ignition delay times and two-stage ignition behavior seen in their RCM tests .

A number of later studies also employed an energy balance formulation, e.g., [264–266], however, it was subsequently demonstrated that volumetrically-averaged state conditions do not realistically represent the dominant, chemically reactive conditions experienced within the reaction chamber [267,268]. As such, significant discrepancies can arise between the HRM and experimental measurements.

Keck and co-workers [269,270] were the first to hypothesize that autoignition chemistry within the reaction chamber proceeds at faster rates within the hottest portion of the mixture, especially when Arrhenius kinetics are applicable. This hypothesis followed from analyses of end gas autoignition within

spark-ignited systems, e.g., spherical combustion vessels, and coincided with their development of piston crevices as a means to suppress the corner vortex development during compression, thereby segregating the colder boundary layer gas from the adiabatic core. Their HRM was constructed as an adiabatic reactor where the experimental pressure history was used, in conjunction with isentropic relations, to prescribe an effective time-varying volume, for both the piston compression and the subsequent delay periods. Their expression is presented in Eq. (2), where this is derived by rearranging Eq. (1) with the heat loss term eliminated, and the ideal gas equation of state is used to convert the volume rate change term into a pressure rate change.

$$\frac{dT}{dt} = \frac{\gamma - 1}{\gamma}\frac{T}{p}\left[\frac{Q_K}{V} + \left.\frac{dp}{dt}\right|_{\exp}\right] \quad (2)$$

Here, the total number of moles in the reactor is approximated as constant throughout the test. Park and Keck [270] suggested using an isochoric assumption, facilitated by setting $dp/dt|_{exp} = 0$, beyond the point of noticeable exothermicity in the test, defined as $dp/dt|_{exp} > 0$.

The adiabatic core approach has been the basis of most HRMs utilized over the past two decades, and is also frequently employed to estimate the thermodynamic state conditions for experimental tests, i.e., T_c, especially for comparison against other datasets, through Arrhenius diagrams. This is achieved by rearranging Eq. (2) with the heat release term set to zero and integrating from the initial, pre-compressed conditions at $t = 0$, yielding

$$\int_{T_i}^{T_c} \frac{\gamma}{\gamma - 1}\frac{dT}{T} = \ln\frac{p_c}{p_i} \quad (3)$$

where the subscripts *i* and *c* denote the initial and compressed conditions, respectively.

Numerous iterations and extensions have been proposed to the adiabatic core HRM for simulating RCM experiments. Minetti and co-workers [80] employed a simplified expression wherein the compression process is modeled using a frozen chemistry assumption, *i.e.*, there are no appreciable changes in composition or exothermicity, while the delay period is modeled under isochoric conditions. Wooldridge and co-workers [271,272] similarly used a frozen chemistry approximation during compression, with this assumption also extended into the ignition delay period in order to derive an effective thermodynamic state (i.e., T_{eff}, p_{eff}), which accounts for heat loss or exothermicity due to ITHR, as well as non-uniform ignition events, as discussed in Section 5. In this approach, the model simulations can then be initiated using the effective temperature and pressure as the starting point, with an isochoric condition applied.

Mohamed [273], Curran *et al*. [274] and others, e.g., [275] demonstrated experimentally and computationally, respectively, that under some conditions chemical reactivity during piston compression can significantly alter the autoignition process and thus induction times, even if the 'compression' limit, as defined in Section 4.1, is not strictly reached. This provides motivation to account for gas reactivity during compression within the simulations. Tanaka *et al*. [276] divided the compression process into two segments where the piston was assumed to travel at constant velocity through the majority of its displacement, with a constant rate of deceleration applied at the end of compression. The assumed velocities were selected to match representative experimental compression histories. During the constant volume period an analytical model was employed to simulate the growth of the thermal boundary layer within the reaction chamber and this was converted into an effective volumetric expansion of the adiabatic core. The constants for the boundary layer model were adjusted in order to match experimental measurements. Mittal and co-workers [268] used a similar approach for the compression process, but added a third phase of constant acceleration at the start of the piston motion. During the delay period they used measurements of representative non-reacting tests with the O_2 replaced with N_2, to directly specify the $dp/dt|_{exp}$ term in Eq. (2). This technique tends to provide very good replication of the pressure falloff due to heat loss without repeated tuning of the model constants. Gallagher *et al*. [277] and Healy *et al*. [278] utilized a similar method where non-reacting mixtures were compared directly against reacting ones, but in a coarser fashion the effective volumetric expansion was approximated by two or three constant velocity segments. Details concerning the implementation of these empirical approaches are discussed in Sung and Curran [39] where comparisons are made to simplified simulation methods, e.g., adiabatic, constant volume.

Refinements to the adiabatic core HRM since its inception have enabled more realistic accountings of piston compression and heat loss, and the influences that they have on the thermodynamic state of the reacting mixture, and thus, the progress to ignition. Some techniques however, can increase the number of tests that must be conducted during an experimental campaign to adequately prescribe the heat loss behavior for each mixture considered. Würmel and co-workers [146,279] demonstrated via CFD simulations and experiments that the pressure decay during the delay period can be significantly altered due to the composition of the test mixture and operating condition used, e.g., nitrogen versus argon as the diluent, so that many additional tests can be required. One approach to address this, as demonstrated by Lee and Hochgreb [141], is to formulate a multiple-zone, physics-based adiabatic core model that can be applied, after proper validation, to any variety of mixtures and test conditions. This model, a schematic of which is presented in Fig. 31, utilizes a single zone to simulate the chemical kinetics, while expressions

for the growth of the thermal boundary and mass flow to the piston crevice are used to account for the various physical processes that occur during the delay period.

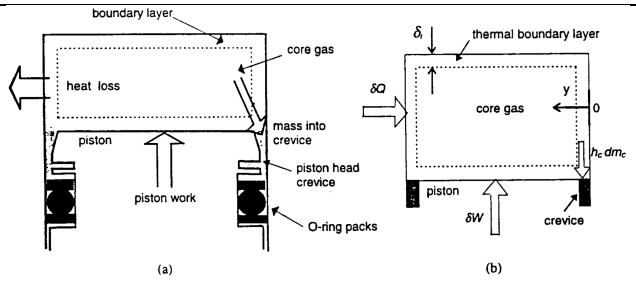

Figure 31. Schematic of (a) experimental reaction chamber and (b) multiple-zone HRM where δQ(<0) represents heat transfer through the wall, δW(<0) denotes work done by system, and dm_c mass transfer to the crevice volume (reprinted from [141] with permission of John Wiley & Sons, Inc.)

In this model the growth of the boundary layer depends on the thermal gradient at the reaction chamber wall; a non-dimensional expression was suggested in Lee and Hochgreb [141] to prescribe the temperature profile across the boundary layer. The rate of mass flow to the crevice depends on the pressure dynamics between the crevice and the reaction chamber, and it was assumed that the flow is fast enough such that no pressure differential can be established between the crevice and the main volume of the chamber. Lee and Hochgreb's formulation also assumed that the mass entering the crevice is immediately cooled to the wall temperature due to the large surface area to volume ratio that exists there. This model inherently implies that the corner vortex is completely suppressed by the piston crevice so that only diffusive heat loss occurs within the reaction chamber. Brett *et al*. [115] extended this model for tests exploring methane autoignition in an opposed-piston geometry.

Goldsborough *et al*. [280] developed enhancements to this multiple-zone HRM wherein many of the original assumptions were relaxed based on observations from detailed CFD simulations. For instance, the growth of the boundary layer in the reaction chamber was determined using a one-dimensional discrete application of the conduction equation so that the imposition of an assumed thermal gradient was not required. The flow rate into, and cooling of the gas in the crevice were based on more physically-realistic approximations using Reynolds- and Nusselt-based correlations, respectively. An approach was also formulated to account for the additional gas transfer into the crevice volume that occurs when there is significant preliminary exothermicity, e.g., LTHR, during a test [152]. As discussed in Section 2, these processes can substantially increase apparent ignition delay times under some conditions [85].

Another advantage of physics-based HRMs is that the boundary layer growth and penetration into the core can be directly monitored for each simulated condition. At long delay times the thickness of the

thermal layer can become significant and the 'loss of adiabaticity' limit may be reached, even if the reacting gas is not quenched. Furthermore, within the NTC regime the ignition delay time may be influenced by reactivity within the boundary layer, particularly after this region has sufficiently grown [140]. More detailed models may be appropriate under these conditions, as discussed next. Finally, once properly parameterized, physics-based HRMs can be used without the need to conduct non-reactive tests at each condition, so that their implementation can be more cost-effective.

4.2.2. Non-uniform reactor models

For RCM tests that explore non-uniform autoignition phenomena, there is a need way to account for spatial variations within the reaction chamber. Reduced-order, non-uniform reactor models are one approach, where these are less computationally expensive than for instance, large eddy simulation (LES) techniques. Such models can be classified as stratified or stochastic, where the former are focused on describing large-scale, one- or two-dimensional gradients, such as those due to non-uniform heating systems or diffusive boundary layer growth, while the latter are focused on small-scale, e.g., particle-by-particle inhomogeneities, such as those caused by turbulent mixing. Stratified reactor models, like the 'onion-layer', or 'concentric-balloon' model, have been applied to simulate RCM conditions in just a few studies [165], but there is an extensive literature on their application to modeling stratified autoignition in HCCI engines [281,282]. Potential exists for their use in various RCM studies, including autoignition chemistry investigations to address and reduce uncertainties under NTC conditions and long ignition delay times where the measurements can be significantly affected by boundary layer gradients [267,283][140]. Furthermore, this approach may be beneficial for tests employing advanced diagnostics (e.g., line-of-sight absorption spectroscopy), where boundary layer gradients have the potential to influence the measurements so that undertaking representative simulations could be important for interpreting these datasets.

Stochastic reactor models (SRMs) have recently been utilized to simulate conditions where turbulence effects are influential. Section 2 discussed ways that turbulence can be generated in RCMs for TCI studies. In addition, turbulent conditions have the potential to develop within the reaction chamber as a result of residual motion from the filling process or at the boundary layer interface, and due to compressive strain within the core, as discussed in [102,170]. Analogous scenarios can be found in shock tubes and flow reactors, and are sometimes taken into account when simulating such non-idealized tests [41]. In reduced-order SRMs, it is generally assumed that statistical homogeneity exists, meaning that the local distributions of composition and temperature are identical at all points throughout the reaction chamber.

These models are limited in the extent to which they can capture processes which are dependent on both small-scale and large-scale phenomena, such as mild ignition and knock, as discussed more in Section 5.

Strozzi *et al*. [126] employed a transported probability distribution function (PDF) approach, where molecular diffusion, chemical production, heat transfer and exothermicity perturb the statistics based on the local conditions. Monte Carlo methods can be used to solve the PDF equation, and Strozzi *et al*. employed 1,000 individual particles to achieve statistical convergence. A variety of approaches were investigated for addressing the micro-mixing process, and some results illustrating the influence of different sub-models are presented in Fig. 32. Particle heat transfer was conducted using a random walk approach and this was coupled to a mean convection term using the IC engine-based, Woschni correlation [284]. In their initial implementation, the authors assumed that the gas in the reaction chamber was initially homogeneous, so that all of the heterogeneities generated during a test were due to heat transfer alone.

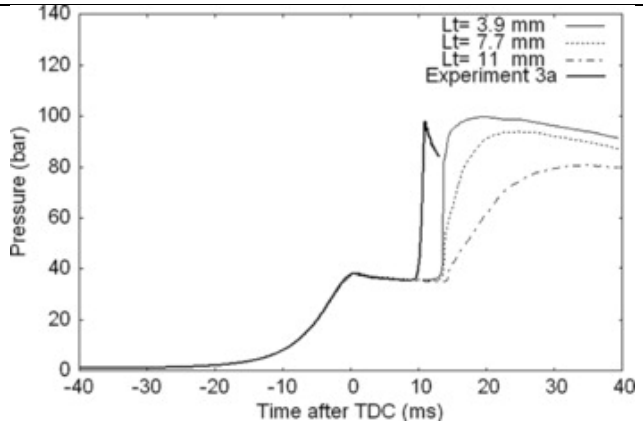

Figure 32. Comparison of experimental and simulated pressures for tests with methane/air mixtures where various molecular mixing sub-models are used in the SRM simulation. 'Lt' indicates the assumed integral length scale. T_c = 945 K, p_c = 38.4 bar, ϕ = 1, diluent:O_2 = 3.76 (reprinted from [126] with permission of Francis & Taylor).

Ihme [170] formulated an SRM in order to simulate the amplification of (presumed) velocity and scalar fluctuations due to piston compression. This reactor model captures the influence of rapid compressive strain on the production of inhomogeneities during a test, which is one way that small-scale non-uniformities can be generated. The model employed rapid distortion theory (RDT) to describe the evolution of initial distributions. RDT is an approach, based on linear analysis, for estimating how turbulent fields are distorted due to large-scale velocity gradients, bounding surfaces, etc., which are applied for a time shorter than the 'turn-over' time of the flow. The effects of heat transfer were not taken into account directly by altering the probability distribution function, for instance, but were

approximated during the delay period using a volumetric expansion model [276] which was easily coupled to the RDT approach. A Lagrangian Fokker-Planck method was employed to account for interactions amongst thermal and compositional inhomogeneities via turbulent mixing and diffusion. Closure was obtained via a k-ε formulation and an Interaction by Exchange with the Mean micro-mixing model. Due to the framework used for this reactor model, initial PDFs for velocity, temperature, and composition, must be specified, and there is some ambiguity associated with the initialization. Representative simulation results presented in [170] covered parametric variations with the reactor model to highlight influences of initial PDF specification, as well as machine operating characteristics, e.g., compression ratio, on the initiation and progress of autoignition for a syngas mixture. Although the necessary dimensionality is missing from this SRM, similar features, including shifts in ignition timing and global rates of pressure rise, were observed between the computed results and RCM measurements under conditions where mild ignition is present, *i.e.*, combined deflagrative/autoignitive combustion,.

4.3. Summary

Investigations of autoignition phenomena using RCMs encompass a variety of autoignition regimes, though the majority target adiabatic, strong behavior. While a range of reduced-order models has been utilized to simulate RCM experiments, a number of open questions remain regarding 'best practices', including the extent of uncertainties associated with various HRM approaches and the level of detail necessary to minimize these for various reacting systems, as well as how to most appropriately represent complex physical-chemical inateractions in a computationally-tractable. Though some attempts to compare different HRM methodologies have been undertaken [280][285], conclusions drawn are dependent on the thermodynamic state conditions, the operating characteristics of the RCM hardware, as well as the fuel/oxidizer/diluent composition. Some mixtures and state conditions are more sensitive to facility effects, such as the rate of piston compression and pressure decay experienced during the delay period, or inhomogeneities that may be present, while other reacting systems are less so. For instance, although Curran *et al*. [274] demonstrated a significant influence of the compression history on computed ignition delay times, if the low temperature chemistry portion of a model has much higher uncertainties associated with it than the intermediate temperature chemistry component [286], and the experiments are conducted at intermediate temperatures, achieved via compression from near-room temperature conditions, then the predictions could be perturbed in a complicated manner if the compression history is simulated. To date there are no definitive metrics or rigorous guidelines that can be used across a wide range of RCM conditions. Furthermore, there are still questions that remain regarding the use of reduced-

order models towards comparing datasets between different RCM facilities, as well as other experimental apparatuses. This is an area needing more investigation.

5. Studies of physical-chemical interactions

Whereas studies of autoignition chemistry represent the primary focus of modern RCM investigations and are discussed in detail in Section 6, some important work has considered physical-chemical interactions, often in specially-designed RCM configurations, as described in Section 2. Phenomena covered in this section include stratified autoignition, turbulence-chemistry interactions (TCI), mild ignition and knock. These classifications refer to a range of possible couplings between chemical reaction and transport. Stratified autoignition and TCI generally occur across different length/time scales, but are directly relevant to combustion processes in operating engines; for example, they can be used to control rates of heat release and pollutant formation in LTC schemes [162]. Mild ignition in RCMs, shock tubes and flow reactors has been observed for many years, and is associated with convolved deflagrative/autoignitive processes. It is identified as undesirable in studies of autoignition chemistry since it complicates the interpretation of datasets, and thus the evaluation and validation of chemical kinetic models [287,288]. The fundamental causes of mild ignition and its mitigation are of continued interest. Finally, knock can lead to unwanted engine noise, and result in structural damage and engine failure if not properly eliminated via operating conditions, fuel selection and/or combustion chamber design [289].

In this section, highlights of RCM studies of chemical-physical interactions are presented, starting with autoignition under stratified thermal and/or compositional conditions, followed by results of work focused on turbulence-chemistry interactions. RCM contributions to understanding the origin of mild, strong and mixed-mode ignition are presented next, and the section ends with a discussion of RCM investigations of knock phenomena.

5.1. Stratified autoignition

The presence of bulk thermal or composition gradients in combustion chambers can lead to localized autoignition. These stratified, or sequential autoignition events were explored by Iida and co-workers [163–167] using an optically accessible RCM, in order to understand the influences of bulk thermal and compositional stratification, as well as effects of fuel structure. Pressure and piston position data were recorded during and post compression, and chemiluminescence images were acquired using a high speed camera (10,000 frames per second or 10 kilo-frames per second (kfps)) with a resolution of 0.67 mm/pixel (improved to 0.40 mm/pixel in later tests). The details of their specialized experimental configuration were described in Section 2. The reactive mixtures utilized a very lean condition (ϕ = 0.17), while comparisons were made to non-reactive tests with air. For all of the reactive tests, autoignition and the

accompanying heat release occurred during the compression stroke, and this altered the piston dynamics by extending the seating duration, i.e., t_{50} changed from 25 ms to 35 ms for unreactive versus reactive experiments.

The tests utilized dimethyl ether (DME), *n*-heptane, *n*-butane and *iso*-octane as the fuels, with the first two selected due to their greater LTHR at the compressed conditions. For cases where there was no compositional stratification, the results indicated that DME and *n*-heptane are less influenced by thermal stratification, since ignition timings and rates of pressure rise were similar across the various conditions. The chemiluminescence images for these fuels demonstrated non-uniformities across the reaction chamber as the mixtures became more stratified, there was delayed autoignition in the cooler regions of the reaction chamber. Contrary to this behavior, *n*-butane and especially *iso*-octane experienced more noticeable differences in the pressure measurements where the ignition timings were shifted (*n*-butane, earlier, *iso*-octane, later) and the rates of pressure rise were reduced. The thermally stratified mixtures were seen to initiate heat release earlier, and had an overall slower heat release process. The chemiluminescence data for these fuels also highlighted changes in the spatial development of autoignition, again starting in the hotter portion of the charge and propagating from there. For the conditions explored in all of these tests autoignition is expected to initiate in the hottest portions of the mixture, since the NTC behavior is rather weak due to the very lean conditions. Differences in observed fuel response may be attributed to the fact that DME and *n*-heptane are more reactive and therefore autoignite earlier in the compression stroke, under conditions where the compressed pressure and temperature are lower and the magnitude of stratification across the reaction chamber is also lower.

For the compositionally stratified cases, only DME was used as the fuel, and the tests revealed that the interactions between thermal and compositional stratification are complex. For instance, at the $\Delta T \approx$ 25 K condition, in which the thermal and compositional gradients are in the same direction (positively correlated), ignited faster, while at the $\Delta T \approx$ 40 K condition, in which the thermal and compositional gradients are in opposite directions (negatively correlated), ignited faster. These features are probably influenced by the behavior of the NTC region for this fuel/air mixture. When simulated EGR was used, the positively correlated mixture ignited earlier and faster, while the negatively correlated mixture ignited later and took longer to complete the heat release process. Nevertheless, these characteristics have implications for controlling the autoignition and heat release rates for conventional and advanced combustion systems. For instance, under most fuel injection scenarios the thermal and compositional gradients are negatively correlated due to the vaporization enthalpy of the fuel.

5.2. Turbulence-chemistry interactions

Strozzi and co-workers [122,126,215] and Guibert and co-workers [113,240] studied the influence of turbulent fluid dynamics on the evolution of autoignition and interactions with flame front propagation under low and high turbulence conditions, respectively, where a range of advanced optical diagnostics were employed, including schlieren, PIV, PLIF and chemiluminescence (described in Section 3). Turbulent motion within the reaction chamber of RCMs, like in IC engines, can be quite different than in canonical configurations like swirl-stabilized flames, due to the presence of fluid–wall interactions and the ensuing generation of shear/mixing as well as thermal inhomogeneities.

Strozzi *et al*. [122,126,215] investigated TCI under conditions where the turbulent fluid motion and succeeding heterogeneities were generated solely due to vortex roll-up within a square cross-section RCM that did not utilize creviced pistons. PIV measurements indicated a maximum turbulent kinetic energy of 0.5 m^2/s^2 within the core of the reaction chamber at 2 ms before the end of compression. Pressure and piston position data were recorded during and post compression, and chemiluminescence imaging was acquired using a high speed camera (5 and 9 kfps)) with a resolution of 0.128 and 0.256 mm/pixel, respectively. Stoichiometric mixtures of methane/air were used in [122,126,215] at compressed temperatures and pressures of T_c = 926–945 K, p_c = 40 bar, respectively. Under these conditions no NTC behavior was expected, so the hotter regions within the reacting mixture are most reactive. The chemiluminescence data revealed the presence of ignition kernels at various locations within the mixture where these evolved during the heat release process. The data were post-processed using a binarization, front-tracking algorithm to determine local propagation velocities, with these corrected to account for thermal expansion of the burned gases. Analysis of the measurements indicated that some fronts propagated with high apparent velocities, near 40–80 m/s, while others had velocities that were moderate, near 5 m/s. The laminar burning velocity at the experimental conditions was estimated to be near 1 m/s. The results suggested different modes of front propagation, and so the PLIF-derived temperature fields were analyzed with the theory of Zeldovich [248], Gu *et al*. [249] and Sankaran *et al*. [290]. Fairly good correlation was found for the delineation between spontaneous autoignition and deflagrative propagation, except during the later stages of heat release, while these modes were significantly dependent on the local gradients in temperature and reactivity. Strozzi *et al*. [215] concluded that under the conditions they investigated, the low-intensity turbulent fields generated in their RCM only influenced the initial development of heterogeneities and thus ensuing global heat release rates, but had little, if any effect on the front propagation behavior, e.g., there was no wrinkling or smoothing of the fronts.

Ben Houidi et al. [291] followed this with investigations of TCI under NTC conditions. Lean (ϕ = 0.4) *n*-hexane and an *n*-heptane/methylcyclohexane blends were used at p_c = 12 and 15 bar, respectively, covering T_c = 700–900 K. As with their earlier work [215], they found that the reaction progress was not significantly influenced by the local turbulence levels, with most of the propagation done by compression waves having velocities on the order of 40–60 m/s, peaking near 1500 m/s. Both cool flame and hot ignition fronts were visualized, and these were observed to initiate in regions of highest reactivity, which could be either coldest or hottest zones, or even both.

Guibert *et al*. [113,240] investigated high turbulence conditions in their RCM using a reaction chamber that had a contracting geometry (relative to the bore of the swept volume), where perforated mesh plates were placed at the chamber's entrance. The intent of their work, like Strozzi *et al*. [122,126,215], was to identify various combustion modes during autoignition, and investigate the influence of turbulence scale and intensity on the combustion modes observed. They altered the turbulence field by changing the mesh hole size, while maintaining similar blockage ratios (~40%). The smallest holes generated higher levels of turbulence with accompanying faster rates of heat loss and pressure drop after TDC. PIV measurements indicated peak turbulent kinetic energies near 70 m^2/s^2 within the core of the reaction chamber, at 1 ms after the end of compression [240]. This is two orders of magnitude greater than the environment within the RCM used in [215]. Pressure and piston position data were recorded during and post compression, with chemiluminescence imaging acquired at 6 or 12.5 kfps using a spatial resolution of 0.1 mm/pixel. Histograms of luminosity were generated from the chemiluminescence data, and bimodal features used to identify the presence of flame fronts. Flame curvatures and PDFs were temporally tracked in order to quantify apparent displacement speeds of the flames, and how these can be wrinkled during the autoignition process. In Guibert *et al*. [113], propane and *iso*-octane were used as the fuels at ϕ = 0.45 and 0.35–0.50, respectively, with compressed conditions near T_c = 920 K and p_c = 35 bar. In Guibert *et al*. [240] four fuels were investigated including *iso*-octane, 1-hexene, primary reference fuel blend of 90% iso-octane / 10% n-heptane (PRF90) and methyl cyclopentane, with ϕ = 0.40 at compressed temperatures and pressures near T_c = 840 K and p_c = 38 bar. At the stoichiometries and state conditions of these studies, NTC behavior is relatively weak so hotter regions within the reacting mixture are expected to be the most reactive.

Guibert *et al*. [113] classified two modes of combustion during their tests. For the propane/air mixture, combustion initiated at a single location and spread in a front-like manner. For the *iso*-octane/air mixtures however, autoignition started at multiple locations, where these spread throughout the reaction

chamber and eventually merged. For both fuel mixtures, at the leanest conditions the displacement speeds increased slightly with time due to compression of the unburned mixture by the expanding burned gases. For the richest *iso*-octane/air mixture, the increases in displacement speed were more significant, while the reacting charge transitioned to volumetric autoignition before the front could consume the unreacted gas. The authors concluded that in the presence of significant turbulent fluid motion and thermal inhomogeneities, kinetic interactions can be important during all stages of combustion. For instance, once initiated, autoignition can enhance the level of inhomogeneity and thus more intensely couple physics and chemical kinetics, inducing volumetric and front-like combustion. Furthermore, with increased fuel loading the ignition times are faster and heat release is more significant, and this leads to a stronger coupling between turbulence and chemistry.

Guibert *et al*. [240] followed this work by more rigorously quantifying the influence of turbulent fluid motion on autoignition, with the fuels studied covering a wide range of ignition delay times, τ_{ign} = 7 to 178 ms. During the induction period the authors observed the turbulent kinetic energy of the mixture dissipated significantly due to wall shear. Furthermore, the PIV measurements highlighted vortex-flame-autoignition interactions. For instance, in the 1-hexene/air mixture, which had the shortest ignition delay times, regions confined by eddies in the flow experienced thermal runaway of the chemical reaction, and thus spontaneous volumetric ignition occurred over a small region of the test section. The ignition kernels significantly increased the local temperature, and thus thermal gradient, since the characteristic time of turbulent mixing dissipation was longer than the chemical time scale. The enhanced temperature gradient then favored the development of a propagation front, where the initially wrinkled front became smooth due to Lewis number effects. Differently, the *iso*-octane/air mixture, which had the longest ignition times, exhibited autoignition in a more volumetric manner, with slight spatial spreading, and this was due to thermal inhomogeneities initially present in the reaction chamber that were homogenized by the local turbulent heat dissipation rates during the induction period.

5.3. Mild ignition

Mild ignition and its causes have been extensively studied in shock tubes, while historical and recent work has also been undertaken using RCMs. Mild ignition refers to a convolved deflagrative/autoignitive process, but generally in a regime where turbulence interactions are weaker than the conditions targeted by, for example, the UPMC's RCM [113,240], i.e. weaker than the high turbulence, stirred uniform reaction regimes. Mild ignition has also been identified and labeled as 'weak ignition' in some literature. These events are characterized by the appearance of a single, or multiple flame kernels at various locations

throughout the reaction chamber, which grow into distinguishable flame fronts. The fronts are generally not cool flames (which are defined in Section 6), but are associated with chemiluminescence due to high temperature chemistry. Mild ignition can transition to strong, i.e., volumetric autoignition, or detonation in shock tubes, for instance when the end gas, or unburned mixture is sufficiently heated by the compressive action accompanying the initial rise in pressure. This evolution can lead to complex phenomena, including the generation of pressure waves, detonation and knock, which are discussed in the next sub-section. Preliminary exothermicity is often noted in the pressure and chemilluminescence emission during mild ignition events, but this is different than LTHR or ITHR. LTHR and ITHR, which are described more in Section 6, usually comprise about 2–15% of the heating value of the fuel, while pre-ignition heat release (PIHR) due to mild ignition and its associated deflagrative processes can be much larger, with fractions approaching 20–80% [292]. Measured ignition delay times during mild ignition events are generally shorter, indicating a difference in reactivity relative to the nominal compressed conditions, for example due to a hot spot. Finally, mild ignition can be associated with high variability or scatter in the measurements depending on the local conditions [288], and this highlights the stochasticity that can accompany the process. There can be noticeable differences between measurements in facilities where mild ignition is present, indicating an influence of machine operating characteristics.

Early studies by Teichmann [293] and Leary and co-workers [69,106], using their optically accessible RCMs, identified important factors governing the rise of mild ignition events, including the presence of thermal inhomogeneities. Taylor *et al*. [69] ruled out fuel condensation due to piston compression as a cause, but noted an influence of fuel loading, where leaner mixtures (e.g., $\phi < 0.5$) did not exhibit deflagrative events. Haskell and co-workers [96,294] highlighted potential catalytic effects of suspended contaminant particles within the mixture, via dust or within the fuel itself. Furutani *et al*. [238] identified flame-like structures in their optical experiments, for both cool flame heat release and hot ignition, where these were presumed to develop from thermal heterogeneities.

5.3.1. Shock tube observations

A brief discussion of important shock tube studies of mild ignition is presented here to supplement and provide insight into work undertaken on this subject using RCMs. The first detailed measurements of mild ignition were conducted by Saytzev and Soloukhin [295] using an optically accessible shock tube where they employed schlieren block photography and moving picture techniques for tests using H_2/O_2 mixtures, as well as inert gases. The tests covered p_c = 1–3 bar and T_c = 900–1700 K. At lower temperatures, they identified distributed combustion centers in the test section located away from the

endwall, which were seen to develop as a result of perturbations in the pressure and temperature fields within the gas behind the reflected shock wave. Local non-uniformities were observed in the inert gas tests; based on the resolution of their images and some simplifying assumptions, temperature variations were estimated to be on the order of ±10 K, or ±1%. Voevodsky and Soloukhin [296] used similar conditions, p_c = 0.5–4.0 bar and T_c = 800–1700 K, again with H_2/O_2 mixtures where they demonstrated that as pressures increased and temperatures decreased the ignition process transitioned from strong to mild. Chemical kinetic analysis was used and the transition was shown to correspond with the shift from chain-branching chemistry via $\dot{H}+O_2=\ddot{O}+\dot{O}H$ to degenerate-branching, or intermediate-temperature chemistry via $\dot{H}+O_2(+M)=H\dot{O}_2(+M)$, where this is described more in Section 6.

Oppenheim and co-workers [297,298][299] used a square cross-section, optically accessible shock tube to perform measurements employing stroboscopic, laser-schlieren imaging techniques to visualize spatial variations in the ignition process. In tests with undiluted, stoichiometric H_2/O_2 mixtures [297] covering p_c = 0.23–1.98 bar and T_c = 900–1350 K, they noted a transition from strong to mild ignition at higher pressure and lower temperatures, similar to Voevodsky and Soloukhin [296]. Localized exothermic centers were observed predominantly in the stagnant regions of the tube near the corners, where the reflected shock wave interacted with the boundary layer leading to bifurcation and the development of inhomogeneities [297]. Flame propagation was initially slow, with practically no pressure rise, but the reaction fronts transitioned to detonation waves as the tests progressed. Meyer and Oppenheim [297] argued that the shift from strong to mild ignition phenomena is predominantly thermo-physically based, influenced by the significant increase in ignition delay times at lower temperatures. For instance, as the degenerate branching controlled regime is approached for H_2/O_2 mixtures, induction times become longer and the tests are therefore more sensitive to temperature variations. Hot spots that form are able to react at significantly faster rates than the surrounding gas. At the same time, as a consequence of the longer induction period, transport phenomena acquire greater influence and this leads to the appearance of small flame kernels. Meyer and Oppenheim [297] constructed a regime diagram based on temperature and pressure, and they identified an empirical limit of $(\partial\tau/\partial T)_p$ = -2 μs/K which demarcated the transition from strong to mild ignition in their facility. This limit was found to roughly correlate with the transition from chain- to degenerate-branching ignition at their experimental conditions.

Vermeer *et al*. [299] and Cheng and Oppenheim [298] extended this work covering *n*-heptane/O_2/Ar, *iso*-octane/O_2/Ar and eleven blends of $CH_4/H_2/O_2$/Ar, respectively. For the *n*-heptane and *iso*-octane mixtures a mild ignition transition was found to occur when $(\partial \ln\tau/\partial T)_p$ = -0.012 and -0.008, respectively,

while the methane/hydrogen mixtures transitioned near $(\partial\tau/\partial T)_p$ = -0.2 to -0.7 μs/K, depending on the CH_4:H_2 ratio. Vermeer *et al*. [299] argued that the hydrocarbon fuels were better characterized by $(\partial \ln\tau/\partial T)_p$ gradients instead of by gradients of $(\partial\tau/\partial T)_p$ due to a coupling that exists between the pulse duration of the exothermic centers and the induction times, which they speculated was not correlated for the fuel blends containing H_2.

Additional experimental insight covering a wider range of fuels, including hydrogen, *n*-heptane, *iso*-octane, PRF blends, benzene, methanol and methyl tert butyl ether (MTBE), as well as *n*-decane, α-methylnaphthalene and DME, and at higher pressures was provided by Adomeit and co-workers [300–304]. They used a square cross-section, optically accessible shock tube rated to $p_c \approx 20$ bar, and a metal shock tube rated to $p_c \approx 50$ bar, and employed shadowgraph imaging techniques combined with pressure measurements and records of CH* emissions (430.7 nm), as well as data from thin-film heat transfer gauges. Their measurements highlighted spatial details of the convolved deflagrative/autoignitive processes, and the transitions to detonation in their devices. Ciezki and Adomeit [300] identified an initial, slowly rising pressure and no merging of the reflected shock and reaction front, while they noted the transition from strong to mild ignition was not abrupt for *n*-heptane, as was seen with other fuels, e.g., hydrogen [297], but occurred over a range of temperatures, where the deflagrative portion of ignition was usually followed by detonation with short transition times. Pfahl *et al*. [302] further described characteristics of mild ignition within their tests covering three diesel-relevant fuels, where they noted the high cetane rated fuels, *n*-decane and DME, more readily transitioned from deflagrative behavior to detonation, while higher temperatures, e.g., $T_c > 960$ K, were required for α-methylnaphthalene to make this transition. Fieweger *et al*. [303] constructed regime diagrams for benzene and *iso*-octane based on temperature and pressure, similar to Meyer and Oppenheim [297], where demarcations were identified between strong and mild ignition with the strong ignition cases classified solely based on whether or not the ignition process transitioned to detonation, even though many of the pressure records contained noticeable PIHR.

Blumenthal *et al*. [301] complemented this work with studies where they identified a range of multi-dimensional phenomena for mixtures using hydrogen, *n*-heptane and *iso*-octane as the fuels. Specifically, they studied the evolution of flame kernels starting at locations far from the endwall, along with ensuing deflagration and detonation waves. The development of spherical and planar waves was described in detail, and correlations between the visual records and recorded data from pressure transducers and photomultiplier detectors were noted. Blumenthal *et al*. [301] distinguished mild ignition from strong

ignition such that flame kernels were absent from strong ignition events. Based on this definition they concluded that over at least some portion of the thermodynamic range explored, all three fuels experienced mild ignition. Under some conditions, the mixture located near the transducer was completely consumed by the propagating deflagrative front, while in others the pressure rise due to the flame caused the gas in this region to volumetrically autoignite. *n*-Heptane was found to always transition to detonation. The behaviors observed in their tests were summarized by again creating a regime diagram using $(\partial\tau/\partial T)_p$ plotted as a function of temperature, with demarcations identified for strong ignition, planar ignition structures, and spherical structures. The strong ignition limit was correlated with a value of -2 μs/K, similar to Meyer and Oppenheim's boundary for hydrogen [297], but unlike Vermeer *et al*. [299], the derivative of the natural log was not used for the hydrocarbon fuels. For the results shown in Blumenthal *et al*. [301], only the low pressure (p_c = 3 bar) hydrogen tests yielded strong ignition behavior over an extensive portion of the temperature regime studied.

Finally, Fieweger *et al*. [304] discussed the influence of mild ignition events on data acquired for autoignition chemistry studies. For most of their dataset they identified deflagrative phenomena, where these transitioned to volumetric ignition and detonation under some conditions. Shortened ignition times relative to purely chemical kinetic processes were observed. Some times were estimated to be a factor of 10 faster due to the non-uniform, multi-dimensional deflagration processes. These phenomena can challenge the interpretation of data from a chemical kinetic perspective [305]. Fieweger *et al*. [304] argued however, that for tests that transition to detonation, the only interactions between the gas at the endwall and the deflagrating front were due to pressure couplings, so by assuming adiabatic compression of the end gas during the induction period to account for exothermicity in other portions of the reacting mixture, shifts or advancements in ignition timing could be taken into account. Formulating comparisons in this manner however, as discussed earlier, requires (at a minimum) access to pressure-time histories for such datasets, e.g., [306], and while it may improve comparisons with homogeneous reactor model calculations, it introduces additional experimental and modeling uncertainties. As such, a constrained reaction volume concept for shock tubes has been developed [307] in an attempt to eliminate mild ignition phenomena, whereby fuel is loaded only near the endwall of the driven section to minimize exothermic effects.

These shock tube investigations identified complex physical and chemical dynamics that influence mild ignition phenomena, where sensitivities to inhomogeneities in the mixture, impurities, wall properties, and the generation of local hot spots were highlighted. More recent experimental works have

extended these insights [308–311], and detailed simulation techniques have been used where the development and evolution of non-uniformities caused by gas dynamic processes, especially boundary layer interactions with the reflected shock wave and shock bifurcation, have been studied [86,312–314]. These phenomena become very important at long induction times. Gas dynamics are generally suppressed in RCMs due to the lower rates of gas compression employed, as highlighted in Section 2. However, inhomogeneities which facilitate mild ignition events can be generated by other mechanisms in RCMs and shock tubes.

5.3.2. RCM measurements

Wooldridge and co-workers have conducted the most extensive work to date using an RCM platform to study mild ignition. They investigated syngas (i.e., H_2/CO blends) [204,272] and *iso*-octane [213,315,316] as fuels. The configuration utilized for their work incorporated a fully accessible optical endwall to enable high speed imaging of the entire reaction chamber. Walton *et al*. [272] studied a wide range of syngas blends covering H_2:CO ratios from 0.25 to 4, with T_c = 855–1051 K and p_c = 7.2–26.7 bar. They used diluent:O_2 ratios near atmospheric conditions, with most of the mixtures near ϕ = 0.4. The pressure records for much of the data revealed noticeable PIHR, followed by a transition to volumetric ignition, but without detonation. The imaging data indicated that deflagration fronts propagated across the mixture starting at one or multiple exothermic centers in the reaction chamber. The visible emissions were noted to correspond with the gradual increase in pressure, preceding the main ignition event. These features can be seen in Fig. 33 where results from a representative test are illustrated. The transition for volumetric ignition occurs here after ~40% of the total combustion reaction enthalpy is released. For the leanest cases, no PIHR or chemiluminescence front were observed. Like Fieweger *et al*. [304], Walton *et al*. [272] suggested for modeling and analysis purposes the deflagrative portion of the ignition process, in particular PIHR, could be taken into account via empirical means, similar to argument by Fieweger *et al*. [304], but specifically by establishing an effective thermodynamic state for each test, as discussed in Section 4. They proposed a time-integrated average condition, beginning from the point of maximum piston compression to the time of maximum pressure rise rate. The measured ignition delay times in this work exhibited a change in activation energy below $T_c \approx 1000$ K, where this was in disagreement with a detailed chemical kinetic model used for comparison. The authors argued the discrepancy could be due to uncertainties in the model, most likely associated with $CO+H\dot{O}_2=CO_2+\dot{O}H$.

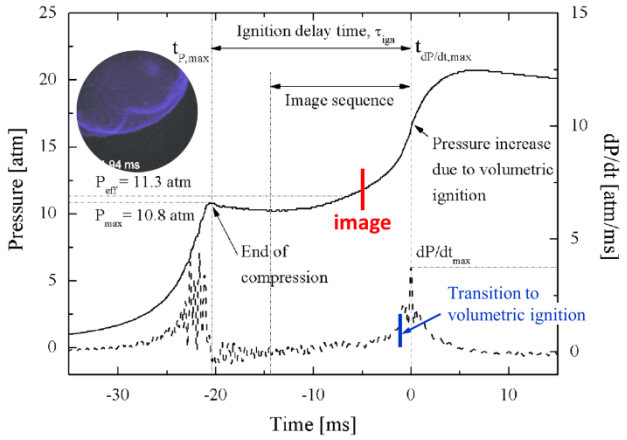

Figure 33. Representative pressure-time history illustrating mild ignition behavior where T_{eff} = 1004 K (see Section 4.2.1), ϕ = 0.4, H_2:CO = 0.25, diluent:O_2 = 3.76. The insert chemiluminescence image illustrates a deflagrative process emanating from localized autoignition near the upper portion of the reaction chamber. The timing of this image is indicated on the pressure trace, while the transition to volumetric ignition is identified on the *dp/dt* curve. (adapted from [272] with permission of Elsevier)

Walton *et al*. [213] investigated mild ignition using *iso*-octane as the fuel. They covered a narrow range of state conditions with T_c = 900–1020 and p_c = 9–15 bar, but used a wide range of fuel loadings with ϕ = 0.2–2.0 and diluent:O_2 levels from 1.4 to 5.9. As with the syngas work, some of the tests exhibited mild ignition and some did not. Effective thermodynamic state conditions were again derived from the measurements, and comparisons with a chemical kinetic model were shown. Using the chemiluminescence records, the speeds of the reacting fronts were estimated and compared with theoretical values, as proposed by Zeldovich [248]. For the theoretical calculations a temperature gradient of 3 K/mm was assumed, which corresponds to bulk gradients that have been experimentally measured in RCMs, as discussed in Section 3. The $(\partial\tau/\partial T)_p$ values for the calculations were based on the experimentally measured results, where these were observed to be reasonably close to predictions by the kinetic model. Poor agreement however, was seen between the measured and theoretically-calculated front speeds, with the measured values substantially greater than theoretical ones. On the other hand, the experimental velocities were found to correlate fairly well with fuel mole fraction. The influence of thermal diffusivity was also considered, and it was argued that mixtures with higher diffusivities should be less susceptible to mild ignition since local non-uniformities created during gas compression can be more effectively homogenized before localized ignition takes place. This hypothesis was evaluated using comparisons to select conditions reported by Fieweger *et al*. [304], and agreeable trends were noted.

Assanis *et al*. [315] investigated spark-assisted autoignition, or what could be considered as 'near' mild ignition conditions, where *iso*-octane was again used as the fuel. For this study a local hot spot was generated via high temperature plasma deposition using a conventional spark plug located on the circumferential wall of the RCM reaction chamber. The timings of the spark discharge were targeted to occur at the end of the first quartile of the chemical induction period. The spark discharge energy was kept constant between each test. Compressed temperatures and pressures covered T_c = 942–1012 K and p_c = 7.9–9.6 bar, with ϕ = 0.2–0.99 and diluent:O_2 = 3.76–7.47. Effective thermodynamic state conditions were derived from the measurements, as per Walton *et al*. [272], in order to account for PIHR in the data traces. Visual records and pressure measurements were made, similar to the previous works. The behaviors of the front propagation process under spark-ignited conditions were found to be comparable to mild ignition seen in the non-sparked, or spontaneous ignition tests studied in Walton *et al*. [272] and [213]. For instance, some mixtures were determined to be incapable of sustaining the imposed flame front, while others could easily do so. The authors labeled the former conditions as 'below flammability limit'. This categorization is analogous to the incapacity of, or propensity for mixtures to exhibit flame propagation during spontaneous ignition tests, as noted in early work by Taylor *et al*. [69]. The front velocities for each mixture were again determined using the chemiluminescence records, and these values correlated very well with the calculated adiabatic flame temperatures, in a manner equivalent to correlations observed with fuel mole fraction [213].

Mansfield and Wooldridge [204] further explored the delineation between strong and mild ignition for syngas mixtures by conducting tests in the University of Michigan RCM covering T_c = 950–1150 K and p_c = 3–15.2 bar, with two fuel loadings, ϕ = 0.1 and 0.5. A blend ratio of H_2:CO = 0.7 was used with diluent:O_2 = 3.76. To correlate their data the authors constructed regime diagrams using pressure and temperature, analogous to the work of Meyer and Oppenheim [297]. Results for two equivalence ratios were presented on two plots. For the higher ϕ condition, data from two previous shock tube studies, [301] and [317], were included in the diagram. Three theoretical approaches were employed in an attempt to explain the demarcation between strong and mild ignition regimes. The first analyzed the classical and extended second explosion limits for H_2/O_2 mixtures, as suggested by Voevodsky and Soloukhin [296]. At low pressure the demarcation agreed well with these limits, however at higher pressures the agreement was not good. The second method was based on the thermal sensitivity of the mixture, as suggested by Meyer and Oppenheim [297]. The gradient of ignition time with respect to temperature, $(\partial\tau/\partial T)_p$, was calculated for the H_2:CO = 0.7 mixture and isopleths were presented at the two equivalence ratios. Values of -700 μs/K and -40 μs/K provided reasonable agreement with the

transition for the ϕ = 0.1 and 0.5 mixtures, respectively. The third methodology compared the laminar flame speeds of the mixtures to the rates of reaction front propagation, where it was identified that the diffusive flame velocity must be large enough for the flame to propagate across the reaction chamber before the upstream, or unburned mixture can autoignite. This criterion was initially proposed by Zeldovich [248], and revisited by Gu *et al*. [249] and Sankaran *et al*. [250]. The reaction front propagation rates were estimated using an assumed thermal gradient, e.g., $(d\tau/dx)^{-1} = ((d\tau/dT)\times(dT/dx))^{-1}$, where this accounts for influences of molecular transport. It was postulated heterogeneous deflagration is more likely to be observed under conditions when the laminar flame speed is much faster than the rate of sequential autoignition, or reaction front propagation rate. Isopleths of presumed *dT/dx* were presented on the regime diagrams and these contours can be seen in the pressure-temperature diagram presented in Fig. 34. For both fuel loadings, it was found that thermal gradients near 5 K/mm, identified as a critical value of thermal sensitivity, correlated well with the demarcation between the strong and mild ignition regimes.

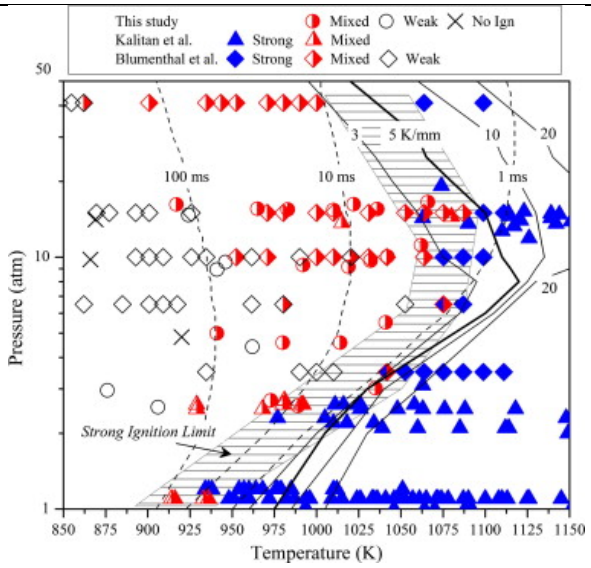

Figure 34. Regime diagram highlighting strong, 'mixed', and mild (termed 'weak') ignition for H_2/O_2 and syngas/air mixtures at ϕ = 0.5. The strong ignition limit is shown as the hashed area. Isopleths of thermal sensitivity of the ignition delay time calculated using the reaction mechanism of Li *et al*. [318] are shown as solid lines. Isopleths of ignition delay time calculated using the same reaction mechanism are shown as dotted lines. The strong ignition limit appears to correlate well with a critical value of thermal sensitivity. (reprinted from [204] with permission of Elsevier)

Finally, Mansfield *et al*. [316] extended their analysis to mixtures with *iso*-octane as the fuel. Experiments were conducted covering T_c = 740–1125 K and p_c = 3–30 bar, while focusing on ϕ = 0.25 and 1.0, with diluent:O_2 ratios near atmospheric levels. A second RCM was used in this work which had

different operating characteristics (e.g., pneumatic/hydraulic actuation vs. pneumatic/impact actuation), in order to complement the data. Both configurations had full optical access through the endwall, and high speed imaging of the tests was conducted along with measurements of pressure. Regime diagrams were constructed using pressure and temperature, while data from two previous shock tube studies ([299] and [304]) were included for comparison. Again, theoretical analyses based on Zeldovich [248], Gu *et al*. [249], and Sankaran *et al*. [250] were used to explain the transition to mild ignition at low temperatures and high pressures. The thermal gradients required to facilitate mild ignition were similarly estimated to be near dT/dx = 5–10 K/mm, and this gave good agreement between the three datasets.

Grogan *et al*. [257] and Im *et al*. [319] have proposed similar regime diagrams based on Damköhler and Reynolds number scaling that can be used as guides when conducting tests under conditions where mild ignition is possible. Figure 35 from Im *et al*. [319] utilizes two ignition Damköhler numbers, namely integral scale Da_ℓ and mixing scale Da_λ, the turbulent Reynolds number, and includes a sensitivity parameter, K, for the ignition delay which is based on the prior work by Zeldovich [248], Gu *et al*. [249] and Sankaran *et al*. [290]. This regime diagram was supported by data from [204] and by recent computational studies of syngas autoignition [292,320] where mild ignition due to local hot spots was investigated. As seen in Fig. 35, strong or volumetric ignition is predicted to occur when the mixture is dominated by turbulent mixing with low reactivity or low Da_ℓ, and when the mixture is dominated by reactivity, regardless of Reynolds number. Between the limit defined by the sensitivity parameter $Da_\ell = K^2$ and $Da_\ell = 1$, the diagram predicts mixed or weak (i.e., mild) ignition will occur. Figure 35 was proposed to serve as a general guideline to identify when combustion systems, not only within RCMs, are controlled by autoignition versus controlled by flame propagation, and this highlights the utility of fundamental RCM investigations.

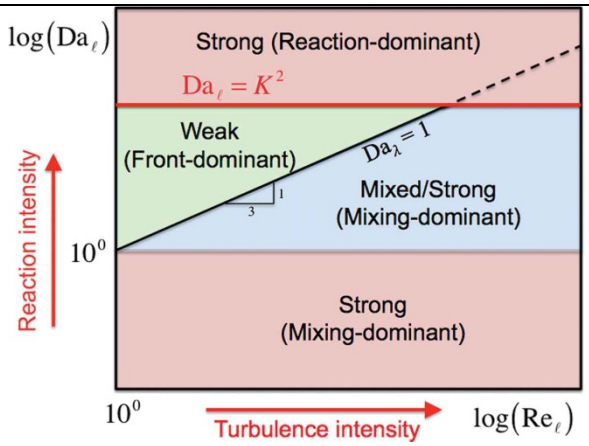

Figure 35. Generalized regime diagram for combustion modes indicating transitions between strong and mild ignition (reprinted from [319] with permission of Elsevier)

5.4. Knock

RCMs have been used as a well-controlled platform to study knock under both spontaneous ignition, as well as forced ignition conditions, *i.e.*, generated from a spark or other ignition source. The RCM knock studies reviewed here cover: (a) influences of fuel structure and autoignition chemistry, (b) flame-autoignition interactions, and (c) gas dynamic evolution after knock initiation.

5.4.1. Fuel structure and autoignition chemistry effects

Taylor et al. [178] acquired some of the first chemiluminescence images and pressure records using an RCM to study the influence of fuel structure and fuel loading on end gas autoignition and the development of knock. *n*-Heptane, *iso*-octane, benzene, triptane (2,2,3-trimethylbutane), and *n*-butane were used in mixtures with air at ϕ = 0.6–1.5, while the effects of tetraethyllead doping were also investigated. The compression ratio and initial temperature were varied to cover a range of compressed conditions, p_c = 20–30 bar and T_c = 750–1050 K. Most of the tests utilized spontaneous ignition of the gas mixture, though some tests employing forced ignition, via a spark plug located in the cylinder wall, were also conducted. Virtually all of the spontaneous ignition cases proceeded through mild ignition, with localized flamelets observed across the reaction chamber, where these compressed the unburned mixture to autoignition, with this followed by oscilations in the pressure trace. Due to the limitations of the data acquisition system, simultaneous visual and pressure measurements were not possible for most of the tests, and there were significant shot-to-shot variations caused by the thermal inhomogeneities within the reaction chamber [106]. Nevertheless, Taylor et al. [178] discussed the influence of fuel structure, and progress of heat release from the flamelets before the initiation of knock.

Affleck and Fish [71] conducted one of the earliest detailed RCM-based investigations into the causes of knock where they employed stoichiometric mixtures of 2-methylpentane/air at p_c = 20 bar and T_c = 653, 743 K. The lower temperature is within the low-temperature chemistry regime where the timing of first-stage heat release, τ_1, is close to the main ignition point, τ_{ign}. The higher temperature is near the transition to NTC chemistry where there is a noticeable time lag between the two stages of ignition, as was identified for the *iso*-octane/air data presented in Fig. 2. They compared the behavior of spontaneous ignition events with forced ignition events, and classified the behaviors as either non-knocking or knocking. A range of knocking behavior was achieved from light to heavy. The spark probes were centrally located in the reaction chamber and they acquired emissions records via spectral filtering techniques, while they also sampled the product gases with analysis conducted using a gas chromatograph coupled with a flame ionization detector.

The emissions records identified OH* at 306.4 nm, and there were lines associated with the metals that had been removed from the reaction chamber walls, e.g., nickel, especially during knocking conditions. Under spontaneous ignition conditions OH* emission was visible, but weak, while under spark-ignited and knocking conditions the OH* emission intensity grew significantly. The GC analysis identified both hydrocarbons and oxygenates as the organic products resulting from spontaneous ignition. C_2 hydrocarbons were the major constituents, along with smaller yields of propylene, *iso*-butene, isopentane, hexenes and benzene. Oxygenates included acetone, butanone, propionaldehyde, isobutyraldehyde, acrolein, methacrolein, 3-methyloxetan, 2,2-dimethyltetrahydrofuran, 2,4-dimethyltetrahydrofuran, methyl vinyl ketone, and larger saturated and unsaturated ketones. Under sparked conditions with no or minimal knock, no oxygenates or products typical of first-stage ignition were formed in detectable concentrations. However, as the intensity of knock increased, products associated with spontaneous ignition were observed with increasing concentration. The results supported the idea that knock in IC engines is primarily related to autoignition of the end gas, as opposed to DDT phenomena.

Griffiths and Nimmo [179] investigated the influence of fuel structure by comparing the knocking tendencies of *n*-butane and *iso*-butane using stoichiometric mixtures with argon as the diluent, at p_c = 10 bar and T_c = 900 K. The mixtures were not ignited by a spark, but proceeded through spontaneous ignition. The authors acquired pressure-time histories (200 kHz) and visualization data through the endwall, using high speed photographs recorded at 6 kfps. Under the conditions they explored, the *n*-butane mixtures were more reactive, with measured τ_{ign} approximately half of the value of the *iso*-butane mixtures. The

data for both fuels indicated the existence of localized flame kernel development and propagation, along with associated PIHR. As discussed previously, these processes can evolve due to thermal non-uniformities within the reaction chamber. The authors found that the *n*-butane mixtures more easily transitioned to rapid heat release where a greater portion of the reaction enthalpy was released simultaneously, after which acoustic waves with large amplitude ensued. For the *iso*-butane mixtures, most of the reactants were consumed by propagating flamelets by the time chain-thermal explosion occurred so that no gas dynamic phenomena ensued.

Griffiths and co-workers [74,180,181], subsequently investigated the thermokinetic interactions leading to the development of knock in three related spontaneous ignition studies. They sought to better understand how the chemical kinetic evolution of ignition influenced the development of gas dynamics within the reaction chamber. Schreiber *et al*. [180] studied stoichiometric mixtures of *n*-heptane/air at p_c = 8 bar. Griffiths and Whitaker [181] utilized lean *n*-pentane/air mixtures (ϕ = 0.5) at p_c = 12.8–14.8 bar. And Griffiths *et al*. [74] used *n*-pentane/air mixtures over a wider range of stoichiometry (ϕ = 0.6, 0.7, 1.0) at two initial pressure ranges yielding p_c = 7.9–8.4 and 13.8–14.8 bar. A range of compressed temperatures was targeted covering the transition from low temperature chemistry to NTC chemistry, i.e., T_c = 650–950 K for *n*-heptane, and T_c = 690–820 K for *n*-pentane, where the diluent gas composition was modified to achieve these conditions. The transition from low temperature chemistry to NTC behavior for the *n*-heptane and *n*-pentane mixtures occurred near T_c = 740–760 K. Pressure-time histories were acquired (200 kHz, in the critical interval of interest) and accompanied by single-shot chemiluminescence photographs of the *n*-pentane tests, taken at various times during the first and second stages of heat release. Spectral filters distinguished spatial locations associated with CH*, C_2* and CH_2O*. Filtered Rayleigh scattering was used in Griffiths and Whitaker [181] to ascertain the relative temperature distribution across the reaction chamber at successive times during the autoignition process. In all of the *n*-pentane tests, thermal inhomogeneities were identified within the reaction chamber at the beginning of the induction period, and this was ascribed to the rollup vortex generated in their flat piston configuration [74,181]. The lowest temperatures outside the boundary layer were located at the center of the reaction chamber (at around 1 ms after the end of compression), and were approximately 50 K cooler than the surrounding gas. For the *n*-heptane tests, most of the pressure-time data indicated the presence of substantial PIHR.

For the two fuels, covering a range of stoichiometry and pressure, the measurements revealed at the lowest compressed temperatures there was minimal gas dynamic development at the point of main

ignition. However, as the compressed temperatures increased, proceeding through the point of minimum τ_{ign}, i.e., entering the NTC region as seen in Fig. 36a, the behavior transitioned to intense pressure ringing, or knock. This became severe at the highest temperatures, as seen in Fig. 36b. The emissions records suggested there were differences in the predominant chemistry associated with the final stage of knocking reaction, as compared to conditions where knock was not observed. For instance, at T_c = 722 K without knock, the degree of uniformity in the chemiluminescence records implied chemical reaction continued to be driven by $H\dot{O}_2$ reactions late into the main heat release. On the other hand, at T_c = 792 K with heavy knock, the second stage of ignition which was induced close to the wall of the reaction chamber, as a consequence of the preceding interactions between the chemical kinetics and fluid mechanics, was able to develop very rapidly to hot ignition through an early transition to Ö atom chain branching. At these conditions, there was a dramatic growth in activity over an interval that was neither uniform spontaneous ignition nor smooth flame development. Griffiths and co-workers [74,181] argued that their results suggested that the development of knock is connected to the competition between $\dot{H}+O_2(+M)=H\dot{O}_2(+M)$ and $\dot{H}+O_2=\ddot{O}+\dot{O}H$ near the point of main heat release, with the latter leading to knock. The production of $H\dot{O}_2$ is favored at lower temperatures, and the stronger pressure dependence of this reaction suggests the $H\dot{O}_2$ propagation route is sustained to higher temperatures when higher pressures prevail.

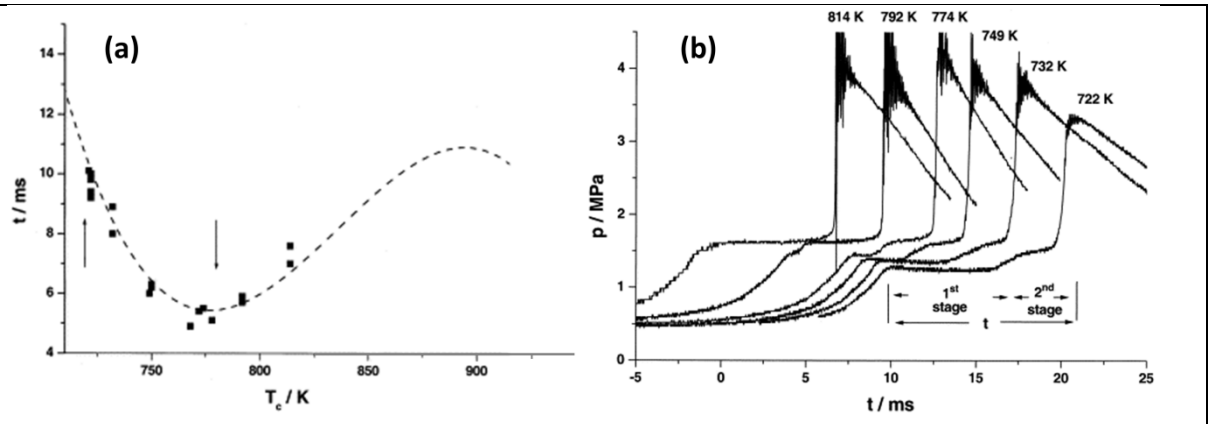

Figure 36. Influence of temperature and associated autoignition chemistry on the evolution of knock during spontaneous ignition tests with *n*-pentane/air with ϕ = 0.5, at p_c = 12.8–14.8 bar. (reprinted from [268] with permission of Elsevier)

Tanaka *et al*. [189], in a study similar to Griffiths and Whitaker [181], investigated knock development from unforced ignition using an optically accessible RCM. They used *n*-heptane as the fuel with diluent:O_2 = 3.76–5.64 covering a range of stoichiometry (ϕ = 0.38–2.0). In their configuration, the fuel was injected directly into the reaction chamber, after which heated O_2 and diluent gases were supplied. The compression process was initiated after a dwell time of 300 s, which suggests thermal and compositional stratification may have been present at the start of piston compression. Three compression ratios were

used to cover p_c = 9.8–14 bar and T_c = 678–736 K. High speed images were acquired (9 kfps) using a Bowditch-style piston, and laser extinction measurements were made via a He-Ne laser directed through the side wall. The imaging measurements indicated that the spontaneous ignition process was not uniform, due to gradients generated by their uncreviced piston, as well as the mixture preparation process. The authors found some of the tests produced strong knocking conditions, as a result of thermokinetic interactions, while others did not. They created a regime diagram as a function of compressed temperature, stoichiometry and extent of dilution, where the resulting transition between non-knocking and knocking behavior corroborated the findings of Griffiths and Whitaker [181], while mapping the behavior over a much wider range of test conditions.

5.4.2. Flame–autoignition interactions

Hayashi *et al*. [182] used an optically accessible rapid compression expansion machine (RCEM) to investigate flame-autoignition interactions where a spark plug located in the cylinder wall was used to force ignition. The spark timing was varied from 60 to 120 degrees before TDC (i.e., 12–25 ms before the end of compression), where $\tau_C \approx 40$ ms. They used mixtures of *n*-butane/air with a narrow range of stoichiometry, ϕ = 0.9–1.1, at compressed conditions (without spark) near p_c = 20 bar and T_c = 650–800 K. High speed color photographs (3 kfps) and schlieren images (100 kfps) were acquired during heavy knocking events. The color images showed a blueish flame produced near the spark which expanded in a circular fashion, increasing in brightness as the pressure increased. When knock started, the unburned region flashed white and expanded into the blue-colored burned region, after which the whole reaction chamber became white. This was followed by radiation indicative of soot. The schlieren images revealed the flame propagation through the mixture, until the point where the end-gas autoignited, followed by pressure waves into the unburned and burned regions. The wave speeds were estimated to initially be near 1300–1500 m/s, which was greater than the sonic velocity of the mixture. As the waves reflected at the far cylinder wall, the propagation magnitude was reduced to the sonic speed.

Pöschl and Sattelmayer [168] followed this work by investigating the influence of large-scale thermal stratification on knock, also using an optically accessible RCEM. They used PRF69 with air at stoichiometric proportions. A range of compression ratios was employed to achieve compressed conditions near p_c = 15–20 bar and T_c = 750–900 K. The mixture was thermally stratified before compression by means of a non-uniform heating system, so a temperature difference of ΔT = 10–20 K was achieved from one side of the reaction chamber to the other. No piston crevice was used in their machine, but the authors conjectured only small-scale turbulence was generated during compression, though no accounting for

piston-induced bulk fluid motion was made. Pressure-time histories were recorded, along with high speed imaging (87.6 kfps) through a Bowditch-style piston and via fiber optics integrated into the endwall (250 kfps). Spontaneous and forced ignition were explored where the latter was achieved by a single spark plug positioned at different locations on the endwall. The three arrangements of the spark allowed the authors to investigate the influence of igniting the mixture in the cooler or hotter portions of the charge.

For the spontaneous ignition conditions it was observed that when ignition started in the hotter portion of the mixture, reaction fronts propagated through the unburned gas with velocities near 50–200 m/s for the cool flame, and near 500 m/s for the hot ignition. The observations were considered indicative of a stratified, or sequential autoignition process, which can propagate at much greater velocities than diffusive/transport limited, flame processes, as discussed in previous sections. Under these conditions, there was no generation of gas dynamic waves within the reaction chamber. For the forced ignition conditions, the authors found severe knocking could most easily be generated when the mixture was sparked in the cooler portion of the charge. Under this scenario the spark-ignited flame could interact with the evolving autoignition front leading to the development of a detonation wave with velocities near 1400 m/s. The pressure waves could be reflected and focused at the nearby convex wall, and then passed through the reactive gas mixture that had high concentrations of radicals and intermediate species, where a bidirectional coupling of the pressure wave and heat release could develop. Such a coupling mechanism has been discussed extensively in the literature, and is often identified as shock wave amplification by coherent energy release, or SWACER [321].

Katsumata *et al*. [183] used an optically accessible RCM ($\tau_C \approx 5$ ms) to investigate forced ignition conditions where a spark probe was inserted into the reaction chamber to generate a spark near the cylinder wall, or in the center of the reaction chamber. The spark was timed to occur during the compression stroke. They used a range of PRF blends from 0 to 90, at stoichiometric concentrations in air, and varied *CR* and T_i to achieve a number of compressed conditions covering T_c = 600–900 K and p_c = 20–30 bar. Both schlieren imaging (45 kfps) and direct photography techniques (180 kfps) were used. The schlieren imaging revealed effects of LTHR in the end gas on flame propagation, specifically wrinkling of the flame. In both spark configurations, they observed SWACER features as spontaneous ignition was induced near the walls of the reaction chamber, similar to the observations of Pöschl and Sattelmayer [168]. It should be noted that SWACER has also been identified in recent LES studies of knock and superknock [26], and this highlights the similarity of the physics within RCMs and those in IC engines.

Wang and co-workers [184–186] also investigated knock under both spontaneous and forced ignition conditions using an optically accessible, single-piston RCM. *iso*-Octane was used as the fuel and this was blended at stoichiometric proportions with either argon [184] or nitrogen [185,186] as the diluent. Pressure data were recorded at 100 kHz, while high speed images were recorded at 45 or 288–360 kfps, respectively. Higher resolution was used under the lower frame rate conditions, e.g., 0.1 mm/pixel versus 0.45 mm/pixel, respectively. Wang *et al*. [184] studied the evolution of knock for situations where combustion is initiated locally due to random suspended particles or thermal non-uniformities, i.e., a hot spot. The nominal compressed conditions were T_c = 930 K and p_c = 20 bar, on the high temperature side of the NTC region. The ignition timing observed during the tests, if due to hot spot initiation, suggested a local temperature about 2–3% greater than the surrounding gas. The authors reported that out of hundreds of tests performed, only a few initiated inhomogeneously, and they argued this behavior was similar to the sporadic nature of superknock. The visual images indicated three distinct stages of combustion. After initial flame kernel formation in the adiabatic core, a deflagration phase ensued where the flame propagated through the bulk mixture with a velocity near 11 m/s. As the flame neared the cylinder wall, the end gas autoignited, and within a period of 20 μs a detonation front formed, and the detonation front then propagated around the circumference of the reaction chamber with a velocity close to 3100 m/s (Mach number = 5.5). Since the Chapman-Jouguet detonation velocity was estimated to be near 2300 m/s, the authors concluded this front was a strong detonation wave. When the remaining unburned mixture was consumed by the detonation front, the waves were reduced to the sonic velocity with pressure oscillations that continued for 3 to 5 ms. The combustion behavior observed in the RCM tests was argued to be similar to superknock, where the timings of deflagration and autoignition kinetics must match so a detonation front can be initiated at just the right time in the cycle; otherwise, the end gas autoignition wave is too weak and leads to only sonic waves.

Qi *et al*. [185,186] followed this work to better understand and quantify the requirements necessary for detonation within the reaction chamber. They used forced ignition conditions and employed a commercial spark plug where the electrodes were extended to the central portion of the reaction chamber. The spark timing was controlled to within 1 ms after the end of compression. The compression ratio of the machine was adjusted to cover T_c = 640 to 730 K, with p_c = 10–30 bar. The compressed conditions were used to represent boosted spark-ignited engines, and differently from their earlier study [184], are in the low temperature autoignition regime for *iso*-octane, i.e., before the transition to NTC chemistry. In this regime there are only small changes in ignition delay time due to pressure differences; however, as the system proceeds to end gas autoignition this feature becomes more complicated, since

the end gas is compression heated into the NTC regime. The pressure and high speed imaging data of this work also indicated three stages of combustion, with two modes of end gas autoignition identified, both of which occurred in the near-wall region. Sequential autoignition with no detonation was detected via high-pass filtering of the image sequence where the luminosity variations could be extracted. They found under these conditions, no flame front propagated after autoignition, although the area associated with autoignition increased and small pressure waves were initiated. Detonation, on the other hand, was detected by extreme pressure rise rates (6.5 kbar/ms), while the imaging sequences revealed front propagation rates were close to 1900 m/s, near the calculated Chapman-Jouguet detonation velocity of 1870 m/s. The authors compared these measurements to the detonation theory of Kalghatgi and Bradley [27] and found the results were consistent with the deflagration-detonation regime diagram described by Gu *et al*. [249]. They noted also, as Pöschl and Sattelmayer [168] did earlier, that the pressure wave initiated due to autoignition could interact with the reaction chamber wall, resulting in what they termed shock wave reflection-induced detonation. The authors also correlated their data to the thermodynamic conditions used in the tests, and identified a threshold energy density of ~17.5 MJ/m^3 required to initiate sequential autoignition, while ~20 MJ/m^3 was required to initiate detonation under their experimental conditions.

Tanoue *et al*. [188] used an optically accessible RCEM to study flame-autoignition interactions, and the transition from sub-sonic to detonation waves during forced ignition events. *n*-Butane:DME fuel blends were used at molar ratios of 0, 0.25, 0.50 and 0.75, where DME was employed to decrease the knock resistance of the fuel. Stoichiometric ratios were used and compressed conditions near p_c = 30 bar and T_c = 700 K were targeted. For their tests an ignition plug was located in the cylinder wall and used to ignite the mixture at 20° before TDC (i.e., 5.1 ms before TDC). Chemiluminescence images were recorded using a high-speed camera and local flame propagation speeds were deduced via image-processing software. The authors noted for all four fuel blends the initial flame speeds were near 5 m/s, and an initial autoignition event close by the ignition plug propagated circumferentially along the cylinder wall at a much higher velocity, near 22–28 m/s. This was interpreted as a subsonic autoignition front. After much of the charge had been consumed, a second autoignition event was observed far from the ignition plug, where this propagated at a velocity near 130–520 m/s, which was close to that of a developing detonation front. The detonation theory described by Gu *et al*. [249] was used to interpret the data, and the knock intensities were demonstrated to be well correlated to the non-dimensional ratio of the autoignition propagation velocity and the sound speed. The data also agreed with the detonation peninsula described by Bradley [322].

5.4.3. Gas dynamic evolution

Kono *et al*. [107] used a single-piston machine with endwall optical access to investigate gas dynamic evolution initiated by forced ignition where blends of diethyl ether / acetone (1:0, 1:0.5, 1:1.5, 1:4.5) were used in stoichiometric concentrations with air at p_c = 19 bar and T_c = 446 K. The diethyl ether was selected for its two-stage ignition behavior. The mixtures were spark-ignited from the side of the cylinder opposite the pressure transducer. The pressure data, recorded at 200 kHz, were analyzed using a Fast Fourier Transform (FFT) method after the main ignition event in order to discern the characteristics of the acoustic energy. They found that the knock intensity, represented by the total acoustic energy, was inversely dependent on the extent that flame propagation had been completed before the onset of end-gas autoignition. Furthermore, most of the energy was contained within the first tangential mode, corresponding to knock typically seen in IC engines [323].

Qi *et al*. [187] also studied the evolution of gas dynamics under forced ignition conditions within an optically accessible RCM. They utilized a commercial spark plug located in the wall of the reaction chamber with stoichiometric mixtures of *iso*-octane/air where the geometric compression ratio of the machine was set to 11.35. The compressed temperatures were close to T_c = 645 K, while three compressed pressures were investigated, p_c = 17, 19.5, 23 bar. The higher pressures were used to increase the intensity of knock, which was consistent with their later work [186]. The pressure measurements were recorded at 100 kHz, and chemiluminescence measurements were recorded at 288 kfps. The signals were post-processed just after ringing onset, analyzing the frequency domain of both the pressure records and the chemiluminescence images with a pixel-by-pixel technique. The images provided spatial detail concerning local pressure and temperature fluctuations since the pixel sensitivity captured small variations in luminosity. The FFT analyses indicated discrepancies between the optical signals and the pressure records, which the authors attributed to the recessed mounting of the transducer. In agreement with Kono *et al*. [107], the FFT analysis also indicated, that the dominant acoustic mode of the gas dynamics was the first tangential mode, while the second tangential mode was also important, particularly at the intermediate pressure condition investigated. Via the high speed images, the authors also detected soot incandescence near the wall of the cylinder, near the point of knock initiation, which they hypothesized to be due to fuel pyrolysis within the crevice volume caused by the intense pressure waves.

5.5. Summary

Summary of stratified autoignition

Summary of turbulence-chemistry interactions

Mild ignition can complicate the interpretation of autoignition data. The shock tube and RCM-based studies reviewed here illustrate complex phenomena and how they can influence experimental measurements of autoignition chemistry. Fundamental insight has been gained indicating that some fuels and mixtures are more susceptible to the evolution of deflagrative behavior, while the critical thermal gradient necessary to facilitate mild ignition within the mixture appears to be very low, and even near levels that have been experimentally measured within the adiabatic core of well-controlled reaction chambers, i.e., those utilizing creviced pistons. Based on this, it is evident that care must be taken when conducting tests under conditions where mild ignition is possible, and diligence should be used in identifying these events.

The knock studies reviewed here illustrate complex phenomena associated with knock initiation and development. The findings highlight that knock fundamentals in RCMs closely reproduce those observed within operating IC engines, and potential exists for investigating still-open questions related to knock including the generation of localized exothermic centers, the characterization of large- and small-scale structures, as well as the ability to adeaquately model relevant processes for engine design purposes. Experimental measurements under these extreme conditions however, can be challenging. At a minimum, kilohertz imaging and pressure diagnostics are necessary to allow access to very high speed phenomena that occur during knock, while the thermodynamic conditions and localized pressure spikes can lead to serious equipment damage. Furthermore, observations of Qi *et al*. [187] raise concerns that soot can form during heavy knocking tests with or without forced ignition, and contaminate the surfaces of the reaction chamber, particularly for undiluted, high pressure conditions. This finding is relevant to autoigntion chemistry studies at high fuel loading conditions.

6. Studies of autoignition chemistry

Much of what we know today about autoignition chemistry has emerged from RCM studies where the device time scales are amenable to reaction time scales at relevant conditions, as described in the Introduction. This section details the vast array of knowledge developed, complementing other experimental platforms and covering a range of fuels using RCMs, progressing from discussion of RCM results for fuels with the simplest-structures, H_2 and CO, to discussion of systematically more complex fuel structures, specifically alkanes, alkenes, aromatics, oxygenates and closing with a discussion of RCM studies of real fuels and fuel additives. In this context, it is useful to consider the series of reaction pathways leading to autoignition at LTC conditions, typical for many fuels, which have been extensively discussed in [324–326], and are illustrated in Fig. 37. At temperatures below about 1200 K, reactions with the fuel molecule, RH, are usually initiated via abstraction of a hydrogen atom from the fuel (R1). O_2 and a variety of radicals, e.g., ȮH, $HȮ_2$, can participate, yielding an alkyl radical, Ṙ, and products such as $HȮ_2$, H_2O, and H_2O_2. In systems with low concentrations of active radicals, the initiation reactions are thought to occur between the fuel and molecular oxygen, which then forms a hydroperoxyl radical, $HȮ_2$, as the product.

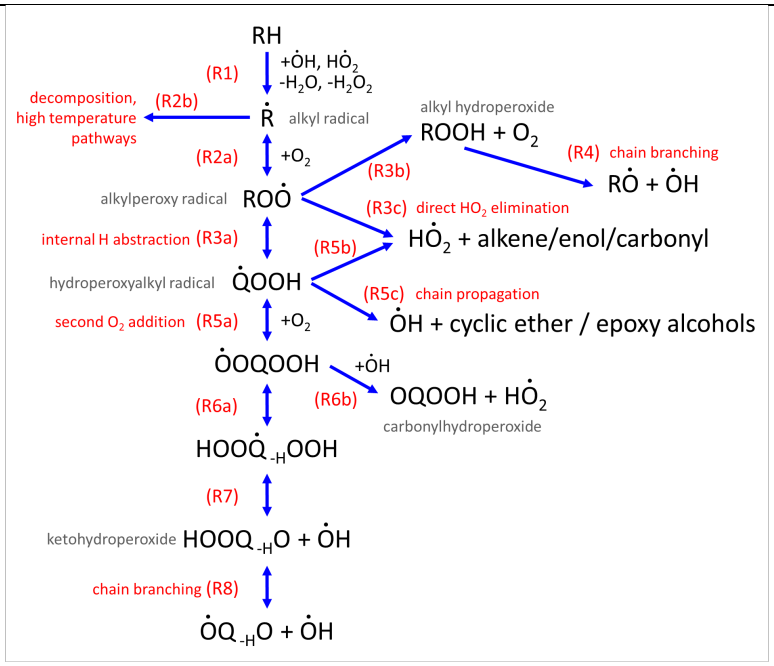

Figure 37. Classical reaction scheme for LTC oxidation of many hydrocarbon fuels, RH, adapted from [325].

At temperatures as low as 500–600 K, the fuel-derived alkyl radicals react rapidly with O_2 to form alkylperoxyl radicals, ROȮ (R2a), which can lead, through various transformations as marked in (R3a) and (R3b), to the formation of hydroperoxide species and hydroperoxyalkyl and other small radicals. These in turn can react with additional fuel molecules by metatheses in order to regenerate alkyl radicals. This causes a propagation chain in which ȮH radicals are the main chain carriers. The formation of hydroperoxides is important, because these species contain a weak O–OH bond whose breaking leads to the formation of two radicals, which can then react again with fuel molecules to give further alkyl radicals. This so-called degenerate branching induces an exponential acceleration of reaction rates, leading to spontaneous autoignition, or explosion.

Cool flames and LTHR are often observed preceding the main ignition event in this regime [61]. These cool flames occur at temperatures much colder than the adiabatic flame temperature of the mixture, and are typically bluish in color, indicative of CH_2O^* chemiluminescence [327]. In stratified mixtures, such as in HCCI engines and diesel sprays [328,329] or fundamental experiments [194,291,330,331], these flames can propagate via advective/diffusive or compressive/advective/diffusive mechanisms. In homogenous mixtures typical of RCM experiments, the observed emissions are mostly-uniform, lacking defined spatial structure indicative of a flame [332]. CH_2O concentrations peak in the mixture as the local temperature rises following the decomposition of ketohydroperoxides which produces multiple ȮH radicals, followed by, for example, $CH_3\dot{O}+\dot{O}H=CH_2O+H_2O$. This first stage of ignition is typically associated with an increase in temperature of 50–200 K, and is identifed as a sharp rise in pressure, e.g., Δp_1, as marked in Fig. 30. After LTHR, the reactivity slows in part due to a shift in equilibrium to the reverse of (R5a), while the concentration of H_2O_2 increases due to H-atom abstraction reactions by $H\dot{O}_2$ radicals, as well as recombination reactions of $H\dot{O}_2$ with $H\dot{O}_2$ and $\dot{C}H_3$. During that time, significant quantities of H_2O_2 accumulate while the pressure and temperature slowly increase in the core because of non-branching exothermic reactions. This slow rise in temperature after LTHR is termed intermediate temperature heat release (ITHR), as indicated in Fig. 30. The second-stage, or main ignition follows when the temperature and pressure are sufficient for H_2O_2 to decompose into two ȮH radicals, causing the intermediate temperature degenerate branching. The terms ‘cool flame’ and ‘first-stage ignition’ have been used interchangeably in historical RCM investigations, however we reserve ‘cool flame’ to designate the low-temperature propagating front, e.g., [291,330,333].

At higher temperatures, e.g., 800–1000 K, the formation of alkenes via (R3c) and (R5b) competes with the isomerization reactions, (R3a) and (R5a), as does the dissociation of alkylperoxyl radicals via the

reverse of (R2a). These aspects lead to a reduction in the overall reaction rate, particularly since alkenes are stable and relatively unreactive, and $H\dot{O}_2$ radicals are much less reactive than $\dot{O}H$ radicals, and this gives rise to NTC behavior, as illustrated in Fig. 2. This distinctive feature of many fuels presents a range of temperatures within which global induction times increase, or at least remain nearly constant, as the temperature increases. The competition between channels leading to low-temperature branching and those producing less reactive products, such as alkenes and cyclic ethers (R5c), accounts for (at least in part) the decrease in reactivity of many fuels when the extent of molecular branching increases, for example from *n*-butane to 2-methylpropane. Analogously, the increase in reactivity when the length of the linear carbon chain increases, for example from *n*-butane to *n*-pentane, results from the larger number of sites at which internal isomerization reactions (R3a,R7) can occur. In the NTC regime, self-heating of the system can also play an important role, where this transitions from LTHR to ITHR. The extent of preliminary exothermicity is typically lower at higher temperatures, with Δp_1 being smaller, and the time from τ_1 to τ_{ign} longer. Reactions associated with ITHR are generally less well understood, but the direct (i.e., concerted) elimination reactions of $RO\dot{O}$ leading to $H\dot{O}_2$+alkene/ether/carbonyl species (R3c), followed by $H\dot{O}_2+H\dot{O}_2=H_2O_2+O_2$, are thought to be important [334].

At temperatures above the NTC regime, for instance, greater than about 1000 K, the decomposition of fuel radicals into smaller alkyl radicals and alkenes is the predominant pathway traversed by most fuel radicals containing more than three carbon atoms. H-atom abstractions followed by isomerization and successive decomposition of alkyl radicals occur until small molecule chemistry (C_0–C_2) dominates.

Autoignition of fuels at LTC conditions, as highlighted in Section 1, proceeds through a range of thermo-chemical states. As such, even though a system may start at low to intermediate temperatures, the coupled self-heating, including LTHR/ITHR, generally results in conditions where higher temperature chemistry evolves, e.g., $H_2O_2(+M)=\dot{O}H+\dot{O}H(+M)$ and $\dot{H}+O_2=\ddot{O}+\dot{O}H$, and this is critically important for the multiplication in radicals leading to high temperature heat release, e.g., via $CO+\dot{O}H=CO_2+\dot{H}$. This complex evolution is responsible for the propagation of combustion in operating engines, and is well replicated in RCM experiments.

Studies of autoignition chemistry can generally be classified based on the fuels investigated. As indicated earlier, they are presented here in hierarchical order, starting with the smallest molecules, hydrogen and carbon monoxide, followed by alkanes, alkenes, cycloalkanes, aromatics, oxygenates, and finally full-boiling range fuels and fuel additives. These structural classes represent the constituents of most market fuels for stationary and transportation applications, including natural gas, LPG, gasoline, jet

fuel, and diesel fuel. LTC of real fuels, which typically consist of hundreds to thousands of components, proceeds through a cascade of fuel fragments and intermediate oxygenated species that are also present during the decomposition and oxidation of small fuels, such as hydrogen and propene. As such, the combustion chemistry of small molecules is not only relevant for their utilization as fuels themselves, e.g., within natural gas, but also spans the development of hierarchical chemical kinetic models for complex fuels at LTC conditions.

This section guides the reader through the evolving understanding of autoignition at LTC conditions, covering the pioneering work of Affleck and Fish [70] as well as current state-of-the-art. Whereas most investigations during the last century focused on trends observed within conventional engine regimes [69,105,293], recent activities are often undertaken to acquire rigorous measurements which can be used to develop and validate detailed chemical kinetic models covering a wide range of conditions. Particular attention is devoted in modern studies towards minimizing uncertainties associated with the measurements, as discussed in [39], so that predictive computational tools can be formulated to aid the design of new fuels and advanced combustion engines. The primary focus of the review in this section is on experimental findings of autoignition chemistry; however, some attention is paid to the development and comparison of chemical kinetic models using the experimental datasets, as well as interpretations facilitated by the modeling results.

6.1. Hydrogen / syngas mixtures

Hydrogen is an important fuel, not only because there is potential to generate hydrogen via electrolysis of water using renewable power, but also because hydrogen oxidation kinetics, as just highlighted, are critically important in the combustion of all hydrogen containing fuels, and thus it is the foundation of all hierarchical kinetic models. Most hydrogen is currently produced by steam reforming of natural gas, or by the gasification of coal, biomass or municipal waste, where the resulting synthesis gas (syngas) also contains significant fractions of CO. Syngas can be utilized as a low pollution fuel for both stationary piston- and turbine-based engines.

There have been a number of studies of hydrogen and syngas oxidation in RCMs (e.g., [204,272,335–341]), the conditions of which are summarized in Table 2. Experiments with hydrogen can be challenging, due to the sensitivity of autoignition to the presence of gas impurities, vessel contamination, and thermal in-homogeneities [305,342]. Early ignition and non-uniform (i.e., mild) ignition has been observed in many historical studies due to such issues. Hydrogen explosion limits at low temperatures have previously been characterized in terms of threshold first and second pressure limits, beyond which no explosion

occurs [343]. Between the first and second explosion limits, i.e., the 'strong ignition' regime, autoignition is controlled primarily by branching via $\dot{H}+O_2=\ddot{O}+\dot{O}H$ and very little coupled self-heating can be found in the experimental pressure records. However, at pressure conditions above the extended second limit, the autoignition of hydrogen follows a degenerate branching process and is controlled primarily by the formation and consumption of $H\dot{O}_2$, e.g., $\dot{H}+O_2(+M)=H\dot{O}_2(+M)$, $H_2+H\dot{O}_2=\dot{H}+H_2O_2$, $H\dot{O}_2+H\dot{O}_2=H_2O_2+O_2$, and $H_2O_2(+M)=\dot{O}H+\dot{O}H(+M)$. Under these conditions, chemical energy release in the pre-ignition period plays an important role, where the rates of pressure/temperature rise evolve from a relatively slow process, transitioning to rapid heat release at the point of main ignition. The rates of heat release are generally lower than in the strong ignition regime, and there is often a detectable level of ITHR in experimental measurements before the system explodes. These features have been classified in historical literature as the 'weak ignition' regime.

Table 2. Studies of hydrogen and syngas mixtures using RCMs.

Fuels	T_c (K)	p_c (bar)	Mixture Composition	Diluent:O_2	ϕ	Reference
Hydrogen	950–1050	6–40	$H_2/O_2/Ar$	5.00	1.0	[335]
Hydrogen	950–1100	15–50	$H_2/O_2/Ar/N_2$	13.0	1.0	[340,341]
Hydrogen	950–1060	15–70	$H_2/O_2/Ar$	5.00	1.0	[336]
Hydrogen/syngas	950–1100	15–50	$H_2/CO/O_2/Ar/N_2$ H_2:CO = 0.25, 0.54, 1, 3, ∞	6.4–31.8	0.36–1.6	[340,341]
Hydrogen/syngas	900–1100	20–80	H_2, H_2/CO	4.00	0.5, 1.0	[338]
Hydrogen/syngas	914–1068	8–70	$H_2/CO/O_2/N_2/Ar$	3.76, 13.0	0.5–2.0	[339]
Syngas	855–1051	7.2–26.7	$H_2/CO/O_2/N_2/CO_2$	3.76	0.1–1.0	[272]
Hydrogen/water	907–1048	10–70	$H_2/O_2/H_2O/N_2/Ar$	13.0	1.0	[344]
Hydrogen/carbon monoxide/syngas/water	895–1140	10, 30	H_2; 70% H_2/30% H_2O; CO; 70% CO/30% H_2O; 35% H_2/35% CO/30% H_2O	3.76	0.5, 1.0, 2.0	[260]
Syngas/CH_4/trimethylsilanol	1010–1110	5, 15	$H_2/CO/O_2/N_2$; H_2:CO = 0.7	3.76	0.1	[337]

Lee and Hochgreb [335] provided some of the first experimental autoignition data for hydrogen significantly above the extended second explosion limit. They identified ITHR in the pressure records at their lower temperature conditions while none was present at higher temperatures. A modification to the rate constant for $H_2+H\dot{O}_2=\dot{H}+H_2O_2$ was seen to improve kinetic model predictions compared to the experimental measurements.

Mittal *et al*. [340,341] studied the autoignition of $H_2/O_2/Ar/N_2$ and $H_2/CO/O_2/Ar/N_2$ mixtures. H_2 was replaced by CO in order to investigate the effect of the change in relative concentrations of both fuels, while keeping the total fuel mole fraction constant. It was found that even replacing small amounts of H_2 with CO led to longer ignition times and a decrease in reactivity. Moreover, the inhibiting effect of CO

addition was found to be much more pronounced with increasing pressure. Chemical kinetic modeling showed that, at the intermediate-temperatures and high-pressures explored in this work, reactions involving the production and consumption of $H\dot{O}_2$ and H_2O_2 were important, consistent with the work of Lee and Hochgreb [335]. The role of $CO+H\dot{O}_2=CO_2+\dot{O}H$ was suggested in Mittal *et al*. [340,341] as a primary source of discrepancies between the kinetic model and the experimental data.

The measurements of Gersen *et al*. [336] confirmed the findings of Lee and Hochgreb [335] and Mittal *et al*. [340,341]. Their further work [338] studied the effect of CO and CH_4 addition to stoichiometric and fuel-lean (ϕ = 0.5) mixtures of H_2, H_2/CO, CH_4, CH_4/CO, CH_4/H_2 and CH_4/CO/H_2. There was no inhibiting effect for replacement of up to 50% of the H_2 with CO, somewhat contrary to the findings of Mittal *et al*. [340,341], but in agreement with detailed chemical kinetic simulations.

Kéromnès *et al*. [339] used RCMs and shock tubes to measure ignition delay times for H_2/CO/O_2/N_2/Ar mixtures over a wide range of stoichiometry, temperature and pressure. Ignition delays decreased with increasing temperature, pressure, and equivalence ratio. For CO concentrations lower than 50%, it was found that syngas mixture reactivity was controlled by hydrogen chemistry, with little or no inhibiting effect of CO addition to H_2, consistent with the work of Gersen *et al*. [338]. However, for CO concentrations higher than 50%, the inhibiting effect of CO addition was found to be noticeable. The experimental behavior was simulated using a detailed chemical kinetic mechanism, showing that the reaction sequence $H_2+H\dot{O}_2=\dot{H}+H_2O_2$ followed by $H_2O_2(+M)=\dot{O}H+\dot{O}H(+M)$ played a central role in hydrogen ignition under intermediate temperature and high-pressure conditions, in agreement with the conclusions of Lee and Hochgreb [335] and Mittal *et al*. [340,341].

Walton et al. [272] studied simulated syngas mixtures for lean to stoichiometric equivalence ratios, initial oxygen mole percentages from 15% to 20%, and H_2:CO molar ratios between 0.25 and 4.0. They found that the model of Davis et al. [345] agreed well with the experimental data, though the trends with temperature and ϕ were not completely in agreement. The chemical kinetic simulations utilized an effective state definition, as discussed in Section 4, to account for early exothermicity (i.e., pre-ignition heat release) observed at some test conditions.

Das et al. [344] studied the effect of water addition on the reactivity of stoichiometric H_2/O_2/N_2/Ar mixtures, for water addition of 0%, 10%, and 40% by mole. Under high-pressure conditions of 30 and 70 bar, the addition of water was seen to promote ignition. However, for relatively lower pressure conditions, the addition of water reduced the reactivity of the mixture. The mechanism of Hong et al. [346] was modified by changing the rate of the reaction $\dot{H}+O_2=\ddot{O}+\dot{O}H$ within the established uncertainty limits.

Changing this rate substantially improved the agreement of the model with both the dry ignition data (i.e., no water) and the moist ignition data (i.e., with water) at low pressures, while not changing the already good agreement at high pressures.

Donohoe et al. [347] studied the influence of steam (i.e., water) dilution on the autoignition behavior of hydrogen, carbon monoxide, and syngas mixtures, with 0%, 10%, and 30% H_2O dilution. For the hydrogen and syngas mixtures there was no significant chemical effect on ignition delay time. However, the higher heat capacity and lower thermal diffusivity of H_2O lead to lower heat losses to the walls and result in shorter observed ignition delay times. For the pure CO mixtures a significant chemical effect was observed. Using a chemical kinetic model to interpret the data it was found that the increased reactivity was due to the following series of reactions: $CO+O_2=CO_2+\ddot{O}$, $H_2O+\ddot{O}=\dot{O}H+\dot{O}H$, $CO+\dot{O}H=CO_2+\dot{H}$, and $\dot{H}+O_2=\ddot{O}+\dot{O}H$. Critically, the presence of water facilitates its reaction with oxygen atoms, producing two $\dot{O}H$ radicals which react with CO producing CO_2 and a hydrogen atom. These hydrogen atoms react with molecular oxygen via $\dot{H}+O_2=\ddot{O}+\dot{O}H$, which, as highlighted earlier, is a critically important high-temperature chain branching reaction.

Mansfield and Wooldridge [337] investigated the effects of chemical impurities on the combustion of syngas, focusing on CH_4, a common component of syngas, and trimethylsilanol (TMS), an unstudied impurity related to those commonly found in landfill-based syngas. Pressure-time history measurements and high-speed imaging of the ignition process were again used to determine autoignition delay times and observe ignition behaviors. The four simulated syngas mixtures used were (1) pure syngas: 30% H_2, 70% CO fuel volume, (2) syngas with CH_4: 27% H_2, 67% CO, 6% CH_4, (3) and (4) pure syngas with 10 or 100 ppm TMS. The results uniquely illustrated the occurrence of two-step ignition behavior at higher pressures, with two distinct regions of heat release and pressure rise. The first and second autoignition delay times were therefore defined and interestingly the times were affected differently by the addition of impurities. The addition of CH_4 consistently increased autoignition delay times up to 40% at 15 bar, while increasing autoignition delay times at 5 bar by up to a factor of three. Conversely, the addition of 10 ppm TMS caused a consistent decrease of ~10–30% in autoignition delay times at 15 bar with insignificant impact at 5 bar, and 100 ppm TMS impurity caused consistent decreases of 50–70% at 15 bar and 20–30% decreases at 5 bar. The marked pressure dependence of the autoignition delay time, typical for syngas at these conditions, was virtually eliminated for the 100 ppm TMS mixture. Kinetic modeling suggested that the promoting effects of TMS were related to enhanced consumption and/or reduced production of $H\dot{O}_2$ radicals. The impact of TMS is remarkably similar to that for SiH_4 in pure H_2 [348,349],

suggesting a possible trend for poorly understood Si-based species to promote autoignition in syngas and hydrogen mixtures.

6.2. Linear and branched chain alkanes

Linear and branched chain alkanes, or paraffins, constitute a major portion of most modern fuels, including natural gas and petroleum-based fuels, and there is a long history of their study using RCMs. They are considered here from the simplest to the more complex.

6.2.1. Methane

Methane is the primary constituent of natural gas and its ignition chemistry is important for a range of conventional and advanced combustion strategies. Yet there have been few studies on the oxidation of pure methane in RCMs, most involving mixtures of methane blended with other fuels such as hydrogen and small alkanes. Methane is a very unreactive fuel, in part due to the high activation energy required for abstraction of its H-atoms and also because of the relative low reactivity of the methyl radicals formed which can, for example, undergo self-recombination producing stable ethane molecules. Hence it is difficult to study methane autoignition at the lower temperature (600–1000 K) conditions typically encountered in RCMs, and high pressures must be utilized and a narrow range of temperatures covered. A summary of studies using methane and methane-blended fuels is provided in Table 3.

Table 3. Studies of methane/natural gas mixtures using RCMs.

Fuels	T_c (K)	p_c (bar)	Mixture Composition	Diluent:O_2	ϕ	Reference
Methane	980–1060	16	$CH_4/O_2/Ar$	3.50	1.0	[115]
Methane	900–1100	20–80	$CH_4/O_2/N_2/Ar$	4.00	0.5, 1.0	[338]
Methane	1050–1100	10	$CH_4/O_2/Ar$	3.76	0.8	[350]
Methane	870–1200	10, 25	$CH_4/O_2/N_2/Ar$	3.76	0.3, 0.5, 1.0, 2.0	[351]
Methane	880–1000	20.5–22.7	$CH_4/O_2/N_2/Ar$	3.76	0.7, 1.0	[352]
Methane/hydrogen	950–1200	10, 30	$CH_4/H_2/O_2/N_2/Ar$ $H_2:CH_4$ = 1.5, 4.0	3.76	0.5, 1.0	[353]
Methane/hydrogen	950–1060	15–70	CH_4, $CH_4/H_2/N_2/Ar$ $H_2:CH_4$ = 0, 0.05, 0.11, 0.25, 1, ∞	4–5	0.5, 1.0	[246]
Methane/hydrogen/carbon monoxide	900–1100	20–80	Fuel/$O_2/N_2/Ar$ CH_4, CH_4/H_2, CH_4/CO, and CH_4/CO/H_2	4.00	0.5, 1.0	[338]
Methane/ethane, methane/propane, methane/*n*-butane	900–1100	10	CH_4/higher HC/O_2/N_2 CH_4/H_xC_y = 1, 3.25, 20, 100	3.76	1.0	[350]
Methane/ethane/propane	870–1000	16, 19, 22	Fuel/$O_2/N_2/Ar$ $CH_4/C_2H_6/C_3H_8$ at 89/9/2	3.76	0.7, 1.0	[352]
Methane/ethane/propane	850–925	13, 21	Fuel/$O_2/N_2/Ar$ $CH_4/C_2H_6/C_3H_8$ at 89/9/2	1.97–3.75	0.625–1.0	[354]
Methane/ethane/propane/hydrogen, carbon	870–1000	18–21	Fuel/$O_2/N_2/Ar$ NG:H_2 = 0.67, 4	3.76	1.0	[352]

monoxide, carbon dioxide, water			NG:CO = 2.33, 4, 9 NG:CO_2 = 2.33, 4, 9 NG:H_2O = 2.33			
Methane/DME	600–1050	10, 20, 30	Fuel/O_2/N_2/Ar CH_4:DME =1.5, 4	3.76	0.3, 0.5, 1.0, 2.0	[351]
Methane/propane	735–1136	10, 20, 30, 40	Fuel/O_2/N_2/Ar CH_4:C_3H_8 = 2.33, 9	3.76	0.3, 0.5, 1.0, 2.0, 3.0	[355]
Methane/ethane/propane	770–1100	10, 20, 30	Fuel/O_2/N_2/Ar CH_4/C_2H_6/C_3H_8 at 90/6.6/3.3, 70/15/15 & 70/20/10	3.76	0.5, 1.0, 2.0	[355]
Methane/*n*-butane	660–1150	10, 20, 30	Fuel/O_2/N_2/Ar CH_4:*n*-C_4H_{10} = 2.33, 9	3.76	0.32, 0.53, 1.07, 2.31	[356]
Quinternary natural gas (methane/ethane/propane /butane/pentane)	630–1136	8, 20, 30	Fuel/O_2/N_2/Ar CH_4/C_2H_6/C_3H_8/*n*-C_4H_{10}/*n*-C_5H_{12} at 81.28/10/5/2.5/1.25 & 62.5/20/10/5/2.5	3.76	0.5, 1.0, 2.0	[278,357, 358]
Quinternary natural gas/ hydrogen (methane/ ethane/propane/butane/ pentane/hydrogen)	850–1136	10, 30	Fuel/O_2/N_2/Ar CH_4/C_2H_6/C_3H_8/*n*-C_4H_{10}/*n*-C_5H_{12} at 81.25/10/5/2.5/1.25 & 62.5/20/10/5/2.5 in various compositions with H_2	3.76	0.3, 0.5, 1.0	[353]
Quinternary natural gas/syngas/water	730–1060	10, 30	Fuel/O_2/N_2/Ar NG:H_2O = 2.33, 9 NG/Syn/H_2O at 70/15/15	3.76	0.5, 1.0, 2.0	[260]
Methane/ethane/NO_2	900–1050	25–50	CH_4/C_2H_6/NO_2/O_2/N_2/Ar NO_2 at 0, 100, 270 ppm	4.00	1.0	[359]
Ethane/NO_2	930–1010	20–40	C_2H_6/NO_2/O_2/N_2/Ar	4.00	1.0	[359]

Brett et al. [115] reported ignition delay times for $CH_4/O_2/Ar$ mixtures over a narrow temperature range. The experimental measurements of ignition delay time were significantly longer than those predicted by two chemical kinetic mechanisms, especially at temperatures below 1000 K. Gersen et al. [338] also studied a stoichiometric $CH_4/O_2/N_2/Ar$ mixture and compared their data with the same models as Brett et al. [115]. While Gersen et al. [338] found that neither model agreed well with their data as well, the data from the study of Gersen et al. [338] agreed well with the model from the work of Petersen et al. [360].

Furutani et al. [350] also reported ignition delay times for $CH_4/O_2/Ar$ mixtures over a narrow temperature range. They compared the measurements to ignition delay times for blends of CH_4/C_2H_6, CH_4/C_3H_8, and CH_4/*n*-C_4H_{10}, albeit at slightly lower temperatures, e.g., 900–1100 K; however, they did not evaluate predictions from any kinetic model. It was found that at 20:1 molar blend ratios, the stimulating influence of ethane and propane were very similar, with reductions in τ_{ign} of 60%, while *n*-butane was

much more effective, reducing τ_{ign} by 80%. Furthermore, their measurements demonstrated a non-linear response to *n*-butane doping for molar blend ratios of CH_4:*n*-C_4H_{10} = 1, 3.25, 20 ,and 100.

Burke et al. [351] studied the ignition of methane as part of a larger study involving methane/DME mixtures using three different shock tubes and an RCM. Under conditions listed in Table 3, they found that the ignition delays agreed well with a new mechanism they developed in their work.

Yu et al. [352] also studied the ignition of methane as part of a larger study involving natural gas (i.e. blends of methane, ethane, and propane). They found that the ignition delays decreased monotonically with increasing temperature, but that τ_{ign} at the lowest temperatures was very sensitive to random uncertainties in the experimental conditions. Near 880 K, for instance, variations of up to $\pm$50% in ignition delay times were seen.

6.2.2. Methane / hydrogen mixtures

Methane/hydrogen fuel blends have recently drawn attention due to interest in increasing the use of carbon-less and low-carbon fuels. There are potential greenhouse gas benefits as well as substantial emissions reductions that could be realized with engines operating on such fuel blends. Furthermore, hydrogen can enhance the reactivity of methane at engine-relevant conditions so that these fuel blends are easier to utilize than pure methane, resulting in lower inlet temperatures and/or reduced compression ratios necessary for effective engine operation.

Methane/hydrogen mixtures were studied by Gersen et al. [336] at stoichiometric conditions in the temperature range of 950–1060 K and at pressures between 15 and 70 bar. Eight fuel blends were considered, ranging from pure methane to pure hydrogen. They found significant non-linear behavior where, for hydrogen addition to methane at hydrogen mole percentages below 20% there was only a slight decrease in reactivity but at mole percentages above 50% there was a substantial decrease in ignition delay times. Results for fuel-lean mixtures showed a slight effect of ϕ on reactivity. All experiments were simulated using the detailed chemical kinetic model of Petersen et al. [360], where generally good agreement was observed between the simulations and the experimental results.

Donohoe et al. [353] measured ignition delay times in both a shock tube and an RCM to determine the increase in reactivity due to the addition of hydrogen to mixtures of methane. Experiments in this dataset were performed over a very wide range of T_c, p_c, ϕ and dilution. Pure methane and hydrogen-blended mixtures were prepared, and it was found that increasing the hydrogen concentration increased

reactivity, reducing ignition delay times, consistent with the findings of Gersen et al. [336] and Yu et al. [352].

6.2.3. Methane / natural gas mixtures

While the primary component of natural gas is methane, small alkanes from C_2 to C_5 can constitute a significant fraction of the fuel, from 15 to 35%, especially when extracted from gas fields that are enhanced via unconventional extraction techniques like hydraulic fracturing. Often, such gas supplies are termed 'wet' natural gas, particularly if the heavier hydrocarbon fraction is large.

Heyne et al. [354] studied the oxidation of a $CH_4/C_2H_6/C_3H_8$ blend containing 89/9/2 molar percentages. The measured ignition delay times were compared to predictions using six chemical kinetic mechanisms and most of the models were found to over-predict the experimental ignition delays. To generate an improved model, components of Gas Research Institute reaction mechanism, GRI-Mech 3.0 [361] were combined with the RAM Accelerator Mechanism (RAMEC) [287], and two additional ethane reactions, and the rate constants for 25 of the most sensitive reactions were adjusted within their established uncertainty bounds by an evolutionary algorithm. It was found that at the experimental conditions, reactions involving peroxy and methylperoxy radicals were most sensitive and required the largest changes in rate constants to adequately match the experimental results.

Healy et al. [355,356] used both a high-pressure shock tube and an RCM to study a series of natural gas mixtures covering a wide composition envelope, and at high-pressure conditions (up to 50 bar) of interest to the gas turbine industry. These were the first such studies to present ignition delay times at conditions that significantly overlapped shock tube and RCM facilities, and demonstrated the influences of facility effects such as heat loss, on the measurements in the two different devices.

Methane/propane mixtures in synthetic air were studied by Healy et al. [355] for blends containing molar ratios of CH_4/C_3H_8 of 90/10 and 70/30. The data showed characteristic NTC behavior which was more pronounced for mixtures containing higher fractions of propane. The findings highlighted the increasing roles of the formation of ROOH and cyclic ethers on the oxidation processes. A detailed chemical kinetic mechanism was used to simulate the experimental data, and the model was able to qualitatively reproduce the influence of temperature, pressure, and equivalence ratio very well. Reasonable quantitative agreement was observed for some mixtures; for the 90/10 blends good agreement was observed over the entire range of conditions. For the 70/30 blends the model tended to over-predict reactivity, with the divergence between the model and the experimental data being more

pronounced at lower temperatures, higher pressures and for fuel-rich mixtures, highlighting the complexities of fuel blend interactions.

Healy et al. [355] also studied the oxidation of $CH_4/C_2H_6/C_3H_8$/air mixtures for blends containing molar ratios of 90/6.6/3.3, 70/15/15, and 70/20/10 of each respective fuel component. The data were simulated using a detailed chemical kinetic model which qualitatively reproduced the effect of change in equivalence ratio and pressure, predicting that fuel-rich, high-pressure mixtures ignited fastest while fuel-lean, low-pressure mixtures ignited slowest. Moreover, the evolution of the reactivity as a function of temperature was well captured, with the model predicting NTC behavior similar to experimental observations. Quantitatively the model was generally in excellent agreement with the experimental results but produced shorter reaction times than measurements for the fuel-rich mixture containing the highest quantity of propane (70/15/15 mixture) at the lowest temperatures (770–900 K), similar to the study for the methane/propane mixtures [355].

Healy et al. [356] studied the autoignition of $CH_4/n\text{-}C_4H_{10}$ mixtures containing molar ratios of 90/10 and 70/30. A detailed chemical kinetic model developed in [355] was shown to quantitatively reproduce the ignition delays, accurately capturing fuel mixture reactivity as a function of fuel composition, equivalence ratio, temperature, and pressure.

Ignition delay times for the oxidation of quinternary ($CH_4/C_2H_6/C_3H_8/n\text{-}C_4H_{10}/n\text{-}C_5H_{12}$) natural gas mixtures [278,357,358] were measured. In an attempt to test a wide range of natural gas composition, two natural gas mixtures were studied, one containing 81.25% methane with decreasing concentrations (10/5/2.5/1.25%) of progressively larger alkanes ($C_2H_6/C_3H_8/n\text{-}C_4H_{10}/n\text{-}C_5H_{12}$) referred to as NG2, and another composed of approximately 62.5% methane and relatively higher concentrations (20/10/5/2.5%) of larger hydrocarbon species, referred to as NG3. A detailed chemical kinetic model was used to simulate the data with good agreement observed between the model and the experimentally measured delay times. The NG3 mixtures produced faster reaction times compared to the NG2 ones, as the former contained higher concentrations of larger alkanes which have greater reactivity along the LTC pathways described in Fig. 37.

Yu et al. [352] studied the effect of several EGR and syngas components on the autoignition of a natural gas mixture composed of 89% methane, 9% ethane and 2% propane. Ignition delay times for methane, natural gas, and mixtures of natural gas with hydrogen, carbon monoxide, carbon dioxide and water were measured. The results showed that H_2 addition accelerated mixture reactivity, similar to the findings of Gersen et al. [336]. The experimental data were simulated using four chemical kinetic

mechanisms from the literature; the model by Heyne et al. [354], the NUIG model [278,357,358], the model by Wang et al. [362], and the GRI-Mech 3.0 model [361] with the RAMEC sub-mechanism [287]. It was found that natural gas ignition delays could be reproduced satisfactorily, but improvements in the mechanisms were needed in order to achieve an accurate, quantitative account of the effect of the inclusion of hydrogen.

As discussed earlier for methane/hydrogen mixtures, Donohoe et al. [353] also measured ignition delay times for natural gas/hydrogen mixtures. Two synthetic natural gas-fueled mixtures were used which contained methane, ethane, propane, *n*-butane and *n*-pentane, with one comprising 81.25/10/5/2.5/1.25% while the other consisted of 62.5/20/10/5/2.5% $C_1/C_2/C_3/C_4/C_5$ components in order to encompass a wide range of possible natural gas compositions. The experimental data showed that τ_{ign} decreased with increasing temperature, pressure, and an increase in long-chain hydrocarbons, similar to earlier findings of [278,357,358]. Moreover, increasing the H_2 concentration also increased reactivity, reducing τ_{ign}, consistent again with the findings of Gersen et al. [336] and Yu et al. [352]. All experiments were simulated using a detailed chemical kinetic model [363] and generally, good agreement was observed between the model and the experiments.

As discussed above for hydrogen/syngas mixtures in the same study, Donohoe et al. [347] also reported the influence of steam (i.e., water) dilution on the autoignition behavior of methane and natural gas mixtures with 0%, 10%, and 30% steam dilution. For all fuel mixtures it was found that there was no significant chemical effect on τ_{ign}, but that significant changes in the thermal properties affected reactivity. Again, the primary effect was via the thermal and transport properties: the addition of water increases the heat capacity and reduces the thermal diffusivity of the mixtures, leading to lower heat losses and shorter observed τ_{ign}.

The findings of many of these recent investigations on natural gas highlight needs to further improve the understanding of the chemical kinetics of higher hydrocarbons and hydrogen, especially at high-pressure and low-temperature, at fuel-rich conditions and the influence of EGR components, and in conjunction, formulate models which can quantitatively capture the experimental trends observed for future LTC engines.

6.2.4 Ethane

Gersen et al. [359] studied the ignition of methane, ethane and methane/ethane mixtures subject to NO_2 doping. As expected from previous work involving carbon chains longer than methane, ethane is more

reactive than methane. Furthermore, the data revealed that NO_2 addition to methane and methane/ethane blends significantly increases the fuel reactivity, and this stimulating effect increases at higher temperatures. Doping of NO_2 to ethane however, was not nearly as effective. Their modeling results suggested that the ignition-promoting effects are due to new conversion channels that appear for $\dot{C}H_3$ and $CH_3O\dot{O}$, namely $NO_2+\dot{C}H_3=NO+CH_3\dot{O}$ and $NO+CH_3O\dot{O}=NO_2+CH_3\dot{O}$, respectively, while $\dot{O}H$ radical generation is stimulated due to the NO–NO_2 loop, i.e., $NO_2+\dot{H}=NO+\dot{O}H$ and $NO+H\dot{O}_2=NO_2+\dot{O}H$.

6.2.5. Propane

Propane is a significant component of 'wet' natural gas, as well as petroleum. These feed-stocks are often refined to produce fuels such as liquefied petroleum gas (LPG), where LPG can be used in vehicles as well as various heating appliances. LPG consists primarily of propane/butane blends, though significant quantities of propene and *iso*-butene can also be present. In addition to its importance as a fuel component, propane is the smallest alkane for which cool flame and NTC behavior can be observed at engine-relevant conditions, as evident in some of the natural gas studies previously described, and discussed recently by Merchant et al. [61]. A summary of the low temperature autoignition work carried out on propane, butane isomers, and pentane isomers mixtures is provided in Table 4.

Table 4. Studies of C_3–C_6 alkane fuels using RCMs.

Fuels	T_c (K)	p_c (bar)	Mixture Composition	Diluent:O_2	ϕ	Reference
Propane	680–970	21, 27, 37	$C_3H_8/O_2/N_2/Ar$	3.76	0.5, 1.0, 2.0	[277]
Propane	690–910	30	$C_3H_8/O_2/N_2$	1.38, 3.76, 8.52	0.5, 1.0, 2.0	[364]
***n*-Butane**	660–880	10–15	*n*-$C_4H_{10}/O_2/N_2/Ar$	3.76	0.8	[365]
***n*-Butane, *iso*-butane**	600–950	7.4–9.7	*n*- and *iso*-$C_4H_{10}/O_2/N_2/Ar$	3.76	1.0	[76]
***n*-Butane**	700–900	8.9–11.4	*n*-$C_4H_{10}/O_2/N_2/Ar$	3.76	08, 1.0, 1.2	[221]
***n*-Butane**	700–900	5.8–11.4	*n*-$C_4H_{10}/O_2/N_2/Ar$	3.76	1.0	[79]
***n*-Butane, propane/*n*-butane**	720–900	16–18	*n*-$C_4H_{10}/O_2/N_2/Ar$ C_3H_8:*n*-C_4H_{10} = 0.25, 0.67	3.76	1.0	[138]
***n*-Butane, *iso*-butane**	660–1010	14–36	*n*- and *iso*-$C_4H_{10}/O_2/N_2/Ar$	3.76–4.00	0.5, 1.0	[366]
***n*-Butane**	645–1050	10, 20, 30	*n*-$C_4H_{10}/O_2/N_2/Ar$	3.76	0.3, 0.5, 1.0, 2.0	[285]
***iso*-Butane**	590–1010	10, 20, 30	*iso*-$C_4H_{10}/O_2/N_2/Ar$	3.76	0.3, 0.5, 1.0, 2.0	[367]
***n*-Pentane**	600–950	7.7–9.9	*n*-$C_5H_{12}/O_2/N_2/Ar$	3.76	1.0	[76]
***n*-Pentane, *iso*-pentane, *neo*-pentane**	650–950	7.5–9.0	*n*-, *iso*-, *neo*-$C_5H_{12}/O_2/N_2/Ar/CO_2$	3.76	1.0	[368]
***n*-Pentane, *neo*-pentane**	650–950	4.5–9.2	*n*-, *iso*-, *neo*-$C_5H_{12}/O_2/N_2/Ar/CO_2$	3.76	1.0	[79]
***n*-Pentane**	675–980	8–20	*n*-$C_5H_{12}/O_2/N_2/Ar/CO_2$	3.76	0.5, 1.0, 2.0	[369]
***n*-Pentane**	720–875	7.8–9.5	*n*-$C_5H_{12}/O_2/N_2/Ar$	3.76	1.0	[77]
***n*-Pentane**	600–900	6.8–9.2	*n*-$C_5H_{12}/O_2/N_2/Ar/CO_2$	3.76	1.0	[81,370]
***n*-Pentane**	650–950	9–11	*n*-$C_5H_{12}/O_2/N_2/Ar/CO_2$	3.76	1.0	[273]

***n*-Pentane, *iso*-pentane, *neo*-pentane**	640–900	4–10	*n*-, *iso*-, *neo*-$C_5H_{12}/O_2/N_2/Ar/CO_2$	3.76	1.0	[371]
***n*-Pentane**	690–820	7.9–14.8	*n*-$C_5H_{12}/O_2/N_2/Ar$	3.76	0.6, 0.75, 1.0	[74]
***n*-Pentane**	660–1000	10	*n*-$C_5H_{12}/O_2/N_2/Ar$	3.76	1.0	[372]
***n*-Pentane, *iso*-pentane, *neo*-pentane**	643–1100	10, 20	*n*-, *iso*-, *neo*-$C_5H_{12}/O_2/N_2/Ar$	3.76	0.5, 1.0, 2.0	[373]
2-Methylpentane	706–730	20	*iso*-$C_6H_{14}/O_2/N_2$	4.00	0.5	[70]
***n*-Hexane, 2-methylpentane, 2,2- & 2,3-dimethylbutane**	710–930	10–50	Fuel/O_2/N_2	3.76	1.0	[72]
2-Methylpentane	650–950	7.5–9.0	*iso*-$C_6H_{14}/O_2/N_2/Ar/CO_2$	3.76	1.0	[368]
***n*-Hexane**	637–1100	15	*n*-$C_6H_{14}/O_2/N_2/Ar$	3.76	1.0, 2.0	[374]

Gallagher et al. [277] investigated the oxidation of propane for the conditions listed in Table 4. These data exhibited the characteristic NTC behavior generated by the competing reaction pathways discussed in connection with Fig. 37. Gallagher et al. [277] found good agreement with a model they developed, both with their RCM data and previously published flow reactor data. Interestingly, it was found that the ignition delay times recorded in the RCM were almost two orders of magnitude longer than those reported by Cadman et al. [375] and Herzler et al. [376,377] in shock tubes at temperatures below approximately 1000 K. These discrepancies have been discussed by Davidson and Hanson [47], Pang et al. [378], Petersen et al. [379], and Chaos and Dryer [305] from the perspective of shock tube experiments. Those studies highlighted the fact that non-ideal effects in shock tubes, including incident shock wave attenuation due to boundary layer growth, as well as other physical interactions may lead to pressure increases during the induction period, resulting in shorter ignition delays than if at a constant internal energy/specific volume condition. Moreover, in the experiments performed by Herzler et al. [376,377] this type of pressure rise was identified and highlighted by Petersen et al. [379], though the cause of it could not be exactly determined. As discussed in Sections 2 and 4, RCMs generally experience a pressure decrease during the induction period due to heat loss, and this extends ignition delay times relative to a constant internal energy/specific volume condition. The different characteristic effects of heat loss in RCMs and in shock tubes can explain some discrepancies in literature data, though further experimental datasets may help to clarify these issues further. Significantly, the discrepancies highlight the need for careful selection of the simulation framework, at the minimum including heat loss and boundary layer effects, as described in Section 5, when comparing simulation results to many experimental datasets.

Recently, Dames et al. [364] developed a binary fuel model for propane and DME under engine-relevant conditions where they studied pure propane over a range of conditions. Both τ_1 and τ_{ign} were measured experimentally for these mixtures and a detailed chemical kinetic model compared favorably

to the data. It was found that the reactions of H-atom abstraction from the fuel by ȮH radicals (R1) and also the reactions *n*-$C_3H_7O\dot{O}=C_3H_6+H\dot{O}_2$ (R3c) and $\dot{O}OCH_2CH_2CH_2OOH$=ketohydroperoxides+ȮH (R6a, R7) all controlled the low-temperature autoignition of propane. Rate constants for these reactions were taken from the work of Goldsmith et al. [380] and Merchant et al. [61] with some small adjustments in activation energies for the key reactions.

6.2.6. Butane isomers

Butane is a component of 'wet' natural gas and as well as petroleum, and it is a primary constituent of refined LPG. Furthermore, it is used as a blending agent for gasoline in cold weather environments due to its relatively high vapor pressure. This improves a gasoline's vaporization characteristics within an engine's intake manifold or combustion chamber and thereby enhances combustion stability while reducing emissions. From a fundamental perspective, butane is the smallest alkane that has isomeric structure branching.

Carlier et al. [365] reported total ignition delay times for an *n*-$C_4H_{10}/O_2/N_2$/Ar mixture, with the proportions of O_2 and N_2+Ar similar to that found in air. Ignition delay times ranged from about 90 to 180 ms, which is close to the 'loss of adiabaticity' limit shown in Fig. 28. Simulations were performed using a chemical kinetic mechanism by Lawrence Livermore National Laboratory (LLNL) [381], and it was found that the model was substantially more reactive than the experiments, in that the NTC region started at a lower temperature (670 K in the model compared to 700 K in the experiments) and ended earlier (710 K in the model, 810 K in the experiments). However, the magnitude of the ignition delays at the start and end of the NTC region was similar between the experiments and the model.

Griffiths et al. [76] studied the autoignition characteristics of *n*-butane and *iso*-butane as part of a study including hydrocarbons between C_4 and C_7. It was found that *n*-butane was much slower to react compared to the larger *n*-alkanes and this corresponded with its higher octane rating. They postulated that, because low-temperature chemistry is driven by alkylperoxyl (RO$\dot{O}$) radical isomerization (R3a) followed by decomposition reactions to oxygenated products and ȮH radicals (R5c), the reduced reactivity of *n*-butane might be associated with the inability to readily form hydroperoxy-peroxy species, e.g., ȮOQOOH via (R5a). It was also considered likely that the reactivities of the more highly branched species, including *iso*-butane, were constrained by similar mechanisms to those controlling *n*-butane. There was no indication however, in either the pressure or light emission records, of a vigorous development of two-stage ignition during the oxidation of *iso*-butane. Its reduced reactivity was thus ascribed to the activation energies associated with the transition states created during intra-molecular H-atom isomerization

reactions as a result of the tighter carbon-atom structure, and the opportunity of only a primary H-atom internal transfer when the initial radical is formed at the tertiary site. This work provided significant contributions of early experimental insights for the effects of branched structures on autoignition behavior in LTC regimes.

Minetti et al. [221] measured τ_1 and τ_{ign} for the oxidation and autoignition of stoichiometric, fuel-lean (ϕ = 0.8) and fuel-rich (ϕ = 1.2) *n*-butane/air mixtures. In addition, concentration measurements for selected major and minor species were recorded using a rapid sampling system and GC-MS analysis, as discussed in Section 3. C_4 heterocycles were identified, which were believed to be formed via isomerization and decomposition of butylperoxyl radicals (ROȮ) via (R5c). These data were simulated using a detailed chemical kinetic mechanism [382] and predicted ignition delay times were found to be of the same order of magnitude as those measured experimentally. Reasonably good agreement was found for the major species profiles, but minor species including 1- and 2-butene, tetrahydrofuran, methyloxetane, and 2,3-dimethyl oxirane were poorly predicted. This work highlighted the utility of employing intermediate species as additional validation targets for chemical kinetic mechanisms, while it has been recently demonstrated that ignition delay times may not sufficiently constrain a model so that measured time-histories of important intermediate species can provide additional constraints [383].

Minetti et al. [79] compared τ_{ign} measured for linear and branch chained alkanes including *n*-butane, *n*-pentane, *neo*-pentane, *n*-heptane, and *iso*-octane. The data for *n*-butane reported in the work of Minetti et al. [221] were compared to data recorded for *n*-pentane and *n*-heptane for stoichiometric fuel-air mixtures. It was shown that *n*-butane was considerably slower to react compared to the larger alkanes, consistent with the findings of Griffiths et al. [76]. Moreover, the minimum ignition temperature was higher for *n*-butane at approximately 700 K, compared to close to 670 K for *n*-pentane, and 625 K for *n*-heptane. Three chemical kinetic mechanisms were used to simulate the *n*-butane results, one taken from Kojima [384], one from Ranzi et al. [385], and the last developed by the authors [79] in their study. It was found that the mechanism from Ranzi et al. [385] best matched the *n*-butane experimental data.

Kim et al. [138] studied the effects of pressure and temperature on the autoignition of stoichiometric *n*-butane/synthetic air, as well as mixtures of propane/*n*-butane containing 20/80 and 40/60 molar volume blends of the two fuels. Compressed gas temperatures were attained by altering the ratio of the inert gas components (Ar and N_2). Two-stage ignition events and NTC behavior were experimentally observed. As the propane concentration was increased, the mixture reactivity decreased; at 750 K, for the blends with 20% and 40% propane, τ_{ign} increased by approximately 41% and 55% respectively, relative to

τ_{ign} measured for pure *n*-butane. These data highlighted the difficulty of achieving ROȮ isomerization with propane compared to *n*-butane (R3a).

Gersen et al. [366] measured ignition delay times of *n*-butane and *iso*-butane. Both butane isomers exhibited two-stage ignition at low temperatures (680–825 K), and also NTC behavior. Interestingly, at temperatures below about 900 K, ignition delay times for *n*-butane were shorter than for *iso*-butane, while above this temperature both isomers showed almost identical ignition delays. This feature highlights the influence that branched structures have on the ROȮ isomerization and decomposition reactions to form oxygenated products and ȮH radicals at lower temperatures. In addition, the authors observed temperature-dependent trends in reactivity in terms of ϕ. Below approximately 720 K, the ignition delays were relatively insensitive to ϕ. However, above that temperature, there was a marked difference in reactivity, resulting in a factor of 2 difference in ignition delay at ϕ = 0.5 versus ϕ = 1.0. The amplitude of the NTC region was decreased by increasing pressure from 15 to 30 bar, while this pressure increase reduced the ignition delay time for both isomers by roughly a factor of 3. In the region where two-stage ignition was observed, the duration of the first ignition stage decreased sharply in the temperature range of 680–770 K, but became essentially constant above 770 K. These data were simulated using a detailed chemical kinetic mechanism [358] and good quantitative agreement was observed between the measurements and calculations for *n*-butane including both ignition delay times in the two-stage region. However, substantial differences were observed for *iso*-butane, particularly in the NTC region, indicating that more work was needed to better understand and predict the influence of *iso*-butane's methyl branch on its LTC behavior.

Healy et al. [285] used both an RCM and a shock tube to measure ignition delay times for *n*-butane/air mixtures for lean to rich equivalence ratios covering a wide range of temperatures and pressure. A detailed chemical kinetic model was used to simulate the data and this was also able to reproduce a range of previously published ignition delay time data for *n*-butane, showing generally good agreement.

Healy et al.[367] followed this with autoignition experiments using *iso*-butane/air mixtures across similar temperature and pressure conditions, conducted within an RCM and a shock tube. The detailed kinetic model for *n*-butane developed previously [285] was updated with new reactions for *iso*-butane combustion. The model again showed good agreement with the data from this study, as well as data available in the literature. The authors further used this model to compare the reactivities of the butane isomers, and their simulations correlated. They found that *n*-butane was more reactive than *iso*-butane, where the difference in reactivity was greater at higher equivalence ratios and lower pressures.

6.2.7. Pentane isomers

Pentane is an intermediate/heavy component of 'wet' natural gas and is also present as a lighter component within petroleum feed-stocks. It is often used as a primary constituent to denature ethanol that is produced for E85 flexible fuel. Since its octane rating is lower than that of gasoline, it can be blended with high fractions of ethanol, which has a research octane number (RON) of 109, and thus achieve an octane rating that is suitable for modern gasoline engines. The three isomers of pentane have provided substantial insight into the influence of molecular structure on autoignition at LTC conditions.

In the study on the autoignition characteristics of C_4–C_7 *n*-alkanes published by Griffiths et al. [76], *n*-pentane was studied using stoichiometric mixtures in synthetic air. In this study greater reactivity was reported as the carbon number of the *n*-alkanes was increased. This was evident in both the measured minimum temperature at which spontaneous ignition first occurred, and in the minimum and maximum duration of the ignition delay times measured in the NTC region (~720–850 K for *n*-pentane and *n*-hexane). These trends corresponded loosely with the octane ratings of these fuels [386]. Moreover, the reactivity of *n*-pentane and *n*-hexane paralleled one another throughout the entire temperature range, with *n*-pentane being consistently a factor of two or so slower compared to *n*-hexane.

In another study, Griffiths et al. [368] measured ignition delay times for a range of alkanes (C_4–C_8) and mixtures of the PRFs, *n*-heptane and *iso*-octane, using stoichiometric fuel/air mixtures. Ignition delay times were reported as a function of temperature for *n*-pentane and 2,2-dimethylpropane (*neo*-pentane), among other fuels including PRF mixtures. The ignition delay times for *neo*-pentane and *n*-pentane were compared to fuels of similar RON covering a range of temperatures and pressures. The reactivity of PRF80 was compared to 2,4-dimethylpentane (RON = 83), 3,3-dimethylpentane (RON = 81), and *neo*-pentane (RON = 85). It was shown that all four fuels exhibited very different reactivities, with *neo*-pentane, which had the highest RON being the fastest to ignite across all temperatures. The same was true when *n*-pentane (RON = 62.5) was compared with PRF60, where *n*-pentane was shown to ignite faster than PRF60 in the temperature range of 700–900 K, even though it has a higher RON. However, at temperatures below 700 K and above 900 K, *n*-pentane was slower to ignite compared to PRF60. These findings, along with those presented in [76] provided early demonstrations of the complexity of autoignition processes within the NTC regime, and this leads to particular challenges associated with using octane ratings as a metric to characterize and predict fuel performance within advanced LTC regimes which are governed, or significantly influenced by autoignition chemistry. Furthermore, the findings highlight challenges of

relating results from fundamental apparatuses like RCMs and flow reactors to fuel performance in combustion engines.

Minetti et al. [79] acquired ignition delay data for linear and branch chain alkanes including *n*-pentane and *neo*-pentane, among other fuels discussed in other sections of this review. Fuel-oxygen-inert mixtures were prepared with inert gases N_2, Ar, and CO_2 used in varying proportions to achieve different compressed gas temperatures. Stoichiometric mixtures were studied for all fuels where the compressed pressure was adjusted depending on the fuel reactivity and the mixture equivalence ratio. *n*-Pentane and *neo*-pentane were studied at intermediate pressures, representing the intermediate reactivity of the fuels investigated. Both two-stage and single-stage ignition were identified in the pressure and natural light output traces. It was demonstrated that for stoichiometric *n*-pentane/air mixtures, τ_{ign} decreased with increasing compressed charge density i.e., pressure. Moreover, at a mean compressed charge density of 89.3 mol/m^3 it was shown that *neo*-pentane was slower to react compared to *n*-pentane in the temperature range of 650–950 K. Furthermore, the minimum ignition temperature of 700 K was higher for *neo*-pentane than the 675 K required for *n*-pentane.

Westbrook et al. [369] used RCM measurements to examine the influences of pressure, temperature, and equivalence ratio on the autoignition of *n*-pentane. The experiments were simulated using a detailed chemical kinetic mechanism where the calculations showed that for most experiments, the fuel exhibited two-stage autoignition except at the highest temperatures where little or no first-stage autoignition occurred. The model predicted that the first-stage ignition was controlled by low-temperature ROȮ radical isomerization pathways (R3a) that are quenched very effectively when the temperature reaches a level such that the dissociation of ROȮ (R3b, R3c) and peroxyl-alkylhydroperoxide (ȮOQOOH) radicals (R5b, R5c), respectively, become more rapid than the reverse addition steps. The second stage of ignition was predicted to be controlled by the dissociation of H_2O_2, leading to the formation of two reactive ȮH radicals. One important point of their work was that, in some cases, LTHR was predicted to occur during the compression stroke. This feature, as discussed in Section 4, can complicate the interpretation of experimental datasets since the 'compression' limit is reached and it is difficult to ascertain a baseline for defining the ignition delay time. Modifications to the test gas conditions, e.g., p_c, or the machine configuration, e.g., t_{50}, can be used to overcome this, while simulations that include the full compression stroke are necessary to compare with experimental measurements.

Cox et al. [77] studied the autoignition of *n*-pentane in stoichiometric mixtures with air. In the lower temperature range, two-stage ignition occurred and the first-stage of ignition consumed approximately

15% of the fuel, based on physical gas sampling and subsequent GC analysis. However, at the higher temperature range, the fuel ignited in one stage with a smoothly increasing extent of fuel consumption. In both cases, there was no measurable fuel decomposition during the compression stroke.

Ribaucour et al. [370] and Minetti and Ribaucour [81] compared the autoignition behavior of *n*-pentane and 1-pentene. They found both fuels showed two-stage ignition and NTC behavior, with 1-pentene being less reactive. Its minimum ignition temperature limit was higher than *n*-pentene, 700 K compared to 650 K, at a compressed pressure of 7.4 bar, while early exothermicity and NTC behavior were stronger for *n*-pentane and were observed over a wider temperature range. These features illustrate differences in the isomerization and formation of diperoxy species which are necessary for low-temperature oxidation, as discussed previously. Using their gas sampling apparatus and GC-MS analysis, these researchers compared typical common products formed at low temperatures, including the extent of fuel consumption as well as concentrations of C_4–C_5 olefins, C_5 cyclic ethers, and C_2–C_4 aldehydes. Very different distribution patterns were observed. *n*-Pentane produced high concentrations of 2-pentene, 1-pentene, and 1-butene, and low concentrations of the di-olefins 1,3-butadiene, and 1,3-pentadiene. Conversely, 1-pentene produced relatively high concentrations of 1,3-butadiene and 1,3-pentadiene. C_5 cyclic ethers (2-ethyl-3-methyloxirane, 2-ethyloxetane, 2,4-dimethyloxetane, and 2-methyltetrahydrofuran) were produced in significant concentrations during the oxidation of *n*-pentane, with 2-methyltetrahydrofuran dominating, whereas only propyloxirane was produced in any significant quantity for 1-pentene. Interestingly, its concentration was almost an order of magnitude higher for 1-pentene compared to *n*-pentane oxidation. Ethanal was the predominant aldehyde formed for both fuels, but significant concentrations of propenal and butanal were produced during the oxidation of 1-pentene, whereas propanal was more substantial for *n*-pentane with little butanal formed. A detailed mechanism was developed to simulate ignition delay times, LTHR and product species distributions. Good results were obtained for 1-pentene, but only when: (1) direct addition channels of $\dot{O}H$ and $H\dot{O}_2$ radicals to the double bond were included, and (2) if a higher rate constant for the decomposition of the hydroperoxyalkyl ($\dot{Q}OOH$) radicals into cyclic ethers (R5c) was used when this radical was formed by direct $H\dot{O}_2$ radical addition instead of isomerization of $RO\dot{O}$ radicals. Analysis of the chemical kinetic mechanism for 1-pentene indicated that the total ignition delay time depended on the competition between $\dot{Q}OOH$ radical addition to molecular oxygen (R5a) followed by reactions leading to chain branching, and the propagation reactions generating smaller alkenes (R5b). τ_1 was found to depend mainly on the rate of decomposition of unsaturated ketohydroperoxides (R8). This work contributed key, detailed experimental and modeling

results which identified influences of double carbon bonds on the chemical kinetic processes leading to cool flame and NTC behavior at LTC conditions.

Ribaucour et al. [371] measured ignition delay times for the three isomers of pentane in order to better understand the influences of variations in fuel molecular structure on autoignition behavior. It was found that under similar conditions, the fuels showed reactivity in the order *n*-pentane > *neo*-pentane > *iso*-pentane, while *iso*-pentane showed a much stronger NTC behavior compared to the other two isomers. The reactivity trends indicated greater flux through (R3c) from the alkyl radical combination with O_2 for *iso*-pentane, relative to the formation of the ROȮ radical (R3a). Simulations were also conducted using a detailed chemical kinetic mechanism where the model indicated that, in most cases, the reactive gases experienced two-stage heat release, except at the highest compressed temperatures, where little or no first-stage ignition was observed. Similar to the work of Westbrook et al. [369], it was indicated that the first-stage ignition is effectively quenched when the decomposition of ROȮ and ȮOQOOH radicals becomes faster than the reverse addition steps. The second-stage ignition was found to be controlled by the dissociation of H_2O_2.

Recently, Bugler et al. [372] used RCM data to re-investigate the kinetics of low-temperature fuel oxidation by studying the three isomers of pentane. By updating the thermochemical parameters associated with the intermediate species, e.g. ROȮ and ȮOOH radicals, and using rate constants calculated from the literature, including Villano et al. [387,388], Miyoshi [389,390], Goldsmith et al. [380], and Sharma et al. [391], it was possible to capture the reactivity of all three isomers using a detailed chemical kinetic model. This work highlighted the importance of consistently representing thermochemical properties towards achieving predictive capability of kinetic models at RCM (i.e., engine-relevant) conditions.

Bugler et al. [373] went on to investigate all three pentane isomers in both an RCM and two shock tubes. The data were recorded over a wide range of stoichiometry and compressed conditions. Comparisons of the reactivity of the three isomers at the higher pressures indicated that at low temperatures (640–900 K), the fuels showed reactivity in the order *n*-pentane > *neo*-pentane > *iso*-pentane, as observed in the study of Ribaucour et al. [371]. However, the reactivity of all three isomers tended to converge at 900 K. At higher temperatures (900–1450 K) the reactivities of *n*-pentane and *iso*-pentane were very similar, both being greater than the reactivity of *neo*-pentane. This was investigated using a chemical kinetic model where it was found at low temperatures *neo*-pentane reacts faster than *iso*-pentane because there is no possible concerted elimination reaction of *neo*-pentyl-peroxyl radicals

whereas these are possible for *iso*-pentyl-peroxyl radicals (and also for *n*-pentyl-peroxyl radicals). At temperatures in the range 900–1100 K, fuel alkyl radicals still add to molecular oxygen forming ROȮ radicals (R2a) and the concerted elimination reactions possible for *n*- and *iso*-pentane lead to the formation of olefins and $H\dot{O}_2$ radicals via (R3c). The lack of a concerted elimination reaction for *neo*-pentane leads to its much reduced reactivity at these temperature (900–1100 K) and pressure (≥ 10 bar) conditions, since the conversion of $H\dot{O}_2$ radicals to H_2O_2, and subsequently two ȮH radicals is prevented. *neo*-Pentane continues to show a much reduced reactivity in comparison to the other two isomers at even higher temperatures because β-scission of the *neo*-pentyl radical leads to the formation of *iso*-butene and a methyl radical. *iso*-Butene, or methylpropene is a particularly unreactive intermediate, as H-atom abstraction from it leads to the generation of relatively unreactive, resonantly stabilized methyl allyl radicals. The unmodified chemical kinetic model developed by Bugler et al. [373] was also used to successfully simulate species profiles measured as a function of temperature at 1 and 10 bar in two different jet-stirred reactors [392].

6.2.8. Hexane isomers

Hexane is a major component of petroleum-derived gasoline, and its five linear and branched chain isomeric structures result in a wide range of autoignition behavior.

Affleck and Fish [70] studied the autoignition of 2-methylpentane under engine-relevant, fuel-lean conditions in an RCM, and sub-atmospheric pressure, fuel-rich conditions in a Pyrex reactor. The work focused on comparing the products of first-stage ignition between the different conditions. In general, the measured products between the cases were very similar, indicating a common chemical mechanism could be operating at the widely varying pressure and equivalence ratio conditions.

Fish and co-workers [72,73,393] studied autoignition processes for four hexane isomers including 2-methylpentane, *n*-hexane, 2,2-dimethylbutane and 2,3-dimethylbutane. The autoignition characteristics were also compared to *iso*-octane and PRF mixtures of 25, 60, and 80 octane ratings. The authors removed gas samples from the reaction chamber for analysis by gas chromatography. These were some of the first speciated data to probe the decomposition and oxidation processes of a gasoline relevant constituent at LTC conditions. By using measurements of τ_1 and τ_{ign}, the authors were able to determine the relationship of the second-stage ignition delay (i.e., the difference between τ_1 and τ_{ign}) with Δp_1. In addition, they used the sampling experiments to elucidate the mechanism of low-temperature oxidation of the fuels they studied, establishing further experimental evidence for the chain carrying and chain branching species during low-temperature oxidation of alkanes under engine-relevant conditions.

Griffiths et al. [368] included 2-methylpentane in their measurements of C_4–C_8 alkanes where stoichiometric fuel/air mixtures were used. Ignition delay times were reported as a function of temperature comparing the reactivity of 2-methylpentane (RON = 73) to a PRF70 mixture. 2-Methylpentane was found to ignite more readily than the PRF70 mixture in the temperature range of 730–950 K. At lower temperatures, however, 2-methylpentane was slower to react and had a higher minimum ignition temperature of 700 K compared to 675 K for the PRF70 mixture. This study further illustrated differences that exist in LTC autoignition behavior for fuels having different molecular structure, but very similar octane ratings.

Zhang et al. [374] measured ignition delay times for *n*-hexane in an RCM at stoichiometric conditions. These data were also complemented by data measured in a shock tube for multiple fuel mixtures and over a range of temperature and pressure. Moreover, to further study the concentration of intermediate species formed during the oxidation process, experiments were performed in a jet-stirred reactor over a wide temperature range of 530–1160 K at 10 bar and at equivalence ratios of ϕ = 0.5, 1.0, and 2.0. A detailed chemical kinetic model was developed to simulate the experimental results, which was largely based on the reaction rate rules developed in the studies of Bugler et al. [372,373] for the pentane isomers. It was found that the new model was able to simulate the hexane results measured in the study, while the rules were successfully applied to simulate *n*-heptane shock tube [300] and JSR speciation results [394] under conditions of pressure, temperature, and mixture composition similar as those for *n*-hexane study.

6.2.9. Heptane isomers

Normal heptane has been used for many years as a reference fuel for gasoline and diesel. Its octane rating of 0 is used to establish one extremum of the octane scale, while its cetane rating is very similar to the rating of typical petroleum-derived diesel sold in North America. Moreover, substantial work has been undertaken using *n*-heptane as a two-component surrogate, i.e., primary reference fuel blend for gasoline and a single-component surrogate for diesel engines. The study of *n*-heptane in RCMs can be challenging due to its high reactivity. Most work to date has utilized low pressures, extensive dilution or very lean conditions in order to overcome this. A summary of the work carried out on *n*-heptane and larger alkanes is provided in Table 5.

Table 5. Studies of C_7 and larger alkane fuels using RCMs.

Fuels	T_c (K)	p_c (bar)	Mixture Composition	Diluent:O_2	ϕ	Reference
***n*-Heptane**	650–900	7.7–9.9	*n*-C_7H_{16}/O_2/N_2/Ar/CO_2	3.76	1.0	[76]

***n*-Heptane**	720–750, 845-875	8.2–9.2	*n*-$C_7H_{16}/O_2/N_2/Ar/CO_2$	3.76	1.0	[77]
***n*-Heptane**	650–950	9–11	*n*-$C_7H_{16}/O_2/N_2/Ar/CO_2$	3.76	1.0	[273]
***n*-Heptane**	640–900	2.7–4.5	*n*-$C_7H_{16}/O_2/N_2/Ar/CO_2$	3.76	1.0	[80,222]
***n*-Heptane**	798–875	41.6	*n*-$C_7H_{16}/O_2/N_2$	3.76	0.2–0.5	[395]
***n*-Heptane, 2-methylhexane, 3,methylhexane, 2,2-, 2,3-, 2,4-, 33-dimethylpentane, 3-ethylpentane, 2,2,3-trimethylbutane**	640–960	15 (10, 20 bar for *n*-C_7H_{16})	$Fuel/O_2/N_2/Ar/CO_2$	3.76	1.0	[396]
***n*-Heptane**	710–814	8–10.4	*n*-$C_7H_{16}/O_2/N_2$	3.76	1.0	[397]
***n*-Heptane**	660–710	9	*n*-$C_7H_{16}/O_2/N_2/CO_2$	5.64	1.0	[228]
***n*-Heptane**	650–900	9	*n*-$C_7H_{16}/O_2/N_2/Ar$	5.63	1.0	[133]
***iso*-Octane**	900–950	9	*iso*-$C_8H_{18}/O_2/N_2/Ar/CO_2$	3.76	1.0	[76]
***iso*-Octane**	640–920	10.7–16	*iso*-$C_8H_{18}/O_2/N_2/Ar/CO_2$	3.76	1.0	[222]
***iso*-Octane**	943–1027	5–23	*iso*-$C_8H_{18}/O_2/N_2/Ar/CO_2$	3.76–10	0.25–1.0	[271]
***iso*-Octane**	650–900	12.6–16.1	*iso*-$C_8H_{18}/O_2/N_2/Ar/CO_2$	3.76	1.0	[398]
***iso*-Octane**	820–900	15–45	*iso*-$C_8H_{18}/O_2/N_2/Ar$	6.07	0.75	[399]
***n*-Heptane/*iso*-octane**	670–760	18–20, 39–43	$Fuel/O_2/N_2/Ar$ (PRF0, 50, 75, 90, 100)	3.77	1.0	[102]
***n*-Heptane/*iso*-octane**	660, 875	20	$Fuel/O_2/N_2$ (PRF0, 72, 82, 91, 100)	3.76	0.1–0.6	[400]
***n*-Heptane/*iso*-octane**	650–950	7.5–9.0	$Fuel/O_2/N_2/Ar/CO_2$ (PRF0, 20, 40, 60, 70, 80, 90, 100)	3.76	1.0	[368]
***n*-Heptane/*iso*-octane**	798–875	41.6	$Fuel/O_2/N_2$ (PRF0, 50, 75, 90, 100)	3.76	0.2–0.5	[395]
***iso*-Octane**	600–800	20	*iso*-$C_8H_{18}/O_2/N_2/Ar/CO_2$	3.76	1.0	[133]
***iso*-Octane**	903–1020	8.7–16.6	*iso*-$C_8H_{18}/O_2/N_2/Ar/CO_2$	1.38–5.89	0.2–1.98	[213]
***iso*-Octane**	680–940	15.5–20.5	*iso*-$C_8H_{18}/O_2/Ar$	3.76	1.0	[85]
***iso*-Octane**	675–792	20	*iso*-$C_8H_{18}/O_2/N_2/Ar$	3.76, 6.0	1.0	[401]
***n*-Decane**	630–770	7–30	*n*-$C_{10}H_{22}/O_2/N_2$	3.76–19	0.5–2.2	[402]

Griffiths et al. [76] studied the ignition of several *n*-alkanes. Under the conditions investigated, *n*-heptane showed the highest level of reactivity and appeared to show the least amount of NTC behavior in the temperature range of 700–850 K, indicating that at these conditions the ROȮ and ȮQOOH isomerization processes, (R3a) and (R5a), respectively, are much quicker than their competing decomposition to $HȮ_2$ + alkene/ether/carbonyl species, (R3c) and (R5b), respectively, for the C_7 normal alkane. This behavior was shown by Curran et al. [274] to be a facility effect caused by heat losses, non-homogeneous effects or reaction during compression, with the model of Curran at al. reproducing these *n*-heptane experiments by incorporating heat losses and reaction during compression.

Cox et al. [77] studied the autoignition characteristics of stoichiometric *n*-heptane/air mixtures. Gas samples were also extracted from the reactive mixture during the chemical induction period and fuel conversion profiles were recorded. Under the higher temperature conditions, a substantial portion of the *n*-heptane was consumed during the compression stroke causing a first-stage of ignition to occur during piston compression, i.e., before the test conditions were reached. At the lower temperature conditions however, little to no fuel was consumed during the compression stroke, and two-stage ignition was present at the end-of-compression condition, consuming about 40% of the fuel in the first-stage, which was much greater than observed in their analogous tests using *n*-pentane.

Minetti et al. [80,222] measured ignition delay times and intermediate species concentrations during autoignition of stoichiometric *n*-heptane/air mixtures. A wide range of species, including cyclic ethers, were identified from their mass spectra. Concentration profiles of alkenes, aldehydes, and ethers were recorded, showing significant formation during the first-stage of ignition and consumption during the main ignition event for most of the LTC intermediates. These studies discussed the primary oxidation pathways of alkylperoxyl and hydroperoxy-alkyl radicals, including isomerizations of the former, (R3a), and scissions of the latter, (R5b) and (R5c).

Tanaka et al. [395] measured ignition delay times of *n*-heptane for varying ϕ = 0.2–0.5. In agreement with the study of Fish et al. [72], τ_{ign} was shown to correlate well with the energy released during the first-stage of ignition, or LTHR, as indicated by the initial pressure rise, Δp_1.

Silke et al. [396] measured ignition delay times of the nine heptane isomers/air mixtures in order to study the influence of molecular structure on ignition propensity. The recorded ignition delays showed good agreement with those reported by Griffiths et al. [76] at compressed pressure of 10 bar. All nine isomers exhibited NTC behavior, while it was found that increased chain substitution resulted in pronounced NTC along with decreased reactivity, highlighting the increasing importance of (R3c) and (R5b), where these compete more effectively with the isomerization steps due to higher strain on the bond angles during hydrogen transfer. The order of reactivity for the isomers was also shown to generally coincide with the individual octane ratings. Di Sante [397] also measured ignition delay times of stoichiometric *n*-heptane mixtures in air, showing good agreement with those from Griffiths et al. [76] and Silke et al. [396].

Karwat et al. [228] conducted ignition delay and species measurements for diluted stoichiometric *n*-heptane mixtures. Comparison of the experiments with a kinetic model showed poor agreement for several intermediates, particularly the heptane species formed from reactions of the ROȮ radicals. The

intermediate species profiles predicted by an updated kinetic model showed better agreement with the measurements, and this again demonstrated the benefit of including intermediate species profiles as additional validation targets for kinetic model development and refinement.

Di et al. [133] studied the effect of buffer (i.e., diluent) gas on the reactivity of *n*-heptane. Two different gases were studied, including nitrogen and argon. The buffer gas composition was found to have no effect on τ_1, but the different specific heat capacities of the diluents caused varying levels of pressure and temperature rise due to LTHR. This, in turn, affected τ_{ign}, with the use of argon as the diluent resulting in substantially shorter overall ignition delays compared to nitrogen.

6.2.10. *iso*-Octane and PRF blends

iso-Octane, or 2,2,4-trimethyl pentane, has been used for many years as a reference fuel for gasoline where its octane rating of 100 is used to establish the higher extremum of the octane scale. Its highly branched configuration yields unique LTC behavior, while its structure is also relevant as a fragment in the decomposition of larger, highly branched hydrocarbons like the diesel reference fuel 2,2,4,4,6,8,8-heptamethyl nonane (*iso*-cetane). Substantial experimental and modeling work has been undertaken using *iso*-octane as a single- or two-component surrogate for gasoline, i.e., PRF blends, in IC engines covering a range of conventional and LTC schemes. Additionally, numerous measurements have been conducted within RCM platforms. The extent of historical data and observed differences in some of the measurements also provided motivation to utilize this fuel as the reference species for the RCM Workshop Characterization Initiative [62], some results of which were presented in Fig. 2.

Griffiths et al. [368] used a reference temperature typical of that experienced in the end gas of spark ignition engines under knocking conditions, T_c = 900 K, to compare ignition delay times of the single-component fuels which had the same RON to comparable PRF mixtures. Ignition delay times of some of the low octane fuels and their corresponding PRF mixtures were shown to be in quantitative agreement. However, the agreement became less satisfactory for fuels with RONs higher than 85. The authors ascribed this difference to the decreasing reactivity of the fuels. For the binary PRF mixtures it was argued that appreciable reaction could occur during piston compression, leading to a sensitization of the mixture in the post-compression period at higher temperatures, whereas the single component alkanes were not similarly reactive. These differences were linked to the relative reactivities of the fuels and to characteristics of reaction rates in the NTC regime, in the temperature range of 750–850 K. It was suggested that the minimum temperature at which autoignition occurs within a given system, rather than ignition delay time, might give a closer correlation of the relationship between reactivity observed in RCMs

and octane numbers measured in operating engines. This idea has not been explored to date, but would entail characterizing the thermo-physical state of the gas over a wider range of conditions than typically explored in RCMs, and could be subject to large uncertainties, based on current understandings of gas motion and heat loss phenomena. More recent work by Mehl et al. [403], and Badra et al. [404] suggested that using a lower temperature and higher pressure, e.g., T_c = 820 or 825 K and p_c = 20 or 25 bar, respectively, would enable better comparison between RON ratings and RCM-measured τ_{ign}.

Park and Keck [102] measured ignition delays for stoichiometric PRF/O_2/N_2/Ar mixtures with five blends including PRF100, 90, 75, 50, and 0. It was found, consistent with the work of Griffiths et al. [368], that the ignition delays were not a linear function of octane rating. In addition, for the experimental conditions utilized, τ_1 decreased significantly as the temperature increased, whereas τ_{ign} stayed unchanged. The authors also highlighted the importance of characterizing the heat loss behavior of their configuration, as well as the procedures used for mixture preparation when conducting RCM tests.

Minetti et al. [222] measured ignition delay times and intermediate species concentrations during autoignition of stoichiometric *iso*-octane/air. In general, the authors found that at the conditions investigated *iso*-octane was much less reactive than *n*-heptane, which had a more significant two-stage ignition zone and required much lower pressures to realize similar τ_{ign}. Intermediate species concentrations recorded using rapid gas sampling aided in understanding the low-temperature reaction pathways where the authors highlighted the importance of β-scission reactions (R5b) in producing unsaturated species, such as methylpropene and substituted pentenes, and noted that the primary stable oxygen containing heterocycle intermediates were tetrahydrofurans.

Tanaka et al. [395] measured ignition delay times of *iso*-octane, as well as PRF blends of 50, 75, and 90. For the fuels explored, the authors attempted to uncover empirical relationships between τ_{ign}, Δp_1, burn rates (defined as *dp/dt* at τ_{ign}), ϕ, and octane rating. The trends observed in the data were highly non-linear where τ_{ign} was found to be inversely proportional to Δp_1, burn rate, and ϕ, and directly proportional to octane rating.

Lim et al. [400] conducted RCM experiments for PRF blends of 0, 72, 82, 91, and 100. In many of their tests, LTHR occurred during the compression stroke, so it was difficult to define t_0. Additionally, as the 'loss of adiabaticity' limit defined in Section 4 was reached for some of the lean mixtures of low *n*-heptane content, autoignition was quenched. Furthermore, the data were not displayed on a conventional Arrhenius diagram so that trends from the pressure traces had to be deduced. Nevertheless, their results showed that as the *n*-heptane mixing ratio was decreased, both τ_1 and τ_{ign} increased while a slightly higher

compressed temperature (~30 K) was required to initiate LTHR. As well, as ϕ increased, the extent of LTHR, and thus Δp_1 increased.

He et al.[271] measured ignition delay times of *iso*-octane and investigated the effect of addition of EGR species CO_2 and H_2O. Measurements showed that H_2O has a chemical effect, with ignition delays decreasing with increasing water content, while CO_2 was found to have no effect for the conditions studied. The performance of various kinetic mechanisms in predicting the ignition delay times was also investigated. He et al. [243] further measured ȮH concentrations using narrow line absorption techniques, as discussed in Section 3, and used these results to evaluate the significance of the rate constants of important reactions, including $H_2O_2(+M)=\dot{O}H+\dot{O}H(+M)$, $\dot{C}H_3+H\dot{O}_2=CH_3\dot{O}+\dot{O}H$, and $\dot{C}H_3+H\dot{O}_2=CH_4+O_2$.

Vanhove et al. [167][398] studied ignition delay times of stoichiometric *iso*-octane/air mixtures, as well as mixtures of this fuel with toluene and 1-hexene. It was found that *iso*-octane was converted to C_8 intermediate products, including *iso*-octenes and cyclic ethers. In addition, it was noted that as *iso*-octane is much less reactive than *n*-heptane, the generation of a pool of radicals at low temperatures requires higher pressure. The evolution of the ignition delays with the addition of toluene or 1-hexene was found to be highly non-linear, which was attributed to the formation of the radical pool by the most reactive species.

Mittal and Sung [399] measured ignition delay times of *iso*-octane/O_2/N_2/Ar mixtures at, along with blends of *iso*-octane and other hydrocarbons, in order to understand the chemical kinetic interactions between different fuel components. For binary fuel blends of toluene and *iso*-octane in particular, it was found that the variation of ignition delay with the relative fuel proportion was highly nonlinear, resulting in greatly enhanced reactivity even with a small addition of *iso*-octane to toluene. This finding correlated with results of octane testing performed by Morgan et al. [405] and ignition delay measurements by Vanhove et al. [398].

Di et al. [133] studied the influence of buffer gas on the autoignition characteristics of *iso*-octane in their study examining the behavior of *n*-heptane. Three diluent gases were studied including nitrogen, argon, and a mixture of argon and CO_2. As with *n*-heptane, using argon as the diluent resulted in similar τ_1 as compared to N_2, but shorter overall ignition delays, due to the larger Δp_1 and temperature rise of LTHR. Furthermore, the effect of third-body collision efficiencies was probed by blending argon with CO_2 such that the specific heat nearly matched that of pure nitrogen. The authors concluded that there was negligible effect due to the third-body collision efficiencies at their experimental conditions.

Zhang et al. [401] investigated two-stage ignition in the NTC region for stoichiometric *iso*-octane/O_2/N_2/Ar mixtures. It was found that τ_1 was sensitive to O_2 concentration, but was insensitive to the dilution gas and fuel concentrations. A detailed model was used to explain the cause of the NTC behavior, and this was predicted to be due to the competition between (R5a), (R3c), (R5c) and (R2b), i.e., the backward reaction of the second $\dot{Q}OOH$ radical addition to O_2, $RO\dot{O}$=alkene+$H\dot{O}_2$, $\dot{Q}OOH$=cyclic-ether+$\dot{O}H$, and the β-scission reactions of the alkyl radicals, respectively.

6.2.11. Decane

Decane is representative of some of the largest alkanes in gasoline, as well as some smaller components in jet fuel and diesel. There has been only one study by Kumar et al. [402] using decane in an RCM due to challenges associated with its high boiling point and high reactivity. Dependence of τ_1 and τ_{ign} on varying fuel concentrations, oxygen mole fractions, pressure, and temperature were investigated in this study. τ_{ign} was found to depend strongly on the equivalence ratio and compressed gas pressure, but τ_1 depended primarily on the compressed gas temperature and did not depend strongly on ϕ or pressure. In addition, through comparison to a kinetic model, the decomposition of ketohydroperoxides via (R5a) was shown to be important in both τ_1 and τ_{ign}.

The understanding of LTC autoignition behavior for paraffinic fuels has been developed over many years with the assistance of successive RCM experiments. In order to expand this towards a comprehensive understanding of LTC autoignition, as well as the formulation of fuel surrogates and the development of chemical kinetic models for transportation liquid fuels, validation datasets of larger alkanes beyond decane, such as dodecane and cetane, under engine relevant conditions are needed. Several groups are currently conducting RCM experiments towards those heavier hydrocarbons.

6.3. Cycloalkanes

Cycloalkanes, or naphthenes, can constitute a significant portion of gasoline, jet fuel, and diesel, with larger fractions found in fuels derived from non-traditional feed-stocks, e.g., shale oil, cellulosic-/sugar-based biomass. The generally 5- and 6-membered ring structures of these components yield unique autoignition and pollutant formation behavior compared to analogous straight and branched chain alkanes, since ring opening and dehydrogenation processes play important roles. Additional complexity in the chemistry arises from multiple stable conformations of the cyclic structure for fuels with ring sizes greater than six carbon atoms, and the influence these conformations have on the internal isomerization reactions. To date there has been little to no work reported investigating the autoignition behavior of 5-

membered ring naphthenes within RCMs, while some studies have been conducted investigating 6-membered ring fuels. A summary of the work performed on cycloalkanes is provided in Table 6, along with that on alkene and aromatic fuels.

Table 6. Studies of cycloalkane, alkene and aromatic fuels using RCMs.

Fuels	T_c (K)	p_c (bar)	Mixture Composition	Diluent:O_2	ϕ	Reference
Cyclohexane	600–900	7–14	*cyc*-$C_6H_{12}/O_2/N_2/Ar/CO_2$	3.76	1.0	[83]
Cyclohexane	680–910	12.5, 20, 40	*cyc*-$C_6H_{12}/O_2/N_2/Ar$	3.76	0.5, 1.0, 2.0	[406]
Methylcyclohexane	650–1050	10, 15, 20	*cyc*-$C_7H_{14}/O_2/N_2/Ar$	3.76	1.0	[407]
Methylcyclohexane	650–900	15–25	*cyc*-$C_7H_{14}/O_2/N_2/Ar$	3.5, 8.0, 12.5	0.5, 1.0, 1.5	[408]
Methylcyclohexane	690–900	50	*cyc*-$C_7H_{14}/O_2/N_2/Ar$	3.5, 8.0, 12.5	0.5, 1.0, 1.5	[409]
Methylcyclohexane	702–802	15	*cyc*-$C_7H_{14}/O_2/N_2/Ar$	8.0	0.5	[401]
Propylcyclohexane	620–930	4.5–13.4	*cyc*-$C_9H_{18}/O_2/N_2/Ar/CO_2$	3.76	0.3, 0.4, 0.5	[224]
Ethylene	850–1050	15, 30, 50	$C_2H_4/O_2/N_2/Ar$	11.28	1.0	[410]
Propene	750–1100	10, 40	$C_3H_6/O_2/N_2/Ar$	3–19	0.5, 1.0, 2.0	[411]
***iso*-Butene**	666–996	10–50	$iC_4H_8/O_2/N_2/Ar$	3.76	0.3, 0.5, 1.0, 2.0	[412]
1-Pentene	600–900	6.8–9.2	$C_5H_{10}/O_2/N_2/Ar/CO_2$	3.76	1.0	[81,370]
1-, 2-, 3-Hexene	630–850	10	$C_6H_{12}/O_2/N_2/Ar/CO_2$	3.76	1.0	[84]
1-Hexene/*iso*-octane	630–900	11–14	Fuel/ $O_2/N_2/Ar/CO_2$ 1-C_6H_{12}:*iso*-C_8H_{18} = 0.22	3.76	1.0	[398]
Cyclohexene, cyclohexa-1,3diene	600–900	7–14	Fuel/$O_2/N_2/Ar/CO_2$	3.76	1.0	[83]
1-, 2-, 3-Heptene	827	41.6	Fuel/O_2/N_2	3.76	0.2–0.5	[395]
Diisobutylene-1	760–950	35, 45	DIB-1/$O_2/N_2/Ar$	3.76–6.37	0.75	[399]
Benzene	~800	20	$C_6H_6/O_2/N_2$	3.76	0.5, 1.0	[413]
Benzene	1040–1100	45	$C_6H_6/O_2/N_2/Ar$	5.87, 12.7	0.5, 1.0	[414]
Benzene/*n*-heptane	620–865	4.63–8.87	Fuel/$O_2/N_2/Ar/CO_2$ C_7H_8:*n*-C_7H_{16} = 0.5	3.76	1.0	[415]
Toluene	920–1100	25, 45	$C_7H_8/O_2/N_2/Ar$	4.72–14.9	0.5, 0.75, 1.0	[414]
Toluene/*n*-heptane	710–814	8–10.4	Fuel/O_2/N_2 C_7H_8:*n*-C_7H_{16} = 0, 0.3, 0.6, 0.8	3.76	1.0	[397]
Benzene/*n*-heptane, toluene/*n*-heptane, toluene/*iso*-octane, toluene/1-hexene, toluene/1-hexene/*iso*-octane	630–900	11–15	Fuel/$O_2/N_2/Ar/CO_2$ C_6H_6:*n*-C_7H_{16} = 1 C_7H_8:*n*-C_7H_{16} = 1 C_7H_8:*iso*-C_8H_{18} = 0.54 C_7H_8:1-C_6H_{12} = 2.33 C_7H_8:1-C_6H_{12}:*iso*-C_8H_{18} = 35/18/47	3.76	1.0	[398]
Toluene/*iso*-octane	910–1060	25, 45	Fuel/$O_2/N_2/Ar$	6.07–8.82	0.75	[399]
Toluene/diisobutylene-1	860–1050			7.40–8.82		
Toluene, ethylbenzene, 2-ethyltoluene, *n*-propylbenzene, *n*-butylbenzene, xylene isomers, and	600–907	6.2–25	Fuel/$O_2/N_2/Ar/CO_2$	3.70	1.0	[416]

trimethylbenzene isomers, *n*-butylbenzene and *o*-xylene						
***n*-Butylbenzene, *o*-xylene and *o*-ethyltoluene**	600–900	14–19	Fuel/O_2/N_2/Ar/CO_2	2.70	1.0	[225]
***n*-Butylbenzene**	640–840	14–18	*n*-BB/O_2/N_2/Ar/CO_2	2.70, 3.76	1.0	[225]
***n*-Propylbenzene**	650–1000	10, 30, 50	*n*-PB/O_2/N_2/Ar	3.76	0.29, 0.48, 0.96, 1.92	[417]
***n*-Butylbenzene**	640–960	13–23	*n*-BB/O_2/N_2/Ar/CO_2	2.70, 3.76	0.3, 0.4, 0.5	[418]
***n*-Butylbenzene**	730–1020	10, 30, 50	*n*-BB/O_2/N_2/Ar	3.76	0.3, 0.5, 1.0, 2.0	[419]
Tetralin (1,2,3,4-tetrahydronaphthalene)	762–950	15, 35, 50	Tetralin/O_2/N_2	3.76, 8.56	0.5, 1.0	[420]

6.3.1. Cyclohexane

Lemaire et al. [83] studied the oxidation of cyclohexane to understand the low-temperature pathways leading to the formation of benzene. The oxidation characteristics of cyclohexene and cyclohexa-1,3-diene were also investigated in this study. Cyclohexane was found to exhibit two-stage ignition at low temperatures and single-stage ignition at intermediate temperatures. NTC behavior was evident at conditions investigated in this study. Pathways leading to the formation of conjugated alkenes were observed to promote the formation of benzene.

Vranckx et al. [406] reported ignition delay times of cyclohexane/air mixtures and compared the measured values with those from Lemaire et al. [83]. τ_{ign} from [406] are consistently longer than those in [83], where these significant differences were suggested to arise partly from the longer compression time in [83] and higher heat losses in [406]. Additionally, simulations were conducted to assess the performance of three available kinetic models. All three models were found to generally capture the autoignition characteristics of cyclohexane but none of the mechanisms was observed to correctly predict the measured τ_{ign} over a wide temperature range. Sensitivity analysis showed differences in the dominant reaction classes controlling ignition for the three mechanisms which was due to the different reaction rates used in three mechanisms. The study of [406] also identified the importance for further understanding the $\dot{Q}OOH$ radical chemistry, e.g., (R5).

6.3.2. Methylcyclohexane

Pitz et al. [407] measured τ_{ign} of stoichiometric methylcyclohexane (MCH) + oxidizer mixtures. MCH was found to exhibit two-stage ignition behavior at low temperatures, and NTC behavior was also

observed. A detailed chemical kinetic model for MCH was developed and the simulated ignition process was observed to be dependent on the isomerization rates of methylcyclohexylperoxyl radicals (R3a). Incorporation of isomerization rates of ROȮ radicals resulted in longer ignition delays and the absence of NTC behavior. A kinetic model using isomerization rates from Gulati and Walker [421] was found to predict τ_{ign} in reasonable agreement with measured values, along with similar NTC behavior.

Mittal and Sung [408] measured ignition delay times of MCH/O_2/N_2/Ar mixtures. In this work ϕ was varied by changing the concentration of oxygen at fixed MCH concentration (1.047%). τ_1 and τ_{ign} were found to depend significantly on oxygen concentration. Simulations conducted using the MCH kinetic model developed by Pitz et al. [407] predicted ignition delay times that were substantially different from the experimental measurements.

Weber et al. [409] measured ignition delay times of MCH/O_2/N_2/Ar mixtures at a higher compressed pressure of 50 bar. A new chemical kinetic model of MCH was developed by updating the mechanism of Pitz et al. [407] with new reaction pathways and more accurate rate constants for many reactions, including (R1), (R2a), (R3a), (R5), and (R8). The updated kinetic model was found to predict τ_{ign} measured in [407–409] with good agreement.

In the same study as that for *iso*-octane discussed above, Zhang et al. [401] investigated autoignition of lean (ϕ = 0.5) MCH/O_2/N_2/Ar mixtures in the temperature range 702–802 K at p_c = 15 bar, where two-stage ignition behavior was observed at T_c = 750–785 K.

6.3.3. Propylcyclohexane

Crochet et al. [224] experimentally obtained τ_{ign} of *n*-propylcyclohexane/air mixtures. Concentrations of 49 intermediate species were also recorded using a rapid gas sampling technique and mass spectrometry. The data indicated that a variety of bicyclic ethers, as well as conjugated alkenes were formed during the first-stage ignition period. In particular, 1-oxa-2-methylsprio[3,5]nonane and 1-oxa-2-ethylspiro[2,5]octane, and 4-propylcyclohex-1-ene and 3-propylcyclohex-1-ene were most abundant. The authors proposed formation pathways for both classes of intermediates starting from the ȮOOH radicals, i.e., (R5b) and (R5c). Measured τ_{ign} were compared with high-pressure shock tube experiments and good agreement was observed. Simulated ignition delay times, conducted using a kinetic model of *n*-propylcyclohexane, were found to differ from the experimental values by two orders of magnitude. These differences were attributed to the absence of low-temperature reaction pathways in the model.

Overall, the state of the art of understanding and simulations for cycloalkanes significantly lag the development of paraffins. These structures can indeed lead to increased complexity in the internal isomerization reactions, and significantly affect the overall reactivity of a multicomponent fuel. The large discrepancies between experiments and model indicate that further work is clearly needed to unravel the overall autoignition mechanism.

6.4. Alkenes

Alkenes or olefins are present in petroleum-based fuels, with especially significant quantities found in some renewable-based fuels. Their autoignition behavior is substantially different from saturated analogues, such that blending of fairly small amounts (5–10% by volume) can alter the octane or cetane rating of a fuel. Unfortunately, the PM and smog-forming potential of high olefin fuels can be substantially greater than low olefin counterparts. Fundamentally, ethylene, propene, and larger alkenes are important intermediates formed in the decomposition of many fuels via (R3c) and (R5b). This section highlights features associated with double carbon bonds located within or branched from the alkyl backbone, which affect the LTC behavior of these fuels, through additional reaction pathways and formation of resonance-stabilized allylic radicalsthat are not shown in Fig. 37.

Ethylene is typically not a component of liquid fuels, but as noted, it is an important intermediate species formed due to β-scission reactions of larger hydrocarbons. Additionally, it is a key intermediate in soot formation where its decomposition can lead to acetylene which participates in the HACA (H-atom abstraction–C_2H_2-addition) mechanism. Kumar et al. [410] measured τ_{ign} of diluted stoichiometric ethylene/oxidizer mixtures. Simulated τ_{ign} using the Center for Energy Research at the University of California at San Diego reaction mechanism [422] exhibited good agreement with the experimental data. Kinetic analyses demonstrated the importance of reactions between ethylene and the $H\dot{O}_2$ radical in the low-to-intermediate temperature range.

To enhance the understanding of propene chemistry, which is also an important intermediate formed during combustion of larger fuels, Burke et al. [411] recently conducted a series of τ_{ign} measurements in six different shock tubes and two RCMs covering a very wide range of pressure and temperature. This study provided a basis for extensive facility cross-comparisons for experimental τ_{ign}, while a large database was generated for model validation. Experimental results were also compared to predictions of the chemical kinetic mechanism developed in this study and good agreement was observed.

Recently, Zhou et al. [412] carried out a detailed experimental and kinetic modeling investigation of the oxidation of *iso*-butene. This study included measurements of τ_{ign} in shock tubes and RCMs, laminar flame speeds, and speciation data measured in flow and jet-stirred reactors. Based on chemical kinetic modeling it was found that the reactivity of the alkene species at very low temperatures (< 800 K) is dominated by $H\dot{O}_2$ addition reactions to the double bond of the alkene followed by addition of O_2 to the resulting radical. At intermediate temperatures (800–1300 K), the reactivity is controlled by the competition between H-atom abstraction from the alkene by O_2 and $\dot{O}H$ radicals with subsequent reaction between resonantly stabilized methyl-allyl radicals, and $H\dot{O}_2$ resulting in chain branching reactions. This work highlighted, similar to earlier studies with larger alkenes which are discussed next, that $H\dot{O}_2$ combination reactions are critically important steps in the chain branching and LTC oxidation of alkene fuels, and this is unique compared to alkane combustion, as discussed above.

Ribaucour et al. [370] and Minetti et al. [81] compared the autoignition behavior of 1-pentene and *n*-pentane and found that both fuels showed two-stage ignition and NTC behavior, with 1-pentene being less reactive. Details of this study are discussed in Section 4.2.7.

Vanhove et al. [84] investigated the autoignition chemistry of stoichiometric mixtures of the three hexene isomers and discussed the effect of the double bond position. Gas samples were also extracted from the reactive mixtures and gas chromatography conducted to analyze the composition of the sampled gas. Selectivities of the main intermediates were reported, including C_6 saturated O-heterocycles, C_6 saturated aldehydes and ketones, C_6 unsaturated O-heterocycles, C_6 unsaturated aldehydes and ketones, hexadienes, C_2–C_5 saturated aldehydes, and C_3–C_5 unsaturated aldehydes. Of the three isomers of hexene, 1-hexene was found to be more reactive while 3-hexene was found to be the least reactive. The NTC behavior was more pronounced for 1-hexene while 3-hexene exhibited very weak NTC behavior. The authors proposed pathways to the formation of the major intermediate species based on analogy to the isomers of pentane. Of particular influence was the addition of $\dot{O}H$ and $H\dot{O}_2$ radicals to the double bond, leading to epoxidation or scission of the double bond, also discussed in [A3]. These features highlight the influence of alkyl chain structure on the isomerization steps (R3a, R5a) necessary for low-temperature ignition. In another study, Vanhove et al. [398] measured the ignition delay times of stoichiometric 1-hexene/toluene, 1-hexene/*iso*-octane, and 1-hexene/*iso*-octane/toluene blends. Gas samples were extracted from the reactive mixtures to understand the kinetic interactions between the hydrocarbons.

Lemaire et al. [83] measured the ignition delay times of stoichiometric fuel/air mixtures of cyclohexene and cyclohexa-1,3diene. In their study, there was neither two-stage ignition or NTC behavior

observed for cyclohexa-1,3-diene. While cyclohexene behaved in an intermediate way without a first-stage ignition, there existed a narrow, not very marked NTC region. Modeling work indicated that by including addition of O_2 to cyclohexenyl radicals (R2a) and the various isomerizations of the resulting peroxyl radicals, most of the C_6 products from cyclohexene could be predicted by the classical scheme for low-temperature oxidation. However, as in [84], in order to predict the formation of 1,2-epoxycyclohexane, addition of ȮH and HO_2̇ radicals to the double bond had to be included in the model. For cyclohexa-1,3-diene, the classical scheme was found to be invalid, as the C_6 oxygenated products are only formed by addition of ȮH and HO_2̇ radicals to the double bond. Furthermore, the pathways to benzene are those leading to conjugated alkenes, which are more efficient than those producing oxygenated products, either by adding HO_2̇ to double bonds, or by addition of O_2 to the initial cyclic radical.

Tanaka et al. [395] measured the ignition delay times of the three linear heptene isomers in air under fuel lean conditions. Of the three isomers, 1-heptene exhibited the shortest ignition delay while 3-heptene exhibited the longest ignition delay. At their experimental conditions, 1-heptene and 2-heptene both showed two-stage ignition, though 3-heptene exhibited only single-stage ignition behavior.

Ignition delay times of diisobutylene-1 (DIB-1)/oxidizer mixtures and binary blends of DIB-1/toluene mixtures were measured by Mittal and Sung [399]. It was shown that, consistent with the work of Vanhove et al. [84], the inclusion of a double bond and the location of its position can significantly alter the fuel ignition characteristics.

Under low-to-intermediate-temperature conditions, the overall chemical kinetic behavior of alkenes is a result of competition between two channels – reactions through hydrogen abstraction from the alkyl chain, and in the main, the addition of ȮH and HO_2̇ radicals to the double bond [84]. When autoignition chemistry is dominated by the reactivity of a double bond, alkenes do not exhibit pronounced NTC behavior [84]. As highlighted in the study of Ribaucour et al. [370] covering the autoignition behavior of *n*-pentane and 1-pentene, the reactions involving direct addition of ȮH and HO_2̇ to the double bond are the controlling steps. Therefore, the less pronounced features of NTC behavior for alkenes, as compared to alkanes, indicate the addition reactions at the double bond dominate over the peroxidation reactions of the alkenyl chain.

6.5. Aromatics

Aromatics are an important class of hydrocarbons within petroleum-derived fuels and their presence significantly influences autoignition and heat release characteristics, as well as PM emissions. The LTC

behavior of fuels with high aromatic content can be quite different than other fuels, even for blends with similar octane ratings [423], and this can have significant implications for engine operation and control, especially under LTC schemes.

6.5.1. Benzene

Beckers and Levedahl [413] studied the kinetics and mechanism of rapid autoignition for benzene/air mixtures using an RCM and a motored engine at the compressed conditions of 800 K and 20 bar in the RCM, and 900 K and 40 bar in the engine. They found the kinetics of the overall reaction can be described by a bimolecular rate equation with a low apparent activation energy near 11.6 kcal/mol (48.53 kJ/mol). Furthermore, the motored engine tests revealed that only 1.5% of the fuel molecules had decomposed, with 2- and 4-carbon acetylenes being the only hydrocarbon intermediates found. Additional species detected included CO_2, H_2O, methanol, and HCHO which were hypothesized to be oxidation products of acetylenes. The lack of phenol derivatives indicated that the breaking of the benzyl ring occurs very shortly after the first attack on the molecule, which was in contrast to reported experiments at lower temperatures, e.g., ~600 K.

Mittal and Sung [414] reported τ_{ign} for benzene/O_2/N_2/Ar mixtures. The mole fraction of benzene was fixed and the amount of oxygen was varied in order to change ϕ. Simulations were also conducted to examine the performance of various chemical kinetic mechanisms for benzene, and these showed that none of the mechanisms existing at the time succeeded in predicting the ignition delay times with good agreement, where the apparent activation energies of the models were much lower than observed in the experimental measurements, and the ITHR was larger.

The co-oxidation of benzene in 50/50 mixtures with *n*-heptane was reported by El Bakali et al. in [415]. Two-stage ignition was observed in their RCM measurements, and qualitative analysis of the intermediate products did not show the formation of aromatic products such as phenol, while a variety of products of *n*-heptane first-stage reactivity were identified. The ignition delay results were compared with predictions of a kinetic model developed by the authors, showing overall good agreement.

6.5.2. Alkyl substituted benzenes

Mittal and Sung [414] reported the ignition delay times of toluene/O_2/N_2/Ar. Experiments were conducted to understand the effects of ϕ and oxygen concentration on ignition delays. It was noted that toluene was much more reactive than benzene under the same conditions. The experimental results were compared to shock tube data [424] to specifically analyze the ITHR. Under similar state conditions and

overall stoichiometry, but with 2.5 times greater fuel loading, i.e., fuel mole fraction of 0.0228 compared to 0.00962, the shock tube pressure records indicated substantially larger ITHR compared to the RCM data. Mittal and Sung [414] argued that this could be due to surface contamination in the shock tube experiments leading to non-uniform, or mild ignition events, and presented evidence for this by conducting tests where the RCM reaction chamber was intentionally vitiated. Based on this, the apparently high ITHR in the shock tube could have been due to deflagrative processes, or pre-ignition heat release. Simulations of the experiments demonstrated that none of the chemical kinetic mechanisms existing at the time succeeded in predicting τ_{ign} with good agreement. As with benzene, the apparent activation energies were too low, while the ITHR appeared to be significantly over-predicted by the models. Moreover, the various models indicated different fuel consumption patterns, extents of intermediates formed, and importance of different reactions.

Di Sante [397] measured ignition delay times of stoichiometric *n*-heptane/toluene mixtures in air. Comparison of ignition delays for pure *n*-heptane/air mixtures with those of *n*-heptane/toluene/air mixtures showed that τ_{ign} increased with increases in the amount of toluene, while *n*-heptane chemistry dominates at low amounts of toluene which is not surprising given the lower reactivity of toluene. Ignition delay times obtained from numerical simulations conducted using gasoline surrogate modeling from LLNL, validated notably on the experimental results from [425] and [414], showed reasonable agreement with experimental measurements.

Vanhove et al. [398] studied oxidation of *n*-heptane/toluene, *iso*-octane/toluene, 1-hexene/toluene binary blends and a three-component surrogate gasoline fuel composed of 1-hexene/*iso*-octane/toluene. Ignition delays and intermediate species profiles were measured using a gas sampling rig. τ_{ign} was, as expected, observed to increase nonlinearly with addition of toluene for the binary blends at low temperatures. In addition, the apparent activation energy in the NTC region was found to decrease with addition of toluene to *iso*-octane, hexane, and *n*-heptane. Speciation measurements during the chemical induction times indicated that toluene is converted to benzaldehyde and benzene, with trace concentrations of cross reaction products such as ethylbenzene and heptenylbenzene observed. Such cross reaction products have typically not detected in work using flow reactors operated in diluted regimes, where this highlights the practical interest of conducting speciation studies at engine-relevant conditions where these interactions may, or may not evolve.

The high-pressure autoignition characteristics of binary fuel blends of toluene/*iso*-octane and toluene/DIB-1 were studied by Mittal and Sung [399]. The relative proportion of the two fuels was

systematically varied in the binary blends, while the total fuel mole fraction and ϕ were kept constant. Experimental results showed that the variation of τ_{ign} with the relative fuel proportion was highly nonlinear, namely a small addition of *iso*-octane or DIB-1 to toluene resulted in greatly enhanced reactivity. Furthermore, the effect of DIB-1 addition to toluene was seen to be more significant than the stimulating effect of *iso*-octane addition.

Roubaud et al. [82,225,416] studied the autoignition characteristics of 11 alkyl substituted benzenes to understand the effect of substituent position and alkyl chain length on ignition delay characteristics. The fuels included toluene, ethylbenzene, 2-ethyltoluene, *n*-propylbenzene, *n*-butylbenzene, xylene isomers, and trimethylbenzene isomers. *n*-Butylbenzene and *o*-xylene were found to be the most reactive. *n*-Butylbenzene was the only fuel that exhibited an NTC behavior, while ignition delay times of *o*-xylene and 1,2,3 trimethylbenzene exhibited two-stage ignition and NTC behavior. The measurements indicated that the fuel reactivity increases as the chain length of the alkyl substitution increases, and the proximity of the substituents also increases the reactivity, since there is a greater capability for intramolecular transformations leading to isomerization, e.g., (R3a).

Roubaud et al. [225] recorded ignition delay times and intermediate species profiles during autoignition of *n*-butylbenzene, *o*-xylene, and *o*-ethyltoluene. The intermediate species identified indicated low-temperature pathways for alkyl substituted benzenes proceeding through the formation of peroxy radicals (R2). Alkyl substituted benzenes, in which isomerization of peroxy radicals is facilitated (R3a), exhibit relatively higher reactivity. In poly-alkyl substituted benzenes, substitution at the *ortho* site facilitates isomerisations leading to chain branching at low temperatures. This explains the trends observed in their earlier study [416], in which *o*-xylene and 1,2,3 trimethylbenzene were found to be reactive at low temperatures. A detailed chemical kinetic model describing the autoignition of *n*-butylbenzene was developed in Ribaucour et al. [82] which was validated based on ignition delays and intermediate species concentrations, where the kinetic model predictions were found to agree well with the experimental values.

Darcy et al. [417] studied the autoignition of *n*-propylbenzene. These RCM data were compared with and complemented shock tube ignition delay data which had previously been recorded under similar conditions of pressure and ϕ [426]. Where overlapping data existed, very good agreement was observed between τ_{ign} measured in the shock tube and the RCM facilities. The experimental data were simulated using an updated detailed chemical kinetic model, which included reactions in the low-temperature oxidation regime with special attention given to ROȮ isomerizations (R3a) and HȮ$_2$ elimination (R3c)

reactions involving the secondary benzylic site on *n*-propylbenzene in order to obtain good agreement with the experimental results.

Husson et al. [418] studied the oxidation of *n*-butylbenzene in various experimental facilities and developed a detailed chemical kinetic model. Measurements included ignition delay times from an RCM and a shock tube, as well as intermediate species from RCM and JSR studies. Ignition delay times measured in the RCM complemented well the data from the shock tube. Simulated results using the detailed mechanism showed satisfactory agreement, while chemical kinetic analyses demonstrated the importance of O_2 addition to resonantly stabilized, 4-phenylbut-4-yl radicals (R2a).

Nakamura et al. [419] studied the autoignition of *n*-butylbenzene. Similar to the study of Darcy et al. [417], the data were compared with previously published shock tube ignition delay data [426]. The RCM data were at lower temperatures, while the shock tube data covered higher temperatures. Where overlap existed, good agreement between the RCM and shock tube data was observed. A detailed chemical kinetic mechanism including low-temperature reactions was developed and used to simulate the data, and generally good agreement was observed between the model and the experiments. Due to the overlapping conditions studied for both *n*-propylbenzene [417] and *n*-butylbenzene [419], the results can be directly compared. It was observed, both experimentally and with model predictions, that the two fuels showed similar reactivity at high temperatures (> 1000 K), but *n*-butylbenzene was faster to ignite compared to *n*-propylbenzene at lower temperatures (650–1000 K). This is consistent with the findings of Roubaud et al. [82,225,416]. The higher reactivity of *n*-butylbenzene compared to *n*-propylbenzene is due to the longer *n*-butyl alkyl chain, allowing for more facile ROȮ and ȮOQOOH radical isomerization reactions, (R3a) and (R6a), respectively.

6.5.3 Other Aromatics

Kukkadapu et al. [420] studied the autoignition of tetralin (1,2,3,4-tetrahydronaphthalene). The authors noted some ITHR behavior at the lowest temperature experiments they conducted, although no two-stage ignition or NTC behavior was found. The measured ignition delays were compared to an existing kinetic model and relatively poor agreement was found. This was attributed to the lack of low-temperature chemistry in the model, such as those steps illustrated in Fig. 37.

There are still to this day large uncertainties linked to the kinetic rate constants associated with aromatics autoignition. These structures lead to resonance-stabilized radicals, undergo radical addition channels and can significantly affect the overall reactivity of a multicomponent fuel because of their

increased complexity. These uncertainties tend to play a smaller role for larger, single-ring molecules, since the presence of a long alkyl chain tends to drive the reactivity.

6.6. Oxygenates

Oxygenates are a special class of fuels that consists of alcohols, esters, ethers, and ketones. They do not occur naturally in natural gas or petroleum reservoirs, but are often added to refined fuels for a variety of reasons. Oxygenates can alter the octane or cetane rating of a fuel, while they can also improve combustion performance within engines so that lower CO, UHCs, and PM emissions can result [326,427]. Oxygenates can be derived from renewable bio-feedstocks and thus hold interest as a means to reduce the impact of carbon dioxide emissions. Data from a variety of high-pressure devices indicate that the mechanisms of oxygenate autoignition are controlled by chemical oxidation routes involved in the oxygen moiety, however as the fuel molecular weight increases without additional oxygen, they become more dominated by the same mechanisms involved in hydrocarbon autoignition. A summary of studies on oxygenated fuels is provided in Table 7.

Table 7. Studies of oxygenated fuels using RCMs.

Fuels	T_c (K)	p_c (bar)	Mixture Composition	Diluent:O_2	ϕ	Reference
Methanol	830–940	24	$CH_3OH/O_2/N_2/Ar$	5.00	1.0	[428]
Methanol	850–1100	7–30	$CH_3OH/O_2/Ar$	3.76	0.25–2.0	[429]
Methanol	817–980	10, 30, 40	$CH_3OH/O_2/N_2/Ar$	3.76	0.5, 1.0, 2.0	[430]
Ethanol	830–1000	32	$C_2H_5OH/O_2/N_2/Ar$	5.00	1.0	[428]
Ethanol	705–910	37	$C_2H_5OH/O_2/N_2/Ar$	3.77	1.0	[431]
Ethanol	825–985	10, 25, 50	$C_2H_5OH/O_2/N_2/Ar$	3.76	0.3, 0.5, 1.0	[432]
***n*-Butanol, *iso*-butanol, *sec*-butanol, *tert*-butanol**	675–925	15, 30	*n*-, *iso*-, *sec*-, *t*-$C_4H_9OH/O_2/N_2$	1.38, 3.76, 8.52	0.5, 1.0, 2.0	[260,433]
***n*-Butanol**	920–1040	2.82–3.30	*n*-$C_4H_9OH/O_2/N_2/Ar$	5.64	1.0	[217]
***n*-Butanol/*n*-heptane**	660–710	9	$Fuel/O_2/N_2/CO_2$ *n*-C_4H_9OH:*iso*-C_8H_{18} = 0.25, 0.5	5.64	1.0	[228]
***n*-Butanol/*n*-heptane** ***n*-Butanol/*iso*-octane**	613–979	20	$Fuel/O_2/N_2/Ar$ *n*-C_4H_9OH:C_xH_y = 0, 0.25, 0.67, 1.5, 4, ∞	3.76, 5.6, 15.6	0.4, 1.0	[434]
***iso*-Butanol**	840–950 K	25	$Fuel/O_2/N_2/Ar$	7.26	0.4	[233]
***iso*-Pentanol**	650–950	7, 20, 40	*iso*-$C_5H_{11}OH/O_2/N_2$	3.76	0.5, 1.0, 2.0	[38,435,436]
***n*-Pentanol,** ***n*-hexanol**	640–850	9, 18	*n*-$C_5H_{11}OH/O_2/N_2/Ar$ *n*-$C_6H_{13}OH/O_2/N_2/Ar$	3.76	1.0	[437]
n-Butyl formate	646–841	20	*n*-$BF/O_2/N_2/Ar$	3.76	1.0	[438]
Methyl butanoate	640–950	10, 20, 40	$MB/O_2/N_2/Ar$	3.76	0.25, 0.5, 1.0, 1.5	[439]
Methyl butanoate, ethyl propanoate	935–1117	4.7–19.6	$Fuel/O_2/N_2/Ar$	3.76	0.3–0.4	[231]

Methyl butanoate	985	10.2	MB/O_2/N_2/Ar	3.76	0.3	[230]
Methyl butanoate, methyl pentanoate, methyl hexanoate, methyl heptanoate	650–850	4–20	Fuel/O_2/N_2/Ar	3.76	1.0	[226]
Methyl tertiary-butyl ether	800–930	24	MTBE/O_2/N_2/Ar	5.00	1.0	[428]
Dimethyl ether	615–715	10, 15, 20	DME/O_2/N_2	3.86, 7.5, 16	0.43, 0.75, 1.5	[275]
Dimethyl ether	625–900	11, 25, 30	DME/O_2/N_2/Ar	3.76	0.3, 0.5, 1.0, 2.0	[351]
Dimethyl ether/propane	603–902	30	Fuel/O_2/N_2	3.76	1.0	[364]
Dimethyl ether/toluene	624–1459	20–40	Fuel/O_2/N_2/Ar	3.76	0.5, 1.0, 2.0	[440]
Ethylene oxide	865–1025	4.7–15	C_2H_4O/O_2/Ar	25, 38, 108, ∞	0.83, 2.5, 11.4, ∞	[441]
Tetrahydrofuran (THF)	640–900	5–10	THF/O_2/N_2/Ar	3.76	1.0	[442]
Diethyl carbonate	660–960	30	DEC/O_2/N_2/Ar	3.76	0.5, 1.0, 2.0	[443]

6.6.1. Alcohols

Alcohols can be produced directly from biomass via fermentation or gasification processes. Bio-alcohols typically include alcohols up to C_6 with a single hydroxyl group, and which have identified biological production pathways. Larger molecules have also been investigated in combustion engines as second-generation biofuels [427]. The combustion chemistry of these fuels has been reviewed recently by Sarathy et al. [326], including steps relevant to autoignition.

6.6.1.1. Methanol

Lee et al. [428] studied the oxidation of alcohols and ethers in an RCM. Although the measured τ_{ign} data for methanol were slightly lower than predicted values using reported reaction mechanisms, the experimental and predicted values for the activation energy were in very good agreement at around 184 kJ/mol.

Kumar and Sung [429] investigated the autoignition of methanol. By comparison to existing kinetic models, the authors found τ_{ign} were under-predicted by an order of magnitude. To ascertain possible reasons for the large discrepancies, a sensitivity analysis was conducted. They found methanol autoignition to be most sensitive to reactions that form the primary fuel radical ($\dot{C}H_2OH$) through H-atom abstraction by $H\dot{O}_2$ radicals. Updating the rate of this reaction with a rate expression from the literature improved the model predictions at low temperatures dramatically, while there was no significant change in the mechanism performance at high temperatures as a consequence of the modification.

Most recently, a detailed chemical kinetic mechanism was used to simulate τ_{ign} measured for methanol oxidation over a wide range of pressures and ϕ using both an RCM and a shock tube [430]. At some conditions there was overlap in the experimental conditions where it was found that the τ_{ign} data in both facilities agreed with one another. This work further demonstrated the effective use of RCMs in measuring τ_{ign} at longer times than would otherwise be available allowing for the exploration of lower temperature conditions.

6.6.1.2. Ethanol

In the RCM study of Lee et al. [428], there were five data points reported for stoichiometric ethanol mixtures. The measured activation energy for ethanol autoignition was in good agreement with previous shock tube results of 130 kJ/mol, despite τ_{ign} predicted by the shock tube correlation being a factor of three lower than the measured values. Lee et al. [431] followed this with more expansive tests, again using ethanol at stoichiometric conditions. The measured ignition delays in this study were used to develop an updated kinetic model for the combustion of ethanol, with good agreement shown between the data and the model.

Mittal et al.[432] studied the autoignition of ethanol over a wide range of stoichiometry, where ϕ was changed by changing the oxygen mole fraction at constant fuel mole fraction. The authors compared their measurements to predictions from several kinetic models and updated one recent model with new rates for the $C_2H_5OH+H\dot{O}_2$ reactions. These updates substantially improved the agreement with the data measured in this study, while not affecting agreement with data from previous work.

6.6.1.3. Propanol

Surprisingly, there have been no experimental RCM studies using propanol, as highlighted in [326], even though the chemical kinetic pathways for propanol ignition at LTC conditions are relevant to the autoignition behavior of larger alcohols.

6.6.1.4. Butanol

Weber and co-workers [260,433] investigated the autoignition of four butanol isomers (*n*-, *iso*-, *sec*- and *t*-). Further, Weber et al. [433] determined the dependence of τ_{ign} of *n*-butanol on the initial fuel and oxygen concentrations by independently varying these to adjust ϕ. No evidence of an NTC region or two-stage ignition was found for any of the isomers. However, *t*-butanol exhibited unique ITHR, which Weber and Sung [260] attributed to different ignition chemistry in *t*-butanol as compared to the other butanol isomers. The authors found that ITHR, which was not associated with NTC behavior, increased with

decreasing temperature and increasing ϕ. They hypothesized that this exothermicity was due, in part, to O_2 addition to the fuel radical to form β–hydroxybutylperoxy, because only β–hydroxybutyl radicals form from *t*-butanol. The other isomers form primarily α-radicals that tend to react with O_2 to directly form $H\dot{O}_2$ and an aldehyde. *n*-Butanol was found to be the most reactive of the butanol isomers due to its facile ROȮ chemistry, but the order of reactivity of the other three butanol isomers was shown to be dependent on pressure. In particular, *t*-butanol was the least reactive at 15 bar, but became the second most reactive at 30 bar, behind only *n*-butanol.

Karwat et al. [217] measured τ_{ign} of stoichiometric *n*-butanol mixtures. Comparison to a kinetic model [444] found good agreement with the experiments in this study. Karwat and co-workers further measured time-resolved species profiles during the induction period at approximately 900 K and 3 bar [217] and *n*-butanol/*n*-heptane mixtures at approximately 9 bar and 700 K [228], using a custom built rapid sampling apparatus described in Section 3. They were able to identify and quantify the mole fractions of important intermediate species, including *n*-butanol, methane, carbon monoxide, ethene, propene, acetaldehyde, 1-butene, and *n*-butyraldehyde [217]; and *n*-heptane, methanol, acetaldehyde, propionaldehyde, methane, ethane, ethene, propane, propene, 1-butene, 1-pentene, 1-hexene, 1,3-butadiene, 3-heptene, 2-heptene, *n*-butyraldehyde, and carbon monoxide [228]. Karwat et al. [217] also compared their *n*-butanol speciation results to the mechanism of Black et al. [444] and found the model was able to predict the time-dependent mole fraction of most intermediates with reasonable accuracy, though ethene was a notable exception. When studying the blends of *n*-butanol/*n*-heptane, Karwat et al. [228] found that *n*-butanol significantly reduced the formation of large unsaturated hydrocarbons from *n*-heptane oxidation, indicating the synergistic effect that fuel blending creates. Karwat et al. [228] further compared their *n*-butanol/*n*-heptane speciation results with a custom model, including sub-mechanisms for *n*-butanol from Sarathy et al. [445], *n*-heptane from Mehl et al. [446], and C_1–C_4 chemistry from Metcalfe et al. [363]. They found the model was largely able to predict the mole fractions of most major species, but intermediates such as *n*-butyraldehyde were strongly over-predicted [228].

Kumar et al. [434] studied the influence of blending *n*-butanol on the ignition delay times of *n*-heptane and *iso*-octane. The effect of *n*-butanol addition on the development of the two-stage ignition for *n*-heptane and *iso*-octane was also illustrated. Experimental results showed that the addition of *n*-butanol to *n*-heptane leads to a decrease in overall reactivity, as manifested by the increase in both τ_1 and τ_{ign} for all the conditions studied. On the other hand, the addition of *n*-butanol to *iso*-octane was found to lead to shorter τ_{ign}. In addition, the experimental results were compared to predictions simulated using a

detailed chemical kinetic model, which was obtained by systematically merging previously reported base models for the individual fuel constituents. This compiled model was found to generally well predict the qualitative and quantitative trends for the autoignition of the binary fuel blends, although some discrepancies between experiments and simulations for *n*-butanol/*iso*-octane blends were noted. A sensitivity analysis on the base and merged models was further performed to understand the dependence of τ_{ign} on the model parameters.

Recently, Ji et al. [233] measured both τ_{ign} and intermediate species formed during lean, *iso*-butanol autoignition. Fast sampling and gas chromatography were used to acquire and quantify the intermediate species during the induction period. The ignition delay times and quantitative measurements of the mole fraction time histories of methane, ethene, propene, *iso*-butene, isobutyraldehyde, *iso*-butanol, and carbon monoxide were compared with predictions from the detailed mechanisms developed by Sarathy et al. [445], Merchant et al. [447], and Cai et al. [448]. It was shown that while the Sarathy et al. mechanism predicted τ_{ign} well, it over-predicted ethane concentrations by a factor of 6–10, under-predicted *iso*-butene by a factor of 2, and over-predicted isobutyraldehyde by a factor of 2.

6.6.1.5. Larger alcohols

Tsujimura et al. [38,435] and Sarathy et al. [436] measured τ_{ign} of *iso*-pentanol over a range of ϕ in air. ITHR behavior similar to *t*-butanol [260] was found at 40 bar for *iso*-pentanol [436]. Comparison with an updated model showed ignition delays were accurately predicted for the stoichiometric condition, but the model was unable to capture ϕ dependence [436]. On the other hand, the model was able to qualitatively capture the ITHR behavior. Similar to *iso*-butanol, the primary radical formed via H-atom abstraction is the α-radical, leading primarily to the formation of an aldehyde and hydroperoxyl radical. However, sufficient chain-branching involving the γ- and δ-radicals is present to produce the observed ITHR behavior, in contrast to the smaller butanol isomers.

Heufer et al. [437] measured the ignition delay times of several *n*-alkanes and *n*-alcohols, including *n*-pentanol and *n*-hexanol in an RCM and a shock tube. The authors noted that *n*-pentanol and *n*-hexanol both exhibit the typical alkane NTC behavior. By comparison to the corresponding alkane of the same carbon chain length, the authors concluded normal alcohols are more reactive than normal alkanes in the high-temperature regime, but less reactive in the low-to-intermediate temperature regime. The authors attributed this to the effect of the alcohol group which reduces the bond dissociation energy of the C–H bonds corresponding to the carbon atom nearest the alcohol group. At high temperatures, this reduction in bond dissociation energy contributes to the reactivity by offering a fast path for H-abstraction and quick

formation of fuel radicals (R1). However, at low-to-intermediate temperatures, the radicals formed by this fast H-atom abstraction in turn form aldehydes instead of ȮOOH radicals through (R3c), reducing the reactivity in comparison to alkanes. Furthermore, the effect of the alcohol group is diminished as the carbon chain length increases, indicating that for very long carbon chains, negligible influence of the alcohol group might be expected, especially for straight chain alkyl structures with the hydroxyl group at the end position.

6.6.2. Esters

Esters are fuels that are structurally representative of biodiesel, which can be produced directly from the trans-esterification of seed oils, such as soybean and palm. This process is typically facilitated using a small alcohol such as methanol or ethanol, so long chain (C_{12} and larger) methyl, or ethyl esters respectively result from the conversion. Studies undertaken to date, within RCMs as well as other laboratory devices, have investigated much smaller ester molecules, such as C_5 esters, as the low vapor pressures of these fuels and their tendency to stick to the walls of the equipment hampers the use of larger, lower volatility compounds.

Vranckx et al. [438] measured ignition delay times of stoichiometric mixtures of *n*-butyl formate. The same study also reported ignition delay measurements from a shock tube and laminar flame speed results. *n*-Butyl formate was found to exhibit two-stage ignition and NTC behavior. The RCM measurements were found to complement shock tube data, and the simulated ignition delay times and laminar flame speeds using the kinetic model developed in this study also showed good agreement.

Dooley et al. [439] measured τ_{ign} of methyl butanoate. The τ_{ign} data exhibited Arrhenius behavior and no evidence of an NTC regime. A chemical kinetic model was also developed in this study and validated with data from other fundamental reactors, and this was found to emulate the qualitative behavior of the ignition delays, but the simulated τ_{ign} differed substantially and further improvements were needed.

Walton et al. [231] measured τ_{ign} of methyl butanoate and ethyl propanoate. Ethyl propanoate was found to be more reactive than methyl butanoate. A detailed kinetic model was developed in this study and was found to predict τ_{ign} of methyl butanoate with excellent agreement while ethyl propanoate predictions were not as good. Walton et al. [230] in a later study conducted rapid sampling experiments to perform speciation measurements during autoignition of methyl butanoate. Evolution profiles of methane, ethane, ethene, propene, and 1-butene were recorded. The kinetic model developed in these

studies was found to predict methane and ethene concentrations with excellent agreement, while comparison of ethane, propene, and 1-butene were not as good.

HadjAli et al. [226] measured ignition delay times of C_4–C_8 methyl esters to understand the influence of the chain length on the ignition of methyl esters. Ignition delay measurements showed that reactivity increases with increases in chain length for the conditions investigated. Methyl pentanoate, methyl hexanoate, and methyl heptanoate exhibited two-stage ignition behavior. Further tests were conducted to understand the characteristics of methyl esters which included comparison of ignition delays with those of *n*-alkanes and intermediate species measurements. Methyl hexanoate was chosen as the representative for methyl esters. Comparison of ignition delay times showed the following reactivity order: *n*-heptane > methyl hexanoate > *n*-pentane > *n*-butane. τ_1 and τ_{ign} of methyl hexanoate were found to be shorter than those of *n*-pentane, indicating the methyl ester functional group has a promoting effect on low-temperature chemistry. Information on the intermediate species formed during the induction period aided in understanding the controlling reaction pathways. Proposed routes were constructed to yield observed methyl epoxyhexanoates, methyl hexenoates, and small unsaturated methyl esters + aldehydes that form via O–O, C–O, and C–C scission, respectively, of the ȮOOH species, (R5b) and (R5c). It was highlighted that most measured intermediates were formed by abstraction of the C_2–H bond, followed by internal H-atom transfer from the 3, 4, 5 or 7 carbon, or H-atom abstraction from the 3, 4, 5 or 7 carbon with H-transfer from the C_2–H bond.

6.6.3. Ethers

Ethers are typically produced via catalytic reformation or dehydration of alcohols. The molecular structure of the alcohol dictates the type of ether that is formed. Some ethers, e.g., dimethyl ether (DME), have been suggested as direct replacements for diesel fuel.

MTBE has been used a gasoline additive to reduce emissions and enhance octane rating. Lee et al. [428] conducted RCM experiments for stoichiometric MTBE mixtures. The measured activation energy of 173 kJ/mol was found to be higher than the value of 117 kJ/mol reported in the shock tube study of Curran et al. [449]. The work of Lee et al. [428] demonstrated that the oxygenated fuels tested (methanol, ethanol, and MTBE) are more resistant to autoignition as compared to primary reference fuels.

Mittal et al. [275] measured ignition delay times of DME, in which ϕ was varied by changing the oxygen concentration while keeping fuel loading constant. DME was found to exhibit two-stage ignition and NTC behavior. τ_1 was observed to be less sensitive to pressure and ϕ. On the other hand, τ_{ign} was observed to

increase with equivalence ratio, as the fuel loading was fixed and the oxygen concentration decreased with increase in ϕ highlighting the importance of O_2 concentration relative to ϕ. Simulations conducted using a DME mechanism showed good agreement with the experimental findings. Additional analyses using novel computational singular perturbation techniques indicated that chemical species formed during the piston compression process, even with negligible evolved exothermicity, can considerably affect the autoignition observations. These results emphasized the importance of constructing physically and chemically realistic simulation frameworks for the experiments, as discussed in Section 4.

Using an RCM and three different shock tubes, Burke et al. [351] provided experimental and chemical kinetic model-predicted ignition delay time data for DME/methane blends, pure DME, and pure methane covering a range of conditions relevant to gas turbine environments,. By incorporating high-level rate constant measurements and calculations available for the reactions of DME, and applying a pressure-dependent treatment to the low-temperature reactions of DME, the detailed chemical kinetic model developed in this study was capable of accurately predicting this wide range of ignition delay data, as well as available literature data including flow reactor, JSR, shock tube ignition delay times, shock tube speciation, laminar flame speed, and flame speciation results.

As mentioned earlier in the discussion of propane oxidation, recently Dames et al. [364] studied binary mixtures of propane and DME using an RCM with a detailed chemical kinetic mechanism analysis. Stoichiometric mixtures in air were used for pure propane and pure DME mixtures in addition to various mixture blends comprising 90/10, 75/25, 50/50, and 25/75 propane/DME. It was found that propane was slowest to ignite, while the mixtures containing higher concentrations of DME were progressively faster in igniting. Much of the kinetics of the propane/DME mixtures was predicted to be controlled by the underlying DME chemistry. It was found that including the pressure-dependent unimolecular decomposition of the $CH_3O\dot{C}H_2$ radical, in addition to other reactions including $2CH_3OCH_2O_2$=products, and $\dot{C}H_2OCHO=CH_2O+H\dot{C}O$, $\dot{O}CH_2OCHO=HOCHO+H\dot{C}O$, $HOCH_2\dot{O}=\dot{H}+HOCHO$, and $CH_3OCH_2\dot{O}=CH_3OCHO+\dot{H}$ all led to a better agreement between the model and the experimental results. It was also concluded that even though many cross reactions between stable and radical species involved in the propane/DME sub-mechanisms were included, they did not have a measurable effect on most simulations. This suggested that important cross reactions that do occur involve competition for $\dot{O}H$ and $H\dot{O}_2$ radicals formed during the combustion process.

These trends were further corroborated by Zhang et al. [440], who investigated binary blends of DME and toluene using a high pressure shock tube and an RCM. Ignition delay time data were acquired

covering a range of ϕ, pressure and DME/toluene blend ratios, including 100/0, 74/26, 42/58, 24/76 and 0/100, respectively, where DME blending was used to facilitate investigation of toluene oxidation at NTC conditions. They observed that the reactivity of the mixtures with low toluene fractions was dominated by DME oxidation processes, but at the 24/76 blend ratio, the global ignition processes shifted to be controlled more by toluene than DME. Furthermore, simulations with an updated kinetic model, extended to include possible cross reactions between the two fuel-derived radicals and ȮH-toluene addition reactions, exhibited significant discrepancies with the experimental measurements, underscoring uncertainties in the chemical kinetics and thermodynamics in existing toluene oxidation pathways in the model, as well as the possible exclusion of necessary oxidation pathways. As was concluded by Dames et al. [364], and somewhat in contrast to the gas sampling work of Vanhove et al. [398], the model indicated that the only interactions between the two fuels were via competition for the ȮH and $H\dot{O}_2$ radical pool, where toluene's ability to act as a radical sink (as well as an anti-knock agent in operating engines) can be traced to its weak allylic C-H bond, the subsequent reactions of $C_6H_5\dot{C}H_2$ radical, and the lack of a rapid oxidation mechanism for this at LTC conditions. Model discrepencies found in this work, and with other experimental observations highlight the need for continued study in this area.

6.6.4. Other oxygenates: Ethylene oxide, tetrahydrofuran, diethyl carbonate

Griffiths and Perche [441] studied the spontaneous decomposition, oxidation and autoignition of ethylene oxide (i.e., oxiran) under rapid compression. Ethylene oxide is the simplest epoxide, and is isomeric with acetaldehyde and vinyl alcohol. Dilute mixtures (1.25–5.0% ethylene oxide) in argon were studied with added amounts of oxygen (0.88%, 2.5%, and 3.75%). Pressure-time profiles and emitted light intensities were recorded, while mixture compositions were measured using mass spectrometry. It was found that trace amounts of oxygen enhanced the rate and extent of reaction of fuel. With approximately equal amounts of ethylene oxide and oxygen, ignition occurred at conditions where none was possible in the absence of oxygen, while τ_{ign} also became significantly shorter. Product compositions of ethylene oxide pyrolysis and oxidation were reported and these included acetaldehyde, methane, ethane, ethylene, carbon monoxide, carbon dioxide, hydrogen, and water. It was found that fuel decomposition occurred rapidly at temperatures of 850 K and higher and that it was highly exothermic (> 100 kJ/mol), in contrast to acetaldehyde which was found to be almost thermo-neutral, with decomposition only occurring at temperatures greater than 1000 K. The results showed that small amounts of ethylene oxide in air can be a potential explosion hazard if modest but adiabatic compression occurs.

Vanhove et al. [442] performed an experimental and modeling study of tetrahydrofuran (THF) at low temperatures using an RCM and JSR. Two-stage ignition was observed within the RCM at temperatures up to 810 K, and the evolution of τ_{ign} with temperature demonstrated a clear deviation from Arrhenius behavior in the temperature range 680–750 K. The JSR measurements, which were conducted at 1 bar and highly diluted conditions, corroborated the RCM data in that an NTC zone was observed in the temperature range of 600–750 K. Reactive mixtures were sampled from the RCM indicating the formation of C_1–C_4 aldehydes and alkenes, a variety of oxygenated heterocycles, including oxirane, methyloxirane, oxetane, furan, both isomers of dihydrofuran, 1,4-dioxene and butyrolactone, as well as cyclopropane carboxaldehyde, formic acid, 2-propenyl ester and butanedial. Speciated samples from the JSR indicated discrepancies with the RCM measurements where many of the aforementioned oxygenated intermediates were not detected, while methylvinylether and dihydrofuranols were observed. The differences between the results for the two experimental platforms indicate that the relative significance of reaction pathways may differ between RCM and JSR devices, and this highlights the importance of conducting autoignition chemistry studies across a wide range of conditions, including at high pressures and undiluted concentrations that are representative of IC engine operation. Furthermore, they emphasize the need for complementary datasets that can provide insight into fuel reactivity, such as the importance of cross reactions between fuel components.

Nakamura et al. [443] measured τ_{ign} for diethyl carbonate (DEC) using both an RCM and a shock tube. The data were complemented by speciation data measured in a JSR. The RCM results showed near-NTC behavior and relatively low reactivity in the low-temperature regime (660–900 K) and these results were interpreted using a chemical kinetic model. Analysis indicated that the chemical structure of DEC does not result in six- and seven-membered ring alkylperoxyl radical isomerization reactions (R3a), but that 5-, 8-, and 9-membered ring isomerization reactions are possible. Six-membered ring isomerization reactions are thought to initiate low-temperature branching reactions leading to high reactivity in the low-temperature regime, and thus the lack of these (and seven-membered ring isomerization reactions) resulted in the reduced reactivity of DEC at low temperatures.

6.7. Full-boiling range fuels

Full-boiling range fuels are liquid fuels that consist of a diverse mix of hydrocarbon species which cover a wide range of molecular weights and isomeric structures. The distillation curves for such fuels span a large range of temperature where the difference between initial and final boiling points can be on the order of 100 to 200 K [450,451]. Gasoline, jet fuel, and diesel are included within this classification.

There are numerous challenges associated with utilizing these fuels in RCMs, as well as other experimental apparatuses including preferential distillation, cracking, and contamination, along with greater susceptibility to perturbations within the reaction chamber, e.g., thermal gradients. Moreover, chemical kinetic modeling of the experiments requires the use of single or multi-component surrogates, which may not be representative of the real fuels. Discussions of these issues can be found in various review papers (e.g., [324,452,453]). Nevertheless, it is often desirable to have direct data from the real fuel as well as surrogate blends at representative conditions, as opposed to just surrogate model comparisons, in order to understand differences and similarities between such representative surrogate blends and the real fuels.

6.7.1. Gasoline and its surrogates

Gasoline contains hydrocarbons that typically range from C_4 to C_{12}, where octane ratings generally fall within RON ≈ 80–95. Like many full-boiling range fuels, gasoline is compositionally variant, meaning its chemical content varies significantly from source to source, and season to season. While an octane rating may be specified for a particular batch, this metric, as highlighted in the work of Griffiths et al. [368] and others, is not an adequate indicator of the autoignition characteristics of a fuel at LTC conditions. As such, comparison of experimental results between studies using different gasolines, IC engine based or otherwise, is not always straightforward. A summary of RCM studies performed on gasoline and its surrogates is provided in Table 8.

Table 8. Studies of gasoline and its surrogates using RCMs.

Fuels	T_c (K)	p_c (bar)	Mixture Composition	Diluent:O_2	ϕ	Reference
Commercial gasoline, TRF blends	890–1000	18	Fuel/O_2/N_2/Ar *n*-C_7H_{16}/*iso*-C_8H_{18}/C_7H_8 at 17/56/28 and 21/47/32 (molar)	3.76	1.0	[111]
RD387 gasoline	645–950	20, 40	Fuel/O_2/N_2	3.76	0.3, 0.5, 1.0	[454]
RD387 surrogates (TRF, TRF/2-pentene blends)	665–950	20, 40	Fuel/O_2/N_2 *n*-C_7H_{16}/*iso*-C_8H_{18}/C_7H_8/2-C_5H_{10} at 17/56/27/0 and 16/51/31/4 (liquid volume)	3.76	0.3, 0.5, 1.0	[455,456]
FACE-A, FACE-C, PRF84	632–745	20, 40	Fuel/O_2/N_2	3.76	0.5, 1.0	[457]

Kim et al. [111] measured the ignition delay times of a commercial gasoline (RON ~ 92) and two, three-component, Toluene Reference Fuel (TRF) surrogate blends containing *iso*-octane, *n*-heptane, and toluene. One surrogate blend (identified as A) was based on the work of Gauthier et al. [458] and formulated at 63/17/20 (liquid volume ratio). The estimated RON/MON rating for surrogate A was

88.8/84.8 [405]. A second blend (identified as B) was proposed by the authors at 54/22/24 (liquid volume ratio), where this had a lower estimated RON/MON rating of 84.9/82.6. The measured ignition delay times of the surrogate B more closely matched results with the commercial gasoline, whereas the surrogate A formulation yielded ignition delay times that were approximately 30–50% longer. The surrogate A measurements were in good agreement with the shock tube data of Gauthier et al. [458], and it is unclear why the commercial gasoline was more reactive than the A surrogate, even though its RON rating was significantly higher. The experimental data were also compared with simulations using a reduced kinetic mechanism which included the main reaction pathways for *iso*-octane, *n*-heptane, and toluene. The simulations indicated that under some conditions there could be significant consumption of the *iso*-octane and *n*-heptane fuel molecules before the test conditions are reached, while the toluene was predicted to hardly decompose. This is similar to the findings of Griffiths et al. [368]. The model did not appear to adequately capture the preliminary heat release seen in the experiments.

Ignition delay times of a research grade gasoline, RD387 (RON = 91, MON = 82.7), were measured by Kukkadapu et al. [454] over a wide range of conditions. The τ_{ign} measurements for this study were also found to complement the earlier shock tube data from Gauthier et al. [458], though the temperature conditions did not directly overlap. Furthermore, simulated ignition delay times using the gasoline surrogate model from LLNL were found to exhibit good agreement with the experiments. Although some model improvements were still needed, the level of agreement was encouraging, considering the complexity of the associated chemistry for fully blended gasoline. A discrepancy in the slope of the NTC region was noted and could be attributed to the lack of fidelity of the surrogate model and/or the inadequacy of the surrogate formulation in question. Further studies were therefore suggested to identify whether this discrepancy was due to the surrogate model being more reactive in the NTC regime, or the absence of naphthenes in the gasoline surrogate.

In subsequent work, Kukkadapu et al. [455,456] measured the ignition delay times of two surrogates of RD387. One was a TRF blend (A from [458]), while the other was a four-component TRF/2-pentene blend, with this formulation intended to account for the olefinic content of the RD387 (~4.7%). No cycloalkanes were used in the four-component surrogate, though the RD387 contained 16% naphthenes. The authors estimated the RON/MON rating of the TRF/2-pentene blend to be 91/83 based on the work of Mehl et al. [459]. Comparison of the measured ignition delays of two gasoline surrogates with those of RD387 reported in [454] showed the four-component surrogate performed better in emulating the autoignition characteristics of RD387. The performance of the LLNL gasoline surrogate model was also

assessed and noted to be pressure dependent. Furthermore, the agreement between the experimental and simulated results was found to depend on the operating conditions. Good agreement was observed at a compressed pressure of 20 bar, while longer ignition delays were predicted by the chemical kinetic model at 40 bar. Chemical kinetic analyses were further conducted at varying pressures, temperatures, and ϕ to identify the reactions that influence simulated ignition delay times. It was found that τ_1 were very sensitive to the H-atom abstraction reactions from *iso*-octane, as well as the successive concerted elimination reactions producing $H\dot{O}_2$ (R3c), and the β-scission reactions of hydroperoxy alkyl radicals (R5b) and (R5c). As is often the case in these systems, the production and decomposition of H_2O_2 via $H\dot{O}_2+H\dot{O}_2=H_2O_2+O_2$ and $H_2O_2(+M)=\dot{O}H+\dot{O}H(+M)$, respectively, were found to be important in controlling τ_{ign}.

Sarathy et al. [457] compared ignition delay times of two gasoline fuels and their conventional two-component PRF surrogate. Two non-oxygenated, alkane-rich FACE (Fuels for Advanced Combustion Engines) gasoline fuels [460], namely FACE A and FACE C, were used. PRF84 was chosen because the octane ratings of FACE A and FACE C are identical with RON=MON=84. The study intended to examine whether two gasoline fuels with similar octane ratings but different chemical composition exhibited identical reactivity and also whether a simple PRF can emulate the autoignition behavior of gasoline with a similar octane rating. Ignition delay times of the gasoline fuels and PRF84 were measured in both an RCM and shock tubes. The measurements showed both gasoline fuels exhibited identical ignition delays over a wide range of temperatures and that PRF84 could emulate the reactivity of these gasolines at temperatures in the NTC and high-temperature regime. PRF84 however, was found to be more reactive than the gasolines at the lowest temperatures. Furthermore, a six-component surrogate blend was also proposed to model the FACE A and C fuels which included *n*-butane, *n*-heptane, *iso*-pentane, 2-methyhexane, *iso*-octane, and toluene, though no experimental measurements were reported with the surrogate mixture. The results of this work are somewhat contradictory to that of Griffiths et al. [368], and may be due to the more complex makeup of the full-boiling range fuels, compared to the single component hydrocarbons studied in [368].

6.7.2. Jet fuel and its surrogates

Jet fuel has a typical range of hydrocarbons from C_8 to C_{16}, which makes it heavier than gasoline, with a molecular weight of 140–180 g/mol compared to 90–105 g/mol for gasoline. It is also more reactive than gasoline, with typical octane ratings near 30. These features make it more difficult to utilize in RCM experiments since it can be challenging to prepare pre-vaporized fuel/oxidizer/diluent mixtures due to

the fuel's lower vapor pressure. Meanwhile, jet fuels can more easily decompose/oxidize during the compression stroke, before the desired test conditions are reached, and this is especially true if the t_{50} of the machine is longer than 4 to 5 ms. As such, the 'compression' limit identified in Fig. 28 is more easily reached so leaner/more dilute mixtures, lower temperature and/or lower pressures must be used to avoid this [31,160,161]. A summary of studies performed on jet fuel and its surrogates is provided in Table 9.

Table 9. Studies of jet fuel and its surrogates using RCMs.

Fuels	T_c (K)	p_c (bar)	Mixture Composition	Diluent:O_2	ϕ	Reference
POSF 4658 Jet-A, JP-8, and Syntroleum S-8 4734	615–1100	7, 15, 30	Fuel/O_2/N_2/Ar	2.12, 3.76, 8.66	0.43–2.29	[461,462]
POSF 4658 Jet-A and two surrogates (*n*-decane/*iso*-octane/toluene, *n*-dodecane/*iso*-octane/1,3,5-trimethylbenzene/*n*-propylbenzene)	645–714	21.7	Fuel/O_2/N_2	3.76	1.0	[463,464]
POSF 4658 Jet-A and six alternative jet fuels (Syntroleum S-8 4734, Shell GTL 5172, Sasol IPK 5642, UOP camelina 6152, UOP tallow 6308, Syntroleum R-8 5469	642–661	22	Fuel/O_2/N_2	3.76	1.15	[465]
JP-8 and camelina hydro-processed renewable jet fuel	670–750	7, 10	Fuel/O_2/N_2	3.76	0.3, 1.0	[160]
JP-8, camelina and tallow hydro-treated renewable jet fuel	625–730	5, 10, 20	Fuel/O_2/N_2	3.76	0.25, 0.5, 1.0	[161]

The autoignition characteristics of conventional and alternative jet fuels, including Jet-A, JP-8, and S-8, were studied by Kumar and Sung [461,462]. All the three jet fuels were observed to exhibit two-stage ignition and NTC behavior. Comparison of τ_{ign} showed that S-8 was the most reactive followed by JP-8 and Jet-A, respectively [461,462]. Dooley et al. [463,464] studied the oxidation of Jet-A, as well as a three- and a four-component surrogate, containing *n*-decane/*iso*-octane/toluene and *n*-dodecane/*iso*-octane/1,3,5-trimethylbenzene/*n*-propylbenzene, respectively, using various fundamental devices. Both of the surrogates were shown to replicate well the τ_{ign} of the target Jet-A [463,464], but there were discrepancies associated with the first-stage ignition characteristics. The four-component blend better matched the molecular weight of the fuel-boiling range fuel, and therefore transport-dominated phenomena like extinction in diffusion flames were better reproduced by this surrogate blend.

Hui et al. [465] studied combustion characteristics of Jet-A and six other alternative jet fuels in various fundamental combustion systems. Laminar flame speeds, DCN values, and RCM ignition delay times of the six alternative fuels were measured and compared in this study. All the six alternative fuels exhibited two-stage ignition behavior and the comparison of ignition delays showed Jet-A was the least reactive of all the jet fuels tested.

Allen et al. [160] studied the autoignition characteristics of stoichiometric JP-8/air and camelina hydro-processed renewable jet fuel (CHRJ)/air mixtures. They employed the direct test chamber method, discussed in Section 2, for this work. Significant discrepancies were observed when comparing τ_1 and τ_{ign} of JP-8 with those measured by Kumar and Sung [461] and issues of fuel vaporization in the mixture preparation process were discussed as a possible cause. Comparison of τ_{ign} of JP-8 and CHRJ in Allen et al. [160] showed that CHRJ was more reactive than JP-8, which is in accordance with theirderived cetane number (DCN) values. Allen et al. [161] further conducted measurements of JP-8, CHRJ, and tallow hydro-treated renewable jet fuel (THRJ)/air mixtures. Ignition delay measurements of Allen et al. [161] showed CHRJ and THRJ were more reactive than JP-8. CHRJ and THRJ exhibited identical τ_{ign} at fuel lean conditions while τ_{ign} values of CHRJ were greater than those of THRJ at stoichiometric conditions. Experimentally measured τ_{ign} results were also compared with those of surrogates from simulations. Two surrogate mixtures were employed, including pure 2-methylnonane and binary blend of *n*-dodecane and 2-methylundecane for CHRJ and THRJ, respectively. It was found the efficacy of the surrogates for emulating ignition propensity decreased with increasing pressure. The two-component surrogate performed relatively well for most of the conditions while the single-component surrogate of 2-methylnonane was superior at low pressures.

6.7.3. Diesel and its surrogates

Diesel contains hydrocarbons that typically range from C_8 to C_{21}, and its molecular weight ranges from 170 to 230 g/mol. Diesel engines generally operate using fuels rated with Cetane values of 40–55. Like jet fuel, there are substantial challenges associated with conducting experiments using diesel associated with volatility and reactivity. Although there have been a considerable number of RCM studies on large molecular weight hydrocarbons as discussed earlier, there has only been one so far covering reference diesel fuels. Kukkadapu and Sung [466] performed an autoignition study of blends of ultra-low sulfer diesel fuel (ULSD#2) and a FACE research diesel fuel blend (FD9A) at p_c of 10, 15, and 20 bar, covering T_c between 678 K and 938 K, at varying ϕ of 0.5, 0.69, and 1.02 for diesel/O_2/N_2 mixtures. The equivalence ratio was varied by changing the oxygen mole percentage while keeping the fuel mole percentage fixed at 0.514%.

The results demonstrated that diesel blends with similar cetane ratings but different compositions can exhibit varying ignition propensities across different temperature regimes. In particular, differences were observed at temperatures where low temperature branching reactions are important, as illustrated in Fig. 37. Furthermore, the RCM measurements were found to complement existing shock tube data in the literature [467][468] and thus provided an addition to the experimental database of diesel blends needed for development and validation of diesel surrogate models.

The collection of studies shows that the still imperfect state of knowledge in kinetic modeling of individual hydrocarbons, added to non-linear interaction effects between different components means that the expected uncertainty in the predicted ignition delays of full boiling fuels relatively to surrogate mixtures under autoignition conditions is still no better than within a factor of two, particularly at high pressures. Whereas there have been significant advances in prediction of fuels that more closely resemble gasolines under engine-like conditions, challenges remain when considering either blends of heavier fuels, or with oxygenated compounds. These difficulties, however, must be put into context of what is an acceptable uncertainty when making predictions for engineering purposes, either for engine design or gas turbine or safety considerations.

6.8. Fuel additives

Fuel additives are chemicals that can be used in very small quantities to significantly modify the ignition propensity and/or combustion behavior of a fuel. These are typically distinguished from blended fuel components, e.g., butane, and are generally added at volume fractions near 1% or less, though they sometimes can be present in larger amounts. Fuel additives have historically been classified as knock inhibitors (anti-knock agents) or cetane improvers, and while they have been explored primarily for conventional SI and CI combustion systems, there are numerous potential applications within LTC schemes [22]. These chemicals however, can be difficult to utilize in RCM tests. Conventional anti-knock agents like organometallics (e.g., tetraethyl lead), in addition to being toxic, have a tendency to form metal oxides on the surfaces of the reaction chamber, leading to contamination that is difficult to remove. Cetane improvers, on the other hand, due to their high reactivity, even at pre-test conditions, can lead to pre-ignition events in the fuel/oxidizer mixing tank, while they can also foul feed lines to the reaction chamber, subsequently perturbing non-additized tests. A summary of studies performed on fuel additives is provided in Table 10.

Table 10. Studies of anti-knock agents and cetane improvers using RCMs.

Fuels	T_c (K)	p_c (bar)	Mixture Composition	Diluent:O_2	ϕ	Reference

Amyl nitrite/*n*-heptane ethyl nitrate/*n*-heptane acetone peroxide/*n*-heptane aniline/*n*-heptane iron pentacarbonyl/*n*-heptane tetraethyl lead (TEL)/*n*-heptane	675–710	16.5–20	fuel/O_2/N_2 amyl nitrite:fuel = 0.055 ethyl nitrate:fuel = 0.086 acetone peroxide:fuel = 0.06 aniline:fuel = 0.064 iron pentacarbonyl:fuel = 0.033 TEL:fuel = 0.008–0.022	3.76	1.0	[64]
TEL/*n*-heptane	600–680	7–26	TEL:fuel = 0.015	3.76	0.55, 1.0, 1.8	[65]
TEL/*iso*-octane	660–800	15.9–35.7	fuel/O_2/N_2 TEL:*iso*-octane = 0–1230 ppm	3.76	0.45–2.55	[469]
TEL/*n*-butane TEL/*n*-heptane TEL/*iso*-octane TEL/benzene	660–900	18–26	fuel/O_2/N_2 TEL:fuel = 0–800 ppm	3.76	0.6–1.4	[69]
Ethyl nitrite/2,2,3-trimethyl butane (triptane)	660–800	15.9–35.7	fuel/O_2/N_2 EN:triptane = 0–0.20	3.76	1.0	[469]
Di-ethyl amine/*n*-pentane Di-ethyl amine/*n*-heptane	650–950	9–11	fuel/O_2/N_2/Ar/CO_2 DEA:fuel = 0–0.053	3.76	1.0	[273]
Ethanal/*n*-butane diethyl ether/*n*-butane *iso*-propyl nitrate/*n*-butane ditertbutyl peroxide (DTBP)/*n*-butane	700–880	10, 15	fuel/O_2/N_2/Ar/CO_2 additive:fuel = 0–0.053	3.76	1.0	[470]
DTBP	500–600	7–10	DTBP/O_2/N_2/CO_2	7.33–∞	2.87–∞	[267]
DTBP/PRF90 DTBP/*iso*-octane 2-ethylhexyl nitrate (2-EHN)/PRF90 2-EHN/*iso*-octane	790–878	41.6	fuel/O_2/N_2/Ar/CO_2 additive:fuel = 0–0.018	3.76	0.4	[395]
2-EHN/PRF91 2-EHN/TRF91	675–1025	21	fuel/O_2/N_2/Ar 2-EHN:fuel = 0–0.027	5.70	1.0	[134]

6.8.1. Anti-knock agents

Jost and Rögener [64] investigated the influence of various anti-knock agents including aniline, iron pentacarbonyl, and TEL doped into *n*-heptane at various levels from 1 to 4% volume basis, using selected test conditions. The compression ratio was adjusted to vary T_c, and p_c shifted accordingly. The τ_{ign} data indicated that the effectiveness of the dopants could be ranked as aniline > iron pentacarbonyl > TEL. However, this is contrary to their respective octane boosting effectiveness [471]. Furthermore, under some conditions, TEL seemed to enhance the low temperature reactivity of the fuel/air mixtures, resulting in shorter τ_{ign}.

Rögener [65] followed this work with measurements using a blend of TEL/*n*-heptane doped at 1.5% mole fraction, covering a similar range of compressed temperatures and pressures, but also exploring fuel-lean and fuel-rich mixtures, in addition to the stoichiometric ones. Comparisons with undoped fuel

tests indicated that for all of the conditions explored, τ_1 was not noticeably affected by the presence of TEL. However, τ_{ign} was significantly lengthened. Additionally, whereas the undoped fuel exhibited an inverse dependency of ($\tau_{ign} - \tau_1$) on the compressed pressure, the doped blend did not, so an increase in p_c did not result in a corresponding decrease in ($\tau_{ign} - \tau_1$). The data for the doped blend therefore exhibited NTC behavior, while this was absent with the undoped fuel. This transition to NTC behavior with TEL addition can be seen in Fig. 10c of Section 2.

Jovellanos et al. [469] studied the effect of TEL addition to *iso*-octane where changes in ignition delays and critical explosion pressures, defined as the maximum pressure observed due to preliminary heat release before autoignition, were recorded. The TEL used in this work was a commercial blend that included 1,2-dichloro- and 1,2-dibromo-ethane, which act as lead scavengers to prevent surface contamination in operating engines. The preliminary heat release measured in these tests, as documented in later work [69], was due to mild ignition, or flame propagation within their reaction chamber. This is discussed more shortly. The critical explosion pressure was chosen as an indicator of the extent of mass burned before transitioning to end gas autoignition, and thus knock. A fuel with higher critical explosion pressure therefore was expected to exhibit higher anti-knocking tendency. To understand the effect of TEL, the authors utilized various fuel/air ratios and different doping levels, where a range of compressed pressures and temperatures were covered via adjustments to *CR*. The initial temperature and pressure were held constant so T_c and p_c changed simultaneously, while doping levels were 0–1230 ppm. In their analysis, there was no attempt to account for the shifts in compressed conditions due to changes in the mixture heat capacities. The experimental measurements indicated that over the full range of conditions investigated, the addition of TEL leads to increases in the critical explosion pressure; however, over the range of ϕ = 0.9–1.35, the addition of TEL results in no discernable effect on τ_{ign}.

Taylor et al. [69] followed this work by studying the influence of TEL on a number of other fuels, including *n*-butane, *n*-heptane, *iso*-octane, and benzene, using doping levels of 0–800 ppm. The TEL used for these tests was not blended with any lead scavengers. In addition to measurements of τ_{ign}, the authors also reported differences in the rates of pressure rise during ignition, as well as combustion progress via high speed photography through the end wall. The optical measurements were not recorded simultaneously with the pressure-time histories due to experimental complications, while changes to τ_1 were not documented in detail for these tests. The authors noted for most of the experiments the chemiluminescence exhibited characteristics of either spotty ignition, with exothermic centers sporadically located throughout the reaction chamber, or where distinct flame front(s) formed and

propagated across the reaction chamber. Often the mixtures transitioned to volumetric autoignition. For only a few tests, the chemiluminescence was observed to be uniformly distributed at ignition. Taylor et al. [69] did not find any discernable effect of TEL on benzene. However, the *n*-heptane/TEL blends at stoichiometric conditions exhibited increased reactivity at temperatures below 720 K, while at temperatures above this τ_{ign} was noticeably lengthened. Furthermore, at T_c = 820 K, the TEL more significantly extended τ_{ign} for the leaner mixtures. The *iso*-octane/TEL blends, on the other hand, as noted by Jovellanos et al. [469], did not experience any substantial changes to τ_{ign}, although the progress of ignition was significantly altered. For instance, it was found that TEL reduced the rates of pressure rise, and thus the violence of explosion by causing the mixture to burn more slowly. The high speed photography data at T_c = 660 K, p_c = 20 bar, and ϕ = 1 revealed that the inflammation process occurred more slowly because a well-defined flame front was established, whereas without TEL there was no flame front. At T_c = 838 K, p_c = 19 bar, TEL did not appear to influence the general appearance or reaction rate in the flame photographs, even though the pressure rise rates were still reduced.

Interactions between TEL and autoigniting mixtures is complex, as demonstrated by the previous RCM studies. At the lowest temperatures, the release of ethyl radicals from the additive can stimulate reactivity resulting in shortened ignition delays. Complete dissociation of TEL is endothermic and requires elevated temperatures however. Fuels with substantial LTHR can enhance this process, so that the time difference between τ_1 and τ_{ign} is increased [65]. After dissociation, Pb radicals act as a significant radical scavenger and thus reduce overall reactivity, while the formation of lead oxide (PbO) precipant leads to a catalytic sink for formaldehyde and other important radicals [472]. Flames that pass through the PbO fog are significantly slowed, as observed in [69]. While TEL has been demonstrated to be an excellent knock inhibitor, lead unfortunately poisons catalytic converters by chemically bonding to active surface sites of the catalyst and forming lead alloys. This reduces catalyst performance by decreaing the fraction of surface area available to promote CO and UHC oxidation, while it increases the distance through which the reactant molecules must diffuse within the pore structure before undergoing reaction. Disposal of lead contaminated catalysts can be environmentally problematic and very costly.

Mohamed [273] investigated the effects of diethylamine (DEA) (doped at ~5% mol) on stoichiometric *n*-pentane and *n*-heptane mixtures in synthetic air. Pressure-time data and total light output data (via a photomultiplier) were recorded. It was found that DEA extended the first-stage of the two-stage ignition of *n*-pentane and *n*-heptane, leading to a decrease in both the pressure rise and the light intensity associated with the LTHR process. This behavior is different than that observed in [473] with TEL.

Moreover, a longer second-stage ignition delay time was measured. Consequently, an increase in τ_{ign} was observed for *n*-heptane throughout the temperature range of 650–950 K, where first-stage reactions persisted to temperatures above 850 K. The τ_{ign} of *n*-pentane was increased in the range 650–850 K by the addition of DEA, but was decreased at compressed gas temperatures greater than 850 K. It was suggested that the inhibiting role of DEA might be derived from its radical scavenging interactions via $\dot{R}+(C_2H_5)_2NH=RH+(C_2H_5)_2\dot{N}$ and $RO\dot{O}+(C_2H_5)_2NH=ROOH+(C_2H_5)_2\dot{N}$, so (R3a) does not proceed effectively, while the aminyl radicals produced from these reactions are not very reactive. The enhancing role at higher temperatures was postulated to be due to the production of H_2O_2 from H-atom abstraction of DEA via $H\dot{O}_2$, and subsequent decomposition of H_2O_2 into two $\dot{O}H$ radicals. These features were not explored or confirmed via chemical kinetic modeling, however.

Investigations with anti-knock agents have provided useful insight into the evolution of, and perturbations to end gas autoignition chemistry for various fuels, and how these influence knock development. It can be difficult to extend the observed shifts in τ_{ign} at selected conditions to the performance of fuel additives in operating engines. As discussed in Section 5, knock ensues from highly coupled chemical-physical phenomena, of which autoignition chemistry is one component. Evaporative cooling, turbulent flame propagation, and pressure wave – wall interactions are also critically important. Some additives are only influential within the high temperature flame zone of the combustion chamber by altering propagation velocities, e.g., via particle condensation/growth and subsequent catalytic activity [474–476]. The work of Taylor et al. [69] illustrated how TEL can affect flame propagation processes. Nevertheless, opportunities exist to utilize RCM platforms to understand the perturbative effects of emerging, non-toxic (e.g., bio-derived) fuel additives under conditions relevant to modern, boosted SI engines [477], as well as LTC regimes.

6.8.2. Cetane Improvers

In their study of anti-knock agents, Jost and Rögener [64] also investigated the influence of various cetane improvers including amyl nitrite, ethyl nitrate, and acetone peroxide doped into *n*-heptane at ~5%, at 675 K and 16.5 bar. The mixtures for these were at stoichiometric ratios with air dilution levels. The limited τ_{ign} data indicated the effectiveness of the dopants could be ranked as ethyl nitrate > acetone peroxide > amyl nitrite.

Jovellanos et al. [469] also studied the effect of ethyl nitrite on the autoignition of 2,2,3 trimethyl butane, commonly referred as triptane. Triptane is a highly branched hydrocarbon and exhibits high anti-knocking tendency with an octane rating of RON/MON = 112/101. Tests used a fixed compression ratio of

11.7 at stoichiometric conditions where doping covered 0–13%, liquid volume basis. This study showed the doping effectiveness of ethyl nitrite was somewhat nonlinear where, in particular, no noticeable change in τ_{ign} was observed when the doping level was less than 0.2% by volume, while doping levels higher than this decreased τ_{ign} monotonically. In addition, the critical explosion pressures decreased monotonically with ethyl nitrite doping. At the highest doping level, the authors found the fuel behaved analogously to *iso*-octane.

Inomata et al. [470] studied the effect of doping *n*-butane with ethanal, diethyl ether, isopropyl nitrate, and DTBP in small amounts (<5% by volume). Comparison of τ_{ign} showed ethanal and diethyl ether had a weak effect on reactivity, while addition of isopropyl nitrate and DTBP had strong effects, where DTBP was found to be more stimulating than isopropyl nitrate. Furthermore, the change in reactivity due to the additives was dependent on the compressed temperature. For temperatures in the NTC regime, between 765 K and 785 K, it was observed that the additives did not affect the reactivity until a critical doping level was reached, and beyond this value the reactivity increased nonlinearly. For temperatures greater than the NTC peak, in the range of 825–880 K, a threshold doping level was not observed and the reactivity increased with increasing volume percentage of the additive. Based on the experimental results, the authors hypothesized the effectiveness of fuel additives on cetane number enhancement is dependent on three main criteria: (1) exothermic decomposition of the additive, (2) provision of multiple free radicals upon decomposition, and (3) supplementary reactivity induced through the molecular products as a result of the oxidation of additives.

Griffiths et al. [267] studied the decomposition of DTBP with and without oxygen. The authors found the decomposition of DTBP under pyrolysis conditions is greatly enhanced at higher temperatures, while oxidation of DTBP for the conditions investigated proceeded through two-stage ignition. Second-stage ignition was observed when the concentration levels of oxygen exceeded an equi-molar proportion with DTBP. Δp_1 was found to be less dependent on oxygen when the oxygen concentrations were higher than equi-molar proportion with DTBP.

Tanaka et al. [395] studied the effect of DTBP and 2-ethyl hexyl nitrate (2-EHN) addition to PRF90 and PRF100 (i.e., *iso*-octane), doped at 0–2% liquid volume basis (0–1.8% molar basis). Comparison of τ_{ign} showed DTBP had a higher ignition accelerating effect than 2-EHN. This finding however, is contrary to recent DCN tests and accompanying HCCI engine studies conducted under fairly similar conditions, albeit at lower doping levels [478]. The DTBP and 2-EHN additives were observed to decrease τ_1 and τ_{ign}, and the pressure rise due to first-stage ignition increased when the mixtures were doped using either additive.

The authors illustrated that the shift in Δp_1 also correlated with the shorter τ_{ign}, and this trend was similar with the undoped fuel measurements. Both DTBP and 2-EHN dissociate quickly at elevated temperatures and produce alkoxyl radicals. The highly reactive alkoxyl radicals abstract H-atoms from fuel molecules, thereby initiating the low-temperature branching chain. DTBP produces two alkoxyl radicals upon dissociation, while 2-EHN produces only one alkoxyl radical. Therefore, for the two additives tested in this study, it was explained that DTBP had a higher ignition accelerating effect.

Goldsborough et al. [134] studied the effect of 2-EHN addition to two gasoline surrogate fuels. Both surrogates were blended to have an anti-knock index, i.e., (RON+MON)/2, of 91. The first was PRF91, and the second a TRF blend containing 20% toluene, 12.8% *n*-heptane, and 67.2% *iso*-octane on a liquid volume basis. The predicted TRF91 octane rating was based on the work of Morgan et al. [405]. Doping levels of 0–3% liquid volume basis (0–2.7% molar basis) were used. The measurements indicated the reactivity of both surrogates increased upon addition of 2-EHN and both surrogates exhibited similar response upon addition of the dopant. However, it was shown that 2-EHN was more effective at low temperatures in TRF91, while in the intermediate temperature range 2-EHN was more effective in PRF91. Although the detailed chemical kinetic model used to complement the measurements was found to replicate the experimental trends observed, the magnitude of accelerative effect of the additive on ignition was significantly over-predicted, and this suggested deficiencies in the base gasoline surrogate model. Nevertheless, the simulations indicated that CH_2O and CH_3O_2 chemistry are very sensitive to the presence of 2-EHN, while dopant-derived 3-heptyl radicals were predicted to play an important role in stimulating autoignition. Furthermore, nitrogen chemistry was found to be important through the NO–NO_2 loop (see Section 6.2.4), which can generate substantial amounts of ȮH. At the highest doping levels, the formation of methyl and ethyl nitrite, and nitric acid competes with this loop so less ȮH is generated, constraining the reactivity enhancement of 2-EHN.

RCM studies investigating cetane improvers have suggested various chemical kinetic processes by which fuel autoignition can be stimulated due to the presence of additive decomposition products, which include different types of radicals. While there is potential to further investigate cetane improvers as they might be applied in LTC engine schemes such as reactivity controlled compression ignition [22], these studies have also highlighted opportunities whereby conventional cetane improvers, or other radical precursors, e.g., tert-butylhydroperoxide, could be used at very small concentrations to perturb the LTC pathways described in Fig. 37 in order to better understand and more rigorously quantify fuel autoignition

chemistry. While this is sometimes undertaken in flow reactor and shock tube studies [479,480], it has not been pursued within RCM platforms.

7. Summary and Outlook

Future internal combustion and gas turbine engines will face increasingly stringent fuel economy, performance and emissions requirements. To meet these, next-generation devices are expected to utilize a range of low temperature combustion approaches as discussed in Section 1. The design of such new engines requires significantly improved fundamental understandings of low- and intermediate-temperature autoignition phenomena, along with the development of robust combustion models that can reliably predict these processes. Additionally, as new fuels, including those which are more carbon-neutral, are integrated into the market, it will be necessary to quantify how their combustion behavior is different from conventional fuels so flexible engine operating schemes can be devised for optimal performance.

This review extends significantly beyond recent works [63][39], and highlights the pivotal role RCM studies have played in understanding LTC/DLE phenomena, including demonstrating novel experimental approaches and advanced diagnostics which have been employed as key tools towards improving our fundamental understanding of, and capability to model relevant chemistry and physics. The excellent diagnostic access and the ability to maintain prescribed test conditions for relatively long periods of time have enabled RCM studies to investigate autoignition processes at the highest densities (e.g., lower temperatures and higher pressures) of any experimental methods.

The range of operation for RCMs overlaps that of shock tubes in the high pressure (10-60 bar), intermediate temperature range around 1000 K, and autoignition information from such devices are typically in good agreement, once appropriate corrections for facility effects are taken into account. The increasing understanding of fluid and gas dynamic processes, which can limit the capabilities of both devices, has greatly improved the agreement between experimental data and model predictions, where these must take into account not only the compressed conditions, but the evolution of boundary layers and other physical phenomena that can be influential during a particular test. Advances in instrumentation and understanding of various physical processes, such as properly suppressing vortex roll-up, has also led to much better consistency between RCM datasets. For example, studies of *iso*-octane autoignition can now be shown to agree to within $\pm$25 % across a variety of different machines [62], where the origin of variations in individual measurements can be traced to the very high dependence of autoignition chemistry on gas temperature history and its spatial distribution. The gas compression trajectory and piston crevice design are accordingly very influential facility parameters [481].

The importance of temperature specification has motivated recent efforts to rigorously quantify experimental uncertainties associated with the evaluation of this parameter [482], and these analyses should be extended to account for, not only random measurement errors, but also systematic errors associated with experimental configurations and operating protocol, e.g., [483,484]. Related to this, as discussed in Section 4, recent efforts have been undertaken to quantify the extent of uncertainties associated with various approaches used to model the experiments, and the level of detail necessary to minimize these for various reacting systems, though open questions still remain. Some mixtures and state conditions are more sensitive to facility effects, while other reacting systems are less so. To date there are no definitive metrics or rigorous guidelines that can be used across a wide range of conditions towards evaluating chemical kinetic models, or comparing datasets between different RCM facilities, and other experimental apparatuses. Theory on ignition phenomena have started to address these issues, as seen by recent advances in defining ignition regimes in terms of dimensionless parameters (presented in Section 4), but this remains a serious need for the entire combustion community.

Significant progress has been made towards generating consensus for 'best practices' towards machine design and operation, some of which were discussed in [39], with additional detail presented in Section 2. Many of these 'best practices' have now become the norm across many devices, while designers of new components and devices are encouraged to leverage past advances, and to publish detailed descriptions and characterization work that demonstrate new capabilities, or limitations of concepts. It is beneficial to apply high-fidelity and/or reduced-order models before prototyping new concepts. A limitation remains however, how to archive and report RCM data which transparently describes the evolution of the state conditions from start of compression to the time of autoignition, particularly for researchers not familiar with RCM experiments. Data conditioning, for instance, can affect the measured pressures and thus computed temperatures, when derived from pressure data. It is stressed that uncertainty analyses should include the effects of different methods of conditioning data, as well as different means to define end-of-compression. The International RCM Workshop Characterization Initiative has made progress towards this [62], but it is still an area of need and potential for considerable contribution to the RCM and combustion communities

Mechanistic information about chemical pathways has traditionally emerged from continuous sampling of flow/jet reactors, often though, under thermodynamic or fuel loading conditions far from those experienced in operating engines. Recent advances in quenching and sampling from RCMs, followed by gas composition analysis has facilitated high impact studies allowing experimental interrogation of

chemical intermediates at high pressures where there are few data to develop theory and benchmark chemistry. Understanding of the behavior of autoignition chemistry for branched and unbranched hydrocarbons across low- and intermediate-temperatures has been derived, in part, from careful RCM sampling work, combined with mechanistic information from other studies. There is a need to extend the current database with increasing use of time-resolved diagnostics, some of which are highlighted in Section 3. Speciation via gas sample analysis along with additional absorption and LIF diagnostics will increase both the extent of mechanistic information for a range of fuels, as well as provide additional constraints on absolute and relative reaction rates, which are critical for the construction and confident use of rate rules [372,485], and for converging on unique solutions to represent combustion chemistry. Challenges of adequately closing the carbon, or atom balance for tests with large molecular weight species can be mitigated by, for example, coupling the sampling and analytical units with heated glass-lined tubing [486]. The use of time-resolved absorption diagnostics tuned to specific species is evolving quickly [487–490][491], and while currently limited, could add further to the arsenal of diagnostics providing mechanistic information, particularly as longer and shorter wavelength sources become more accessible and reliable. Additionally, approaches which could exploit the isomeric selectivity and radical detection capabilities of synchrotron-based, molecular beam mass spectroscopy techniques, as has been recently implemented with novel shock tube configurations [45], could yield extremely valuable information at LTC conditions. Implementation of advanced and emerging diagnostics will need to consider and mitigate issues associated with non-idealities such as boundary layer development, etc. at longer test times.

High speed, spatially-resolved imaging diagnostics have provided a wealth of information on the effects of thermal stratification and charge motion governing, for instance, the onset of mild ignition as well as other physical-chemical interactions, as discussed in Section 5. These phenomena are significantly more complex than pure chemical kinetic processes, yet are central to the overall understanding of how autoignition takes place in practical devices. Significantly more work needs to be done with the help of advanced (kHz-range) diagnostics [492,493], as well as DNS and LES simulations, in order to come to a clearer picture of the development of non-uniformities, and the interplay between transport and chemistry on the overall heat release rate in autoigniting mixtures. New and evolving techniques such as schlieren image (particle-free) velocimetry [494] and plentopic imaging [495,496] have potential to provide additional insight into these phenomena. Application of such high speed, spatially-resolved diagnostics could also help elucidate complex processes associated with emerging LTC approaches such as plasma-assisted autoignition [191,192][193].

A growing set of fuels has been considered covering a range of conditions in RCMs, yet there are still a number of quantitative gaps, particularly at extreme densities (lower temperatures and higher pressures (upwards of 100+ bar)) where neither RCMs nor shock tube can maintaing high quality experimental conditions, and where diagnostics, even accurate/robust pressure transducers, are limited. Additionally, there is a lack of sufficiently reliable information concerning real fuels, including natural gas blends and full-boiling range fuels. The relatively lower reactivity of natural gas components, which are currently very relevant for use in industrial and large engines, means that the high pressures and/or temperatures required for autoignition are often beyond the capabilities of many existing devices. Furthermore, only recently have well-characterized, research grade transportation fuels been formulated for standardized testing [497]. Challenges associated with the involatility of jet fuels and diesels, as well as some oxygenates, are difficult to overcome, though new experimental approaches as described in Section 2, hold promise for conducting tests over a range of conditions. There is a relative dearth of data for the many non-conventional fuels currently being considered for greenhouse gas emissions reductions, where unique functional groups or moieties within the molecular structures can significantly affect combustion behavior.

The mechanisms of alkane autoignition are fairly well understood, though a variety of quantitative gaps for specific compounds still exist. In addition, new data has indicated the existence unique kinetic pathways not previously considered, such as the addition of a third O_2 to alternatively isomerized $\dot{O}OQOOH$ species (i.e., $\dot{P}(OOH)_2$), where this could compete with (R6a) in Fig. 37, offering an additional route to chain branching [498,499]. The situation is not nearly as clear for alkenes, cyclic and aromatic hydrocarbons, for which both mechanistic and rate information are lacking. For instance, predictions of preliminary exothermic temperature rise can be off by an order of magnitude, especially at high concentrations. Furthermore, highly non-linear synergistic and antagonistic effects that arise from fuel blending, particularly observed with compounds of very different reactivity, pose a significant challenge to predictive models, where data from different devices/regimes can indicate different interactive behavior. These effects are responsible for many of the difficulties in achieving closure between multi-component surrogate blends and practical, full-boiling range fuels [500]. There is also a need for more studies covering the influences of real EGR (including minor constituents) and fuel additives on LTC processes. While major combustion products such as CO_2 and H_2O have been studied, there is very limited data for pollutants such as NO_x and UHCs, which can have significantly greater perturbing characteristics. Opportunities to use fuel additives as radical precursors to better quantify autoignition chemistry are highlighted in Section 6. Finally, uncertainties in chemical models are not well quantified and not

consistently reported [286,383], but these must be addressed in order to more rigorously validate model results, and more effectively design new RCM experiments that can constrain simulation predictions. These issues will continue to provide an impulse for further experimentation, modeling and fine attention to detail in generating reliable information from RCMs.

8. Acknowledgements

The inspiration for this paper stems from many fruitful discussions during the 1st and 2nd International RCM Workshops organized by Argonne National Laboratory. The authors would like to thank the participants of those meetings for the stimulating conversations.

This manuscript has been created in part by UChicago Argonne, LLC, Operator of Argonne National Laboratory ("Argonne"). Argonne, a U.S. Department of Energy Office of Science laboratory, is operated under Contract No. DE-AC02-06CH11357. The U.S. Government retains for itself, and others acting on its behalf, a paid-up non-exclusive, irrevocable worldwide license in said article to reproduce, prepare derivative works, distribute copies to the public, and perform publicly and display publicly, by or on behalf of the Government. The Department of Energy will provide public access to these results of federally sponsored research in accordance with the DOE Public Access Plan. http://energy.gov/downloads/doe-public-access-plan. SSG acknowledges support through the U.S. DOE Vehicle Technology Program with Gurpreet Singh and Leo Breton as program managers. MSW acknowledges support throught the U.S. DOE Basic Energy Sciences via contract No. DE-SC0002645. CJS acknowledges support through the U.S. National Science Foundation under Grant No. CBET-1402231. Michael Pamminger and Toby Rockstroh assisted in the translation of some of the early works by Jost, Rögener and co-workers.

9. References

[1] Johnson T V. Review of CO2 Emissions and Technologies in the Road Transportation Sector. SAE Int J Engines 2010;3:1079–98. doi:10.4271/2010-01-1276.

[2] Johnson T V. Review of diesel emissions and control. Int J Engine Res 2009;10:275–85. doi:10.1243/14680874JER04009.

[3] Saxena S, Bedoya ID. Fundamental phenomena affecting low temperature combustion and HCCI engines, high load limits and strategies for extending these limits. Prog Energy Combust Sci 2013;39:457–88. doi:10.1016/j.pecs.2013.05.002.

[4] Musculus MPB, Miles PC, Pickett LM. Conceptual models for partially premixed low-temperature diesel combustion. Prog Energy Combust Sci 2013;39:246–83. doi:10.1016/j.pecs.2012.09.001.

[5] Lu X, Han D, Huang Z. Fuel design and management for the control of advanced compression-ignition combustion modes. Prog Energy Combust Sci 2011;37:741–83. doi:10.1016/j.pecs.2011.03.003.

[6] Onishi S, Jo S, Shoda K, Jo P. Active Thermo-Atmosphere Combustion (ATAC) - A New Combustion Process for Internal Combustion Engines. SAE Tech. Pap., 1979, p. SAE 790501. doi:10.4271/790501.

[7] Najt PM, Foster DE. Compression ignited homogeneous charge combustion. SAE Pap., 1983, p. SAE Paper 830264. doi:10.4271/830264.

[8] Christensen M, Johansson B, Einewall P. Homogeneous Charge Compression Ignition (HCCI) Using Isooctane, Ethanol and Natural Gas - A Comparison with Spark Ignition Operation. 1997. doi:10.4271/972874.

[9] Christensen M, Hultqvist A, Johansson B. Demonstrating the Multi Fuel Capability of a Homogeneous Charge Compression Ignition Engine with Variable Compression Ratio. 1999. doi:10.4271/1999-01-3679.

[10] Christensen M, Johansson B. Supercharged Homogeneous Charge Compression Ignition (HCCI) with Exhaust Gas Recirculation and Pilot Fuel. 2000. doi:10.4271/2000-01-1835.

[11] Thring RH. Homogeneous – charge compression ignition (HCCI) engines. SAE Pap 892068 1989. doi:10.4271/892068.

[12] Ryan TW, Callahan TJ. Homogeneous charge compression ignition of diesel fuel. SAE Tech Pap 1996;961160. doi:10.4271/961160.

[13] Gray, A.W., Ryan TW. Homogeneous Charge Compression Ignition (HCCI) of Diesel Fuel. SAE Tech Pap 1997;971676. doi:10.4271/971676.

[14] Takeda, N., Keiichi, N., Keiichi N. Emission Characteristics of Premixed Lean Diesel Combustion with Extremely Early Staged Fuel Injection. SAE Tech Pap 1996;961163. doi:10.4271/961163.

[15] Nakagome, K., Shimazaki, N. , Niimura, K., Kobayashi S. Combustion and Emission Characteristics of Premixed Lean Diesel Combustion Engine. SAE Tech Pap 1997;970898. doi:10.4271/970898.

[16] Akihama K, Takatori Y, Inagaki K, Sasaki S, Dean AM. Mechanism of the Smokeless Rich Diesel Combustion by Reducing Temperature. SAE Tech Pap 2001;2001-01-06. doi:10.4271/2001-01-0655.

[17] Hasegawa R, Yanagihara H. HCCI Combustion in DI Diesel Engine. SAE Tech Pap 2003;2003–01–07. doi:10.4271/2003-01-0745.

[18] Kimura S, Aoki O, Ogawa H, Muranaka S, Enomoto Y. New combustion concept for ultra-clean and high-efficiency small DI diesel engines. SAE Pap. 1999-01-3681, 1999. doi:10.4271/1999-01-3681.

[19] Kalghatgi GT, Risberg P, Angstrom H-E. Partially Pre-Mixed Auto-Ignition of Gasoline to Attain Low Smoke and Low NOx at High Load in a Compression Ignition Engine and Comparison with a Diesel Fuel. 2007. doi:10.4271/2007-01-0006.

[20] Kalghatgi G, Hildingsson L, Johansson B. Low NO[sub x] and Low Smoke Operation of a Diesel Engine Using Gasolinelike Fuels. J Eng Gas Turbines Power 2010;132:092803. doi:10.1115/1.4000602.

[21] Splitter DA, Reitz RD. Fuel reactivity effects on the efficiency and operational window of dual-fuel compression ignition engines. Fuel 2014;118:163–75. doi:10.1016/j.fuel.2013.10.045.

[22] Reitz RD, Duraisamy G. Review of high efficiency and clean reactivity controlled compression ignition (RCCI) combustion in internal combustion engines. Prog Energy Combust Sci 2015;46:12–71. doi:10.1016/j.pecs.2014.05.003.

[23] Hülser T, Grünefeld G, Brands T, Günther M, Pischinger S. Optical Investigation on the Origin of Pre-Ignition in a Highly Boosted SI Engine Using Bio-Fuels. SAE Tech Pap 2013–01–1636 2013. doi:10.4271/2013-01-1636.

[24] Amann M, Alger T, Mehta D. The Effect of EGR on Low-Speed Pre-Ignition in Boosted SI Engines. SAE Tech. Pap., 2011. doi:10.4271/2011-01-0339.

[25] Peters N, Kerschgens B, Paczko G. Super-Knock Prediction Using a Refined Theory of Turbulence. SAE Int J Engines 2013;6:2013–01 – 1109. doi:10.4271/2013-01-1109.

[26] Robert A, Richard S, Colin O, Poinsot T. LES study of deflagration to detonation mechanisms in a downsized spark ignition engine. Combust Flame 2015;162:2788–807. doi:10.1016/j.combustflame.2015.04.010.

[27] Kalghatgi GT, Bradley D. Pre-ignition and “super-knock” in turbo-charged spark-ignition engines. Int J Engine Res 2012;13:399–414. doi:10.1177/1468087411431890.

[28] Lefebvre AH, Ballal DR. Gas Turbine Combustion: Alternative Fuels and Emissions. CRC Press; 2010.

[29] Felix Güthe, Jaan Hellat PF. The Reheat Concept: The Proven Pathway to Ultra-Low Emissions and High Efficiency and Flexibility. ASME Turbo Expo 2007 Power Land, Sea, Air, Montreal, Canada: ASME; 2007, p. GT2007–27846, 641–8. doi:10.1115/GT2007-27846.

[30] Güthe F, Hellat J, Flohr P. The Reheat Concept: The Proven Pathway to Ultralow Emissions and High Efficiency and Flexibility. J Eng Gas Turbines Power 2008;131:21503.

[31] Valco DJ, Gentz G, Allen C, Colket M, Edwards T, Gowdagiri S, et al. Autoignition behavior of synthetic alternative jet fuels: An examination of chemical composition effects on ignition delays at low to intermediate temperatures. Proc Combust Inst 2015;35:2983–91. doi:10.1016/j.proci.2014.05.145.

[32] Stachler RD, Heyne JS, Stouffer SD, Miller JD, Roquemore WM. Investigation of Combustion

Emissions from Conventional and Alternative Aviation Fuels in a Well-Stirred Reactor. 55th AIAA Aerosp. Sci. Meet., American Institute of Aeronautics and Astronautics; 2017. doi:doi:10.2514/6.2017-0382.

[33] Sigfrid IR, Whiddon R, Collin R, Klingmann J. Influence of reactive species on the lean blowout limit of an industrial DLE gas turbine burner. Combust Flame 2014;161:1365–73. doi:http://dx.doi.org/10.1016/j.combustflame.2013.10.030.

[34] Won SH, Windom B, Jiang B, Ju Y. The role of low temperature fuel chemistry on turbulent flame propagation. Combust Flame 2014;161:475–83. doi:http://dx.doi.org/10.1016/j.combustflame.2013.08.027.

[35] Windom B, Won SH, Reuter CB, Jiang B, Ju Y, Hammack S, et al. Study of ignition chemistry on turbulent premixed flames of n-heptane/air by using a reactor assisted turbulent slot burner. Combust Flame 2016;169:19–29. doi:http://dx.doi.org/10.1016/j.combustflame.2016.02.031.

[36] Cummins CL. Internal Fire. 3rd Editio. Wilsonville, OR: Carnot Press; 1989.

[37] Mehl M, Pitz WJ, Sjöberg M, Dec JE. Detailed Kinetic Modeling of Low-Temperature Heat Release for PRF Fuels in an HCCI Engine. SAE Tech Pap 2009;2009-01-18. doi:10.4271/2009-01-1806.

[38] Tsujimura T, Pitz WJ, Yang Y, Dec JE. Detailed Kinetic Modeling of HCCI Combustion with Isopentanol. SAE Int J Fuels Lubr 2011;4:257–70. doi:10.4271/2011-24-0023.

[39] Sung C-J, Curran HJ. Using rapid compression machines for chemical kinetics studies. Prog Energy Combust Sci 2014;44:1–18. doi:10.1016/j.pecs.2014.04.001.

[40] Kang D, Lilik G, Dillstrom V, Agudelo J, Lapuerta M, Al-Qurashi K, et al. Impact of branched structures on cycloalkane ignition in a motored engine: Detailed product and conformational analyses. Combust Flame 2015;162:877–92. doi:10.1016/j.combustflame.2014.09.009.

[41] Dryer FL, Haas FM, Santner J, Farouk TI, Chaos M. Interpreting chemical kinetics from complex reaction–advection–diffusion systems: Modeling of flow reactors and related experiments. Prog Energy Combust Sci 2014;44:19–39. doi:10.1016/j.pecs.2014.04.002.

[42] Herbinet O, Dayma G. Jet Stirred Reactors. In: Battin-Leclerc F, Simmie JM, Blurock E, editors. Clean. Combust., Springer-Verlag London; 2013, p. 183–210. doi:10.1007/978-1-4471-5307-8.

[43] Hanson RK, Davidson DF. Recent advances in laser absorption and shock tube methods for studies of combustion chemistry. Prog Energy Combust Sci 2014;44:103–14. doi:10.1016/j.pecs.2014.05.001.

[44] Tranter RS, Amoorthy HR, Raman A, Brezinsky K, Allendorf MD. High-pressure single-pulse shock tube investigation of rich and stoichiometric ethane oxidation. Proc Combust Inst 2002;29:1267–75. doi:http://dx.doi.org/10.1016/S1540-7489(02)80156-0.

[45] Lynch PT, Troy TP, Ahmed M, Tranter RS. Probing Combustion Chemistry in a Miniature Shock Tube with Synchrotron VUV Photo Ionization Mass Spectrometry. Anal Chem 2015;87:2345–52. doi:10.1021/ac5041633.

[46] Campbell MF, Parise T, Tulgestke AM, Spearrin RM, Davidson DF, Hanson RK. Strategies for obtaining long constant-pressure test times in shock tubes. Shock Waves 2015;25:651–65. doi:10.1007/s00193-015-0596-x.

[47] Davidson DF, Hanson RK. Recent advances in shock tube/laser diagnostic methods for improved

chemical kinetics measurements. Shock Waves 2009;19:271–83. doi:10.1007/s00193-009-0203-0.

[48] Tranter R, Brezinsky K. Shock Tube Studies of Combustion Relevant Elementary Chemical Reactions and Submechanisms. In: Battin-Leclerc F, Simmie JM, Blurock E, editors. Clean. Combust., Springer-Verlag London; 2013, p. 629–52. doi:10.1007/978-1-4471-5307-8.

[49] Al-Abdeli YM, Masri AR. Review of laboratory swirl burners and experiments for model validation. Exp Therm Fluid Sci 2015;69:178–96. doi:http://dx.doi.org/10.1016/j.expthermflusci.2015.07.023.

[50] O'Connor J, Acharya V, Lieuwen T. Transverse combustion instabilities: Acoustic, fluid mechanic, and flame processes. Prog Energy Combust Sci 2015;49:1–39. doi:http://dx.doi.org/10.1016/j.pecs.2015.01.001.

[51] Xu S, Huang S, Huang R, Wei W, Cheng X, Ma Y, et al. Estimation of turbulence characteristics from PIV in a high-pressure fan-stirred constant volume combustion chamber. Appl Therm Eng 2017;110:346–55. doi:http://dx.doi.org/10.1016/j.applthermaleng.2016.08.149.

[52] Galmiche B, Mazellier N, Halter F, Foucher F. Turbulence characterization of a high-pressure high-temperature fan-stirred combustion vessel using LDV, PIV and TR-PIV measurements. Exp Fluids 2013;55:1636. doi:10.1007/s00348-013-1636-x.

[53] Maes N, Meijer M, Dam N, Somers B, Baya Toda H, Bruneaux G, et al. Characterization of Spray A flame structure for parametric variations in ECN constant-volume vessels using chemiluminescence and laser-induced fluorescence. Combust Flame 2016;174:138–51. doi:http://dx.doi.org/10.1016/j.combustflame.2016.09.005.

[54] Yu H, Chen Z. End-gas autoignition and detonation development in a closed chamber. Combust Flame 2015;162:4102–11. doi:http://dx.doi.org/10.1016/j.combustflame.2015.08.018.

[55] Pan J, Shu G, Zhao P, Wei H, Chen Z. Interactions of flame propagation, auto-ignition and pressure wave during knocking combustion. Combust Flame 2016;164:319–28. doi:http://dx.doi.org/10.1016/j.combustflame.2015.11.030.

[56] Krisman A, Hawkes ER, Talei M, Bhagatwala A, Chen JH. Characterisation of two-stage ignition in diesel engine-relevant thermochemical conditions using direct numerical simulation. Combust Flame 2016;172:326–41. doi:http://dx.doi.org/10.1016/j.combustflame.2016.06.010.

[57] Minamoto Y, Chen JH. DNS of a turbulent lifted DME jet flame. Combust Flame 2016;169:38–50. doi:http://dx.doi.org/10.1016/j.combustflame.2016.04.007.

[58] Courtine E, Selle L, Poinsot T. DNS of Intrinsic ThermoAcoustic modes in laminar premixed flames. Combust Flame 2015;162:4331–41. doi:http://dx.doi.org/10.1016/j.combustflame.2015.07.002.

[59] Fiorina B, Mercier R, Kuenne G, Ketelheun A, Avdić A, Janicka J, et al. Challenging modeling strategies for LES of non-adiabatic turbulent stratified combustion. Combust Flame 2015;162:4264–82. doi:http://dx.doi.org/10.1016/j.combustflame.2015.07.036.

[60] Doisneau F, Arienti M, Oefelein J. On Multi-Fluid models for spray-resolved LES of reacting jets. Proc Combust Inst 2017;36:2441–50. doi:http://dx.doi.org/10.1016/j.proci.2016.07.120.

[61] Merchant SS, Goldsmith CF, Vandeputte AG, Burke MP, Klippenstein SJ, Green WH. Understanding low-temperature first-stage ignition delay: Propane. Combust Flame

2015;162:3658–73. doi:10.1016/j.combustflame.2015.07.005.

[62] Goldsborough SS, Curran HJ, Sung C-J, Vanhove G, Wooldridge MS, Farooq A, et al. RCM Workshop iso-Octane Initiative: identifying and quantifying facility influences on autoignition measurements of a prototypical gasoline surrogate. Combust Flame n.d.

[63] Kéromnès A. Rapid Compression Machines. In: Battin-Leclerc F, Simmie JM, Blurock E, editors. Clean. Combust., Springer-Verlag London; 2013, p. 163–83. doi:10.1007/978-1-4471-5307-8.

[64] Jost W, Rögener H. Uber die Wirkung von Zusatzen auf die Selbstzundung adiabatisch komprimierter Heptan-Luft-Gemische. Zeitschrift Für Elektrochemie 1941;47:307–9. doi:10.1002/bbpc.19410470405.

[65] Rögener H. Entzündung von Kohlenwasserstoff-Luft-Gemischen durch adiabatische Verdichtung. Zeitschrift Für Elektrochemie 1949;53:389–97. doi:10.1002/bbpc.19490530614.

[66] Jost W. Reactions of adiabatically compressed hydrocarbon-air mixtures. Symp Combust 1949;3:424–32. doi:10.1016/S1062-2896(49)80053-5.

[67] Jost W. Knock reaction. Symp Combust 1963;9:1013–22. doi:10.1016/S0082-0784(63)80107-1.

[68] Leary WA, Taylor ES, Taylor CF, Jovellanos JU. A rapid compression machine suitable for studying short ignition delays. Natl Advis Comm Aeronaut 1948. doi:19930081958.

[69] Taylor CF, Taylor ES, Livengood JC, Russell WA, Leary WA. Ignition of Fuels by Rapid Compression. SAE 500178, 1950. doi:10.4271/500178.

[70] Affleck WS, Fish A. Two-stage ignition under engine conditions parallels that at low pressures. Symp Combust 1967;11:1003–13. doi:10.1016/S0082-0784(67)80227-3.

[71] Affleck WS, Fish A. Knock: Flame acceleration or spontaneous ignition? Combust Flame 1968;12:243–52. doi:10.1016/0010-2180(68)90021-7.

[72] Fish A, Read IA, Affleck WS, Haskell WW. The controlling role of cool flames in two-stage ignition. Combust Flame 1969;13:39–49. doi:10.1016/0010-2180(69)90026-1.

[73] Fish A, Haskell WW, Read IA. The Non-Isothermal Oxidation of 2-Methylpentane. III. The Reaction at High Pressure. Proc R Soc A Math Phys Eng Sci 1969;313:261–97. doi:10.1098/rspa.1969.0192.

[74] Griffiths JF, MacNamara JP, Sheppard CGW, Turton DA, Whitaker BJ. The relationship of knock during controlled autoignition to temperature inhomogeneities and fuel reactivity. Fuel 2002;81:2219–25. doi:10.1016/S0016-2361(02)00134-5.

[75] Griffiths JF, Hasko SM. Two-Stage Ignitions During Rapid Compression: Spontaneous Combustion in Lean Fuel-Air Mixtures. Proc R Soc A Math Phys Eng Sci 1984;393:371–95. doi:10.1098/rspa.1984.0063.

[76] Griffiths JF, Halford-Maw PA, Rose DJ. Fundamental features of hydrocarbon autoignition in a rapid compression machine. Combust Flame 1993;95:291–306. doi:10.1016/0010-2180(93)90133-N.

[77] Cox A, Griffiths JF, Mohamed C, Curran HJ, Pitz WJ, Westbrook CK. Extents of alkane combustion during rapid compression leading to single-and two-stage ignition. Proc Combust Inst 1996;26:2685–92. doi:10.1016/S0082-0784(96)80104-4.

[78] Franck J, Griffiths J, Nimmo W. The Control of Spontaneous Ignition under Rapid Compression.

Symp Combust 1986;21:447–54. doi:10.1016/S0082-0784(88)80272-8.

[79] Minetti R, Ribaucour M, Carlier M, Sochet LR. Autoignition Delays of a Series of Linear and Branched Chain Alkanes in the Intermediate Range of Temperature. Combust Sci Technol 1996;113:179–92. doi:10.1080/00102209608935493.

[80] Minetti R, Carlier M, Ribaucour M, Therssen E, Sochet LR. A rapid compression machine investigation of oxidation and auto-ignition of n-Heptane: Measurements and modeling. Combust Flame 1995;102:298–309. doi:10.1016/0010-2180(94)00236-L.

[81] Minetti R, Roubaud A, Therssen E, Ribaucour M, Sochet LR. The chemistry of pre-ignition of n-pentane and 1-pentene. Combust Flame 1999;118:213–20. doi:10.1016/S0010-2180(98)00151-5.

[82] Ribaucour M, Roubaud A, Minetti R, Sochet LR. The low-temperature autoignition of alkylaromatics: Experimental study and modeling of the oxidation of n-butylbenzene. Proc Combust Inst 2000;28:1701–7. doi:10.1016/S0082-0784(00)80570-6.

[83] Lemaire O, Ribaucour M, Carlier M, Minetti R. The production of benzene in the low-temperature oxidation of cyclohexane, cyclohexene, and cyclohexa-1,3-diene. Combust Flame 2001;127:1971–80. doi:10.1016/S0010-2180(01)00301-7.

[84] Vanhove G, Ribaucour M, Minetti R, Zheng X. On the influence of the position of the double bond on the low-temperature chemistry of hexenes. Proc Combust Inst 2005;30 I:1065–72. doi:10.1016/j.proci.2004.08.042.

[85] Mittal G, Chomier M. Effect of crevice mass transfer in a rapid compression machine. Combust Flame 2014;161:398–404. doi:10.1016/j.combustflame.2013.09.008.

[86] Grogan KP, Ihme M. Weak and strong ignition of hydrogen/oxygen mixtures in shock-tube systems. Proc Combust Inst 2015;35:2181–9. doi:10.1016/j.proci.2014.07.074.

[87] Wu H, Ihme M. Effects of flow-field and mixture inhomogeneities on the ignition dynamics in continuous flow reactors. Combust Flame 2014;161:2317–26. doi:10.1016/j.combustflame.2014.02.007.

[88] Chen JH, Hawkes ER, Sankaran R, Mason SD, Im HG, Pébay PP, et al. Direct numerical simulation of ignition front propagation in a constant volume with temperature inhomogeneities. Combust Flame 2006;145:128–44. doi:10.1016/j.combustflame.2005.09.017.

[89] Mastorakos E, Baritaud TA, Poinsot TJ. Numerical simulations of autoignition in turbulent mixing flows. Combust Flame 1997;109:198–223. doi:10.1016/S0010-2180(96)00149-6.

[90] Oppenheim AK, Cohen LM, Short JM, Cheng RK, Hom K. Dynamics of the exothermic process in combustion. Symp Combust 1975;15:1503–13. doi:http://dx.doi.org/10.1016/S0082-0784(75)80408-5.

[91] Filimonov VY. Thermal explosion in homogeneous mixtures – a novel approach to analysis. Combust Theory Model 2015;19:260–77. doi:10.1080/13647830.2015.1013991.

[92] Sokolik A. Self-Ignition, Flame and Detonation in Gases. Jerusalem: Israel Program for Scientific Translations; 1963.

[93] Falk KG. The ignition temperatures of hydrogen-oxygen mixtures. J Am Chem Soc 1906;28:1517–34. doi:10.1021/ja01977a001.

[94] Falk KG. The ignition temperatures of gaseous mixtures. J Am Chem Soc 1907;29:1536–57. doi:10.1021/ja01965a002.

[95] Dixon HB, Crofts JM. CXC.-The firing of gases by adiabatic compression. Part II. The ignition-points of mixtures containing electrolytic gas. J Chem Soc Trans 1914;105:2036–53. doi:10.1039/ct9140502036.

[96] Elsworth JE, Haskell WW, Read IA. Non-Uniform Ignition Processes in Rapid Compression Machines. Combust Flame 1969;13:437–8. doi:10.1016/0010-2180(69)90115-1.

[97] Dixon HB, Bradshaw L, Campbell C. The firing of gases by adiabatic compression. Part I. Photographic analysis of the flame. J Chem Soc Trans 1914;105:2027–35. doi:10.1039/ct9140502027.

[98] Cassel H. Über Entflammung und Verbrennung von Sauerstoff–Wasserstoff-Gemischen. Ann Phys 1916;23:685–704. doi:10.1002/andp.19173562302.

[99] Shepherd WCF. The Ignition of gas mixtures by impulsive pressures. Symp Combust Flame, Explos Phenom 1948;3:301–16. doi:http://dx.doi.org/10.1016/S1062-2896(49)80037-7.

[100] Fay JA. Some experiments on the initiation of detonation In 2H2−O2 mixtures by uniform shock waves. Symp Combust 1953;4:501–7. doi:http://dx.doi.org/10.1016/S0082-0784(53)80071-8.

[101] Steinberg M, Kaskan WE. The ignition of combustible mixtures by shock waves. Symp Combust 1955;5:664–72. doi:http://dx.doi.org/10.1016/S0082-0784(55)80092-6.

[102] Park P, Keck J. Rapid Compression Machine Measurements of Ignition Delays for Primary Reference Fuels. 1990. doi:10.4271/900027.

[103] Smith VC. A Study of Homogeneous Combustion in Gases. M.I.T., 1930.

[104] Rögener H. Untersuchungen über klopfende Verbrennung. Strassburg, Germany: 1945.

[105] Jost W. The self-ignition of mixtures of hydrocarbons and air subjected to very sudden adiabatic compression. 1946.

[106] Livengood JC, Leary WA. Autoignition by Rapid Compression. Ind & Eng Chem 1951;43:2797–805. doi:10.1021/ie50504a046.

[107] Kono M, Shiga S, Kumagai S, Iinuma K. Thermodynamic and experimental determinations of knock intensity by using a spark-ignited rapid compression machine. Combust Flame 1983;54:33–47. doi:10.1016/0010-2180(83)90020-2.

[108] Donovan MT, He X, Zigler BT, Palmer TR, Wooldridge MS, Atreya A. Demonstration of a free-piston rapid compression facility for the study of high temperature combustion phenomena. Combust Flame 2004;137:351–65. doi:10.1016/j.combustflame.2004.02.006.

[109] Yang Z, Qian Y, Yang X, Wang Y, Wang Y, Huang Z, et al. Autoignition of n-Butanol/n-Heptane Blend Fuels in a Rapid Compression Machine under Low-to-Medium Temperature Ranges. Energy & Fuels 2013;27:7800–8. doi:10.1021/ef401774f.

[110] Shiga S, Ozone S, Machacon HTC, Karasawa T, Nakamura H, Ueda T, et al. A study of the combustion and emission characteristics of compressed-natural-gas direct-injection stratified combustion using a rapid-compression-machine. Combust Flame 2002;129:1–10. doi:10.1016/S0010-2180(01)00367-4.

[111] Kim Y, Min K, Kim MS, Chung SH, Bae C. Development of a Reduced Chemical Kinetic Mechanism and Ignition Delay Measurement in a Rapid Compression Machine for CAI Combustion. SAE Tech Pap 2007;2007-01-02. doi:10.4271/2007-01-0218.

[112] Saanum I, Bysveen M, Almås T, Sønju OK. Ignition and Combustion Characterization of Hydrogen/Methane Mixtures by Visualization in a Rapid Compression Machine (RCM). SAE Tech Pap 2005;2005-24-00. doi:10.4271/2005-24-009.

[113] Guibert P, Keromnes A, Legros G, Jean I, Rond L. Development of a Turbulence Controlled Rapid Compression Machine for HCCI Combustion. SAE Tech Pap 2007-01-1869 2007:1086–96. doi:10.4271/2007-01-1869.

[114] Affleck WS, Thomas A. An opposed piston rapid compression machine for preflame reaction studies. Proc Inst Mech Eng 1968;183:365–87. doi:10.1243/PIME_PROC_1968_183_034_02.

[115] Brett L, Macnamara J, Musch P, Simmie JM. Simulation of methane autoignition in a rapid compression machine with creviced pistons. Combust Flame 2001;124:326–9. doi:10.1016/S0010-2180(00)00193-0.

[116] Rogowski A. A New Machine for Studying Combustion of Fuel Sprays with Controlled Air Motion. SAE Tech Pap 1961;610134. doi:10.4271/610134.

[117] Voinov AN, Skorodelov DI, Sokolov FP. Variation with temperature and pressure of ignition delay of hydrocarbon-air mixtures on adiabatic compression. Kinet I Katal 1964;5:388.

[118] Beeley P, Griffiths JF, Gray P. Rapid Compression Studies on Spontaneous Ignition of Isopropyl Nitrate - 2. Rapid Sampling, Intermediate Stages and Reaction Mechanisms. Combust Flame 1980;39:269–81. doi:10.1016/0010-2180(80)90023-1.

[119] Tizard HT, Pye DR. Experiments on the ignition of gases by sudden compression. Philos Mag Ser 6 1922;44:79–121. doi:10.1080/14786440708633981.

[120] Ribaucour M, Minetti R, Carlier M, Sochet L-R. Autoinflammation à haute pression. conception, réalisation et test d'une machine à compression rapide. J Chim Phys 1992;89:2127–52.

[121] J. Guézet, Kageyama T. Etude aérodynamique dans une machine à compression rapide. Rev Gén Therm 1997;36:17–25. doi:10.1016/S0035-3159(99)80062-2.

[122] Strozzi C, Sotton J, Mura A, Bellenoue M. Characterization of a two-dimensional temperature field within a rapid compression machine using a toluene planar laser-induced fluorescence imaging technique. Meas Sci Technol 2009;20:125403. doi:10.1088/0957-0233/20/12/125403.

[123] Murase E, Hanada K. Control of the Start of HCCI Combustion by Pulsed Flame Jet. SAE Tech Pap 2002. doi:10.4271/2002-01-2867.

[124] Hashimoto K. Effect of Ethanol on the HCCI Combustion. SAE Tech Pap 2007-01-2038 2007. doi:10.4271/2007-01-2038.

[125] Gabano JD, Kageyama T, Fission F. Experimental study of n-butane autoignition in a rapid compression machine. In: Kuhl AL, editor. Dyn. Deflagrations React. Syst. Flames, Ann Arbor: AIAA; 1989, p. 407–17. doi:10.2514/5.9781600866043.0407.0417.

[126] Strozzi C, Sotton J, Mura A, Bellenoue M. Experimental and Numerical Study of the Influence of Temperature Heterogeneities on Self-Ignition Process of Methane-Air Mixtures in a Rapid Compression Machine. Combust Sci Technol 2008;180:1829–57.

doi:10.1080/00102200802260656.

[127] Watanabe Y, Morikawa K, Kuwahara T, Tanabe M. Evaluation of Homogeneous Charge Compression Ignition at High Engine Speeds using a Super Rapid Compression Machine. SAE Pap 2008. doi:10.4271/2008-01-2403.

[128] Evezard G. An Innovative Rapid Compression Machine in Theory and Practice. University of Cape Town, 2012.

[129] Maccormac M, Townend DTA. The spontaneous ignition under pressure of typical knocking and non-knocking fuels : heptane, octane; isooctane, diisopropyl ether, acetone, benzene. J Chem Soc 1938:238–46. doi:10.1039/JR9380000238.

[130] Ikegami M, Miwa K, Ohmija T, Nishitani T. Study of the Ignition Delay of Diesel Fuel Spray using a Rapid Compression Machine. Trans Jap Soc Mech Eng Ser B 1987;53:274–81.

[131] Schmidt FAF. The internal combustion engine. Chapman and Hall; 1965.

[132] Liu H, Zhang H, Shi Z, Lu H, Zhao G, Yao B. Performance Characterization and Auto-Ignition Performance of a Rapid Compression Machine. Energies 2014;7:6083–104. doi:10.3390/en7096083.

[133] Di H, He X, Zhang P, Wang Z, Wooldridge MS, Law CK, et al. Effects of buffer gas composition on low temperature ignition of iso-octane and n-heptane. Combust Flame 2014;161:2531–8. doi:10.1016/j.combustflame.2014.04.014.

[134] Goldsborough S, Johnson M, Banyon C, Pitz W, McNenly M. Experimental and modeling study of fuel interactions with an alkyl nitrate cetane enhancer, 2-ethyl-hexyl nitrate. Proc Combust Inst 2015;35:571–9.

[135] Aubert M. Etude physico-chimique de quatre combustibles liquides extraits d'un goudron primaire, obtenu à partir des déchets d'extraction des Mines domaniales françaises de la Sarre. Chal Ind 1925;6:373–9. doi:10.1016/j.proci.2014.06.048.

[136] Yang Z, Qian Y, Yang X, Wang Y, Wang Y, Huang Z, et al. Autoignition of n-Butanol/n-Heptane Blend Fuels in a Rapid Compression Machine under Low-to-Medium Temperature Ranges. Energy & Fuels 2013;27:7800–8. doi:10.1021/ef401774f.

[137] Werler M, Cancino LR, Schiessl R, Maas U, Schulz C, Fikri M. Ignition delay times of diethyl ether measured in a high-pressure shock tube and a rapid compression machine. Proc Combust Inst 2015;35:259–66. doi:http://dx.doi.org/10.1016/j.proci.2014.06.143.

[138] Kim H, Lim Y, Min K, Lee D. Investigation of autoignition of propane and n-butane blends using a rapid compression machine. KSME Int J 2002;16:1127–34. doi:10.1007/bf02984023.

[139] Tizard HT, Pye DR. Ignition of gases by sudden compression. Philos Mag Ser 7 1926;1:1094–105. doi:10.1080/14786442608633711.

[140] Griffiths JF, Jiao Q, Schreiber M, Meyer J, Knoche KF. Development of thermokinetic models for autoignition in a CFD Code: Experimental validation and application of the results to rapid compression studies. Symp Combust 1992;24:1809–15. doi:10.1016/S0082-0784(06)80212-2.

[141] Lee D, Hochgreb S. Rapid compression machines: Heat transfer and suppression of corner vortex. Combust Flame 1998;114:531–45. doi:10.1016/S0010-2180(97)00327-1.

[142] Chen K, Karim GA. An Examination of the Effects of Charge Inhomogeneity on the Compression Ignition of Fuel-Air Mixtures. SAE Tech Pap 982614 1998. doi:10.4271/982614.

[143] Frolov SM, Emans M, Ivanov VS, Basara B, Leshevich VV, Penyazkov OG. 3D simulation of hydrogen ignition in a rapid compression machine. J Loss Prev Process Ind 2013;26:1558–68. doi:10.1016/j.jlp.2013.08.013.

[144] Desgroux P, Gasnot L, Sochet LR. Instantaneous temperature measurement in a rapid-compression machine using laser Rayleigh scattering. Appl Phys B 1995;61:69–72. doi:10.1007/bf01090974.

[145] Desgroux P, Minetti R, Sochet LR. Temperature Distribution Induced by Pre-lgnition Reactions in a Rapid Compression Machine. Combust Sci Technol 1996;113:193–203. doi:10.1080/00102209608935494.

[146] Würmel J, Simmie JM. CFD studies of a twin-piston rapid compression machine. Combust Flame 2005;141:417–30. doi:10.1016/j.combustflame.2005.01.015.

[147] Mittal G, Sung C-J. A rapid compression machine for chemical kinetics studies at elevated pressures and temperatures. Combust Sci Technol 2007;179:497–530. doi:10.1080/00102200600671898.

[148] Mittal G, Sung C-J. Aerodynamics inside a rapid compression machine. Combust Flame 2006;145:160–80. doi:10.1016/j.combustflame.2005.10.019.

[149] Mittal G, Raju MP, Sung C-J. Vortex formation in a rapid compression machine: Influence of physical and operating parameters. Fuel 2012;94:409–17. doi:10.1016/j.fuel.2011.08.034.

[150] Yousefian S, Gauthier F, Morán-Guerrero A, Richardson RR, Curran HJ, Quinlan NJ, et al. Simplified Approach to the Prediction and Analysis of Temperature Inhomogeneity in Rapid Compression Machines. Energy & Fuels 2015;29:8216–25. doi:10.1021/ef501961s.

[151] Mittal G, Raju MP, Sung CJ. CFD modeling of two-stage ignition in a rapid compression machine: Assessment of zero-dimensional approach. Combust Flame 2010;157:1316–24. doi:10.1016/j.combustflame.2010.02.019.

[152] Goldsborough SS, Mittal G, Banyon C. Methodology to account for multi-stage ignition phenomena during simulations of RCM experiments. Proc Combust Inst 2013;34:685–93. doi:10.1016/j.proci.2012.05.094.

[153] Mittal G, Chomier M. Interpretation of experimental data from rapid compression machines without creviced pistons. Combust Flame 2014;161:75–83. doi:10.1016/j.combustflame.2013.08.020.

[154] Mittal G, Bhari A. A rapid compression machine with crevice containment. Combust Flame 2013. doi:10.1016/j.combustflame.2013.06.027.

[155] Allen C, Mittal G, Sung CJ, Toulson E, Lee T. An aerosol rapid compression machine for studying energetic-nanoparticle- enhanced combustion of liquid fuels. Proc Combust Inst 2011;33:3367–74. doi:10.1016/j.proci.2010.06.007.

[156] Davidson DF, Haylett DR, Hanson RK. Development of an aerosol shock tube for kinetic studies of low-vapor-pressure fuels. Combust Flame 2008;155:108–17. doi:10.1016/j.combustflame.2008.01.006.

[157] Haylett DR, Davidson DF, Hanson RK. Second-generation aerosol shock tube: an improved design. Shock Waves 2012;22:483–93. doi:10.1007/s00193-012-0383-x.

[158] Goldsborough SS, Johnson M V., Zhu GS, Aggarwal SK. Fuel and diluent property effects during wet compression of a fuel aerosol under RCM conditions. Fuel 2012;93:454–67. doi:10.1016/j.fuel.2011.06.027.

[159] Goldsborough SS, Johnson MV, Zhu GS, Aggarwal SK. Gas-phase saturation and evaporative cooling effects during wet compression of a fuel aerosol under RCM conditions. Combust Flame 2011;158:57–68. doi:10.1016/j.combustflame.2010.07.018.

[160] Allen C, Toulson E, Edwards T, Lee T. Application of a novel charge preparation approach to testing the autoignition characteristics of JP-8 and camelina hydroprocessed renewable jet fuel in a rapid compression machine. Combust Flame 2012;159:2780–8. doi:10.1016/j.combustflame.2012.03.019.

[161] Allen C, Valco D, Toulson E, Edwards T, Lee T. Ignition behavior and surrogate modeling of JP-8 and of camelina and tallow hydrotreated renewable jet fuels at low temperatures. Combust Flame 2013;160:232–9. doi:10.1016/j.combustflame.2012.10.008.

[162] Sjöberg M, Dec JE. Smoothing HCCI Heat-Release Rates Using Partial Fuel Stratification with Two-Stage Ignition Fuels. SAE Tech Pap 2006-01-0629 2006. doi:10.4271/2006-01-0629.

[163] Lim OT, Nakano H, Ilda N. The Research About the Effects of Thermal Stratification on n-Heptane/iso-Octane-Air Mixture HCCI Combustion Using a Rapid Compression Machine. SAE Tech Pap 2006-01-3319 2006:776–90.

[164] Nakano H, Lim OT, Iida N. An Investigation of the Effect of Thermal Stratification on HCCI Combustion by using Rapid Compression Machine. SAE Tech Pap 2007-01-1870 2007. doi:10.4271/2007-01-1870.

[165] Odajima R, Shirota D, Iida N. An investigation of the potential of EGR stratification for reducing pressure rise rate in HCCI combustion by using rapid compression machine. SAE Tech Pap 2011. doi:10.4271/2011-01-1762.

[166] Lim OT, Iida N. The investigation about the effects of thermal stratification in combustion chamber on HCCI combustion fueled with DME/n-Butane using Rapid Compression Machine. Exp Therm Fluid Sci 2012;39:123–33. doi:10.1016/j.expthermflusci.2012.01.016.

[167] Shirota D, Iida N. An Investigation of the Potential of Thermal and Mixing Stratifications for Reducing Pressure Rise Rate on HCCI Combustion by using Rapid Compression Machine. SAE Tech Pap 2009. doi:10.4271/2009-32-0089.

[168] Pöschl M, Sattelmayer T. Influence of temperature inhomogeneities on knocking combustion. Combust Flame 2008;153:562–73. doi:10.1016/j.combustflame.2007.11.009.

[169] Yoo CS, Luo Z, Lu T, Kim H, Chen JH. A DNS study of ignition characteristics of a lean iso-octane/air mixture under HCCI and SACI conditions. Proc Combust Inst 2013;34:2985–93. doi:10.1016/j.proci.2012.05.019.

[170] Ihme M. On the role of turbulence and compositional fluctuations in rapid compression machines: Autoignition of syngas mixtures. Combust Flame 2012;159:1592–604. doi:10.1016/j.combustflame.2011.11.022.

[171] Kojima S, Suzuoki T. Autoignition-delay measurement over lean to rich mixtures of n-butane/air under swirl conditions. Combustion and Flame. 1993;92(3):254-265. Combust Flame 1993;92:254–65. doi:10.1016/0010-2180(93)90037-4.

[172] Bradley D, Kalghatgi GT. Influence of autoignition delay time characteristics of different fuels on pressure waves and knock in reciprocating engines. Combust Flame 2009;156:2307–18. doi:10.1016/j.combustflame.2009.08.003.

[173] Amer A, Babiker H, Chang J, Kalghatgi G, Adomeit P, Brassat A, et al. Fuel Effects on Knock in a Highly Boosted Direct Injection Spark Ignition Engine. SAE Int J Fuels Lubr 2012;5:2012–01 – 1634. doi:10.4271/2012-01-1634.

[174] Poulos SG, Heywood JB. The Effect of Chamber Geometry on Spark-Ignition Engine Combustion. SAE Tech Pap 830334 1983. doi:10.4271/830334.

[175] Konig G, Sheppard CGW. End Gas Autoignition and Knock in a Spark Ignition Engine 1990. doi:10.4271/902135.

[176] ASTM International. ASTM D2699-16 Standard Test Method for Research Octane Number of Spark-Ignition Engine Fuel. West Conshohocken, PA: n.d. doi:https://doi.org/10.1520/D2699-16.

[177] ASTM International. ASTM D2700-16a Standard Test Method for Motor Octane Number of Spark-Ignition Engine Fuel. West Conshohocken, PA: 2016. doi:https://doi.org/10.1520/D2700-16A.

[178] Taylor CF, Taylor ES, Livengood JC, Russell WA, Leary WA. Ignition of Fuels by Rapid Compression. SAE 500178, 1950. doi:10.4271/500178.

[179] Griffiths JF, Nimmo W. Spontaneous ignition and engine knock under rapid compression. Combust Flame 1985;60:215–8. doi:10.1016/0010-2180(85)90009-4.

[180] Schreiber M, Sakak AS, Poppe C, Griffiths JF, Halford-Maw P, Rose DJ. Spatial Structure in End-Gas Autoignition. SAE Tech Pap 932758 1993. doi:10.4271/932758.

[181] Griffiths JF, Whitaker BJ. Thermokinetic interactions leading to knock during homogeneous charge compression ignition. Combust Flame 2002;131:386–99. doi:10.1016/S0010-2180(02)00417-0.

[182] Hayashi T, Taki M, Kojima S KT. Photographic observation of knock with a rapid compression and expansion machine. SAE Tech Pap 1984. doi:10.4271/841336.

[183] Katsumata M, Morikawa K, Tanabe M. Behavior of shock wave and pressure wave of SI knocking with super rapid compression machine. SAE Tech Pap 2011. doi:10.4271/2011-01-1875.

[184] Wang Z, Qi Y, He X, Wang J, Shuai S, Law CK. Analysis of pre-ignition to super-knock: Hotspot-induced deflagration to detonation. Fuel 2015;144:222–7. doi:10.1016/j.fuel.2014.12.061.

[185] Wang Z, Qi Y, Liu H, Zhang P, He X, Wang J. Shock wave reflection induced detonation (SWRID) under high pressure and temperature condition in closed cylinder. Shock Waves 2016;26:687–91. doi:10.1007/s00193-016-0677-5.

[186] Qi Y, Wang Z, Wang J, He X. Effects of thermodynamic conditions on the end gas combustion mode associated with engine knock. Combust Flame 2015;162:4119–28. doi:10.1016/j.combustflame.2015.08.016.

[187] Qi Y, He X, Wang Z, Wang J. Frequency domain analysis of knock images. Meas Sci Technol

2014;25:125001. doi:10.1088/0957-0233/25/12/125001.

[188] Tanoue K, Chado Y, Jimoto T, Nomura T, Shimada F, Hashimoto J. Effect of autoignition characteristics of fuels on knocking properties. Int J Engine Res 2015. doi:10.1177/1468087415601785.

[189] Tanaka K, Endo H, Imamichi A, Oda Y, Takeda Y, Shimada T. Study of Homogeneous Charge Compression Ignition Using a Rapid Compression Machine. SAE Tech Pap 2001. doi:10.4271/2001-01-1033.

[190] Ju Y, Sun W. Plasma assisted combustion: Dynamics and chemistry. Prog Energy Combust Sci 2015;48:21–83. doi:10.1016/j.pecs.2014.12.002.

[191] Stepanyan S, Vanhove G, Desgroux P, Starikovskaia S. Time-resolved electric field measurements in nanosecond surface dielectric discharge. Comparison of different polarities. Ignition of combustible mixtures by surface discharge in a rapid compression machine. 51st AIAA Aerosp. Sci. Meet. Incl. New Horizons Forum Aerosp. Expo., Reston, Virigina: American Institute of Aeronautics and Astronautics; 2013. doi:10.2514/6.2013-1053.

[192] Boumehdi MA, Stepanyan SA, Desgroux P, Vanhove G, Starikovskaia SM. Ignition of methane- and n-butane-containing mixtures at high pressures by pulsed nanosecond discharge. Combust Flame 2015;162:1336–49. doi:10.1016/j.combustflame.2014.11.006.

[193] Takahashi E, Kojima H, Furutani H. Control of pressure increase rate in compression ignition by pulsed plasma irradiation. Jpn J Appl Phys 2015;54:01AG03. doi:10.7567/JJAP.54.01AG03.

[194] Nayagam V, Dietrich DL, Ferkul P V., Hicks MC, Williams FA. Can cool flames support quasi-steady alkane droplet burning? Combust Flame 2012;159:3583–8. doi:10.1016/j.combustflame.2012.07.012.

[195] Kim H, Baek SW. Combustion of a single emulsion fuel droplet in a rapid compression machine. Energy 2016;106:422–30. doi:http://dx.doi.org/10.1016/j.energy.2016.03.006.

[196] Kim H, Baek SW, Chang D. A single n-heptane droplet behavior in rapid compression machine. Int J Heat Mass Transf 2014;69:247–55. doi:10.1016/j.ijheatmasstransfer.2013.10.028.

[197] Kim H, Baek SW, Chang D. Auto-Ignition Characteristics of Single n -Heptane Droplet in a Rapid Compression Machine. Combust Sci Technol 2014;186:912–27. doi:10.1080/00102202.2014.890598.

[198] Kim H, Baek SW, Han SH. Ignition of a Binary Component Fuel Droplet in a Rapid Compression Machine: Comparative Analysis. Combust Sci Technol 2015;187:659–77. doi:10.1080/00102202.2014.960563.

[199] Eckbreth AC. Laser Diagnostics for Combustion Temperature and Species. 2nd ed. Gordon and Breach; 1996.

[200] Linne MA. Spectroscopic Measurement: An Introduction to the Fundamentals. 2002.

[201] Rogers DR. Engine Combustion: Pressure Measurement and Analysis. SAE Book R-388. 2010-08-19; 2010.

[202] Rosseel E, Sierens R, Baert RSG. Evaluating piezo-electric transducer response to thermal shock from in-cylinder pressure data. SAE Tech Pap 1999-01-0935 1999. doi:10.4271/1999-01-0935.

[203] Ausserer JK, Rowton AK, Grinstead KD, Litke PJ, Polanka MD. Comparison of in-cylinder pressure measurement methods in a small spark ignition engine. SAE Tech Pap 2014-32-0007 2014. doi:10.4271/2014-32-0007.

[204] Mansfield AB, Wooldridge MS. High-pressure low-temperature ignition behavior of syngas mixtures. Combust Flame 2014;161:2242–51. doi:10.1016/j.combustflame.2014.03.001.

[205] Matekunas FA. Schlieren study of combustion in a rapid compression machine simulating the spark ignition engine. Proc Combust Inst 1979;17:1283–94. doi:10.1016/S0082-0784(79)80121-6.

[206] Solomon ASP. A photographic study of fuel spray ignition in a rapid compression machine. SAE Tech Pap 860065 1986. doi:10.4271/860065.

[207] Solomon ASP. Plasma jet ignition of fuel sprays in a rapid compression machine. SAE Tech Pap 880205 1988. doi:10.4271/880025.

[208] Yatsufusa T, Kawakami J, Kidoguchi Y, Khalid A, Fujita Y, Omae K. Effects of supercharging, swirl strength and fuel injection pressure on development and combustion of diesel spray. Trans Soc Automot Eng Japan 2009;40:755–61. doi:10.11351/jsaeronbun.40.755.

[209] Lee K, Tabuchi T, Tsukamoto T, Senda J, Fujimoto H. Clarification of knocking phenomena in flow field by means of rapid compression and expansion machine. SAE Tech Pap 948250 1994. doi:10.4271/948250.

[210] Kawai T, Hattori F, Tsukamoto T, Senda J, Fujimoto H. Knocking phenomena in a rapid compression and expansion machine. SAE Tech Pap 920064 1992. doi:10.4271/920064.

[211] Hayakawa A, Miki Y, Kobayashi S, Nagano Y KT. Effects of CO2 and N2 dilutions on laminar and turbulent flame propagation. SAE Tech Pap 2011. doi:10.4271/2011-01-1878.

[212] Griffiths JF, MacNamara JP, Mohamed C, Whitaker BJ, Pan J, Sheppard CG. Temperature fields during the development of autoignition in a rapid compression machine. Faraday Discuss 2001;119:287–303; discussion 353–70. doi:10.1039/b102002l.

[213] Walton S, He X, Zigler B, Wooldridge M, Atreya A. An experimental investigation of iso-octane ignition phenomena. Combust Flame 2007;150:246–62. doi:10.1016/j.combustflame.2006.07.016.

[214] Clarkson J, Griffiths JF, MacNamara JP, Whitaker BJ. Temperature fields during the development of combustion in a rapid compression machine. Combust Flame 2001;125:1162–75. doi:10.1016/S0010-2180(01)00236-X.

[215] Strozzi C, Mura A, Sotton J, Bellenoue M. Experimental analysis of propagation regimes during the autoignition of a fully premixed methane – air mixture in the presence of temperature inhomogeneities. Combust Flame 2012;159:3323–41. doi:10.1016/j.combustflame.2012.06.011.

[216] Nasir EF, Farooq A. Time-resolved temperature measurements in a rapid compression machine using quantum cascade laser absorption in the intrapulse mode. Proc Combust Inst n.d. doi:http://dx.doi.org/10.1016/j.proci.2016.07.010.

[217] Karwat DM, Wagnon SW, Teini PD, Wooldridge MS. On the chemical kinetics of n-Butanol: Ignition and speciation studies. J Phys Chem A 2011;115:4909–21. doi:10.1021/jp200905n.

[218] Martinengo A, Melczer J, Schlimme E. Analytical investigations of stable products during reaction of adiabatically compressed hydrocarbon air mixtures. Symp Combust 1965;10:323–30.

doi:10.1016/S0082-0784(65)80179-5.

[219] Roblee LHS. A technique for sampling reaction intermediates in a rapid compression machine. Combust Flame 1961;5:229–34. doi:10.1016/0010-2180(61)90101-8.

[220] Bertsch W. Multidimensional Gas Chromatography. In: Cortes HJ, editor. Multidimens. Chromatogr. Tech. Appl., New York and Basel: CRC Press; 1990, p. 75–144.

[221] Minetti R, Ribaucour M, Carlier M, Fittschen C, Sochet LR. Experimental and modeling study of oxidation and autoignition of butane at high pressure. Combust Flame 1994;96:201–11. doi:10.1016/0010-2180(94)90009-4.

[222] Minetti R, Carlier M, Ribaucour M, Therssen E, Sochet LR. Comparison of oxidation and autoignition of the two primary reference fuels by rapid compression. Proc Combust Inst 1996;26:747–53. doi:10.1016/S0082-0784(96)80283-9.

[223] Vanhove G, Minetti R, Touchard S, Fournet R, Glaude P a., Battin-Leclerc F. Experimental and modeling study of the autoignition of 1-hexene/isooctane mixtures at low temperatures. Combust Flame 2006;145:272–81. doi:10.1016/j.combustflame.2005.10.007.

[224] Crochet M, Minetti R, Ribaucour M, Vanhove G. A detailed experimental study of n-propylcyclohexane autoignition in lean conditions. Combust Flame 2010;157:2078–85. doi:10.1016/j.combustflame.2010.04.012.

[225] Roubaud A, Minetti R, Sochet L. High pressure auto-ignition and oxidation mechanisms of o-xylene, o-ethyltoluene, and n-butylbenzene between 600 and 900 K. Combust Flame 2000;123:561–71. doi:10.1016/S0010-2180(00)00174-7.

[226] Hadjali K, Crochet M, Vanhove G, Ribaucour M, Minetti R. A study of the low temperature autoignition of methyl esters. Proc Combust Inst 2009;32 I:239–46. doi:10.1016/j.proci.2008.09.002.

[227] Karwat DM, Wagnon SW, Wooldridge MS, Westbrook CK. Low-temperature speciation and chemical kinetic studies of n-heptane. Combust Flame 2013;160:2693–706. doi:10.1016/j.combustflame.2013.06.029.

[228] Karwat DM, Wagnon SW, Wooldridge MS, Westbrook CK. On the combustion chemistry of n-heptane and n-butanol blends. J Phys Chem A 2012;116:12406–21. doi:10.1021/jp309358h.

[229] He X, Walton SM, Zigler BT, Wooldridge MS, Atreya A. Experimental investigation of the intermediates of isooctane during ignition. Int J Chem Kinet 2007. doi:10.1002/kin.20254.

[230] Walton SM, Karwat DM, Teini PD, Gorny AM, Wooldridge MS. Speciation studies of methyl butanoate ignition. Fuel 2011;90:1796–804. doi:10.1016/j.fuel.2011.01.028.

[231] Walton SM, Wooldridge MS, Westbrook CK. An experimental investigation of structural effects on the auto-ignition properties of two C5 esters. Proc Combust Inst 2009;32 I:255–62. doi:10.1016/j.proci.2008.06.208.

[232] Wagnon SW, Karwat DM, Wooldridge MS, Westbrook CK. Experimental and Modeling Study of Methyl trans-3-Hexenoate Autoignition. Energy and Fuels 2014;28:7227–34. doi:10.1021/ef501806s.

[233] Ji W, Zhang P, He T, Wang Z, Tao L, He X, et al. Intermediate species measurement during iso-butanol auto-ignition. Combust Flame 2015;162:3541–53.

doi:http://dx.doi.org/10.1016/j.combustflame.2015.06.010.

[234] Van Blarigan P, Paradiso N, Goldsborough S. Homogeneous charge compression ignition with a Free Piston: A New Approach to ideal Otto cycle performance. SAE Tech Pap 982484 1998. doi:doi:10.4271/982484.

[235] Moreau RA, Sorenson SC, Hull WL. A technique for time resolved nitric oxide measurements in auto-igniting mixtures. Combust Flame 1975;25:197–205. doi:10.1016/0010-2180(75)90085-1.

[236] Das AK, Uddi M, Sung CJ, Kumar A, Uddi M, Sung CJ. Two-line thermometry and H2O measurement for reactive mixtures in rapid compression machine near 7.6μm. Combust Flame 2012;159:3493–501. doi:10.1016/j.combustflame.2012.06.020.

[237] Werblinski T, Kleindienst S, Engelbrecht R, Zigan L, Will S. Supercontinuum based absorption spectrometer for cycle-resolved multiparameter measurements in a rapid compression machine. Appl Opt 2016;55:4564–74. doi:10.1364/AO.55.004564.

[238] Furutani M, Ohta Y, Komatsu K. Onset Behavior of Low Temperature Flames Caused by Piston Compresssion. JSAE Rev 1993;14:12–7.

[239] Mansfield AB, Wooldridge MS, Di H, He X. Low-temperature ignition behavior of iso-octane. Fuel 2015. doi:10.1016/j.fuel.2014.08.019.

[240] Guibert P, Keromnes A, Legros G. An experimental investigation of the turbulence effect on the combustion propagation in a rapid compression machine. Flow, Turbul Combust 2010;84:79–95. doi:10.1007/s10494-009-9225-z.

[241] Hibi T, Kohata T, Tsumori Y, Namiki S, Shima K, Katsumata M, et al. Study on Knocking Intensity under In-Cylinder Flow Field in SI Engines Using a Rapid Compression Machine. J Therm Sci Technol 2013;8:460–75. doi:10.1299/jtst.8.460.

[242] Hasegawa T, Kinoshita M, Arima T, Sato K, Tanabe M. Characteristics of HCCI Combustion in Homogenized Temperature Fields using a Super Rapid Compression Machine. SAE Pap 2011:147–54. doi:10.4271/2011-01-1761.

[243] He X, Zigler BT, Walton SM, Wooldridge MS, Atreya A. A rapid compression facility study of OH time histories during iso-octane ignition. Combust Flame 2006;145:552–70. doi:10.1016/j.combustflame.2005.12.014.

[244] Uddi M, Das AK, Sung C-J. Temperature measurements in a rapid compression machine using mid-infrared H_2O absorption spectroscopy near 76 μm. Appl Opt 2012;51:5464. doi:10.1364/AO.51.005464.

[245] Kitsopanidis, I, Cheng W. Soot formation study in a rapid compression machine. J Eng Gas Turb Power 2006;128:942–9. doi:10.1115/1.2180279.

[246] Di Sante R. Laser extinction technique for measurements of carbon particles concentration during combustion. Opt Lasers Eng 2013;51:783–9. doi:10.1016/j.optlaseng.2013.01.019.

[247] Song Y, Hong J, Lee J. The turbulence measurement during the intake and compression process for high-turbulence generation around spark timing. Proc Inst Mech Eng Part D J Auto Eng 2001;215:493–501. doi:10.1243/0954407011528103.

[248] Zeldovich YB. Regime classification of an exothermic reaction with nonuniform initial conditions. Combust Flame 1980;39:211–4. doi:10.1016/0010-2180(80)90017-6.

[249] Gu XJ, Emerson DR, Bradley D. Modes of reaction front propagation from hot spots. Combust Flame 2003;133:63–74. doi:10.1016/S0010-2180(02)00541-2.

[250] Sankaran R, Im H, Hawkes E, Chen J. The effects of non-uniform temperature distribution on the ignition of a lean homogeneous hydrogen-air mixture. Proc Combust Inst 2005;30:875–82. doi:10.1016/j.proci.2004.08.176.

[251] Melton L, Lipp C. Criteria for quantitative PLIF experiments using high-power lasers. Expts Fluids 2003;35:310–6. doi:10.1007/s00348-003-0632-y.

[252] Meyer T, King G, Martin G, Lucht R, Schauer F, Dutton J. Accuracy and resolution issues in NO/acetone PLIF measurements of gas-phase molecular mixing. Expts Fluids 2002;32:603–11. doi:10.1007/s00348-001-0372-9.

[253] Böhm B, Heeger C, Gordon RL, Dreizler A. New perspectives on turbulent combustion: multi-parameter high-speed planar laser diagnostics. Flow Turb Combust 2011;86:313–41. doi:10.1007/s10494-010-9291-2.

[254] Schulz C, Sick V. Tracer-LIF diagnostics: quantitative measurement of fuel concentration, temperature and fuel/air ratio in practical combustion systems. Prog Energy Combust Sci 2005;31:75–121. doi:10.1016/j.pecs.2004.08.002.

[255] Sick V. High speed imaging in fundamental and applied combustion research. Proc Combust Inst 2013;34:3509–30. doi:10.1016/j.proci.2012.08.012.

[256] Egolfopoulos FN, Hansen N, Ju Y, Kohse-Höinghaus K, Law CK, Qi F. Advances and challenges in laminar flame experiments and implications for combustion chemistry. Prog Energy Combust Sci 2014;43:36–67. doi:10.1016/j.pecs.2014.04.004.

[257] Grogan KP, Goldsborough SS, Ihme M. Ignition regimes in rapid compression machines. Combust Flame 2015;162:3071–80. doi:10.1016/j.combustflame.2015.03.020.

[258] Gonçalves de Azevedo F, Griffiths JF, Cardoso SSS. Effects of kinetic and transport phenomena on thermal explosion and oscillatory behaviour in a spherical reactor with mixed convection. Phys Chem Chem Phys 2014;16:23365–78. doi:10.1039/C4CP02990A.

[259] Ju Y. Recent progresses in fundamental combustion research. Adv Mech 2014;201402:1–72. doi:10.6052/1000-0992-14-011.

[260] Weber BW, Sung C-J. Comparative autoignition trends in the butanol isomers at elevated pressure. Energy & Fuels 2013;27:1688–98. doi:10.1021/ef302195c.

[261] Lodier G, Merlin C, Domingo P, Vervisch L, Ravet F. Self-ignition scenarios after rapid compression of a turbulent mixture weakly-stratified in temperature. Combust Flame 2012;159:3358–71. doi:http://dx.doi.org/10.1016/j.combustflame.2012.07.006.

[262] Halstead MP, Kirsch LJ, Prothero A, Quinn CP. A Mathematical Model for Hydrocarbon Autoignition at High Pressures. Proc R Soc A Math Phys Eng Sci 1975;346:515–38. doi:10.1098/rspa.1975.0189.

[263] Halstead MP, Kirsch LJ, Quinn CP. The Autoignition of Hydrocarbon Fuels at High Tempertures and Pressures - Fitting of a Mathematical Model. Combust Flame 1977;30:45–60. doi:10.1016/0010-2180(77)90050-5.

[264] Cox R, Cole J. Chemical Aspects of the Autoignition of Hydrocarbon-Air Mixtures. Combust Flame

1985;60. doi:10.1016/0010-2180(85)90001-X.

[265] Cavanagh J, Cox R. Computer Modeling of Cool Flames and Ignition of Acetaldehyde. Combust Flame 1990;82:15–39. doi:10.1016/0010-2180(90)90075-3.

[266] Westbrook CK, Pitz WJ, Boercker JE, Curran HJ, Griffiths JF, Mohamed C, et al. Detailed chemical kinetic reaction mechanisms for autoignition of isomers of heptane under rapid compression. Proc Combust Inst 2002;29:1311–8. doi:10.1016/S1540-7489(02)80161-4.

[267] Griffiths J, Jiao Q, Kordylewski W, Schreiber M, Meyer J, Knoche K. Experimental and numerical studies of di-tertiary butyl peroxide combustion at high pressures in a rapid compression machine. Combust Flame 1993;93:303–15.

[268] Mittal G, Raju MP, Sung CJ. Computational fluid dynamics modeling of hydrogen ignition in a rapid compression machine. Combust Flame 2008;155:417–28. doi:10.1016/j.combustflame.2008.06.006.

[269] Hu H, Keck J. Autoignition of Adiabatically Compressed Combustible Gas Mixtures. SAE 872110, 1987. doi:10.4271/872110.

[270] Park P, Keck J. Ignition Delays for Iso-octane: Measurement using a Rapid Compression Machine and Prediction using a Reduced Kinetic Model. SAE 912553, 1991. doi:10.4271/912553.

[271] He X, Donovan MT, Zigler BT, Palmer TR, Walton SM, Wooldridge MS, et al. An experimental and modeling study of iso-octane ignition delay times under homogeneous charge compression ignition conditions. Combust Flame 2005;142:266–75. doi:10.1016/j.combustflame.2005.02.014.

[272] Walton SM, He X, Zigler BT, Wooldridge MS. An experimental investigation of the ignition properties of hydrogen and carbon monoxide mixtures for syngas turbine applications. Proc Combust Inst 2007;31:3147–54. doi:10.1016/j.proci.2006.08.059.

[273] Mohamed C. Suppression of reaction during rapid compression and its effect on ignition delay. Combust Flame 1998;112:438–44. doi:10.1016/S0010-2180(97)00135-1.

[274] Curran HJ, Gaffuri P, Pitz WJ, Westbrook CK. A Comprehensive Modeling Study of n-Heptane Oxidation. Combust Flame 1998;114:149–77. doi:DOI: 10.1016/S0010-2180(97)00282-4.

[275] Mittal G, Chaos M, Sung CJ, Dryer FL. Dimethyl ether autoignition in a rapid compression machine: Experiments and chemical kinetic modeling. Fuel Process Technol 2008;89:1244–54. doi:10.1016/j.fuproc.2008.05.021.

[276] Tanaka S, Ayala F, Keck JC. A reduced chemical kinetic model for HCCI combustion of primary reference fuels in a rapid compression machine. Combust Flame 2003;133:467–81. doi:10.1016/S0010-2180(03)00057-9.

[277] Gallagher SM, Curran HJ, Metcalfe WK, Healy D, Simmie JM, Bourque G. A rapid compression machine study of the oxidation of propane in the negative temperature coefficient regime. Combust Flame 2008;153:316–33. doi:10.1016/j.combustflame.2007.09.004.

[278] Healy D, Kalitan DM, Aul CJ, Petersen EL, Bourque G, Curran HJ. Oxidation of C1-C5 alkane quinternary natural gas mixtures at high pressures. Energy and Fuels 2010;24:1521–8. doi:10.1021/ef9011005.

[279] Würmel J, Silke EJ, Curran HJ, Ó Conaire MS, Simmie JM. The effect of diluent gases on ignition delay times in the shock tube and in the rapid compression machine. Combust Flame

2007;151:289–302. doi:10.1016/j.combustflame.2007.06.010.

[280] Goldsborough SS, Banyon C, Mittal G. A computationally efficient, physics-based model for simulating heat loss during compression and the delay period in RCM experiments. Combust Flame 2012;159:3476–92. doi:10.1016/j.combustflame.2012.07.010.

[281] Sjöberg M, Dec JE, Cernansky NP. Potential of Thermal Stratification and Combustion Retard for Reducing Pressure-Rise Rates in HCCI Engines, Based on Multi-Zone Modeling and Experiments. SAE 2005-01-0113, 2005. doi:10.4271/2005-01-0113.

[282] Kodavasal J, Keum S, Babajimopoulos A. An extended multi-zone combustion model for PCI simulation. Combust Theory Model 2011;15:893–910. doi:10.1080/13647830.2011.578663.

[283] Wilson D, Allen C. Application of a multi-zone model for the prediction of species concentrations in rapid compression machine experiments. Combust Flame 2016;171:185–97. doi:http://dx.doi.org/10.1016/j.combustflame.2016.05.018.

[284] Woschni G. A Universally Applicable Equation for the Instantaneous Heat Transfer Coefficient in the Internal Combustion Engine. SAE Tech Pap 670931 1967. doi:10.4271/670931.

[285] Healy D, Donato NS, Aul CJ, Petersen EL, Zinner CM, Bourque G, et al. n-Butane: Ignition delay measurements at high pressure and detailed chemical kinetic simulations. Combust Flame 2010;157:1526–39. doi:10.1016/j.combustflame.2010.01.016.

[286] Fridlyand A, Johnson MS, Goldsborough SS, West RH, McNenly MJ, Mehl M, et al. The role of correlations in uncertainty quantification of transportation relevant fuel models. Combust Flame n.d. doi:http://dx.doi.org/10.1016/j.combustflame.2016.10.014.

[287] Petersen E, Davidson D, Hanson R. Kinetics modeling of shock-induced ignition in low-dilution CH4/O2 mixtures at high pressures and intermediate temperatures. Combust Flame 1999;117:272−290. doi:10.1016/S0010-2180(98)00111-4.

[288] Petersen EL, Kalitan DM, Barrett AB, Reehal SC, Mertens JD, Beerer DJ, et al. New syngas/air ignition data at lower temperature and elevated pressure and comparison to current kinetics models. Combust Flame 2007;149:244–7. doi:10.1016/j.combustflame.2006.12.007.

[289] Leone TG, Anderson JE, Davis RS, Iqbal A, Reese RA, Shelby MH, et al. The Effect of Compression Ratio, Fuel Octane Rating, and Ethanol Content on Spark-Ignition Engine Efficiency. Environ Sci Technol 2015;49:10778–89. doi:10.1021/acs.est.5b01420.

[290] Sankaran R, Im HG, Hawkes ER, Chen JH. The effects of non-uniform temperature distribution on the ignition of a lean homogeneous hydrogen–air mixture. Proc Combust Inst 2005;30:875–82. doi:10.1016/j.proci.2004.08.176.

[291] Ben Houidi M, Sotton J, Bellenoue M. Interpretation of auto-ignition delays from RCM in the presence of temperature heterogeneities: Impact on combustion regimes and negative temperature coefficient behavior. Fuel 2016;186:476–95. doi:http://dx.doi.org/10.1016/j.fuel.2016.08.089.

[292] Pal P, Mansfield AB, Arias PG, Wooldridge MS, Im HG. A computational study of syngas auto-ignition characteristics at high-pressure and low-temperature conditions with thermal inhomogeneities. Combust Theory Model 2015;19:587–601. doi:10.1080/13647830.2015.1068373.

[293] Teichmann H. Die Selbstentzundung von Kohlenwasserstoff-Luftgemischen und das Klopfen im Otto-Motor. Zeitschrift Für Elektrochemie 1941;47:297–307. doi:10.1002/bbpc.19410470404.

[294] Haskell WW. Fuel Ignition in a Rapid Compression Machine: Sensitivity to Flame Ignition by Particles. SAE Tech. Pap. 700059, 1970. doi:10.4271/700059.

[295] Saytzev SG, Soloukhin RI. Study of combustion of an adiabatically-heated gas mixture. Symp Combust 1961;8:344–7. doi:10.1016/S0082-0784(06)80522-9.

[296] Voevodsky V, Soloukhin R. On the mechanism and explosion limits of hydrogen-oxygen chain self-ignition in shock waves. Proc Combust Inst 1965;10:279–83.

[297] Meyer JW, Oppenheim AK. On the shock-induced ignition of explosive gases. Symp Combust 1971;13:1153–64. doi:10.1016/S0082-0784(71)80112-1.

[298] Cheng RK, Oppenheim AK. Autoignition in methane/hydrogen mixtures. Combust Flame 1984;58:125–39. doi:10.1016/0010-2180(84)90088-9.

[299] Vermeer DJ, Meyer JW, Oppenheim AK. Auto-Ignition of Hydrocarbons behind Reflected Shock Waves. Combust Flame 1972;18:327–36. doi:10.1016/S0010-2180(72)80183-4.

[300] Ciezki HK, Adomeit G. Shock-tube investigation of self-ignition of n-heptane-air mixtures under engine relevant conditions. Combust Flame 1993;93:421–33. doi:10.1016/0010-2180(93)90142-P.

[301] Blumenthal R, Fieweger K, Komp KH, Adomeit G. Gas Dynamic Features of Self Ignition of Non Diluted Fuel/Air Mixtures at High Pressure. Combust Sci Technol 1996;113:137–66. doi:10.1080/00102209608935491.

[302] Pfahl U, Fieweger K, Adomeit G. Self-ignition of diesel-relevant hydrocarbon-air mixtures under engine conditions. Symp Combust 1996;26:781–9. doi:10.1016/S0082-0784(96)80287-6.

[303] Fieweger K, Blumenthal R, Adomeit G. Shock-tube investigations on the self-ignition of hydrocarbon-air mixtures at high pressures. Symp Combust 1994;25:1579–85. doi:10.1016/S0082-0784(06)80803-9.

[304] Fieweger K, Blumenthal R, Adomeit G. Self-ignition of S.I. engine model fuels: A shock tube investigation at high pressure. Combust Flame 1997;109:599–619. doi:10.1016/S0010-2180(97)00049-7.

[305] Chaos M, Dryer FL. Syngas Combustion Kinetics and Applications. Combust Sci Technol 2008;180:1053–96. doi:10.1080/00102200801963011.

[306] Li H, Owens ZC, Davidson DF, Hanson RK. A simple reactive gasdynamic model for the computation of gas temperature and species concentrations behind reflected shock waves. Int J Chem Kinet 2008;40:189–98. doi:10.1002/kin.20305.

[307] Hanson RK, Pang GA, Chakraborty S, Ren W, Wang S, Davidson DF. Constrained reaction volume approach for studying chemical kinetics behind reflected shock waves. Combust Flame 2013;160:1550–8. doi:10.1016/j.combustflame.2013.03.026.

[308] Wang BL, Olivier H, Grönig H. Ignition of shock-heated H2-air-steam mixtures. Combust Flame 2003;133:93–106. doi:10.1016/S0010-2180(02)00552-7.

[309] Huang J, Hill PG, Bushe WK, Munshi SR. Shock-tube study of methane ignition under engine-

relevant conditions: experiments and modeling. Combust Flame 2004;136:25–42. doi:10.1016/j.combustflame.2003.09.002.

[310] Medvedev SP, Gelfand BE, Khomik SV, Agafonov GL. Compression ignition of hydrogen-containing mixtures in shock tubes. J Eng Phys Thermophys 2010;83:1170–7. doi:10.1007/s10891-010-0440-1.

[311] Uygun Y, Ishihara S, Olivier H. A high pressure ignition delay time study of 2-methylfuran and tetrahydrofuran in shock tubes. Combust Flame 2014;161:2519–30. doi:10.1016/j.combustflame.2014.04.004.

[312] Ihme M, Sun Y, Deiterding R. Detailed Simulations of Shock-Bifurcation and Ignition of an Argon-diluted Hydrogen/Oxygen Mixture in a Shock Tube. 51st AIAA Aerosp. Sci. Meet. Incl. New Horizons Forum Aerosp. Expo., Reston, Virigina: American Institute of Aeronautics and Astronautics; 2013. doi:10.2514/6.2013-538.

[313] Yamashita H, Kasahara J, Sugiyama Y, Matsuo A. Visualization study of ignition modes behind bifurcated-reflected shock waves. Combust Flame 2012;159:2954–66. doi:10.1016/j.combustflame.2012.05.009.

[314] Grogan KP, Ihme M. Regimes describing shock boundary layer interaction and ignition in shock tubes. Proc Combust Inst 2017;36:2927–35. doi:http://dx.doi.org/10.1016/j.proci.2016.06.078.

[315] Assanis D, Wagnon SW, Wooldridge MS. An experimental study of flame and autoignition interactions of iso-octane and air mixtures. Combust Flame 2015;162:1214–24. doi:10.1016/j.combustflame.2014.10.012.

[316] Mansfield AB, Wooldridge MS, Di H, He X. Low-temperature ignition behavior of iso-octane. Fuel 2015;139:79–86. doi:10.1016/j.fuel.2014.08.019.

[317] Kalitan DM, Mertens JD, Crofton MW, Petersen EL. Ignition and Oxidation of Lean CO/H2 Fuel Blends in Air. J Propuls Power 2007;23:1291–301. doi:10.2514/1.28123.

[318] Li J, Zhao Z, Kazakov A, Chaos M, Dryer FL, Scire JJ. A comprehensive kinetic mechanism for CO, CH2O, and CH3OH combustion. Int J Chem Kinet 2007;39:109–36. doi:10.1002/kin.20218.

[319] Im HG, Pal P, Wooldridge MS, Mansfield AB. A Regime Diagram for Autoignition of Homogeneous Reactant Mixtures with Turbulent Velocity and Temperature Fluctuations. Combust Sci Technol 2015;187:1263–75. doi:10.1080/00102202.2015.1034355.

[320] Pal P, Im HG, Wooldridge MS, Mansfield AB. Auto-ignition phenomena in thermally inhomogeneous turbulent reacting flows: Numerical validation of a regime diagram. ASPACC 2015 - 10th Asia-Pacific Conf. Combust. 2015, ASPACC 2015 - 10th Asia-Pacific Conf. Combust., 2015.

[321] Lee JH, Knystautas R, Yoshikawa N. Photochemical initiation of gaseous detonations. Acta Astronaut 1978;5:971–82. doi:10.1016/0094-5765(78)90003-6.

[322] Bradley D. Autoignitions and detonations in engines and ducts. Philos Trans R Soc A Math Phys Eng Sci 2012;370:689–714. doi:10.1098/rsta.2011.0367.

[323] Borg JM, Saikalis G, Oho S, Cheok KC. Knock Signal Analysis Using the Discrete Wavelet Transform. SAE Tech Pap 2006-01-0226 2006. doi:10.4271/2006-01-0226.

[324] Battin-Leclerc F. Detailed chemical kinetic models for the low-temperature combustion of

hydrocarbons with application to gasoline and diesel fuel surrogates. Prog Energy Combust Sci 2008;34:440–98. doi:10.1016/j.pecs.2007.10.002.

[325] Zádor J, Taatjes CA, Fernandes RX. Kinetics of elementary reactions in low-temperature autoignition chemistry. Prog Energy Combust Sci 2011;37:371–421. doi:10.1016/j.pecs.2010.06.006.

[326] Sarathy SM, Oßwald P, Hansen N, Kohse-Höinghaus K. Alcohol combustion chemistry. Prog Energy Combust Sci 2014;44:40–102. doi:10.1016/j.pecs.2014.04.003.

[327] Ohta, Y., Furutani H. Identification of Cool and Blue Flames in Compression Ignition. Arch Combust 1991;11:43–52.

[328] Dahms RN, Paczko GA, Skeen SA, Pickett LM. Understanding the ignition mechanism of high-pressure spray flames. Proc Combust Inst 2017;36:2615–23. doi:http://dx.doi.org/10.1016/j.proci.2016.08.023.

[329] Anders H, Christensen M, Johansson B, Franke A, Richter M, Aldén M. A Study of the Homogeneous Charge Compression Ignition Combustion Process by Chemiluminescence Imaging. SAE Tech Pap 1999-01-3680 1999. doi:10.4271/1999-01-3680.

[330] Reuter CB, Won SH, Ju Y. Experimental study of the dynamics and structure of self-sustaining premixed cool flames using a counterflow burner. Combust Flame 2016;166:125–32. doi:http://dx.doi.org/10.1016/j.combustflame.2016.01.008.

[331] Yamamoto A, Oshibe H, Nakamura H, Tezuka T, Hasegawa S, Maruta K. Stabilized three-stage oxidation of gaseous n-heptane/air mixture in a micro flow reactor with a controlled temperature profile. Proc Combust Inst 2011;33:3259–66. doi:10.1016/j.proci.2010.05.004.

[332] Murase E, Hanada K, Miyaura T, Ikeda J. Photographic Observation and Emission Spectral Analysis of Homogeneous Charge Compression Ignition Combustion. Combust Sci Technol 2005;177:1699–723. doi:10.1080/00102200590959242.

[333] Ju Y. On the propagation limits and speeds of premixed cool flames at elevated pressures. Combust Flame 2017;178:61–9. doi:http://dx.doi.org/10.1016/j.combustflame.2017.01.006.

[334] Vuilleumier D, Kozarac D, Mehl M, Saxena S, Pitz WJ, Dibble RW, et al. Intermediate temperature heat release in an HCCI engine fueled by ethanol/n-heptane mixtures: An experimental and modeling study. Combust Flame 2014;161:680–95. doi:10.1016/j.combustflame.2013.10.008.

[335] Lee D, Hochgreb S. Hydrogen Autoignition at Pressures above the (0 . 6 – 4 . 0 MPa) 1998.

[336] Gersen S, Anikin N, Mokhov A, Levinsky H. Ignition properties of methane/hydrogen mixtures in a rapid compression machine. Int J Hydrogen Energy 2008;33:1957–64. doi:10.1016/j.ijhydene.2008.01.017.

[337] Mansfield AB, Wooldridge MS. The effect of impurities on syngas combustion. Combust Flame 2015;162:2286–95. doi:10.1016/j.combustflame.2015.01.026.

[338] Gersen S, Darmeveil H, Levinsky H. The effects of CO addition on the autoignition of H2, CH4 and CH4/H2 fuels at high pressure in an RCM. Combust Flame 2012;159:3472–5. doi:10.1016/j.combustflame.2012.06.021.

[339] Kéromnès A, Metcalfe WK, Heufer K a., Donohoe N, Das AK, Sung C-J, et al. An experimental and detailed chemical kinetic modeling study of hydrogen and syngas mixture oxidation at elevated

pressures. Combust Flame 2013;160:995–1011. doi:10.1016/j.combustflame.2013.01.001.

[340] Mittal G, Sung C, Yetter R. Autoignition of H2/CO at elevated pressures in a rapid compression machine. Int J Chem Kinet 2006;38:516–29. doi:10.1002/kin.20180.

[341] Mittal G, Sung CJ, Fairweather M, Tomlin AS, Griffiths JF, Hughes KJ. Significance of the HO2+CO reaction during the combustion of CO+H2 mixtures at high pressures. Proc Combust Inst 2007;31:419–27. doi:10.1016/j.proci.2006.07.068.

[342] Burke MP, Chaos M, Ju Y, Dryer FL, Klippenstein SJ. Comprehensive H2/O2 kinetic model for high-pressure combustion. Int J Chem Kinet 2012;44:444–74. doi:10.1002/kin.20603.

[343] Gray P, Sherrington ME. Explosive oxidation of hydrogen sulphide: self-heating, chain-branching and chain-thermal contributions to spontaneous ignition. J Chem Soc Faraday Trans 1 Phys Chem Condens Phases 1974;70:2338–50. doi:10.1039/F19747002338.

[344] Das AK, Sung C-J, Zhang Y, Mittal G. Ignition delay study of moist hydrogen/oxidizer mixtures using a rapid compression machine. Int J Hydrogen Energy 2012;37:6901–11. doi:10.1016/j.ijhydene.2012.01.111.

[345] Davis SG, Joshi A V., Wang H, Egolfopoulos F. An optimized kinetic model of H2/CO combustion. Proc Combust Inst 2005;30:1283–92. doi:10.1016/j.proci.2004.08.252.

[346] Hong Z, Davidson DF, Barbour EA, Hanson RK. A new shock tube study of the H+O2→OH+O reaction rate using tunable diode laser absorption of H2O near 2.5μm. Proc Combust Inst 2011;33:309–16. doi:10.1016/j.proci.2010.05.101.

[347] Donohoe N, Heufer KA, Aul CJ, Petersen EL, Bourque G, Gordon R, et al. Influence of steam dilution on the ignition of hydrogen, syngas and natural gas blends at elevated pressures. Combust Flame 2015;162:1126–35. doi:10.1016/j.combustflame.2014.10.005.

[348] Petersen E, Kalitan D, Rickard M. Reflected Shock Ignition of SiH4/H2/O2/Ar and SiH4/CH4/O2/Ar Mixtures. J Propuls Power 2004;20:665–74. doi:10.2514/1.11380.

[349] McLain A, Jachimowski C, Rogers R. Ignition of SiH4-H2-O2-N2 behind reflected shock waves. NASA Tech Pap 2114 1983.

[350] Furutani M, Isogai T, Ohta Y. Ignition Characteristics of Gaseous Fuels and Their Difference Elimination for SI and HCCI Gas Engines. SAE Tech Pap 2003-01-1857 2003. doi:10.4271/2003-01-1857.

[351] Burke U, Somers KP, O'Toole P, Zinner CM, Marquet N, Bourque G, et al. An ignition delay and kinetic modeling study of methane, dimethyl ether, and their mixtures at high pressures. Combust Flame 2015;162:315–30. doi:10.1016/j.combustflame.2014.08.014.

[352] Yu Y, Vanhove G, Griffiths JF, De Ferrieìres S, Pauwels JF. Influence of EGR and syngas components on the autoignition of natural gas in a rapid compression machine: A detailed experimental study. Energy and Fuels 2013;27:3988–96. doi:10.1021/ef400336x.

[353] Donohoe N, Heufer A, Metcalfe W, Curran H, Davis M, Mathieu O, et al. Ignition delay times, laminar flame speeds, and mechanism validation for natural gas/hydrogen blends at elevated pressures. Combust Flame 2014;161:1432–43. doi:10.1016/j.combustflame.2013.12.005.

[354] Heyne S, Roubaud A, Ribaucour M, Vanhove G, Minetti R, Favrat D. Development of a natural gas reaction mechanism for engine simulations based on rapid compression machine experiments

using a multi-objective optimisation strategy. Fuel 2008;87:3046–54. doi:10.1016/j.fuel.2008.04.004.

[355] Healy D, Curran HJ, Dooley S, Simmie J, Kalitan D, Petersen E, et al. Methane/propane mixture oxidation at high pressures and at high, intermediate and low temperatures. Combust Flame 2008;155:441–8. doi:10.1016/j.combustflame.2008.07.003.

[356] Healy D, Kopp MM, Polley NL, Petersen EL, Bourque G, Curran HJ. Methane/n-Butane Ignition Delay Measurements at High Pressure and Detailed Chemical Kinetic Simulations. Energy & Fuels 2010;24:1617–27. doi:10.1021/ef901292j.

[357] Healy D. Experimental and modelling studies of natural gas mixtures in a rapid compression machine. National University of Ireland Galway, 2009.

[358] Bourque G, Healy D, Curran H, Zinner C, Kalitan D, de Vries J, et al. Ignition and flame speed kinetics of two natural gas blends with high levels of heavier hydrocarbons. J Eng Gas Turbines Power 2010;132:021504.

[359] Gersen S, Mokhov A V., Darmeveil JH, Levinsky HB, Glarborg P. Ignition-promoting effect of NO2 on methane, ethane and methane/ethane mixtures in a rapid compression machine. Proc Combust Inst 2011;33:433–40. doi:10.1016/j.proci.2010.05.097.

[360] Petersen E, Kalitan D, Simmons S, Bourque G, Curran H, Simmie J. Methane/propane oxidation at high pressures: experimental and detailed chemical kinetic modeling. Proc Combust Inst 2007;31:447–54. doi:10.1016/j.proci.2006.08.034.

[361] Frenklach M, Wang H, Yu C-L, Goldenberg M, Bowman C, Hanson R, et al. GRI 3.0: available at http://www.me.berkeley.edu/gri_mech/ n.d.

[362] Wang H, You X, Joshi A, Davis S, Laskin A, Egolfopoulos F, et al. USC mechanism available at http://ignis.usc.edu/USC_Mech_II.htm. n.d.

[363] Metcalfe W, Burke S, Ahmed S, Curran H. A hierarchical and comparative kinetic modeling study of C1–C2 hydrocarbon and oxygenated fuels. Int J Chem Kinet 2013;45:638–75. doi:10.1002/kin.20802.

[364] Dames EE, Rosen AS, Weber BW, Gao CW, Sung C-J, Green WH. A detailed combined experimental and theoretical study on dimethyl ether/propane blended oxidation. Combust Flame 2016;168:310–30. doi:http://dx.doi.org/10.1016/j.combustflame.2016.02.021.

[365] Carlier M, Corre C, Minetti R, Pauwels J-F, Ribaucour M, Sochet L-R. Autoignition of butane: A burner and a rapid compression machine study. Proc Combust Inst 1990;23:1753–8. doi:10.1016/S0082-0784(06)80453-4.

[366] Gersen S, Mokhov A V., Darmeveil JH, Levinsky HB. Ignition properties of n-butane and iso-butane in a rapid compression machine. Combust Flame 2010;157:240–5. doi:10.1016/j.combustflame.2009.10.012.

[367] Healy D, Donato NS, Aul CJ, Petersen EL, Zinner CM, Bourque G, et al. Isobutane ignition delay time measurements at high pressure and detailed chemical kinetic simulations. Combust Flame 2010;157:1540–51. doi:10.1016/j.combustflame.2010.01.011.

[368] Griffiths JF, Halford-Maw PA, Mohamed C. Spontaneous ignition delays as a diagnostic of the propensity of alkanes to cause engine knock. Combust Flame 1997;111:327–37.

doi:10.1016/S0010-2180(97)00004-7.

[369] Westbrook CK, Curran HJ, Pitz WJ, Griffiths JF, Mohamed C, Wo SK. The effects of pressure, temperature, and concentration on the reactivity of alkanes: Experiments and modeling in a rapid compression machine. Symp Combust 1998;27:371–8. doi:10.1016/S0082-0784(98)80425-6.

[370] Ribaucour M, Minetti R, Sochet LR. Autoignition of n-pentane and 1-pentene: Experimental data and kinetic modeling. Symp Combust 1998;27:345–51. doi:10.1016/S0082-0784(98)80422-0.

[371] Ribaucour M, Minetti R, Sochet LR, Curran HJ, Pitz WJ, Westbrook CK. Ignition of isomers of pentane: An experimental and kinetic modeling study. Proc Combust Inst 2000;28:1671–8. doi:10.1016/S0082-0784(00)80566-4.

[372] Bugler J, Somers KP, Silke E, Curran H. Revisiting the kinetics and thermodynamics of the low-temperature oxidation pathways of alkanes: A case study of the three pentane isomers. J Phys Chem A 2015;119:7510–27.

[373] Bugler J, Marks B, Mathieu O, Archuleta R, Camou A, Grégoire C, et al. An ignition delay time and chemical kinetic modeling study of the pentane isomers. Combust Flame 2015;163:138–56. doi:10.1016/j.combustflame.2015.09.014.

[374] Zhang K, Banyon C, Togbé C, Dagaut P, Bugler J, Curran H. An experimental and kinetic modeling study of n-hexane oxidation. Combust Flame 2015;162:4194–207. doi:doi:10.1016/j.combustflame.2015.08.001.

[375] Cadman P, Thomas G, Butler P. The auto-ignition of propane at intermediate and high pressures. Phys Chem Chem Phys 2000;2:5411–9. doi:10.1039/B003665J.

[376] Herzler J, Jerig L, Roth P. Shock-tube study of the ignition of propane at intermediate temperatures and high pressures. Comb Sci Tech 2004;176:1627–37. doi:10.1080/00102200490487201.

[377] Herzler J, Jerig L, Roth P, Schulz C. Shock tube study of the ignition of propane at intermediate temperatures and high pressures. Proc Euro Combust Mtg, 2005, p. 195.

[378] Pang G, Davidson D, Hanson R. Experimental study and modeling of shock tube ignition delay times for hydrogen-oxygen-argon mixtures at low temperatures. Proc Combust Inst 2009;32:181–8. doi:10.1016/j.proci.2008.06.014.

[379] Petersen E, Lamnaouer M, de Vries J, Curran H, Simmie J, Fikri M, et al. Discrepancies between shock tube and rapid compression machine ignition at low temperatures and high pressures. Shock Waves 2009:739–44. doi:10.1007/978-3-540-85168-4_119.

[380] Goldsmith CF, Green WH, Klippenstein SJ. Role of O2 + QOOH in Low-Temperature Ignition of Propane. 1. Temperature and Pressure Dependent Rate Coefficients. J Phys Chem A 2012;116:3325–46. doi:10.1021/jp210722w.

[381] Pitz W, Wilk R, Westbrook C, Cernansky N. The oxidation of n-butane at low and intermediate temperatures: an experimental and modeling study. 1998.

[382] Wilk R, Green R, Pitz W, Westbrook C, Addagarla S, Miller D, et al. An experimental and kinetic modeling study of the combustion of n-butane and iso-butane in an internal combustion engine. SAE Tech Pap 1990;Paper SAE-. doi:10.4271/900028.

[383] Hébrard É, Tomlin AS, Bounaceur R, Battin-Leclerc F. Determining predictive uncertainties and global sensitivities for large parameter systems: A case study for n-butane oxidation. Proc Combust Inst 2015;35:607–16. doi:10.1016/j.proci.2014.06.027.

[384] Kojima S. Detailed modelling of n-butane autoignition chemistry. Combust Flame 1994;99:87–136. doi:10.1016/0010-2180(94)90084-1.

[385] Ranzi E, Faravelli T, Gaffuri P, Pennati G, Sogaro A. A wide range modelling study of propane and n-butane oxidation. Combust Sci Tech 1994;100:299–330. doi:10.1080/00102209408935458.

[386] Ghosh P, Hickey KJ, Jaffe SB. Development of a Detailed Gasoline Composition-Based Octane Model. Ind Eng Chem Res 2006;45:337–45. doi:10.1021/ie050811h.

[387] Villano SM, Huynh LK, Carstensen H-H, Dean AM. High-Pressure Rate Rules for Alkyl + O2 Reactions. 1. The Dissociation, Concerted Elimination, and Isomerization Channels of the Alkyl Peroxy Radical. J Phys Chem A 2011;115:13425–42. doi:10.1021/jp2079204.

[388] Villano SM, Huynh LK, Carstensen H-H, Dean AM. High-Pressure Rate Rules for Alkyl + O2 Reactions. 2. The Isomerization, Cyclic Ether Formation, and β-Scission Reactions of Hydroperoxy Alkyl Radicals. J Phys Chem A 2012;116:5068–89. doi:10.1021/jp3023887.

[389] Miyoshi A. Systematic Computational Study on the Unimolecular Reactions of Alkylperoxy (RO2), Hydroperoxyalkyl (QOOH), and Hydroperoxyalkylperoxy (O2QOOH) Radicals. J Phys Chem A 2011;115:3301–25. doi:10.1021/jp112152n.

[390] Miyoshi A. Molecular size dependent falloff rate constants for the recombination reactions of alkyl radicals with O2 and implications for simplified kinetics of alkylperoxy radicals. Int J Chem Kinet 2012;44:59–74. doi:10.1002/kin.20623.

[391] Sharma S, Raman S, Green WH. Intramolecular Hydrogen Migration in Alkylperoxy and Hydroperoxyalkylperoxy Radicals: Accurate Treatment of Hindered Rotors. J Phys Chem A 2010;114:5689–701. doi:10.1021/jp9098792.

[392] Bugler J, Rodriguez A, Herbinet O, Battin-Leclerc F, Togbé C, Dayma G, et al. An experimental and modelling study of n-pentane oxidation in two jet-stirred reactors: The importance of pressure-dependent kinetics and new reaction pathways. Proc Combust Inst 2017;36:441–8. doi:http://dx.doi.org/10.1016/j.proci.2016.05.048.

[393] Fish A. The Cool Flames of Hydrocarbons. Angew Chemie, Int Ed English 1968;7:45–60. doi:10.1002/anie.196800451.

[394] Herbinet O, Husson B, Serinyel Z, Cord M, Warth V, Fournet R, et al. Experimental and modeling investigation of the low-temperature oxidation of n-heptane. Combust Flame 2012;159:3455–71. doi:10.1016/j.combustflame.2012.07.008.

[395] Tanaka S, Ayala F, Keck JC, Heywood JB. Two-stage ignition in HCCI combustion and HCCI control by fuels and additives. Combust Flame 2003;132:219–39. doi:10.1016/S0010-2180(02)00457-1.

[396] Silke EJ, Curran HJ, Simmie JM. The influence of fuel structure on combustion as demonstrated by the isomers of heptane: A rapid compression machine study. Proc Combust Inst 2005;30 II:2639–47. doi:10.1016/j.proci.2004.08.180.

[397] Di Sante R. Measurements of the auto-ignition of n-heptane/toluene mixtures using a rapid compression machine. Combust Flame 2012;159:55–63.

doi:10.1016/j.combustflame.2011.05.020.

[398] Vanhove G, Petit G, Minetti R. Experimental study of the kinetic interactions in the low-temperature autoignition of hydrocarbon binary mixtures and a surrogate fuel. Combust Flame 2006;145:521–32. doi:10.1016/j.combustflame.2006.01.001.

[399] Mittal G, Sung C-J. Homogeneous charge compression ignition of binary fuel blends. Combust Flame 2008;155:431–9. doi:10.1016/j.combustflame.2008.05.003.

[400] Lim OT, Sendoh N, Iida N. Experimental Study on HCCI Combustion Characteristics of n-Heptane and iso-Octane Fuel/Air Mixture by the use of a Rapid Compression Machine. SAE Tech Pap 2004. doi:10.4271/2004-01-1968.

[401] Zhang P, Ji W, He T, He X, Wang Z, Yang B, et al. First-stage ignition delay in the negative temperature coefficient behavior: Experiment and simulation. Combust Flame 2016;167:14–23. doi:http://dx.doi.org/10.1016/j.combustflame.2016.03.002.

[402] Kumar K, Mittal G, Sung CJ. Autoignition of n-decane under elevated pressure and low-to-intermediate temperature conditions. Combust Flame 2009;156:1278–88. doi:10.1016/j.combustflame.2009.01.009.

[403] Mehl M, Chen JY, Pitz WJ, Sarathy SM, Westbrook CK. An Approach for Formulating Surrogates for Gasoline with Application toward a Reduced Surrogate Mechanism for CFD Engine Modeling. Energy & Fuels 2011;25:5215–23. doi:10.1021/ef201099y.

[404] Badra JA, Bokhumseen N, Mulla N, Sarathy SM, Farooq A, Kalghatgi G, et al. A methodology to relate octane numbers of binary and ternary n-heptane, iso-octane and toluene mixtures with simulated ignition delay times. Fuel 2015;160:458–69. doi:10.1016/j.fuel.2015.08.007.

[405] Morgan N, Smallbone A, Bhave A, Kraft M, Cracknell R, Kalghatgi G. Mapping surrogate gasoline compositions into RON/MON space. Combust Flame 2010;157:1122–31. doi:10.1016/j.combustflame.2010.02.003.

[406] Vranckx S, Lee C, Chakravarty HK, Fernandes RX. A rapid compression machine study of the low temperature combustion of cyclohexane at elevated pressures. Proc Combust Inst 2013;34:377–84. doi:10.1016/j.proci.2012.06.071.

[407] Pitz WJ, Naik C V., Ní Mhaoldúin T, Westbrook CK, Curran HJ, Orme JP, et al. Modeling and experimental investigation of methylcyclohexane ignition in a rapid compression machine. Proc Combust Inst 2007;31 I:267–75. doi:10.1016/j.proci.2006.08.041.

[408] Mittal G, Sung CJ. Autoignition of methylcyclohexane at elevated pressures. Combust Flame 2009;156:1852–5. doi:10.1016/j.combustflame.2009.05.009.

[409] Weber BW, Pitz WJ, Mehl M, Silke EJ, Davis AC, Sung C-J. Experiments and modeling of the autoignition of methylcyclohexane at high pressure. Combust Flame 2014;161:1972–83. doi:10.1016/j.combustflame.2014.01.018.

[410] Kumar K, Mittal G, Sung CJ, Law CK. An experimental investigation of ethylene/O2/diluent mixtures: Laminar flame speeds with preheat and ignition delays at high pressures. Combust Flame 2008;153:343–54. doi:10.1016/j.combustflame.2007.11.012.

[411] Burke SM, Burke U, Mc Donagh R, Mathieu O, Osorio I, Keesee C, et al. An experimental and modeling study of propene oxidation. Part 2: Ignition delay time and flame speed measurements.

Combust Flame 2015;162:296–314. doi:10.1016/j.combustflame.2014.07.032.

[412] Zhou C-W, Li Y, O'Connor E, Somers KP, Thion S, Keesee C, et al. A comprehensive experimental and modeling study of isobutene oxidation. Combust Flame 2016;167:353–79. doi:http://dx.doi.org/10.1016/j.combustflame.2016.01.021.

[413] Beckers A, Levedahl WJ. Mechanism of Autoignition in Benzene-Air Mixtures. Ind Eng Chem 1956;48:411–2. doi:10.1021/ie51398a021.

[414] Mittal G, Sung CJ. Autoignition of toluene and benzene at elevated pressures in a rapid compression machine. Combust Flame 2007;150:355–68. doi:10.1016/j.combustflame.2007.04.014.

[415] El Bakali A, Ribaucour M, Saylam A, Vanhove G, Therssen E, Pauwels JF. Benzene addition to a fuel-stoichiometric methane/O2/N 2 flat flame and to n-heptane/air mixtures under rapid compression machine. Fuel 2006;85:881–95. doi:10.1016/j.fuel.2005.10.009.

[416] Roubaud A, Minetti R, Sochet L. Oxidation and combustion of low alkylbenzenes at high pressure: comparative reactivity and auto-ignition. Combust Flame 2000;121:535–41. doi:10.1016/S0010-2180(99)00169-8.

[417] Darcy D, Nakamura H, Tobin CJ, Mehl M, Metcalfe WK, Pitz WJ, et al. A high-pressure rapid compression machine study of n-propylbenzene ignition. Combust Flame 2014;161:65–74. doi:10.1016/j.combustflame.2013.08.001.

[418] Husson B, Bounaceur R, Tanaka K, Ferrari M, Herbinet O, Glaude PA, et al. Experimental and modeling study of the oxidation of n-butylbenzene. Combust Flame 2012;159:1399–416. doi:10.1016/j.combustflame.2011.12.006.

[419] Nakamura H, Darcy D, Mehl M, Tobin CJ, Metcalfe WK, Pitz WJ, et al. An experimental and modeling study of shock tube and rapid compression machine ignition of n-butylbenzene/air mixtures. Combust Flame 2014;161:49–64. doi:10.1016/j.combustflame.2013.08.002.

[420] Kukkadapu G, Weber BW, Sung C-J. Autoignition study of tetralin in a rapid compression machine at elevated pressures and low-to-intermediate temperatures. Fuel 2015;159:436–45. doi:10.1016/j.fuel.2015.06.093.

[421] Gulati SK, Walker RW. Addition of cyclohexane to slowly reacting H2-O2 mixtures at 480-degree C. J Chem Soc Faraday Trans 2 1989;85:1799. doi:10.1039/f29898501799.

[422] Center for Energy Research (Combustion Division) University of California at San Diego. Chemical Kinetic Mechanism for Combustion Applications, http://web.eng.ucsd.edu/mae/groups/combustion/mechanism.html. n.d.

[423] Lacey JS, Filipi ZS, Sathasivam SR, Peyla RJ, Cannella W, Fuentes-Afflick PA. Impact of Refinery Stream Gasoline Property Variation on Load Sensitivity of the HCCI Combustion. J Eng Gas Turbines Power 2013;135:052803. doi:10.1115/1.4023028.

[424] Davidson D, Gauthier B, Hanson R. Shock tube ignition measurements of iso-octane/air and toluene/air at high pressures. Proc Combust Inst 2005;30:1175–82. doi:10.1016/j.proci.2004.08.004.

[425] Vanhove G, Petit G, Minetti R. Experimental study of the kinetic interactions in the low-temperature autoignition of hydrocarbon binary mixtures and a surrogate fuel. Combust Flame

2006;145:521–32. doi:10.1016/j.combustflame.2006.01.001.

[426] Darcy D, Tobin CJ, Yasunaga K, Simmie JM, Würmel J, Metcalfe WK, et al. A high pressure shock tube study of n-propylbenzene oxidation and its comparison with n-butylbenzene. Combust Flame 2012;159:2219–32. doi:10.1016/j.combustflame.2012.02.009.

[427] Agarwal A. Biofuels (alcohols and biodiesel) applications as fuels for internal combustion engines. Prog Energy Combust Sci 2007;33:233–71. doi:10.1016/j.pecs.2006.08.003.

[428] Lee D, Hochgreb S, Keck JC. Autoignition of Alcohols and Ethers in a Rapid Compression Machine. SAE Tech Pap 932755 1993. doi:10.4271/932755.

[429] Kumar K, Sung C. Autoignition of methanol: experiments and computations. Int J Chem Kinet 2011;43:175–84. doi:10.1002/kin.20546.

[430] Burke U, Metcalfe WK, Burke SM, Heufer KA, Dagaut P, Curran HJ. A detailed chemical kinetic modeling, ignition delay time and jet-stirred reactor study of methanol oxidation. Combust Flame 2016;165:125–36. doi:http://dx.doi.org/10.1016/j.combustflame.2015.11.004.

[431] Lee C, Vranckx S, Heufer K a., Khomik S V., Uygun Y, Olivier H, et al. On the Chemical Kinetics of Ethanol Oxidation: Shock Tube, Rapid Compression Machine and Detailed Modeling Study. Zeitschrift Für Phys Chemie 2012;226:1–28. doi:10.1524/zpch.2012.0185.

[432] Mittal G, Burke SM, Davies VA, Parajuli B, Metcalfe WK, Curran HJ. Autoignition of ethanol in a rapid compression machine. Combust Flame 2014;161:1164–71. doi:10.1016/j.combustflame.2013.11.005.

[433] Weber BW, Kumar K, Zhang Y, Sung CJ. Autoignition of n-butanol at elevated pressure and low-to-intermediate temperature. Combust Flame 2011;158:809–19. doi:10.1016/j.combustflame.2011.02.005.

[434] Kumar K, Zhang Y, Sung C, Pitz W. Autoignition Response of n-Butanol and its Blends with Primary Reference Fuel Constituents of Gasoline. Combust Flame 2015;162:2466–79. doi:10.1016/j.combustflame.2015.02.014.

[435] Tsujimura T, Pitz WJ, Gillespie F, Curran HJ, Weber BW, Zhang Y, et al. Development of Isopentanol Reaction Mechanism Reproducing Autoignition Character at High and Low Temperatures. Energy & Fuels 2012;26:4871–86. doi:10.1021/ef300879k.

[436] Sarathy SM, Park S, Weber BW, Wang W, Veloo PS, Davis AC, et al. A comprehensive experimental and modeling study of iso-pentanol combustion. Combust Flame 2013;160:2712–28. doi:10.1016/j.combustflame.2013.06.022.

[437] Heufer KA, Bugler J, Curran HJ. A comparison of longer alkane and alcohol ignition including new experimental results for n-pentanol and n-hexanol. Proc Combust Inst 2013;34:511–8. doi:10.1016/j.proci.2012.05.103.

[438] Vranckx S, Beeckmann J, Kopp W, Lee C, Cai L, Chakravarty H, et al. An experimental and kinetic modelling study of n-butyl formate combustion. Combust Flame 2013;160(12):26:2680–92. doi:10.1016/j.combustflame.2013.06.012.

[439] Dooley S, Curran HJ, Simmie JM. Autoignition measurements and a validated kinetic model for the biodiesel surrogate, methyl butanoate. Combust Flame 2008;153:2–32. doi:10.1016/j.combustflame.2008.01.005.

[440] Zhang Y, Somers KP, Mehl M, Pitz WJ, Cracknell RF, Curran HJ. Probing the antagonistic effect of toluene as a component in surrogate fuel models at low temperatures and high pressures. A case study of toluene/dimethyl ether mixtures. Proc Combust Inst 2017;36:413–21. doi:http://doi.org/10.1016/j.proci.2016.06.190.

[441] Griffiths J, Perche A. The spontaneous decomposition, oxidation and ignition of ethylene oxide under rapid compression. Proc Combust Inst 1981;18:894–901. doi:10.1016/S0082-0784(81)80093-8.

[442] Vanhove G, Yu Y, Boumehdi M, Frottier O, Herbinet O, Glaude P-A, et al. Experimental study of tetrahydrofuran oxidation and ignition in low-temperature conditions. Energy & Fuels 2015. doi:10.1021/acs.energyfuels.5b0105.

[443] Nakamura H, Curran H, Córdoba A, Pitz W, Dagaut P, Togbé C, et al. An experimental and modeling study of diethyl carbonate oxidation. Combust Flame 2015;162:1395–405. doi:10.1016/j.combustflame.2014.11.002.

[444] Black G, Curran H, Pichon S, Simmie J, Zhukov V. Bio-butanol: combustion properties and detailed chemical kinetic model. Combust Flame 2010;157:363–73.

[445] Sarathy SM, Vranckx S, Yasunaga K, Mehl M, Oßwald P, Metcalfe WK, et al. A comprehensive chemical kinetic combustion model for the four butanol isomers. Combust Flame 2012;159:2028–55. doi:10.1016/j.combustflame.2011.12.017.

[446] Mehl M, Pitz WJ, Westbrook CK, Curran HJ. Kinetic modeling of gasoline surrogate components and mixtures under engine conditions. Proc Combust Inst 2011;33:193–200. doi:10.1016/j.proci.2010.05.027.

[447] Merchant SS, Zanoelo EF, Speth RL, Harper MR, Van Geem KM, Green WH. Combustion and pyrolysis of iso-butanol: Experimental and chemical kinetic modeling study. Combust Flame 2013;160:1907–29. doi:http://dx.doi.org/10.1016/j.combustflame.2013.04.023.

[448] Cai J, Yuan W, Ye L, Cheng Z, Wang Y, Dong W, et al. Experimental and kinetic modeling study of i-butanol pyrolysis and combustion. Combust Flame 2014;161:1955–71. doi:http://dx.doi.org/10.1016/j.combustflame.2014.02.004.

[449] Curran H, Dunphy M, Simmie J, Westbrook C, Pitz W. Shock tube ignition of ethanol, isobutene and MTBE: Experiments and modeling. Proc Combust Inst 1992;24:769–76. doi:10.1016/S0082-0784(06)80094-9.

[450] Burger JL, Schneider N, Bruno TJ. Application of the Advanced Distillation Curve Method to Fuels for Advanced Combustion Engine Gasolines. Energy & Fuels 2015;29:4227–35. doi:10.1021/acs.energyfuels.5b00749.

[451] Burger JL, Bruno TJ. Application of the Advanced Distillation Curve Method to the Variability of Jet Fuels. Energy & Fuels 2012;26:3661–71. doi:10.1021/ef3006178.

[452] Dagaut P, Cathonnet M. The ignition, oxidation, and combustion of kerosene: A review of experimental and kinetic modeling. Prog Energy Combust Sci 2006;32:48–92. doi:10.1016/j.pecs.2005.10.003.

[453] Pitz WJ, Mueller CJ. Recent progress in the development of diesel surrogate fuels. Prog Energy Combust Sci 2011;37:330–50. doi:10.1016/j.pecs.2010.06.004.

[454] Kukkadapu G, Kumar K, Sung CJ, Mehl M, Pitz WJ. Experimental and surrogate modeling study of gasoline ignition in a rapid compression machine. Combust Flame 2012;159:3066–78. doi:10.1016/j.combustflame.2012.05.008.

[455] Kukkadapu G, Kumar K, Sung CJ, Mehl M, Pitz WJ. Autoignition of gasoline and its surrogates in a rapid compression machine. Proc Combust Inst 2013;34:345–52. doi:10.1016/j.proci.2012.06.135.

[456] Kukkadapu G, Kumar K, Sung C, Mehl M, Pitz W. Autoignition of Gasoline Surrogates at Low Temperature Combustion Conditions. Combust Flame 2015;162:2272–85. doi:10.1016/j.combustflame.2015.01.025.

[457] Sarathy SM, Kukkadapu G, Mehl M, Wang W, Javed T, Park S, et al. Ignition of alkane-rich FACE gasoline fuels and their surrogate mixtures. Proc Combust Inst 2015;35:249–57. doi:10.1016/j.proci.2014.05.122.

[458] Gauthier BM, Davidson DF, Hanson RK. Shock tube determination of ignition delay times in full-blend and surrogate fuel mixtures. Combust Flame 2004;139:300–11. doi:10.1016/j.combustflame.2004.08.015.

[459] Mehl M, Chen JY, Pitz WJ, Sarathy SM, Westbrook CK. An Approach for Formulating Surrogates for Gasoline with Application toward a Reduced Surrogate Mechanism for CFD Engine Modeling. Energy & Fuels 2011;25:5215–23. doi:10.1021/ef201099y.

[460] Cannella W, Foster M, Gunter G, Leppard W. FACE Gasolines and Blends with Ethanol: Detrailed Characterization of Physical and Chemical Properties. 2014.

[461] Kumar K, Sung C. An experimental study of the autoignition characteristics of conventional jet fuel/oxidizer mixtures: Jet-A and JP-8. Combust Flame 2010;157:676–85. doi:10.1016/j.combustflame.2010.01.001.

[462] Kumar K, Sung CJ. A comparative experimental study of the autoignition characteristics of alternative and conventional jet fuel/oxidizer mixtures. Fuel 2010;89:2853–63. doi:10.1016/j.fuel.2010.05.021.

[463] Dooley S, Won SH, Chaos M, Heyne J, Ju Y, Dryer FL, et al. A jet fuel surrogate formulated by real fuel properties. Combust Flame 2010;157:2333–9. doi:10.1016/j.combustflame.2010.07.001.

[464] Dooley S, Won SH, Heyne J, Farouk TI, Ju Y, Dryer FL, et al. The experimental evaluation of a methodology for surrogate fuel formulation to emulate gas phase combustion kinetic phenomena. Combust Flame 2012;159:1444–66. doi:10.1016/j.combustflame.2011.11.002.

[465] Hui X, Kumar K, Sung CJ, Edwards T, Gardner D. Experimental studies on the combustion characteristics of alternative jet fuels. Fuel 2012;98:176–82. doi:10.1016/j.fuel.2012.03.040.

[466] Kukkadapu G, Sung C-J. Autoignition study of ULSD#2 and FD9A diesel blends. Combust Flame 2016;166:45–54. doi:http://dx.doi.org/10.1016/j.combustflame.2015.12.022.

[467] Haylett DR, Davidson DF, Hanson RK. Ignition delay times of low-vapor-pressure fuels measured using an aerosol shock tube. Combust Flame 2012;159:552–61. doi:http://dx.doi.org/10.1016/j.combustflame.2011.08.021.

[468] Gowdagiri S, Wang W, Oehlschlaeger MA. A shock tube ignition delay study of conventional diesel fuel and hydroprocessed renewable diesel fuel from algal oil. Fuel 2014;128:21–9.

doi:http://dx.doi.org/10.1016/j.fuel.2014.02.064.

[469] Jovellanos BJU, Taylor ES, Taylor CF, Leary WA. An Investigation of the Effect of Tetraethyl Lead and Ethyl Nitrite on the Autoignition Characteristics of Isooctane and Triptane. Natl Advis Comm Aeronaut 1950;Technical .

[470] Inomata T, Griffiths J, Pappin A. The role of additives as sensitizers for the spontaneous ignition of hydrocarbons. Proc Combust Inst 1991;23:1759–66. doi:10.1016/S0082-0784(06)80454-6.

[471] Seyferth D. The Rise and Fall of Tetraethylead. 2. Organometrallics 2003;22:5154–78. doi:10.1021/om030621b.

[472] Chamberlain GHN, Hoare DE, Walsh AD. The mode of action of lead tetraethyl as an inhibitor of combustion processes. Discuss Faraday Soc 1953;14:89–97. doi:10.1039/DF9531400089.

[473] Rifkin EB, Walcutt C. A Basis for Understanding Antiknock Action. SAE Tech. Pap. 570046, 1957. doi:10.4271/570046.

[474] Rumminger MD, Linteris GT. The role of particles in the inhibition of premixed flames by iron pentacarbonyl. Combust Flame 2000;123:82–94. doi:10.1016/S0010-2180(00)00153-X.

[475] Rumminger MD, Linteris GT. Inhibition of premixed carbon monoxide–hydrogen–oxygen–nitrogen flames by iron pentacarbonyl. Combust Flame 2000;120:451–64. doi:10.1016/S0010-2180(99)00114-5.

[476] Linteris G. Inhibition of premixed methane flames by manganese and tin compounds. Combust Flame 2002;129:221–38. doi:10.1016/S0010-2180(02)00346-2.

[477] Sudholt A, Cai L, Heyne J, Haas FM, Pitsch H, Dryer FL. Ignition characteristics of a bio-derived class of saturated and unsaturated furans for engine applications. Proc Combust Inst 2015;35:2957–65. doi:10.1016/j.proci.2014.06.147.

[478] Ji C, Dec JE, Dernotte J, Cannella W. Effect of Ignition Improvers on the Combustion Performance of Regular-Grade E10 Gasoline in an HCCI Engine. SAE Int J Engines 2014;7:2014–01 – 1282. doi:10.4271/2014-01-1282.

[479] Ludwig W, Brandt B, Friedrichs G, Temps F. Kinetics of the Reaction C2H5+HO2 by Time-Resolved Mass Spectrometry. J Phys Chem A 2006;110:3330–7. doi:10.1021/jp0557464.

[480] Pang GA, Hanson RK, Golden DM, Bowman CT. Experimental Determination of the High-Temperature Rate Constant for the Reaction of OH with sec -Butanol. J Phys Chem A 2012;116:9607–13. doi:10.1021/jp306977e.

[481] Goldsborough SS, Santner J. Mining an experimental autoignition database to hierarchically identify facility influences on the measurements. Combust Flame n.d.

[482] Weber BW, Sung C-J, Renfro MW. On the uncertainty of temperature estimation in a rapid compression machine. Combust Flame 2015;162:2518–28. doi:http://dx.doi.org/10.1016/j.combustflame.2015.03.001.

[483] Sciacchitano A, Neal DR, Smith BL, Warner SO, Vlachos PP, Wieneke B, et al. Collaborative framework for PIV uncertainty quantification: comparative assessment of methods. Meas Sci Technol 2015;26:74004. doi:10.1088/0957-0233/26/7/074004.

[484] Ayass WW, Nasir EF, Farooq A, Sarathy SM. Mixing-structure relationship in jet-stirred reactors.

Chem Eng Res Des 2016;111:461–4. doi:10.1016/j.cherd.2016.05.016.

[485] Prager J, Najm HN, Sargsyan K, Safta C, Pitz WJ. Uncertainty quantification of reaction mechanisms accounting for correlations introduced by rate rules and fitted Arrhenius parameters. Combust Flame 2013;160:1583–93. doi:http://dx.doi.org/10.1016/j.combustflame.2013.01.008.

[486] Fridlyand A, Goldsborough SS, Brezinsky K. Chemical Kinetic Influences of Alkyl Chain Structure on the High Pressure and Temperature Oxidation of a Representative Unsaturated Biodiesel: Methyl Nonenoate. J Phys Chem A 2015;119:7559–77. doi:10.1021/acs.jpca.5b00914.

[487] Sajid MB, Farooq A. Applications of cw Quantum Cascade Laser near 8 μm in Gas Sensing Research. Imaging Appl. Opt. 2014, Seattle, Washington : Optical Society of America; 2014, p. LW1D.3. doi:10.1364/LACSEA.2014.LW1D.3.

[488] Chrystie RSM, Nasir EF, Farooq A. Propene concentration sensing for combustion gases using quantum-cascade laser absorption near 11 μm. Appl Phys B 2015;120:317–27. doi:10.1007/s00340-015-6139-4.

[489] Lyakh A, Barron-Jimenez R, Dunayevskiy I, Go R, Tsvid E, Patel KC. Progress in Rapidly-Tunable External Cavity Quantum Cascade Lasers with a Frequency-Shifted Feedback. Photonics 2016;3. doi:10.3390/photonics3020019.

[490] Chrystie RSM, Nasir EF, Farooq A. Towards simultaneous calibration-free and ultra-fast sensing of temperature and species in the intrapulse mode. Proc Combust Inst 2015;35:3757–64. doi:http://dx.doi.org/10.1016/j.proci.2014.06.069.

[491] Goldenstein CS, Spearrin RM, Jeffries JB, Hanson RK. Infrared laser-absorption sensing for combustion gases. Prog Energy Combust Sci 2017;60:132–76. doi:http://doi.org/10.1016/j.pecs.2016.12.002.

[492] McManus TA, Papageorge MJ, Fuest F, Sutton JA. Spatio-temporal characteristics of temperature fluctuations in turbulent non-premixed jet flames. Proc Combust Inst 2015;35:1191–8. doi:http://dx.doi.org/10.1016/j.proci.2014.08.017.

[493] Arndt CM, Papageorge MJ, Fuest F, Sutton JA, Meier W, Aigner M. The role of temperature, mixture fraction, and scalar dissipation rate on transient methane injection and auto-ignition in a jet in hot coflow burner. Combust Flame 2016;167:60–71. doi:http://dx.doi.org/10.1016/j.combustflame.2016.02.027.

[494] Hargather MJ, Lawson MJ, Settles GS, Weinstein LM. Seedless Velocimetry Measurements by Schlieren Image Velocimetry. AIAA J 2011;49:611–20. doi:10.2514/1.J050753.

[495] Lillo PM, Greene ML, Volker S. Plenoptic Single-Shot 3D Imaging of In-Cylinder Fuel Spray Geometry. Zeitschrift Für Phys Chemie 2015;229:549. doi:10.1515/zpch-2014-0601.

[496] Chen H, Lillo PM, Sick V. Three-dimensional spray–flow interaction in a spark-ignition direct-injection engine. Int J Engine Res 2016;17 :129–38. doi:10.1177/1468087415608741.

[497] Cannella W, Foster M, Gunter G, Leppard W. FACE Gasolines and Blends with Ethanol: Detrailed Characterization of Physical and Chemical Properties. 2014.

[498] Wang Z, Sarathy SM. Third O2 addition reactions promote the low-temperature auto-ignition of n-alkanes. Combust Flame 2016;165:364–72.

doi:http://dx.doi.org/10.1016/j.combustflame.2015.12.020.

[499] Wang Z, Zhang L, Moshammer K, Popolan-Vaida DM, Shankar VSB, Lucassen A, et al. Additional chain-branching pathways in the low-temperature oxidation of branched alkanes. Combust Flame 2016;164:386–96. doi:http://dx.doi.org/10.1016/j.combustflame.2015.11.035.

[500] Foong TM, Morganti KJ, Brear MJ, da Silva G, Yang Y, Dryer FL. The octane numbers of ethanol blended with gasoline and its surrogates. Fuel 2014;115:727–39. doi:http://dx.doi.org/10.1016/j.fuel.2013.07.105.